



The
University
Of
Sheffield.

**Impact of Voids on Buried Utility Pipes
Subjected to Surface Traffic Loading**

Centre for Energy and Infrastructure Ground Research
(CEIGR)

Tawfeg A. A. Elmrom

A thesis submitted in partial fulfilment of the requirement
for the degree of Doctor of Philosophy

Department of Civil and Structural Engineering

The University of Sheffield

October, 2021

Declaration

I, Tawfeg Elmrom, hereby declare that the contents of this PhD thesis titled “*Impact of Voids on Buried Utility Pipes Subjected to Surface Traffic Loading*” are original and have not been submitted in whole, or in part, for consideration for any other qualification at this, or any other, university or institution. The work done as part of this thesis is the result of my own work, except where specific reference is made to the work of others.

Tawfeg A. A. ELMROM

October, 2021

A handwritten signature in black ink, appearing to read 'Tawfeg Elmrom', written in a cursive style.

Acknowledgements

I would like to express my sincere gratitude to my supervisor. It was a great opportunity and it was pleasure and privilege to work in the Geotechnical group. I also would like to give my thanks to my second supervisor Dr Richard P Collins for his help throughout this research. Many thanks to all academic staff in particularly Dr Elisabeth Bowman for her academic and social support also Prof. Sam Clarke for his academic support.

I am also very happy to give my great thanks to technical staff at the Department of Civil and Structural Engineering, in particular Alex Cargill for his technical support, without whose assistance and support throughout the centrifuge testing periods, and beyond, this PhD work would not have been a success. Also, many thanks to Mark Foster and Paul Blackburn for their support to develop the experimental systems.

Although The COVID-19 pandemic became the concern of the globe in general, and on a personal level in which I had suffered from this virus for a long period in hospital and still suffering from post-COVID-19. This crisis has not stopped me to continue achieving my PhD research.

Finally, I would like to take this opportunity to extend my thanks and great gratitude to my parents, beloved wife, kids and my brothers and sisters. for their endless love and support, and continual source of inspiration. Also, a moment of reflection to my older brother who recently passed and was always wished to see this moment; we miss you dearly and pray for his mercy.

شكر وتقدير

نحمد الله عز وجل علي النعمة التي أنعم بها علينا في إتمام هذا البحث فهو العلي التقدير والصلاة والسلام علي سيد المرسلين وعلي اله وصحبه اجمعين قال تعالى:-

بسم الله الرحمن الرحيم

وَأَنْزَلَ اللَّهُ عَلَيْكَ الْكِتَابَ وَالْحِكْمَةَ وَعَلَّمَكَ مَا لَمْ تَكُنْ تَعْلَمُ وَكَانَ فَضْلُ اللَّهِ عَلَيْكَ عَظِيمًا

صدق الله العظيم (النساء-113)

أود أن أعرب عن شكري لمشرفي وكان من دواعي سروري وامتناني أيضاً للعمل مع الفريق الجيوتقني في هذه الجامعة. لم يكن هذا البحث ليكتمل ويرى النور لولا إرادة الله سبحانه وتعالى فله الحمد دائما وابدأ . كما أود أن أشكر الدكتور ريتشرد كولانس علي دعمه طيلة فترة دراستي. وشكر حاص الي الدكتوراة الفاضلة اليزابيت يومان علي دعمها الاكاديمي والمعنوي.

يسعدني أيضاً أن أتقدم بجزيل الشكر إلى الكادر الفني في قسم الهندسة المدنية والإنشائية بجامعة شيقيلد ، ولا سيما أليكس كارجيل علي دعمه الفني ، والذي بدون مساعدته ودعمه طوال فترات اختبارات أجهزة الطرد المركزي ، وما بعدها ، لن يكون عمل الدكتوراة هذا سهلاً. أيضاً ، شكر كبير لمارك فوستر وبول بلاكبورن اللذان ساعداني في تطوير الجهاز الخاص بالاختبارات .

علي الرغم من أن جائحة فيروس كورونا COVID-19 أصبحت مصدر قلق للعالم بشكل عام ، وخاص علي المستوى الشخصي التي بسببها عانيت فيه من هذا الفيروس لفترة طويلة في المستشفى وحتى بعد خروجي ما زلت أعاني من اثار هذا الفيروس .لم تمنعني هذه الأزمة من مواصلة إنجاز بحث الدكتوراه الخاص بي بتوفيق من الله.

أخيراً ، أود أن أعنتم هذه الفرصة لأقدم شكري وامتناني الكبير لوالدي وزوجتي الحبيبة وأولادي واخوتي وأخواني لحبهم ودعمهم اللامتناهي ، ومصدر الإلهام المستمر. وأيضاً ، رسالة شكر للشخص الذي تركنا مبكراً وكان يتمنى دائماً رؤية هذه اللحظة (أخي الأكبر المتوفى الذي ادعو له دائماً بالرحمة).

والله ولي التوفيق

ABSTRACT

The integrity and performance of buried pipe infrastructure is vital to our society for the provision of safe potable water and, transportation of sewage. For this purpose, a diverse range of buried utility pipes are deployed ranging from large diameter concrete sewer pipes to small diameter fresh water pipes, historically manufactured from cast iron and more recently plastic. Municipal water distribution and wastewater infrastructure systems are of national importance for any country and the aspect of water leakage; coupled with water scarcity, has become a serious problem in many countries around the world. For example, in the UK up to 22% of potable water can be lost from source to tap to leakage or failure of the pipe network (Laspidou, 2014). Currently we cannot predict when an individual pipe will reach the end of its serviceable life due to the complex, range of factors that contribute to their deterioration. For example, due to their shallow burial depth they are vulnerable to (i) the impact of increasing surface traffic load intensity, (ii) initial and temporal burial conditions and (iii) climate effects that contribute to increased variability of moisture content and temperature within the soil.

This project focuses on examining the impact of surface loading and burial conditions, specifically the role of void formation on plastic pipe behaviour. Small scale physical experiments using the University of Sheffield 4m diameter centrifuge have been undertaken to provide insight of the role of these factors in the pipe-soil interaction behaviour. The results have shown increased pipe bending moment and deflection were observed with the increase of void size confirming that void formation may contribute in the overall failure of pipe infrastructure. Moreover, a decrease in bending moment and pipe deflection were noticed with increase of internal water pressure of the pipe, burial depth and the presence of a road surface. Thesis also covers traffic effects or cyclic loading (Impact of Voids on Buried Utility Pipes Subjected to Surface Traffic Loading). Therefore, These will support the main findings of this research, particularly the academic / intellectual contribution..

Table of Contents

DECLARATION	I
ACKNOWLEDGEMENTS	II
ABSTRACT	III
TABLE OF CONTENTS	IV
LIST OF FIGURES	VII
LIST OF TABLE.....	XIII
NOMENCLATURE.....	XV
1 INTRODUCTION AND MOTIVATION FOR RESEARCH	1
1.1 BACKGROUND TO BURIED UTILITY PIPES.....	1
1.2 RESEARCH AIM AND OBJECTIVES.....	6
1.3 THE NOVELTY OF THE RESEARCH.....	7
1.4 THE OUTLINE OF THE THESIS	8
2 LITERATURE REVIEW	9
2.1 INTRODUCTION.....	9
2.2 BACKGROUND	10
2.2.1 <i>Experimental Studies</i>	11
2.2.2 <i>Numerical Studies</i>	19
2.2.3 <i>Theoretical Modelling</i>	26
2.3 BURIED FLEXIBLE PIPE DESIGN.....	28
2.3.1 <i>Elastic Models for Soil Backfill Response</i>	29
2.3.2 <i>Subgrade Reaction Theory</i>	30
2.4 CONCLUSION AND SUMMARY	34
3 GEOTECHNICAL MODELLING APPROACHES	35
3.1 INTRODUCTION.....	35
3.2 CENTRIFUGE MODELLING	36
3.2.1 <i>The University of Sheffield Centrifuge (UoS50gT)</i>	36
3.3 PRINCIPLES OF CENTRIFUGE MODELLING	39
3.3.1 <i>Scaling Laws</i>	39
3.3.2 <i>Scaling Laws for Vertical Stress (σ_v)</i>	43
3.3.3 <i>Scaling Laws for the Second Moment of Area (I)</i>	44

3.3.4	<i>Scaling Laws of Bending Moment (M)</i>	45
3.3.5	<i>Scaling Laws for Bending Stiffness (EI)</i>	46
3.3.6	<i>Scaling Laws for the Applied Load</i>	47
4	EXPERIMENTAL METHODOLOGY	47
4.1	SCOPE OF CHAPTER	47
4.2	EXPERIMENTAL SETUP	47
4.2.1	<i>Material Properties</i>	48
4.2.2	<i>Model Design</i>	59
4.2.3	<i>Mechanical Design</i>	64
4.2.4	<i>Instrumentation and Calibration</i>	75
4.2.5	<i>Electronic/ Control Design</i>	83
4.2.6	<i>Sample Preparation Equipment</i>	85
4.2.7	<i>Analysis of the test</i>	89
4.2.8	<i>Introduction to the Analysis</i>	89
4.2.9	<i>Data Processing</i>	89
4.3	MODEL CONFIGURATION AND PREPARATION	90
5	PIPE-SOIL BEHAVIOUR UNDER MONOTONIC LOADING	96
5.1	MONOTONIC LOADING	96
5.1.1	<i>Effect of Burial Depth</i>	99
5.1.2	<i>Effect of Eccentricity</i>	110
5.1.3	<i>Effect of void size at the pipe invert (180deg)</i>	114
5.1.4	<i>Effect of a void at the pipe springline (270deg)</i>	117
5.1.5	<i>Effect of internal water pressure via axial force</i>	120
5.1.6	<i>Effect of Road Surface</i>	124
5.1.7	<i>Model Verification</i>	129
6	DISCUSSION AND INTERPRETATION OF STATIC LOADING RESULTS	130
7	PIPE-SOIL BEHAVIOUR UNDER CYCLIC LOADING	133
7.1	INTRODUCTION.....	133
7.2	CYCLIC LOADING RESPONSE	133
7.2.1	<i>Effect of surface loading on soil stiffness</i>	134
7.2.2	<i>Effect of Burial Depth</i>	135
7.2.3	<i>Effect of Eccentricity</i>	141
7.2.4	<i>Effect of Void Size and Location</i>	145

7.2.5	<i>Influence of internal water pressure via axial load modelling.....</i>	150
7.2.6	<i>Effect of Road Surface</i>	155
8	DISCUSSION AND INTERPRETATION OF CYCLIC LOADING RESULTS	159
9	CONCLUSIONS AND RECOMMENDATIONS FOR FUTURE WORK	162
9.1	MAJOR AND MINOR CONTRIBUTIONS	162
9.2	CONCLUSIONS	163
9.3	RECOMMENDATION FOR FUTURE WORK	166
10	REFERENCES	168
	APPENDIX A	176
	APPENDIX B	183
	APPENDIX C.....	195
	PUBLICATIONS	198

List of Figures

Figure 1-1 Image of underground potable water leakage (Water matters UK.2013).....	1
Figure 1-2 Total water leakage in England and Wales (Ofwat.2007).....	2
Figure 1-3 Leakage rate in water distribution utilities pipes world-wide. Average based on country-level leakage percentage (Laspidou, 2014).....	3
Figure 1-4 Erosion and void formation around a breached pipe (Water matters UK.2013).....	4
Figure 1-5 Buried pipe infrastructure and impact of support/void formation (Black,2014).....	5
Figure 2-1 Comparison of buried sewer pipe bending moment for full scale and model studies (Rakitin and Xu, 2014).....	11
Figure 2-2 Impact of load eccentricity on pipe deformation. Hosseini and Tafreshi (2000).....	15
Figure 2-3 (a) Centrifuge model tests of voids and (b) pipe deflection with increasing void size. Sales et al. (2015a).....	17
Figure 2-4 Maximum soil pressure Chapman et al. (2016).....	20
Figure 2-5 Finite element analysis for rigid sewers considering erosion voids and Increase in circumferential stresses at crown due to erosion voids (Tan and Moore, 2007).....	22
Figure 2-6 Plaxis mesh discretization of the buried pipe subjected to earthquake shake Alzabeebee et al. (2018).....	23
Figure 2-7 Soil constitutive model effect on pipe bending moment: a and b for good installation condition, c and d for poor installation condition.....	23
Figure 2-8 Mechanical representation of the Winkler Model (Yang and Li, 2021).....	28
Figure 2-9 Soil pressure on the pipe (Kavitha et al., 2011).....	29
Figure 2-10 Elastic continuum model (Kavitha et al., 2011).....	30
Figure 2-11 Original Winkler model (Hetényi and Hetbenyi, 1946).....	31
Figure 2-12 Beam on Winkler foundation (Hetényi and Hetbenyi, 1946).....	32

Figure 3-1 Centrifuge facility(UoS50gT) at CEIGR Sheffield University (Black J 2014)	37
Figure 3-2 The basic concept of the centrifuge modelling (after Wood, 2004)	39
Figure 3-3 Prototype radial gravity field and model scale test (Madabhushi, 2017).....	42
Figure 3-4 Under-stress and over stress in a centrifuge model (Madabhushi, 2017)	42
Figure 3-5 Concept of geotechnical centrifuge modelling(Abuhajar, 2013).....	44
Figure 3-6 Scaling of prototype scale to model scale of the pipe.....	45
Figure 4-1 HST95 silica sand and model pipe (PE100).....	48
Figure 4-2 Particle size distribution curve of HST95 sand	50
Figure 4-3 Idealised ground stress condition	52
Figure 4-4 Soil-pipe interface shear test.....	53
Figure 4-5 Shear stress- Shear strain response for sand-sand	53
Figure 4-6 Volumetric response during sand- sand shearing	54
Figure 4-7 Shear stress- Shear strain response for sand-pipe.....	54
Figure 4-8 Volumetric response during sand-pipe shearing.....	55
Figure 4-9 Sand-sand and sand-pipe friction angle.....	55
Figure 4-10 Oedometer test for HST95 silica sand	56
Figure 4-11 Dimensions of pipe specimens	57
Figure 4-12 Test machine and sample shape.....	58
Figure 4-13 PE100 plastic pipe tensile test results	58
Figure 4-14 scaling concept for plastic pipe	60
Figure 4-15 Rectangular prism of sponge used to replicate voids in the model.....	63
Figure 4-16 Model sponge location	63
Figure 4-17 Strong box centrifuge model (CEIGR).....	64

Figure 4-18 Approach used to show vertical stress increase in soil (2V:1H).....	65
Figure 4-19 AASHTO H20 and HS20 wheel loads	66
Figure 4-20 Illustration of Timoshenko soil pressure Timoshenko (1953).....	67
Figure 4-21 Illustration of Boussinesq strip loading (Boussinesq, 1885).	67
Figure 4-22 (a) Single axle footing (b) double axle footing	68
Figure 4-23 Wheel load surface contact area at 1g and 19g.....	69
Figure 4-24 Aluminium frame mounted on the strong box.....	70
Figure 4-25 Plan view schematic of the aluminium frame.....	70
Figure 4-26 Cross section a-a schematic of the aluminium frame	71
Figure 4-27 Cross section b-b schematic of the aluminium frame	71
Figure 4-28 Axial stress end restraints on pipe	72
Figure 4-29 Schematic of the actuation system apparatus	74
Figure 4-30 Actuation system apparatus.....	74
Figure 4-31 Graph showing line of best fit for LVDT calibration	75
Figure 4-32 The LVDT's location	76
Figure 4-33 Schematic for the load cell layout	77
Figure 4-34 Example of load cell1 calibration graph.....	78
<i>Figure 4-35 Strain gauge insulation</i>	<i>79</i>
<i>Figure 4-36 Schematic for the strain gauge locations</i>	<i>80</i>
Figure 4-37 Example of strain gauges Calibration graph.....	82
Figure 4-38 Centrifuge DAS cabinet (NI PIXe 1085).....	84
Figure 4-39 NI cDAQ-9188XT Chassis with two different modules.....	84
<i>Figure 4-40 Sheffield University (CEIGR) automatic point pluviation.....</i>	<i>85</i>

Figure 4-41 Schematic of the x, y paths of the automatic pluviator.....	86
Figure 4-42 Sand collection tray and both boxes	87
Figure 4-43 Hydraulic jack and forklift	88
Figure 4-44 peakfinder threshold function graph.....	90
<i>Figure 4-45 General experimental schematic of the tests</i>	91
Figure 5-1 Spin-up stages and sand self-weight effect on the modelled pipe	97
Figure 5-2 Schematic of the pipe behaviour and non-dimensional ratio.....	98
Figure 5-3 Schematic of pipe behaviour for different burial depths	100
Figure 5-4 Maximum bending moment half pipe length for the major axis (repeated test).....	100
Figure 5-5 Maximum bending moment half pipe length for the major axis (average of repeated test).....	101
Figure 5-6 Maximum bending moment along the length of the pipe for the minor axis.....	102
Figure 5-7 Resultant bending moment	103
Figure 5-8 (b) Shear force along the length of the pipe for the minor axis	105
Figure 5-9 Variation in footing stiffness with pipe burial depth	106
Figure 5-10 Soil surface settlements near the loading area.	107
Figure 5-11 Schematic of the traffic load and soil self-weight load.....	107
Figure 5-12 The technique of finite difference method depends on discretising a function on a grid	108
Figure 5-13 Pipe deflection under monotonic load at various burial depths	109
Figure 5-14 Schematic of the pipe behaviour under 6tonnes eccentric load.....	110
<i>Figure 5-15 Schematic of the zone of stress influence.</i>	111
Figure 5-16 Variation in bending moment with load eccentricity at burial depth of $Z_c=1.00m$ and applied load of 6 tonnes.	112

Figure 5-17 Identification of load eccentricity for a 1 m deep pipe.	113
Figure 5-18 Schematic of the pipe behaviour with eccentricity of load and in the presence of different void size at the pipe invert (180deg)	115
Figure 5-19 Pipe monotonic response with the presence of a void; (a) Bending moment;	116
Figure 5-20 Variation in footing stiffness with different void size	117
<i>Figure 5-21 Schematic of the pipe behaviour with an eccentricity load($2D_p$) and void size of $0.5D_p$, $1D_p$ and $2D_p$ at the pipe springline (270deg)</i>	<i>118</i>
Figure 5-22 Void size and location effect at $e=2$; (a) Major and minor bending moment;	119
Figure 5-23 Schematic illustration of pipe behaviour due to axial load.....	120
Figure 5-24 Pipe behaviour under axial force; (a) bending moment; (b) shear force	122
Figure 5-25 Pipe deflection no-axial force compared with axial force applied to the pipe.....	123
Figure 5-26 Inverse correlation between internal pressure and pipe deflection.	123
Figure 5-27 Schematic of the pipe behaviour: (a) with road surface; (b) without road surface..	124
Figure 5-28 Schematic of the pipe behaviour in the presence of a $2D_p$ void located at pipe invert (180deg): (a) with road surface; (b) without road surface.....	125
Figure 5-29 Schematic of the pipe behaviour with road surface: (a) with $2D_p$ void located at pipe invert (180deg) ; (b) without void	126
Figure 5-30 (b) pipe deflection where is V is void and Rs is road surface.....	128
Figure 5-31 Shear force diagram of the pipe with and with presence of road surface/ void	128
Figure 5-32 Comparison of deflection of pipe from centrifuge test and FDM model.....	129
Figure 7-1 Example of the cyclic load time history.	134
Figure 7-2 Soil stiffness comparison with number of cycles at 6 tonne load per cycle	135
Figure 7-3 Bending moment under cyclic load with different burial depth (a) $Z=0.5m$ (b) $Z=0.75m$; (c) $Z=1m$	138
Figure 7-4 Peak and residual major bending moment with increases in cycles	138

Figure 7-5 Pipe deflection under cyclic loading; (a) $Z=0.5\text{m}$; (b) $Z=0.75\text{m}$; (c) $Z=1\text{m}$	140
Figure 7-6 Variation in bending moment with load eccentricity at a burial depth of $Z_c=1\text{m}$ and applied load of 6tonns	142
Figure 7-7 Identification of load eccentricity monotonic and cyclic (2500cycles) loading for 1m deep pipe.	143
Figure 7-8 Variation in pipe deflection with load eccentricity at burial depth of $Z_c=1.00\text{m}$ and applied load of 6 tonnes (a, b, c, d and e).....	144
Figure 7-9 Major and minor bending moment for $2D_p$ void located at pipe invert(180deg).....	146
Figure 7-10 Major and minor bending moment for $2D_p$ void located at pipe springline (270deg)	147
Figure 7-11 Effect of void size on the maximum bending moment	147
Figure 7-12 Major pipe deflection: (a) void located at 180deg ; (b) void located at pipe springline (270deg).	148
Figure 7-13 Variation in footing stiffness with presence of different void size	149
Figure 7-14 Bending moment under cyclic loading with internal pressure; (a) $p=1.5\text{bar}$; (b) $p=2.5\text{bar}$; (c) $p=5\text{bar}$	152
Figure 7-15 Maximum bending moment under internal pressure; i, monotonic loading ii, cyclic loading.....	152
Figure 7-16 Pipe deflection under cyclic loading with internal pressure; (a) $p=1.5\text{bar}$; (b) $p=2.5\text{bar}$; (c) $p=5\text{bar}$	154
Figure 7-17 Comparison between monotonic and cyclic loading under axial force.	155
Figure 7-18 Bending moments: (a) no void no road surface ;.....	157
Figure 7-19 Pipe deflection: (a) no void, no road surface ;.....	158

List of Table

Table 2-1 Compiling of multi-parameter models(Aron and Jonas, 2012).....	32
Table 3-1 UoS50gT Centrifuge specification and performance (Black J 2014)	38
Table 3-2 Geotechnical centrifuge scaling laws (Taylor,1995)	40
Table 4-1 Properties of HST95 silica sand.....	51
Table 4-2 Ultimate strength test results for PE100 plastic pipe	57
Table 4-3 Comparison of properties between prototype HDPE and the model for PE100	61
Table 4-4 Summary of the LVDT calibration	76
Table 4-5 Summary of load cells calibration	78
<i>Table 4-6 Strain gauge locations</i>	<i>81</i>
Table 4-7 Summary of the strain gauge calibration	83
Table 4-8 Experimental matrix of the groups	92
Table 4-9 Test matrix	93
Table 5-1 Non-dimensional ratio	98
Table 5-2 Effect of burial depth (Z_c).....	99
Table 5-3 Effect of eccentricity (e) half axle (6Tonnes)	110
Table 5-4 Pipe bending moment magnitude and direction due to eccentricity of load	112
Table 5-5 Effect of void size at the pipe invert (180deg).....	114
<i>Table 5-6 Effect of Void Size at the pipe springline (270deg).....</i>	<i>118</i>
Table 5-7 Effect of Axial Load “from internal pressure“	120
Table 5-8 Effect of Road Surface (No Void Presence).	124

Table 5-9 Effect of road surface with the presence of a $2D_p$ void located at the pipe invert (180deg).	125
Table 5-10 Effect of a $2D_p$ void located at the pipe invert (180deg) with presence of a road surface.	126
Table 7-1 Effect of burial depth (Z_c).	136
Table 7-2 Effect of eccentricity (e) half axle (6Ton).	141
Table 7-3 Pipe bending moment magnitude and direction due to eccentricity of load.	142
Table 7-4 Effect of void size at the pipe invert (180deg).....	145
Table 7-5 Effect of Void Size at the pipe springline (270deg).....	145
Table 7-6 Effect of internal pressure.....	150
<i>Table 7-7 Effect of road surface (No void Present).</i>	156
Table 7-8 Effect of a road surface with the presence of a $2D_p$ void located at the pipe invert (180deg).	156
Table 7-9 Effect of a $2D_p$ void located at the pipe invert (180deg) with the presence of a road surface.	156

Nomenclature

Latin alphabet

<i>Symbol</i>	<i>Quantity</i>	<i>Units</i>
a	Centrifugal acceleration	[LT ²]
A	Area	[L ²]
B	Footing width	[L]
C_u	Uniformity coefficient C_u	[-]
d_{10}, d_{50}, d_{60}	Particle size at 10%, 50% and 60% passing	[L]
DAQ	Data acquisition system	[-]
D_p	Diameter of the pipe	[L]
D_{p-in}	Inner pipe diameter	[L]
D_{p-out}	Outer pipe diameter	[L]
E	Young's modulus	[M ⁻¹ LT ²]
E_s	Soil elastic modulus	[M ⁻¹ LT ²]
e	Void ratio	[-]
e_0, e_1, e_2, e_3, e_4	Load eccentricity	[L]
E_{avg}	Average of ultimate tensile strength	[M ⁻¹ LT ²]
EI	Bending stiffness	[M ⁻¹ LT ⁴]
e_{max}	Maximum void ratio	[-]
e_{min}	Minimum void ratio	[-]
E_{oed}	Young's Modulus based on the oedometer test	[M ⁻¹ LT ²]
F	Force on the spring foundation	[MLT ²]
f	Frequency	[Hz]
HDPE	High density polyethylene	[-]
g	Acceleration due to earth's gravity	[LT ²]
G_s	Specific gravity	[-]
H	Height of the model soil	[-]
H	Height	[-]
HST95	Silica sand (fraction E sand)	[-]

<i>Symbol</i>	<i>Quantity</i>	<i>Units</i>
Hz	Hertz	[T ⁻¹]
<i>I</i>	Second moment of area	[L ⁴]
<i>k</i>	Relative soil stiffness value	[MLT ²]
<i>L</i>	Length	[L]
LVDTs	linearly varying differential transformers	[-]
<i>m</i>	Mass	[M]
<i>P</i>	Soil pressure per unit pipe length	[M ⁻¹ LT ²]
<i>p</i>	Pipe internal pressure	[M ⁻¹ LT ²]
PSD	Particle size distribution	[-]
PVC	Polyvinyl Chloride	[-]
<i>r</i>	Constant radius	[L]
<i>R_d</i>	Relative density	[ML ⁻³]
<i>R_e</i>	Effective centrifuge radius	[L]
<i>R_t</i>	Top-of-model radius	[L]
<i>t</i>	Thickness	[L]
<i>V_s</i>	Volume of the soil	[L ³]
<i>V_v</i>	Volume of the voids	[L ³]
<i>W</i>	Width	[L]
<i>W_L</i>	Wheel load	[MLT ²]
<i>y_p</i>	Pipe deflection	[L]
<i>z</i>	Soil cover depth	[L]
0deg	at pipe crown	[-]
270deg	at pipe springline	[-]
180deg	at pipe invert	[-]

Greek alphabet

<i>Symbol</i>	<i>Quantity</i>	<i>Units</i>
σ	Stress	[ML ⁻¹ T ⁻²]
ϵ	Strain	[-]
σ_{vp}	Vertical effective stress (prototype)	[ML ⁻¹ T ⁻²]
σ_{vm}	Vertical effective stress (model)	[ML ⁻¹ T ⁻²]
$\Delta\sigma_z$	Change in total vertical stress	[ML ⁻¹ T ⁻²]
φ_{crit}	Effective critical angle of internal friction	[°]
φ_{peak}	Effective peak angle of internal friction	[°]
β, θ	angle	[°]
ρ	Density	[ML ⁻³]
ν	Poisson's ratio	[-]
γ	Soil unit weight	[ML ⁻² T ⁻²]
δ	Deflection	[L]
δ_r	Change in pipe radius	[L]
ω	Angular velocity	[T ⁻¹]
v	velocity	[LT ⁻¹]

Dimensionless parameters

$$\text{Normalized bending moment} \quad \tilde{M} = \frac{M}{\gamma D_p^4}$$

$$\text{Normalized shear force} \quad \tilde{Q} = \frac{Q}{\gamma D_p^3}$$

$$\text{Normalized pressure} \quad \tilde{p} = \frac{p}{\gamma D_p}$$

$$\text{Normalized pipe displacement} \quad \tilde{y}_p = \frac{y_p}{D_p}$$

$$\text{Vertical applied load} \quad \tilde{F} = \frac{F_p}{\gamma D_p^3}$$

$$\text{Normalized pipe length} \quad \tilde{L}_p = \frac{L_p}{D_p}$$

CHAPTER 1

Introduction and Motivation for Research

1.1 Background to Buried Utility Pipes

Utility pipes are very important to our daily lives as they underpin modern society by providing distribution of drinking water and collection of sewage but also extend to energy and communication networks. Water distribution systems are among some of the oldest infrastructure assets with much of the UK network being built during the industrial revolution at the start of the 20th century (Sales et al., 2015a). An acute issue is water scarcity due to availability of water resource, increasing demand and leakage from aging distribution systems (Figure 1-1). For instance, in the UK over 3 billion litres of water is lost through leakage every day (DiscoverWater, 2019), representing up to 22% loss of the potable water from source to the consumers tap in England and Wales (Laspidou, 2014).



Figure 1-1 Image of underground potable water leakage (Water matters UK.2013)

Comparatively, the United States of America estimate approximates 9.8 trillion litres (17%) of all pumped water is lost while this level is about 6 trillion litres of treated drinking water leaked annually in China (China, 2010). While the UK annual leakage rates have declined since 1995, current levels remain unacceptability high (Figure 1-2). This is unsustainable and no longer socially unacceptable. Leakage rates in drinking water distribution pipes world-wide reported and confirm urgent intervention is required , see Figure 1-3 (Laspidou, 2014). Water leakage has serious consequences for our economy as billions of money are wasted in lost electricity generation each year pumping water that is ultimately lose from the system (Cohen, 2012). This has a significant impact on the ability to achieve reduced carbon targets from energy generation.

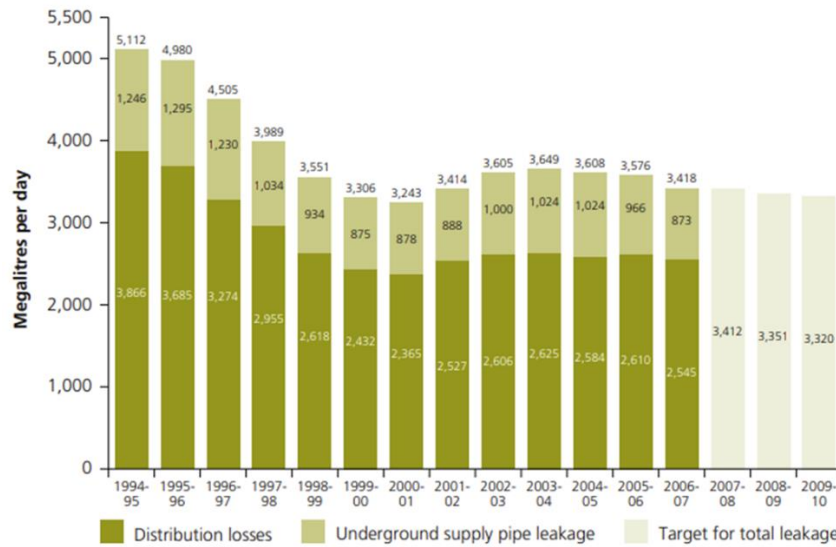


Figure 1-2 Total water leakage in England and Wales (Ofwat.2007)

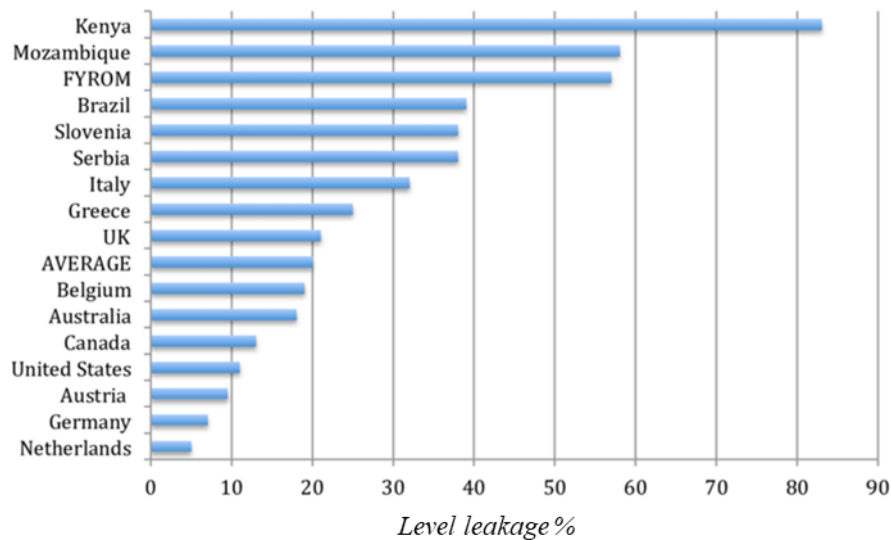


Figure 1-3 Leakage rate in water distribution utilities pipes world-wide. Average based on country-level leakage percentage (Laspidou, 2014)

Buried infrastructure systems operate in harsh environmental conditions and thus are prone to deterioration over their serviceable life. Pipe systems in the UK can be up to 100 years old and are now operating well beyond their planned design life. The rate of network renewal is far below what is required thus it is imperative to better understand the factors that contribute to pipe detrition to mitigate against further failure (Industry, 2014).

Water pipe networks are typically located close to the ground surface at minimum depth of 750 mm and up to a maximum depth of 1350 mm below ground level (BSI,1295) and frequently adjacent to transportation corridors; hence, are susceptible to the influence of external static and dynamic loading from vehicles Smith (1991). Assessment of the effects of surface traffic loading on pipes for an idealised theoretical condition are reasonable well developed and documented in historical literature; for example, Marston (1913), Burns and Richard (1964) Young and Oreilly (1983); with subsequent design codes being established (BSI (1997) and AASHTO (2010)). However, in reality current levels of traffic now exceed historical design limits as road freight has increased in magnitude and intensity (DfT, 2018).

Furthermore, natural variations in ground water and more recently, increasing climate stresses are producing extreme wetting/drying and higher temperature variation within the soil This yields continually evolving complex soil conditions in the vicinity of pipes that undoubtable affect their performance further, yet little is known about these impacts (Nielsen et al. (1972)). In addition to these external factors, variations in internal water supply pressure (transients) due to intermittent service can also be problematic as these increase pipe axial and radial loading. These combined internal and external influences can generate additional stresses in the pipe lining that can ultimately give rise to deterioration of the pipe element itself or the connecting joints (Farshad, 2011).



Figure 1-4 Erosion and void formation around a breached pipe (Water matters UK.2013)

Leakage from pressurised water distribution pipes causes secondary effects including fluidisation of the bed and erosion of the supporting soil materials that can create localised voids around the pipe as seen in Figure 1-4. Such observations were reported by Balkaya et al. (2012) around exhumed pipes during maintenance and replacement works. If a situation develops where the pipe is unsupported, traffic loading and axial thrust forces can generate additional bending stress in the pipe sections and joints. If undetected, this can contribute to premature pipe failure through local buckling or cyclic fatigue (Sales et al., 2015a). Also interesting is that the initial burial conditions of the pipe being laid in a pea-gravel trench is rarely observed around exhumed pipes, this in case of bad bedding area with well graded soil,, suggesting that migration of fines/suffusion processes occur with ground water flow, which may exacerbate the possibility of void formation (Sales et al., 2015a).

The complexities surrounding buried utility pipes and the challenges created by voids in the soil are summarised in Figure 1-5. Little is understood about this condition and pipe behaviour is affected. it is very deffecult to predict how void formed beneath the pipe or any other location this as a result of deffeculty of observing or investigate that for the existing buried pipe system. Thus, if any pipe defect occurs leading to water leakage, this requires excavation work for pipe maintenance resulting in soil collapse and void disappearance. That means void size and shap It remains a hypothesis and only prediction relying on previous studies. Therefore, there is a high motivation to understand the impact of voiding around pipes at a shallow depth and the subsequence impact on pipe performance.

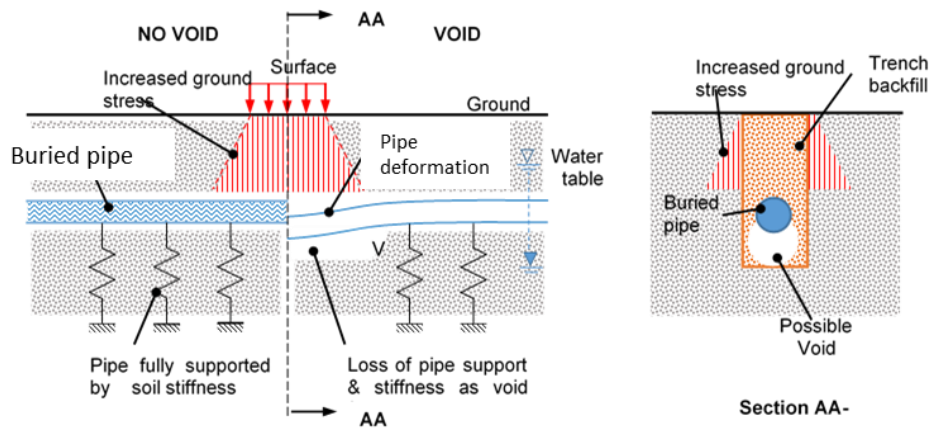


Figure 1-5 Buried pipe infrastructure and impact of support/void formation (Black,2014)

1.2 Research Aim and Objectives

The aim of this thesis is to improve the knowledge on a buried pipe that has a void located beneath it as there is relatively little existing literature relating to the impact of voids on buried pipes. There are even fewer relating to the impact of voids combined with surface traffic loading, so this will also be investigated. Most existing research looks at the effects on the cross-sectional deformation rather than the deflection in the longitudinal direction and ignores the effects of internal water pressure. The focus of this research will be on the effects of the loading on the bending moment of the length of a plastic pipe, high-density polyethylene (HDPE), with a void present beneath it as well as the effects of internal water pressure. An outline of the specific objectives of this thesis is presented below:

1. To explore the understanding of basic modelling effects in centrifuge testing of plastic buried utility pipes (HDPE) in dry sand, and conduct lateral loading (axial load) coupled with long-term cyclic vertical loading experiment to go above and beyond currently available datasets;
2. To develop a suitable experimental apparatus capable of investigating the performance of buried plastic pipes, with and without presence of voids, at representative field stresses, and subject to surface loading;
3. To develop a new apparatus for the first time to be capable of investigating the effect of water pressure in the pipe. The apparatus will provide a design tool simulating the internal water pressure. Thus, investigating the effect of water pressure in the pipe which is subject to surface traffic loading;
4. To evaluate the influence of surface traffic loading (magnitude, orientation, position, monotonic/cyclic) on buried plastic pipes, with and without presence of voids;
5. To evaluate the impact of void size, shape and location on the performance of buried plastic pipe subjected to combined surface loading;
6. To investigate the effect of the road surface in the pipe which is subjected to both surface loading and axial force.

1.3 The novelty of the research

The novel contribution of this research to the field of knowledge is divided into two important parts in term of experimental condition, which allows to have new information and new insight into the soil-structure and actual aspects of pipes buried in the ground; and that can be through a number of mechanisms. Therefore, the overall methodology looks at axially loaded, eccentrically loaded, with and without void, different burial depths, and with and without road surface. These aspects constitute a novel area for investigation.

The first novelty is facing the challenge for how to model and simulate void (unsupported area). In practice the void can occur in the fill material as a result of several processes e.g., washing out of fines through suffusion process and moisture change due to the fluctuation of ground water table, in addition to the soil movement which could affect the pipe joint and cause water leakage from the pipe (that is the worst scenario). The sand in the centrifuge will collapse because of the self-weight stress condition. Therefore, the aim is not to simulate the process of erosion of the void in flight, but rather to observe the effect of the modelled void. In other words, it is not to model the cause but, the effect. Since it is difficult to model a space, the challenge is how to model the area of the void (without soil) or unsupported pipe so as to allow for similar conditions in reality. A subsequent solution was to use a sponge as an alternative space model, on the basic concept that it offers low stiffness with a provision for soil to create that cavity.

The second novelty is related to the difficulties in simulating internal water pressure and understanding the role that hoop stress conditions play on buried plastic pipes. Therefore, it is necessary to reveal the future of such effects on buried pipes by designing a new apparatus to simulate the internal pressure. The novel aspect of this experimental apparatus is its complete uniqueness in that it has ability to apply axial tension or compression forces on the pipe simulating the internal pressure. Nobody else has designed an apparatus with such capabilities. Consequently, this degree of novelty informs new understanding of soil-pipe interaction; with the design being a new piece of apparatus which has unlocked opportunity for deeper understanding in pipe based studies. So, the developed equipment allows for more comprehensive simulation of actual field conditions. The axial tension is generated through pressurising and this allows to capture new datasets which show that under vertical loading (direct or eccentric), the behaviour of the pipe with and/or without axial force that simulate pressurised pipe in the field can be observed.

Conclusively, this piece of research demonstrates key additions to the field of knowledge, by offering novel aspects for consideration when modelling and simulating unsupported portions of soil under buried pipes. In addition, this research addresses the difficulties in simulating internal water pressure and suggests a solution towards understanding the role played by hoop stress conditions.

1.4 The Outline of the Thesis

The research material is presented in this thesis and organized within 7 chapters described as below.

Chapter 1 presents an introduction on the problem of buried pipe, a background of the study and a description of the aim and objectives of the research study.

Chapter 2 reports on recent literature of previous studies related to the performance of buried pipes and current design approaches, focusing on the impacts of external loading and burial conditions.

Chapter 3 introduces the method/concept of centrifuge modelling for a plastic pipe model and an overview of the centrifuge facility at the University of Sheffield.

Chapter 4 provides details of experimental set-up design including; model design, mechanical design and instrumentation and calibration. Results from classification and mechanical properties of the materials are reported.

Chapter 5 presents the results obtained from buried plastic pipe tests subjected to monotonic loading. Pipe deflection and bending observations are reported with respect to a number of variables, compared to several baseline tests, in order to understand their impact on pipe performance.

Chapter 6 presents additional discussion and interpretation of static loading results on Chapter 5

Chapter 7 extends this approach, focusing on cyclic loading conditions and in depth analysis.

Chapter 8 presents discussion and interpretation of cyclic loading results on Chapter 7

Chapter 9 concludes with a summary of the new understanding that has been gained from the study and provides recommendations for future research.

.

CHAPTER 2

Literature Review

2.1 Introduction

The installation of pipes is typically completed through the construction of a trench where the pipe is laid, surrounded by soil backfill and compacted. It is possible that voids can be present within the pipe zone material as a result of poor embedment zone, especially at the haunching area which located between the pipe springline and the bedding. This layer of backfill is necessary for the performance of the pipes. However, owing to its location, the convenient placement of backfill in this layer is usually overlooked. Therefore, care must be considered taken to place and compact the backfill in the haunching area (McGrath et al., 1990). Pipe trenches act as linear drains and water can easily pass through the granular backfill material. If this material is not graded and compacted properly smaller particles can be eroded, weakening the fill and increasing the possibility of internal collapse causing voids (Brachman and Krushelnitzky, 2005). Furthermore, leakages of high pressure water mains at segmented pipe joints or longitudinal cracks in pipes can wash out and erode the neighbouring soil to form a void. Indeed, voids are frequently reported in operator inspection logs when repairing damaged pipes (Gumbel et al., 2003). However, it is not yet known what role they play in the mechanical response of a buried pipe and the potential detrimental impact to their long term serviceability. Voids in soil can cause increased bending of buried pipes because of a loss of support which can contribute to structural failure of a joint or the pipe body due to large deflections and stress concentrations. Jones (1984) stated that flowing water through pipe cracks may induce ground loss resulting in less soil support due to soil density loss or void formation surrounding the pipe. Currently design guidance in the UK (BSI,2020), and other regions (AASHTO, 2010) do not consider the possibility of voiding in the ground and the influence on the pipe. The research conducted in this thesis is aimed to explore the mechanical response of a pipe that is effected by a void in the surrounding area as this is currently an area where there is little research.

Previous research has observed that an increase in vehicle axle loading also has a detrimental effect of increased bending strains (Taylor et al., 1984). This is especially important considering vehicle surveys have confirmed that the current legal drive-axle load limit of 10.5 tonnes for a loaded vehicle is often exceeded (Glover and Shane, 1983). The impact of a localised void on pipe bending could be further exacerbated by traffic loading. A marked increase in pipe strain is observed as vehicle speed decreases below 16 km/h (Pocock et al., 1980), which suggests that pipes will experience greatest strains when buried beneath heavy vehicle parking areas. Vehicles with a twin axle impart reduced bending strains on underground pipes, due to the superposition from each individual axle (Taylor et al., 1984).

In practice, the cyclic nature of traffic loads tends to present a significant problem to shallow buried pipes alone. Cyclic load amplitude causes the maximum pipe deflection. pipe under repeated load with low amplitude may have the same deflection value of the pipe under a repeated load with high amplitude, provided that the cycles of the load continue for a long period (Hosseini and Tafreshi, 2000). The strain caused by cyclic loading in comparison to other types of loading was investigated by Carder et. al (1984), and they concluded that this type of loading was likely to play a major role in contributing to pipe failure. Therefore, this type of loading will be used in the following research in this thesis when looking at the effects of voids (size/location) on buried utility pipes.

2.2 Background

The pipeline network that supplies drinking water, and other services, plays a key role in modern societies. Generally, these buried pipes laid beneath the road surface are subject to a range of different stresses, whether external loads due to traffic load, or internal loads due to pipe internal water pressure(AASHTO, 2010). A high percentage of pipes have been buried for a considerable period and thus their precise condition is largely unknown; but it is highly probable that they will have deteriorated during their serviceable life as failure rate confirm. Therefore even without changes in operational conditions, long term weakening of the pipe element leads to an increase in the stresses experienced by pipes (Rajah et al., 2014).

An understanding of the interaction between soil and the pipe interface is essential in characterising and evaluating performance. Therefore, pipeline designers rely on different guidelines like the AWWA standard (American Water Works Association Manual M23, 2002), WIS UK standard(Water, 2000) or pipe design manual. These guidance documents offer simplifying assumptions, hypotheses, theories and philosophies of design, in some cases with uncertainty due to the unknown soil-pipe interaction behaviour. This leads to contradictory instructions on the selection of soil parameters for use in the soil-structure interface analysis of various pipe materials, which makes it exceedingly difficult to develop design practises. Regardless of the contact between the soil and the pipe, the nature of a buried pipe is substantially different from an idealised case (Rajah et al., 2014). Therefore, it is difficult to evaluate the actual magnitude and distribution of the soil pressure around the pipe accurately as a result of the external load that acts on a buried pipe. This relies on several factors, including pipe burial depth, pipe stiffness, soil mechanical properties and the depth of the water table. For real situations, the pipe and soil are unbounded (the soil only has a contact on the outward surface of the pipe) either full slippage or non-slippage and that depends on the type of pipe material (Ng, 1994). On the other hand, the parameters of the soil utilised to evaluate soil-structure interaction are associated with the method of analysis adopted, for example, there are several modelling approaches related to soil-structure interactions for buried pipes for instance Finite Element modelling Winkler Spring and Subgrade Reaction theory (Bayton, 2020).

2.2.1 Experimental Studies

2.2.1.1 Effect of burial depth

Early investigations carried out at Iowa State University in the United States and the Building Research Station and Transport and Road Research Laboratory in the United Kingdom focused on the performance of pipes with circular cross-section under plane strain conditions created by uniform loading. The work was concentrated on the pipe diameter deflection change into soil-pipe interaction. Thus, the Iowa formula developed at the university of Iowa state by Spangler for estimating vertical deflection of flexible pipe (Spangler, 1956). The method of the design is to determine the ring deflection of the pipe (Ng, 1994). However, in case of plastic pipe, the passive lateral soil resistance upward deflections of the pipe spring lines are taken into account. Rakitin and Xu (2014) conducted centrifuge testing using a hollow aluminium cylinder to simulate a typical reinforced concrete sewer. The study was done to examine the behaviour of a 1400mm diameter reinforced concrete pipe under varying vehicle loading with a maximum load 850kN. The consequence of soil depth between 1-4m was also studied and no rigid or flexible pavement structure was simulated. The results obtained from the centrifuge found to be in reasonable agreement with those which were obtained from full-scale tests. Strong correlation was observed as presented in Figure 2-1 and therefore confirmed the suitability of centrifuge modelling for pipe-interaction studies.

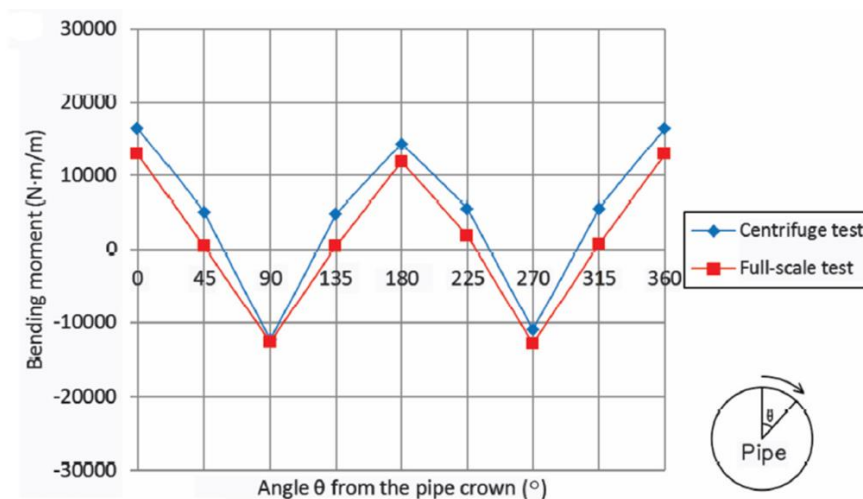


Figure 2-1 Comparison of buried sewer pipe bending moment for full scale and model studies
(Rakitin and Xu, 2014)

Srivastava et al. (2012) studied the load-settlement response of a buried flexible pipe due to surface loading. The test was completed using a model plate load of 150mm, which simulate a prototype surface footing of 1.50m test on a scaled 110mm diameter PVC plastic pipe buried in sand which simulates a prototype pipe of 0.42m diameter. Experiments were conducted in various relative densities (R_D), first was targeted for high relative density and second is targeted for low relative density, $R_D=88\%$ and $R_D=55\%$ respectively. Different scenarios were carried out to understand the combined behaviour of pipe-soil system. The first test scenario was conducted with a footing placed over low relative density of 50% presence of with and without presence of the plastic pipe at two different burial depths (1B and 0.5B; where B is the footing width). The second test scenario was performed similarly to the first one except that the footing placed over very dense sand with high relative density of 80%. Srivastava et al. (2012), stated observations on the ultimate bearing capacity of buried pipe-systems. The bearing capacity of the soil-pipe depends on two important factors; pipe stiffness and soil density. Therefore, when a pipe is buried in the dense sand the overall capacity of the system reduced, whereas in the case of loose sand it showed the opposite response. This might be due to the fact that the stiffness of the buried pipe-soil system increased by reason of the introduction of a stiffer material or less stiff material. This also depends on the sand relative density and pipe stiffness. The results showed the same observations of the bearing capacity trend for the test conducted for both relative density and pipe buried depths of 1B and 0.5B, except this test was performed once with the existence of the buried flexible pipe and others without the existence of the buried flexible pipe.

While overall pipe deflection is important, the connecting joints are extremely important. Balkaya and Moore (2009) suggested defects at the pipe joints are also commonly responsible for failure. Furthermore, additional complexities of infiltration and exfiltration are created that could lead to contamination of the pipe's water supply (Balkaya and Moore, 2009), as well as erosion of the soil surrounding the pipe, which can ultimately produce pipe failure as the joints considered to be the weakest points between the pipe segments. Rahman and Bird (2006) suggested a spigot and bell system offers high resistance to exfiltration. This "Rieber" system is commonly used to join PVC pipes in North America and so both Balkaya and Moore (2009) and Rahman and Bird (2006) focused on PVC pipes, which limits the applicability of the findings to plastic pipes. However, spigot and bell joints are used commonly in the UK for most pipe materials, including cast iron. Moore et al. (2012) presented the effect of longitudinal bending on joints in rigid and flexible culverts through experimental and computational studies. The study compares joints that allow rotation, for instance bell and spigot joints, and joints that transfer longitudinal bending moments through pipes, like butt-welded joints. Tests were carried out by Moore et al. (2012) to investigate the influence of longitudinal bending moment on both reinforced concrete and flexible pipe. The authors provide evidence to show that when a load is applied directly over a pipe joint the deformations are almost symmetrical about the joint. Laboratory experiments were used to assess the behaviour of jointed pipeline system for four different pipe diameters, two different burial depths, and response to external vertical loading with different load

eccentricity. So, thus it was found that when a load is applied offset from a joint, the deformations are almost a reflected image of those experienced if the load is offset on the opposite side of the joint. The paper's findings enabled further studies to be simplified by assuming symmetry in deformations. The cyclic loading experiments clearly demonstrated an unload-reload path in soil behaviour, reinforcing that the sand backfill could be assumed to be elastic.

Carder et al. (1981) produced an analytical model based on experimental studies to evaluate the bending moments in poorly bedded sections of pipeline subjected to traffic loading. It was found that bending moments increased if the subgrade is weaker as a result of non-uniform backfill during pipe installation. The behaviour of a cast iron pipe buried at a shallow depth under the influence of static and rolling wheel loads was investigated also by Pocock et al. (1980). The strain developed on the pipe was found to increase linearly with the axle load, as expected for a static load. Furthermore, it was observed that the strains decreased when tested with faster vehicle speed over the longitudinal direction of the pipe. The argument could be made that this validates the use of cyclic loading in centrifuge testing by applying repeated load directly to the surface, where the ageing of soil under a load can be investigated in the centrifuge to longer durations due to the capability of modelling extended periods of time due to scaling laws. This is a useful assumption to make in clay soils especially like the study used in Pocock et al. (1980), whereas sand tends to have an instant deformation response. However, ageing, particle breakage, and grain re-orientation in sand can be significant (Peng et al., 2021).

Pocock et al. (1980) observed nearly double the amount of strain on the pipes with poorly bedded pipes under both static and rolling wheel loads, which further supports the findings of Young and O'Reilly (1983). It has been stated that the influence of constructed pavement on which the traffic load was applied was not considered, therefore it may have an impact on the results. However, it is reasonable to assume that this would not significantly change the trend of poorly bedded pipes developing much higher strains. The results of the tests carried out by Moore et al. (2012) underpin the findings of Pocock et al. (1980), and allow for better understanding of the data presented. The experiment was performed at prototype scale, meaning there were fewer opportunities for discrepancies between the in situ condition and the experiment through scaling and modelling. The paper concludes that the largest strain and moment were experienced directly below the vehicle axle and the value varied linearly with load. The loading explores several variables, vehicle speed, twin or single wheel, adjacent axles and soil bedding type; noting the maximum axle load used was 10 tonnes. The research offers insight study into the effects of vehicle loading on cast iron pipes, noting, however, that increased values would be observed due to the higher maximum axle load of 12 tonnes in the UK.

Pocock et al. (1980) was further validated when Rakitin and Xu (2013) took advantage of centrifuge modelling to simulate heavy vehicular loading, axle load of 9 tonnes, on large 1.4m diameter underground concrete pipes in a 50g beam centrifuge facility in Tsinghua University. The centrifuge allowed for a test at 20 times normal gravity, meaning the test geometry was 20 times smaller than

prototype. This enabled a large prototype area to be investigated whilst the model was still possible to construct. Position and magnitude of the applied traffic loads were considered with bending moment observations made with respect to the soil cover depth. The concrete pipes were modelled using aluminium and so the Young's Modulus, E , differed between prototype and model scales. Adjusting the second moment of area (I) of the pipe's cross section preserved the bending stiffness (EI) of the model pipe to scale. Details analysis of scaling bending stiffness is reported in Al-Defae and Knappett (2014) that investigated prototype behaviour of concrete piles using aluminium model surrogates.

An experiment study by Cao et al. (2016) suggests that the deeper a pipe is buried, the less deformation the road surface will experience. This conclusion is based on the behaviour of steel reinforced HDPE pipes and assumes the bending of the pipe itself to be negligible, focusing only on the deformation of soil during loading. This assumption was validated by McGrath (2005), which used prototype scale testing to measure the displacement and bending resistance of large diameter corrugated HDPE pipes under real highway loading with shallow depth. The study found the thermoplastic pipe deflection was relatively small compared to the allowable limit. Thermoplastic pipes are considered flexible and this assumption can be considered applicable to materials with a higher bending stiffness, like rigid cast iron. McGrath's prototype experiment study lasted 3.5 years, which makes it significant in evaluating long-term pipe behaviour and repetitive vehicular loads. McGrath (2005) concludes that the minimum cover depth to be used should be 0.5 times the diameter of the pipe, with pavement cracking being the governing design factor.

2.2.1.2 Effect of cyclic loading

A limitation of the aforementioned studies is that they do not consider the effects of cyclic loading and focussed solely on static loading. However, many studies consider only the static condition and then apply a cyclic degradation factor for these cases. Rakitin and Xu (2013) found similar results to those experiments conducted at prototype scale, however it could be said that they are less conservative than other studies. This divergence could be explained by the lack of cyclic loading, as other studies observed more deformation with each cycle as the soil fatigued. This was only observed with high cyclic load in contrast to when the number of cycles was low. The study suggests that pipes at deeper burial depths experience more initial stress, most likely because of higher vertical effective stress from the soil's self-weight, but are affected less by vehicular loading. This conforms to the widely accepted rule of thumb that a load spreads as stress through soil layers at a 2:1 ratio.

Hosseini and Tafreshi (2000) conducted experiments simulating and monitoring flexible pipes subjected to cyclic loading in which they measured radial deflections. The model was capable monitoring and simulating flexible pipes under various scenarios. The burial depth, load position and soil density could be change and controlled. The repeated loads with different amplitude as well as the static loads could be applied to the soil surface. The main factors effecting the buried pipe behaviour were studied. The

authors concluded that soil-pipe interaction was most affected by embedment depth and soil density. From a depth of 1-1.5 diameter of the pipe (D_p), they noticed a sharp decrease in maximum pipe deflection. Although they conducted static loading experiments, Rakitin and Xu (2013) also observed the most significant changes in the bending moment induced in the pipe from $0.5D_p$ - $2D_p$ depth of burial. The bending moment imparted on the pipe more than doubled due to the sensitivity of soil weight in this range, but more interestingly, the bending moment imparted on the pipe due to axle load decreased by over 5 times due to increased burial depth. This suggests that the preventative measure of burying pipes deeper to reduce their deflection works by mitigating the bending moment and thus deflection imparted on the pipe due to axle loading, especially considering axle load plays a major role in contributing to pipe deflection.

2.2.1.3 Effect of eccentric load

Hosseini and Tafreshi (2000) found that the effect of load eccentricity is reduced by over 55% when the load is applied a distance $2D_p$ from the centreline of the pipe. Any distance greater than $2.5D_p$ had a negligible effect. One of the major findings of their experiments was that the compaction of soil surrounding the buried pipe is important in reducing the probability of damage to the pipe. If left uncompacted, the pipe could be seriously damaged when load is applied. Carder et al. (1984) found that cyclical traffic loading had negligible effect on the residual strains of a buried pipe when it was well-bedded, compared to a more than twofold increase in strain in a poorly-bedded soil. Also, later on Mohamed and Moghadas (2002) evaluated the aspect of load position on full scale tests of flexible pipes buried at 1 times the pipe diameter. They reported significant reductions in pipe deformation and ovalisation when the load was relocated from the crown of the pipe to $1D_p$ and $2D_p$ as shown in Figure 2-2.

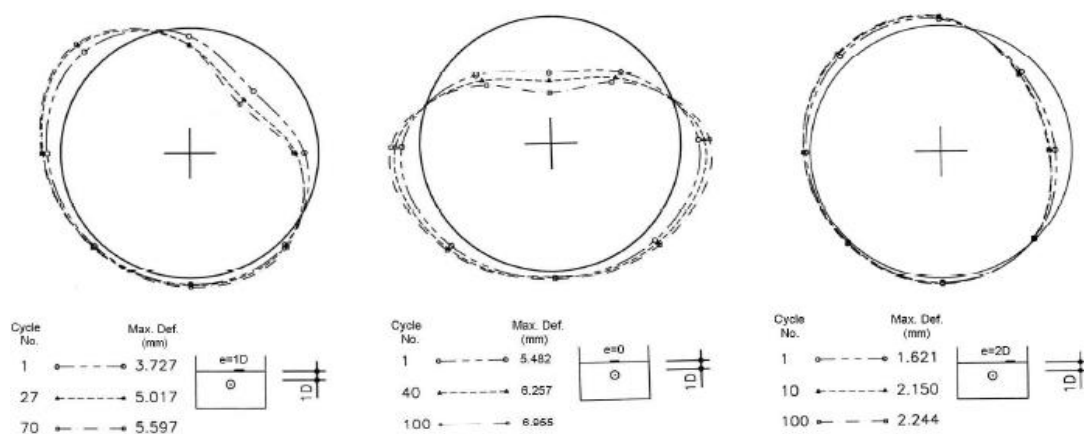


Figure 2-2 Impact of load eccentricity on pipe deformation. Hosseini and Tafreshi (2000)

2.2.1.4 Effect of void size and location

Peter et al. (2018) produced a paper which investigated the impact of voids in concrete pipe (reinforced concrete) subjected to external loading. The experiment was conducted in full-scale on a pipe with internal diameter of 900mm with a modelled void neighbouring the buried pipe. This experiment was performed to record the change in bending moment in the pipe circumference with change in void size, at 90mm pipe depth. Tests were repeated after using different void size by using low strength material (grout). Test results for both void erosion and grout material shows different pipe behaviours. An increase of 70% in the bending moment at the pipe invert in presence of a small void was found, compared with the case of non-supported area of the pipe (no void); whereas an 26% increase in bending moment was observed when a large void was presented. In contrast, grouting the large void and small void showed an improvement in pipe bending moment response. Nevertheless, it was seen that the bending moment at the pipe invert increased by 50% and 22% for large void and small void, respectively compared with intact soil. Also it was seen that soil collapses at large voids and increases of contact angle led to a change in the failure mode.

More recently Sales et al. (2015b) carried out a series of centrifuge model tests to evaluate the influence of void size on a prototype flexible pipe of 0.3m diameter. Four void geometries were considered ranging from 2 to 5 times the pipe diameter, simulating unsupported conditions that were benchmarked to the reference case of no void. The results of the investigation show that the magnitude of the pipe deflection in dry sand increased significantly in the presence of a void and that the magnitude of deflection increased with void size. This is presented in Figure 2-3 (a and b). Also presented was the soil displacement behaviour from image analysis whereby it was observed that the level of soil displacement from a surface loading plate increased with void size which served to increase the extent of loading on the pipe. Also confirmed was the suitable methodology implemented of using a sponge to simulate a sub-surface region of reduced stiffness mimicking a prototype void. The bending moments of the pipe were evaluated using displacements recorded from images and were found to be both sagging and hogging which corresponded to the points of inflection from the pipe deflection response. The relevant deflection of the pipe was found to exceed the allowable deflection criteria (5% of the pipe diameter) for void sizes larger than 3 times the pipe diameter which resulted in large sagging and hogging moments in the pipe at the point of inflection. This study served to provide valuable preliminary data and insight of the behaviour of flexible utility pipes in the presence of a void subjected to surface loading.

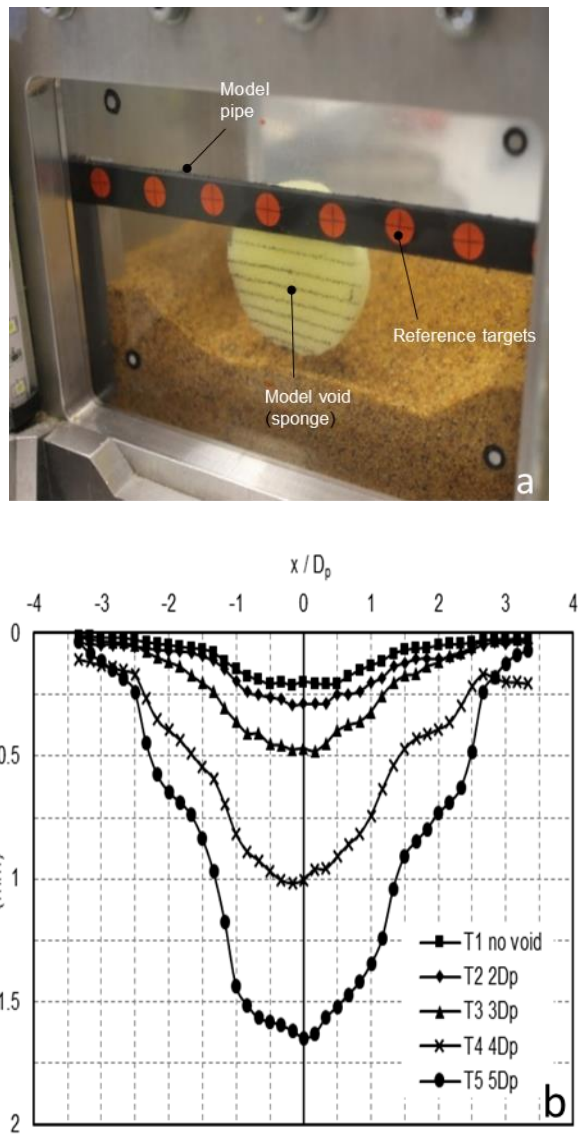


Figure 2-3 (a) Centrifuge model tests of voids and (b) pipe deflection with increasing void size.

Sales et al. (2015a)

2.2.1.5 Effect of pipe stiffness

The comparison between the performance of flexible and rigid pipes has been widely explored in literature. Fernando (1992) investigated and compared the structural properties of PVC and HDPE pipes under external loads with deep burial pipe depth to investigate the pipe behaviour in such conditions. The use of different backfill materials was aimed to investigate the comparison between design methods used at the time. The results of the tests obtained were then used to study the failure mechanisms of the pipes in their respective simulated environments. These tests were overall successful in producing a reliable set of data that allowed the two different types of pipes - flexible and rigid - to be compared and failure mechanisms to be identified. Nevertheless, the test condition ignored the effect of wheel loading on the pipe, which could be added on in future research in the field by simple modifications to the loading platform.

Arockiasamy et al. (2006) performed full scale field test on flexible pipes (HDPE, PVC and metal large diameter) subjected to external live load with consideration of soil cover. The study investigated the soil-pipe responses under the live load and the effect of cyclic loading. The result showed an increase in pipe deflection when additional soil covers of 1.52m were introduced. The soil pressure decreased from 2 to 3 times at the pipe crown of the large pipe diameter compared to smaller pipes. The literature suggests that the amount of soil depth covering the pipe is a crucial factor when analysing the pipe-soil interaction behaviour. Cao et al. (2016) conducted a laboratory test of an unpaved road with a buried steel-reinforced high-density polyethylene (SRHDPE) pipe. The pipe was buried in a compacted sand trench covered by aggregate. Tests were carried out to investigate the impact of the shallowly-buried SRHDPE pipe under repeated traffic loading. The author came to the conclusion that the bigger the soil cover depth to the pipe, the less the road surface deformation would be. However, it is worth noting that Cao et al. (2016) only looked at the deformation of the soil and its behaviour under loading, therefore not taking into account the bending of the SRHDPE pipe itself.

The previous studies into soil-pipe interaction investigate a broad range of factors using both prototype and centrifuge models, but as buried utility pipe behaviour is such a complex issue, more research is still necessary to further understand the subject. There have been many studies conducted that investigate the effect of lateral displacement on pipes buried in sand – both small and large scale. Audibert and Nyman (1977) conducted one of the earlier studies into soil-pipe interaction using a small-scale model in which soil behaviour was analysed when pipes displaced laterally. Audibert and Nyman (1977) presents an analytical method to determine the load-displacement curve for a pipe with diameter of any size at an embedded depth of any size. This dimensionless load displacement relation corroborated a previous relationship suggested by Das and Seeley (1975) and was reported again by Trautmann (1983). The result of the laboratory testing presents the complex soil interaction and associated failure mechanisms. Thus, an analytical method was presented to explore the load-displacement curve for any size pipe buried at any given depth. A moderate size in-situ test was

performed, which confirmed that the results of the laboratory model tests could be successfully applied to in-situ conditions.

Hsu (1993) conducted a large-scale experiment consisting of 120 tests into the effect that sand density, pipe diameter, burial depth had on lateral soil restraint. The study found that the generalized maximum force coefficients increase with depth of burial. It was also found that the same hyperbolic equation could represent the force displacement relationship of soil-pipe interaction, as mentioned above. Hsu (1993) also found that scaling effects on the soil restraints were very minor when considering pipe diameters up to 304.8 mm. Hsu et al. (2001) and Hsu et al. (2006) investigated the soil restraint to oblique movement of buried pipes in both loose and dense sand, respectively. Similar conclusions are made to the previous paper in 1993, with three theoretical models predicting transverse soil restraints to lateral movement of buried pipes. Scaling effects are deemed minor up to a pipe diameter of 304.8 mm. All three papers contain dimensionless force/displacement graphs, which could be used to compare data gathered in this experiment. Several other large-scale tests into pipe-soil interactions under various types of loading (lateral, transverse, axial) have been carried out, all of which have come to similar conclusions (Paulin et al., 1995, Konuk et al., 1999).

None of the papers above have investigated the effects of a void located in the material around the pipe, apart from one that looked at the cross-section of the pipe in 2D and they didn't take a direct measure, rather, they used PIV. Arockiasamy et al. (2006) stated that further studies may necessary to examine the effect of the cyclic loading in small HDPE pipe diameters with shallower depth. Therefore, it can be seen that this is an area that has previously been unexplored, showing the state of the art of this thesis.

2.2.2 Numerical Studies

2.2.2.1 Effect of void size and location

Significant enhancements in computational power and software technologies have helped to improve numerical modelling techniques. Finite element programmes can be used to analyse non-linear soil behaviour, soil-structure interface behaviour, and any complex systems (Madabhushi, 2017). A critical choice for the modeller is whether to implement a two-dimensional (2D) plane strain model or full three-dimensional (3D) model. It is common that the use of simplified 2D analysis is preferred in the majority of cases owing to computational efficiency (Ariyaratne et al., 2013). Moore (1988) demonstrated the success of using 2D plane strain half space model investigation to investigate flexible pipe buckling due to varying pipe cover depth in order to take advantage of the pipe symmetry. Conversely, Lee et al. (2014) suggested that a simplified 2D analysis for examining pipe lateral buckling would be unsuitable highlighting the need for care in modelling approach.

Numerical study has been performed by Chapman et al. (2016) to examine the effect of the soil pressure on a rigid pipe (concrete pipe with diameter 760mm) that experienced vertical repetitive loading

considering poor backfilling at the haunch area of the pipe. Thus, soil pressure rotated on the pipe as a result of traffic loading. The numerical 3D model was based on the Duncan-Chang hyperbolic constitutive model to represent the material of the utilized soil while a linear elastic model was considered to simulate pipe behaviour. In order to simulate the unsupported area around the haunch, the soil element was removed to mimic the worst scenario of the unsupported pipe. It was found that the maximum soil pressure significantly increased once the soil element was removed (poor haunch support). This indicates huge implications on the design of concrete pipes. The outcome of the study showed that maximum soil pressure on the pipe crown coupled with external vertical loading reduced non-linearly with a 12 % increase in pipe depth. However, it was seen that poorly supported soil at the haunch does not remarkably affect soil pressure at the pipe crown. In contrast, maximum soil pressure significantly increases at the pipe invert as a result of both soil weight and external vertical loading by 210% (see Figure 2-4).

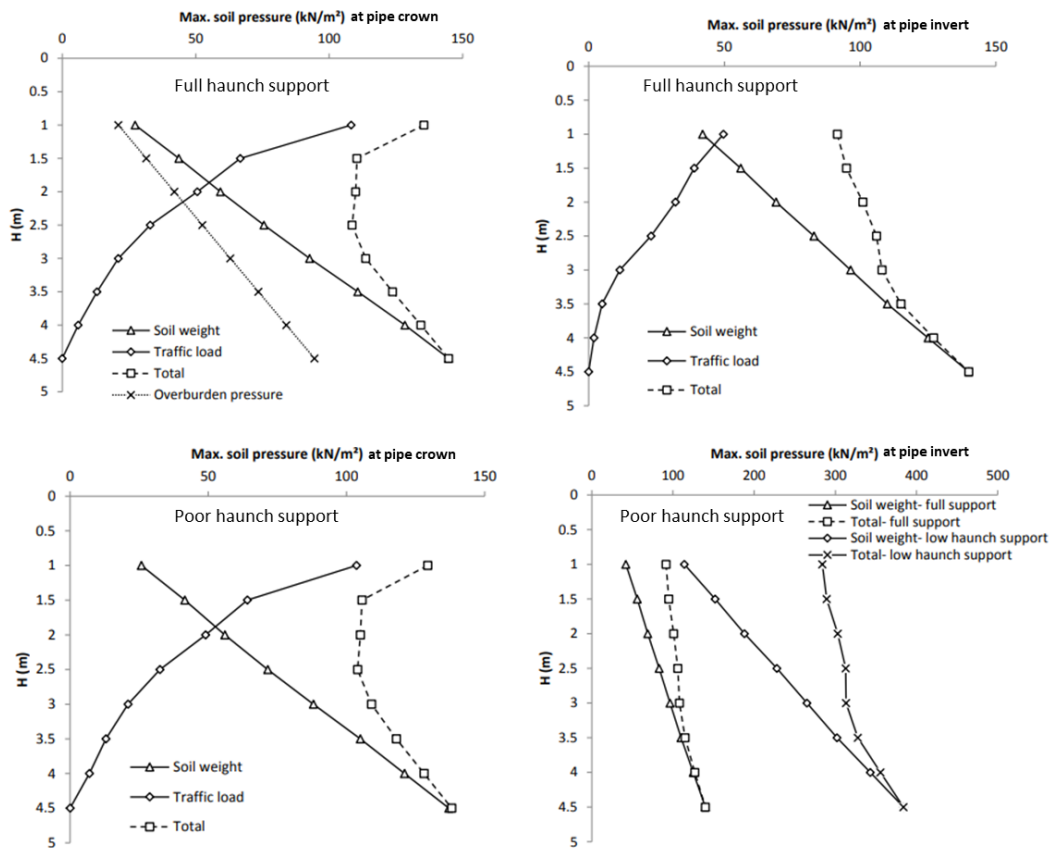
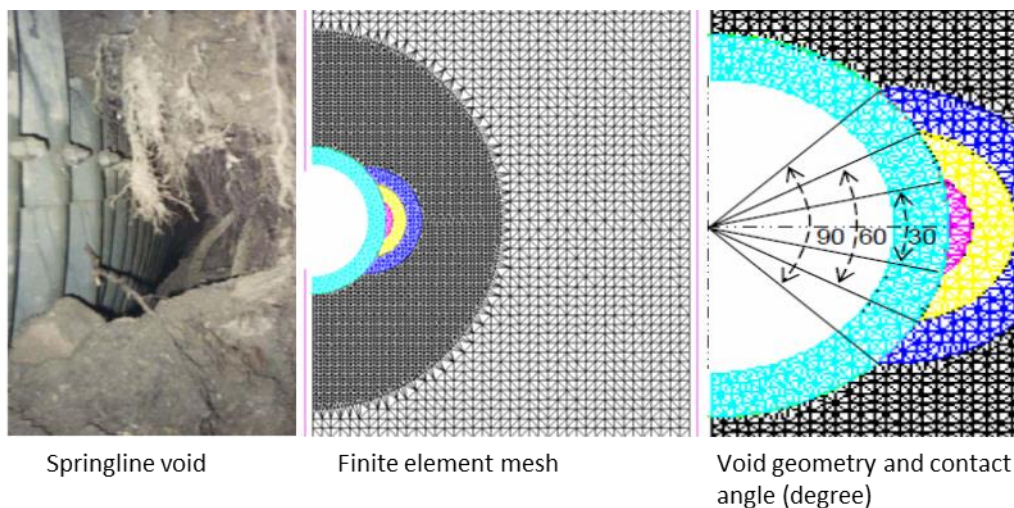


Figure 2-4 Maximum soil pressure Chapman et al. (2016)

Several numerical studies into pipe performance have been conducted by Tan and Moore (2007) to investigate the influence of backfill erosion on buried rigid pipes. The influence of soil voids on the stability of buried rigid pipes is investigated, considering the effects of void size, void location and void shape. A number of simplified void geometries are defined, and their influence on bending moments in the rigid pipe is numerically investigated through finite element analysis. Elastic analysis indicates that the bending moments from expanding voids at the springline will increase slowly, accelerating once the void spans a 45° arc, approximately doubling at 90° , and tripling if the loosened backfill is modelled for shear failure. This preliminary study suggests that the growth of erosion voids should be stopped before they reach 45° , but validation through physical testing is necessary. Elastic and elastic-plastic finite element analyses is utilised to examine the rigid pipe deformation with different thicknesses. Figure 2-5 shows the work from this study established that larger void sizes increased bending moments in the pipe considerably and observed a critical void size beyond which considerable levels of increased stress occurred. A key aspect noted by the authors was that it was acknowledged that “all results presented are theoretical in nature, and physical testing is needed to evaluate the performance of these calculations.”



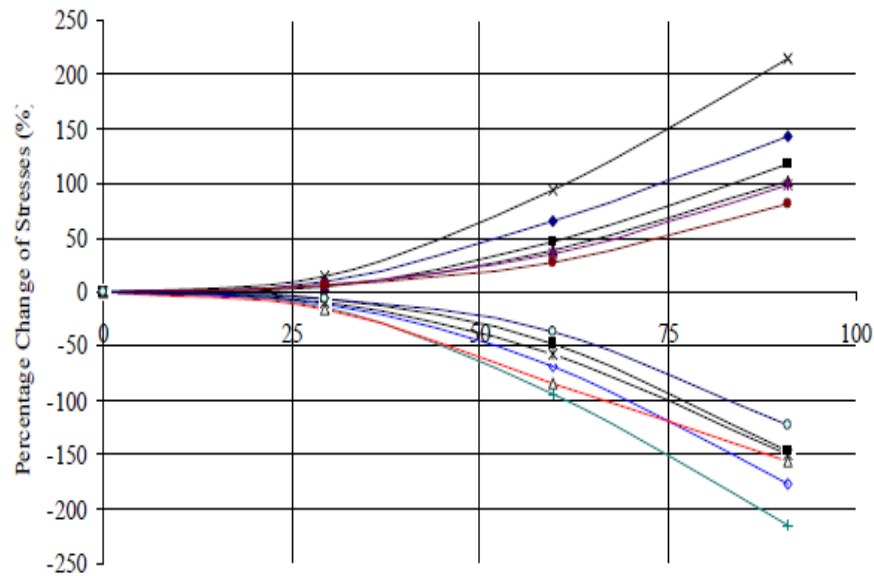


Figure 2-5 Finite element analysis for rigid sewers considering erosion voids and Increase in circumferential stresses at crown due to erosion voids (Tan and Moore, 2007)

There has been much work conducted by Alzabeebee et al. (2018), however perhaps most noticeable is their study of pipe-soil interactions in concrete pipes. This study was conducted in order to assess the effect of the soil constitutive model on the seismic response of buried concrete pipes. The study used the finite element method (Plaxis 2D) to model the problem by using the linear elastic model, elasto-plastic Mohr-Coulomb model, stiffening soil model, and stiffening soil model with small strain stiffness. Both good and poor conditions of installation were taken into account in the analyses (see Figure 2-6). Dynamic seismic load was applied in order to have insight into the effect of the range of earthquakes applied to the model. It was found that a bending moment developed at the circumference of the pipe due to monotonic and seismic conditions when pipe burial was at 2 metre depth. Therefore, all employed models in the present study provide a similar trend of bending moment for pipe circumference with respect of both cases, good and poor installation conditions. Figure 2-7 shows the comparison between linear elastic model, elasto-plastic Mohr-Coulomb model, stiffening soil model, and stiffening soil model with small strain stiffness. Whereby, the both stiffening soil model provide higher bending moment compared to the linear-elastic and Mohr-coulomb model in both conditions static and seismic shaking. Thus, small strain stiffness and degradation of the stiffness over a small range does not have significant effect on the seismic response of a buried rigid pipe that is exposed to soil self-weight.

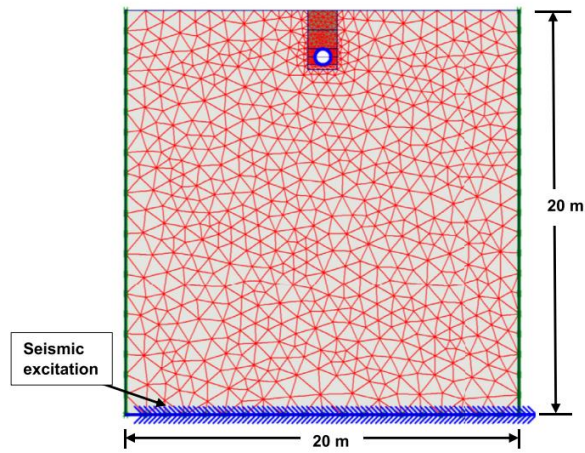


Figure 2-6 Plaxis mesh discretization of the buried pipe subjected to earthquake shake
Alzabeebe et al. (2018)

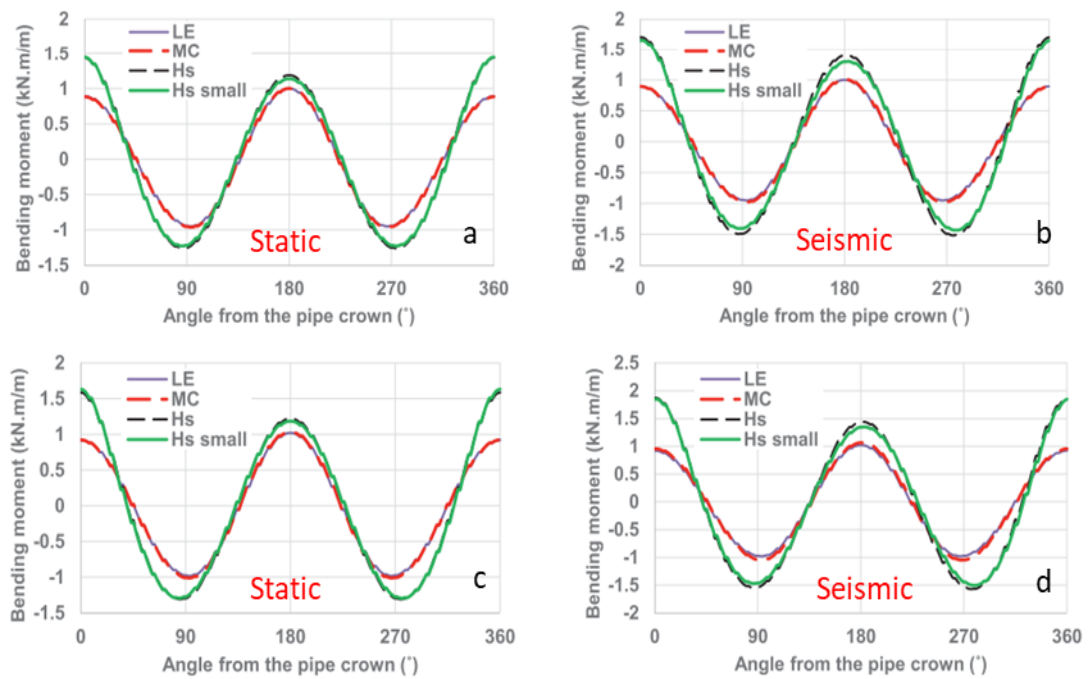


Figure 2-7 Soil constitutive model effect on pipe bending moment: a and b for good installation condition, c and d for poor installation condition

Balkaya et al. (2012) utilised the software ABAQUS to investigate change in stresses and deformations as a function of void shape under the pipe located at the invert and to determine the effect of bedding material on pipe response. Key aspects of the study included the analyses of soil burial conditions whereby medium-dense sand and loose silty sand were considered. They found that higher vertical displacement occurred on the pipe buried in loose silty sand compared to the pipe buried in medium-dense sand, indicating that stiffness of the support material could be important to minimise local stress concentrations in the soil. Also discussed was the importance of limiting pipe deflection criteria and it was commented that the current AASHTO guidance for limiting pipe deflection of 5% of the pipe diameter for flexible pipes was often breached when a void was present (Katona and McGrath, 2007). This contributes to high internal stresses occurring in the pipe at the point of inflection which generated local failure. However, it was also noted that the authors did not simulate a pavement structure in the model and thus the applied surface loading would have overestimated the stresses acting on the pipe that would cause higher localised stress concentrations in the presence of voids. This is true of many pipe-soil studies, numerical or experimental, whereby loads are usually directly applied to the soil surface without typical road surface stiffness being correctly modelled.

More recently there have been studies surrounding tunnel-pipe interaction (Klar et al., 2005, Vorster et al., 2005) that have sought to assess the impact of the underground construction processes on buried infrastructure owing to subsidence. Tunnelling generates sub-surface disturbance and thus where a tunnel intersects a buried pipe, a loss of support may occur. This is an interesting juxtaposition for the proposed work and has demonstrated that loss of soil support results in increased deflection and bending moments in the pipe.

2.2.2.2 Effect of cyclic loading

O'Reilly et al. (1989) undertook numerical analysis of tested rigid sewer pipes using CCTV surveying to investigate the structure of the damaged pipe. Damage was found in marginally less than 5.6% cent of the total length surveyed with large displaced and open joints being found in some 0.8%. In addition to that, the increases in cyclic load, which represent higher traffic flow, appear to be related to slight increases in structural defect rates on minor and major roads compared to other highways. Nevertheless, the defect rate was discovered to be smaller in less-used roads, suggesting that this was due to better road pavements and potentially higher care in design and construction at such sites. The outcome of this study partly endorsed the early experiment studied by Lester and Farrar (1979), who reported a higher occurrence of cracked and fractured sewers on primary highways compared to principal and non-principal roads. Approximately 5 times more fractured and cracked pipes were observed and 30 times as many broken pipes. Longitudinally broken pipes were the most prevalent type of harm, happening most often at the springline (3-9 o'clock), and at the crown (12 o'clock) position. No cracks were noted at the invert (6 o'clock), as flow or debris generally obscured the pipe invert. It was noticed that over 90% of the longitudinal cracks occurred along the pipe length and often occurred as multiple cracks.

Likewise, 90% of the circumferential cracks took place adjacent to the pipe joints. Most of the multiple cracks seemed to have an angle of more than 240° around the circumference of the pipe and the majority of the circumferential cracks were less than 180° . It was observed that the majority of the cracks around the pipe happened in the upper quadrant as a result of the inspection of the lower part in the pipe obscured again by flow or debris. It was also reported that the road type and the inverted depth have a direct effect on the pipeline. Therefore, the type of the road was divided into minor roads and major roads for the analysis purpose that shows that type of road and depth have a major influence on the proportion of longitudinally damaged pipes (i.e. pipes cracked fractured or broken longitudinally).

Clayton et al. (2010) provided the study on how stresses developed in cast-iron pipe by shrink-swell action of clay using finite element analysis through investigation into the measured deflections. Test was conducted on buried water pipe and, over a period of two years, vertical and horizontal deflection were measured a long two plastic pipe which was buried in London Clay. It was calculated that the stresses at mid-point of the pipe were low for flexible pipes. This could be due to the flexible pipe being able to deflect and therefore reducing the remaining stresses on the pipe. The observation implies that higher local stress is applied directly onto the pipe when the soil surrounding the pipe is weaker, which complements the findings of Srivastava et al. (2012).

2.2.2.3 Effect of lateral load

Daiyan et al. (2010) conducted a numerical investigation of 3D continuum finite element model using ABAQUS on the behaviour of buried pipes under axial-lateral soil interaction for buried pipelines. Three-dimensional model developed was then calibrated against centrifuge tests, and the ultimate loads gathered from the model were similar to the experimental data. Results from numerical and experimental centrifuge test were compared. Thus, it showed that the ultimate lateral displacement from centrifuge tests were higher than the results in the literature, although, recent experimental and FDM have shown that pipe-soil interaction can considerably increase the soil restraint on pipeline. Therefore, the numerical model can then be used to simulate buried pipe behaviours under vertical loading and axial force with presence of voids. This supports further numerical studies side by side with experimental studies to examine the findings and more investigation to the effect of voids on buried utility pipes.

The performance of a pipe is affected by the soil in which it is buried. Davies et al. (2001) illustrated the failure mechanism of a rigid sewer pipe as a three staged process involving an initial defect, deterioration and collapse. Flexible pipes would involve a more complex failure process but according to Young and O'Reilly (1983), the bending moment produced will be lower for buried pipes where the soil around the pipe is able to distribute loads and pressures more uniformly. This property of the soil is known as the bedding factor, which is different for each soil type.

Zhan and Rajani (1997) carried out load transfer analysis of Polyvinyl Chloride (PVC) buried pipe in different trench backfills using nonlinear finite element analysis to evaluate the influence of different backfill materials as well as pipe burial depth from 0.65 to 1.65m. A uniformly distributed load was used as a traffic load along the trench width. It was identified that the amount of load transfer onto the pipe was more significant if the burial depth and pipe stiffness was decreased. It concluded that pipes buried in sand backfill experienced higher stresses than that of a pipe buried under clay backfill. This is independent of burial depth and pipe material. Thus, clay backfill provides better protection to a buried pipe system from repeated traffic loading than backfill composed of sand, irrespective of buried pipe depth and stiffness. However, settlement in the clay backfill clearly will be more than settlement when the material of the backfill is a sand. Therefore, this can significantly effect long term pavement performance. However, further investigation may be required if the backfill materials are different.

The papers above have investigated the effects of voids on pipe behaviour. However, most are numerical investigations and fewer experimental. The experiments conducted by Peter et al. (2018) in a full-scale laboratory was only looking at the bending moment at the pipe ring rather than the longitudinal bending moment. As Tan and Moore (2007) stated, physical testing is needed to evaluate the performance of these calculations. This preliminary study suggests that the growth of erosion voids should be stopped before they reach 45°, but validation through physical testing is necessary. The research in this thesis can provide this information.

2.2.3 Theoretical Modelling

It is essential to utilise some established theories from the areas of Geotechnics and Structural Mechanics in addition to relevant theories proposed by other research findings in order to study the displacements and bending of water supply pipes situated near a void and subject to surface loading. How much load is experienced by the pipe from the weight of soil it is buried under and the loads applied at the surface is a much debated subject. Matyas and Davis (1983) reviews various techniques and compares them to relevant design standards at the time of publication. It was shown that the design standards tend to under predict loading experienced by the buried pipes as the load factor values were found to be lower than the experimental values. Thus, it is noted that the current design applications in the UK for evaluating the soil pressure on a buried pipeline under vertical traffic loading is based on a simple equation derived using a Boussinesq solution. In addition, the author reviewed existing techniques used to calculate vertical earth loads on rigid pipes where fill is settling around a pipe. These available methods were again compared to relevant design standards for the time. It was also found that the design standards according to (Spangler and Shafer, 1938) underestimates the earth loads when related to the recommendations of field studies. The conclusion is that, for buried pipes (particularly rigid pipes), the load experienced is more than the dead weight of the overcapping soil when the pipe is installed in a trench. However, in current design standards (BSI, 2004), pressure on flexible pipes due to backfill is still determined by just the vertical stress calculation in the soil. These concerns raised by

Matyas and Davis (1983) have not yet been fully investigated. The effect of concentrated surcharge (e.g. traffic loading) causes further complexities and have yet to be fully appreciated or implemented in the design guidance or validated through a programme of experimental research. Often the evaluation of increased stress in the ground is based on simplified increases in ground stress centred on Newmark's integration of the theory of dissipating stress with depth taken from Boussinesq (1885) and (BSI, 2004). Stresses at any depth and horizontal distance from the application of a load can be calculated depending on the position of analysis and Poisson's ratio of the soil, ν , using Boussinesq's theory. The theory is also known as the "bulbs of pressure" concept, which contours non-dimensionalised stress dissipation beneath the point of the applied load. However, currently no information is provided with respect to the role of the road surface stiffness in dissipating the surface stress, or complex aspects for instance non-uniform pipe burial conditions within a trench.

Winkler (1867b) presents a model which is the most known form of a global simplified model employed to represent the structural properties of a soil in a mechanical way. This leads to the soil interaction with a structure, in this case a pipe, being more simply analysed. Attewell et al. (1986) derived a numerical solution based on the Winkler problem which models soil pipe interactions (see Figure 2-8). The Winkler method models soil as a sequence of individual elastic springs that push back a reaction proportional to the force applied to them. Combining this with elastic continuum beam mechanics leads to the possibility of the investigation of theoretical behaviour of a pipe buried in 'Winkler' type soil – that which is homogenous with a uniform 'spring constant' stiffness value, (k). Figure 2-8 show four different spring groups that model the soil and the pipe displacement.

- i. *Axial spring is representing the resistance of the soil along the pipe in X axis.*
- ii. *Lateral spring is representing the resistance of the soil to the transverse pipe movement.*
- iii. *Vertical bearing and uplift springs are representing the resistance of the soil at the top and bottom of the pipe.*

A linear relationship is assumed, on the basis of Hooke's law, between the force on the spring foundation (F) and the deflection (δ).

$$F = K \cdot \delta \qquad \text{Equation 2-1}$$

The sub-grade reaction module, K (F/L), is the ratio between the soil pressure per unit pipe length, P , and the displacement produced at that point (δ) by the load application.

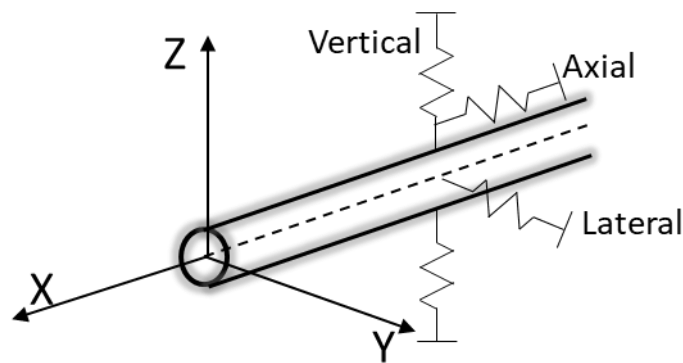


Figure 2-8 Mechanical representation of the Winkler Model (Yang and Li, 2021)

2.3 Buried Flexible Pipe Design

The buried pipeline theory and design application was developed in 1913 by Anson Marston's premiere paper published on earth loads applied to the piping system (Moser and Folkman, 2008). Later in 1914, Spangler, in collaboration with Marston, developed a new theory of flexible pipe design which studies buried pipes in different scenarios. Combined with finite element techniques and sophisticated soil models, computer devices have provided the engineering profession with design resources that have produced, and will continue to produce more precise designs (Moser and Folkman, 2008).

The fundamental aims of the structural design of buried pipelines are to ensure that they are designed to guarantee the optimum embedment and the type utilised pipe materials, whilst meeting all the design requirements and control parameters that are required (BSI, 2020). It is proved from the previous studies that flexible buried pipes derive much of their structural strength from the backfill surrounding them. Therefore, the backfill material selection and compaction is very important where controlling the ovalisation is required. However, it should be taken into account that there are some flexible pipes that have lower stiffness which will take all energy of the compactor to achieve so called Proctor density and soil reaction modulus (Moser and Folkman, 2008).

According to BSI (2020), the Guide to the Structural Design of Buried Pipelines, it can be seen that the soil pressure is varied before and after the pipe installation (see Figure 2-9). Therefore, these factors are taken into consideration during the calculations and the designs of the pipeline as described in (BSI, 1997).

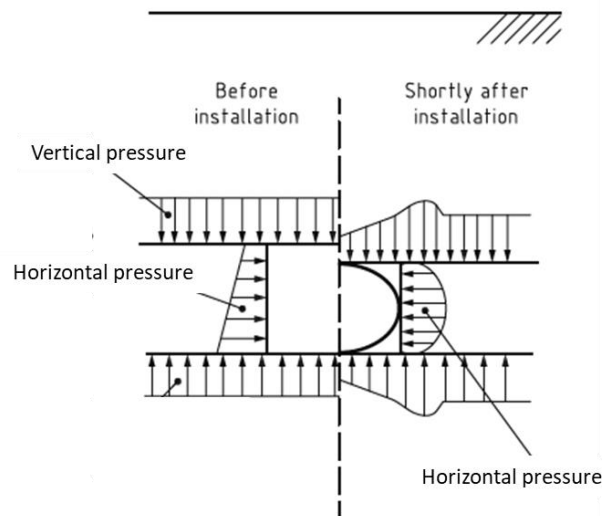


Figure 2-9 Soil pressure on the pipe (Kavitha et al., 2011)

However, subsequent research has looked at buried pipes combined with the soil behaviour complexity, which has resulted in several developments of soil models that are based on the classical elastic theories. The subsequent subsections summarise the basic idea behind a number of the main concepts of the model approaches found in the literature.

2.3.1 Elastic Models for Soil Backfill Response

Overall, the contact pressures between a buried pipe and the surrounding soil are usually not statically determined. Therefore, this depends on the relative deformation at the pipe-soil interface. Thus, characterisation of pipes and soil stiffnesses are essential to any detailed analysis of the pipe-soil structure. All current theories typically are based on the assumption that both pipe and soil respond in a linear elastic manner, at least to small increases in load. However, two alternative models are used for elastic soil response. These are:

i. Continuum Model

In the continuum model, the continuous behaviour of soil is idealised as a three dimensional continuous elastic solid. In this case, the soil surface deflections due to loading will occur under and around the loaded region. Figure 2-10 illustrates a schematic of the surface profile displacement of a soil medium which is exposed to uniform load (p) of radius area (a). Under the external force system action, the distribution of displacements and stresses in the medium remains continuous. In this case, it is presumed that some continuous function describes the behaviour of the soil medium. For the sake of consistency, the soil is believed to be semi-infinite and isotropic in continuum idealisation (Kavitha et al., 2011). furthermore, the assumption of the continuum model usually considers the soil as isotropic and

homogeneous also; hence, the soil response is defined by two elastic parameters, typically the Young's Modulus (E) and Poisson's ratio (Gumbel, 1983).

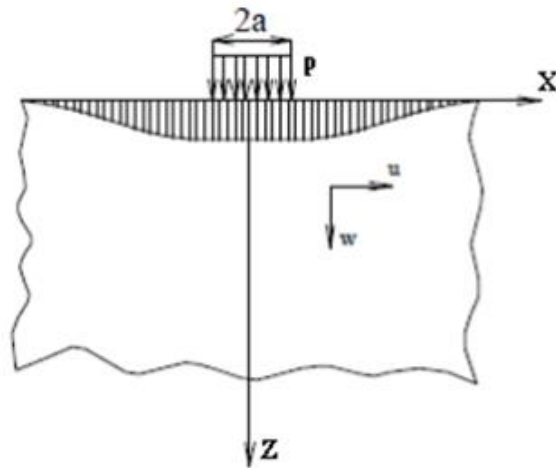


Figure 2-10 Elastic continuum model (Kavitha et al., 2011)

ii. Winkler Model (Discrete Spring)

The Winkler foundation model's idea is to idealise the soil as a series of springs that displace because of the load acting upon it (Winkler, 1867a). But, the model's disadvantage is that the interaction between the springs is not taken into consideration and also is that it uses only one parameter known as k . The soil is described using linear stress-strain behaviour. This linear relationship makes the calculation easier, but in reality, the soil does not behave linearly elastically (Caselunghe and Eriksson, 2012).

2.3.2 Subgrade Reaction Theory

Generally, the subgrade reaction theory is one of the methods developed method from the early Winkler spring model. This method has been used as it is the most convenient representation of soil (linear elastic) for pipe-soil interaction analyses (Winkler, 1867a). The Winkler spring model is currently the most well- known and most used model for soil-structure interaction (SSI) research by structural engineers. Modelling the subgrade that consists of an infinite number of springs on a rigid layer is also

the oldest and simplest form (Ng, 1994). The spring is attached to the top of the rigid layer and below the structure to replace the soil below the foundation (Figure 2-11). Subgrade reaction modulus or subgrade reaction coefficient, k , is the ratio between the pressure, p , at any given point in the contact surface and the settlement, y , at that point produced by the load Equation 2-2:

$$p(y) = ky \quad \text{Equation 2-2}$$

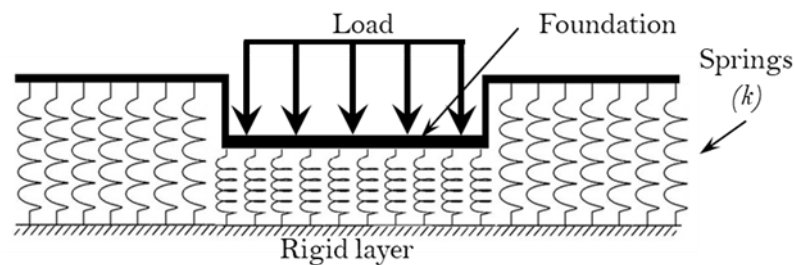


Figure 2-11 Original Winkler model (Hetényi and Hetbenyi, 1946)

In soil-structure interaction applications, Winkler's theory is still being used as the principal subgrade model. While this method does not portray the settlement in particularly accurate way, it can provide a simple method for determining the pipe's behaviour. However, it is limited to certain idealized conditions of support, and the loadings are only by the surface overload pressure and surcharge. For more demanding loading and support conditions, a more general approach is needed.

Therefore, it can be seen that there are several structural models that have been developed to include the transfer of load into the vertical direction. The elements of interaction may be including springs, flexural elements, shear layers and pre-tensioned membranes. Once elements of interaction are added between the springs, multiple parameters define the response of the subgrade and thus are called multi-parameter models. Some multi-parameter models produced are listed in Table 2-1 (Caselunghe and Eriksson, 2012). Significant improvements have been made to the Winkler Spring approach in order to reflect the different physical aspects of the soil-structure interaction (SSI). Hetényi (1971) presented a solution for a single load concentrated on the beam on the Winkler foundation in which an elastic member contact with the springs represents elastic soil support, as shown in Figure 2-12. In addition to

that, the reaction of the soil force is related to the pipe deflection, y , at any depth. Therefore, it can be calculated by the governing equation of the Euler-Bernoulli elastic beam theory (Timoshenko, 1983), defined below in Equation 2-3:

Table 2-1 Compiling of multi-parameter models(Aron and Jonas, 2012)

Subgrade model	Physical elements used to visualize model
Winkler's Hypothesis	springs
Filonenko-Borodich	deformed, pre-tensioned membrane + springs
Pasternak's Hypothesis	shear layer + springs
Loof's Hypothesis	
Kerr model	springs + shear layer + springs
Haber-Shaim	plate + springs
Hetenyi	springs + plate + springs
Rhines	springs + plate + shear layer + springs

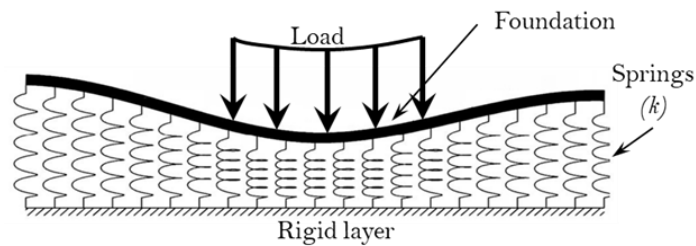


Figure 2-12 Beam on Winkler foundation (Hetényi and Hetbenyi, 1946)

$$EI \frac{d^4 y}{dx^4} - p(y) = 0 \quad \text{Equation 2-3}$$

Where y is the pipe deflection, x the pipe length, EI the flexural stiffness of the pipe, $p(y)$ the subgrade (soil) reaction from the adjacent soil.

2.4 Conclusion and Summary

There have been numerous studies conducted into the soil-pipe interactions when surface loading is applied which provides the groundwork for this experiment to build on. Multiple variables have been tested including soil density, pipe burial depth and pipe displacement under various types of loading. Permanent ground deformation was a key factor in many studies with analytical and numerical models developed for soil-pipe interaction under surface loading. However, the literature relating to soil-pipe interactions is limited, demonstrating that considerable uncertainties remain with respect to the role and impact that voids have in the performance of buried pipe systems. The literature has identified several limitations associated with previous numerical and experimental studies which invites opportunities to make positive contributions to this field, specially:

(a) Design guidance: current design codes/guidance do not accommodate for the presence of a void/loss of local support to the pipe; yet numerical and physical investigations confirm that the presence of voids generate increased pipe deflection and bending that breach current design recommendations. New knowledge is required on aspects relating to void geometry and pipe deformation with respect to applied surface loadings in order to connect the role of voids with pipe performance.

(b) Improved modelling requirements: it is clear that neither numerical studies nor physical model tests accurately study the effect of void size/location, besides, investigating the effect of the road stiffness, therefore the applied surface loads may vary from those in reality. The current literature demonstrates that voids can cause localised pipe stresses and generate additional deformation. Therefore, modelling voids may give better understanding of soil-pipe behaviour subjected to surface traffic loading.

In conclusion, this literature review has examined experimental research and discrete numerical work on the impact external loading on buried pipe looking at only pipe deformation but, none of them has considered the effect of void size/location on the longitudinal bending moment and the deflection of the plastic pipes. Thus, more investigations have to be completed to investigate the effect of void size/location. This sets the state of the art for the following experimentally based investigations.

The following research, therefore, has been conducted to address this gap by investigating the behaviour of a buried plastic pipe with presence of void that subjected to traffic loading and internal water pressure to provide greater understanding of soil-pipe-void interactions. This work also aims to explore the effect of the internal water pressure inside the pipe while under the application of the vertical loads.

CHAPTER 3

Geotechnical Modelling Approaches

3.1 Introduction

The use of various methodologies to investigate geotechnical problems will often lead to a better appreciation of the uncertainties and challenges. Burland (1987) outlines this concept in the well-known “Burland Triangle” in which a range of investigative methodologies are proposed, for instance, experimental, numerical and analytical. Full-scale experimental testing is one such approach whereby testing is conducted on a prototype structure where neither scaling of the materials or geometry are needed. The main disadvantage of this approach is that it is often costly, hence an extensive test suite is prohibitive. Reduced scaled experimental modelling at 1g provides a low stress representation of the full scale prototype system. This offers a manageable experimental scale with the ability to control the test environment and variables, and a more cost effective approach enabling a greater number of parametric experiments. The largest drawback associated with small scale 1g tests is that the prototype soil stress levels are not reproduced; thus care and consideration of scale effects are needed when understanding observations. Centrifuge testing of reduced scale models at elevated gravity (Ng) overcomes many of these drawbacks at 1g, most importantly providing more representative prototype soil stress conditions. Although consideration of scaling is still an important factor (Madabhushi, 2017).

Numerical and analytical methods are reliant on many assumptions in their implementation. A constitutive model is used to represent the actual physical behaviour of soil and despite the increasing number of complex models produced, simplifications regarding how they describe the soil are unavoidable. This impacts on the observations from these approaches so that the modeler must therefore be aware of the limitation of the mathematical descriptors and test the sensitivity of the soil model and other numerical inputs on the results. Further complexities exist when trying to capture soil-structure effects, like pipe-soil interaction to ensure the modelled behaviour reflects an actual interface. Numerical and analytical methods are often validated against physical observations in order to verify input properties and suitability of the underlying model before then conducting more comprehensive parametric studies. The latter is where this approach comes into its own and offers a superior advantage over physical model counterparts as once validated, additional scenarios can be considered with relative ease (Madabhushi, 2017).

The investigative approach used in this work is reduced scale models tested at elevated gravity in a geotechnical centrifuge. Details of the centrifuge modelling technique, technology and scaling are described in Section 4.2, in conjunction with relevant scaling relationships for the model pipes that ensure they offer comparative bending stiffness to the prototype situation described in Section 4.3.

3.2 Centrifuge Modelling

1g model testing is limited by the reduced soil stress levels which affect soil stiffness and dilation characteristics. Centrifuge modelling has become a widely used technique as it affords the opportunity to make direct comparisons with full-scale as field stresses are maintained. Centrifuge testing has been successfully performed to investigate a varied range of soil-pipeline interaction problems and the principles and scaling laws for geotechnical centrifuge testing are described in detail by Schofield (1980) and briefly summarised herein.

Pokrovsky (1936) first developed geotechnical centrifuge modelling in the former USSR in 1931. In spite of the fact that its introduction was in the early 20th century, it was not until developments in electronics/instrumentation in the 1970's where the method found favour for use in geotechnical research. Schofield (1980) was one of the first to describe this technique and operations of the Cambridge 10m diameter geotechnical centrifuge. The number of centrifuges across the world have increased considerably and it is now a commonly used in academia and industry (Taylor, 1995). The key premise of centrifuge modelling is that it provides prototype stress-strain relationships in small-scale models as the self-weight force of soil is magnified by centrifugal acceleration. Section 4.3.1 and 4.3.2 discuss in more detail the governing scaling laws.

3.2.1 The University of Sheffield Centrifuge (UoS50gT)

The University of Sheffield, Centre for Energy and Infrastructure Ground Research (CEIGR), in the Department of Civil and Structural Engineering operates a 4m diameter 50g-ton geotechnical beam centrifuge facility (Figure 3-1). The centrifuge was designed and manufactured by Thomas Broadbent and Son limited, United Kingdom, and commissioned in 2014. This system can accommodate a payload of up to 500kg accelerated to 100 gravities (g). On board sensors and cameras allow the capture of experimental data during testing like strain gauges, force and displacement sensors (Black et al., 2014). Table 3-1 reports the centrifuge technical specifications.

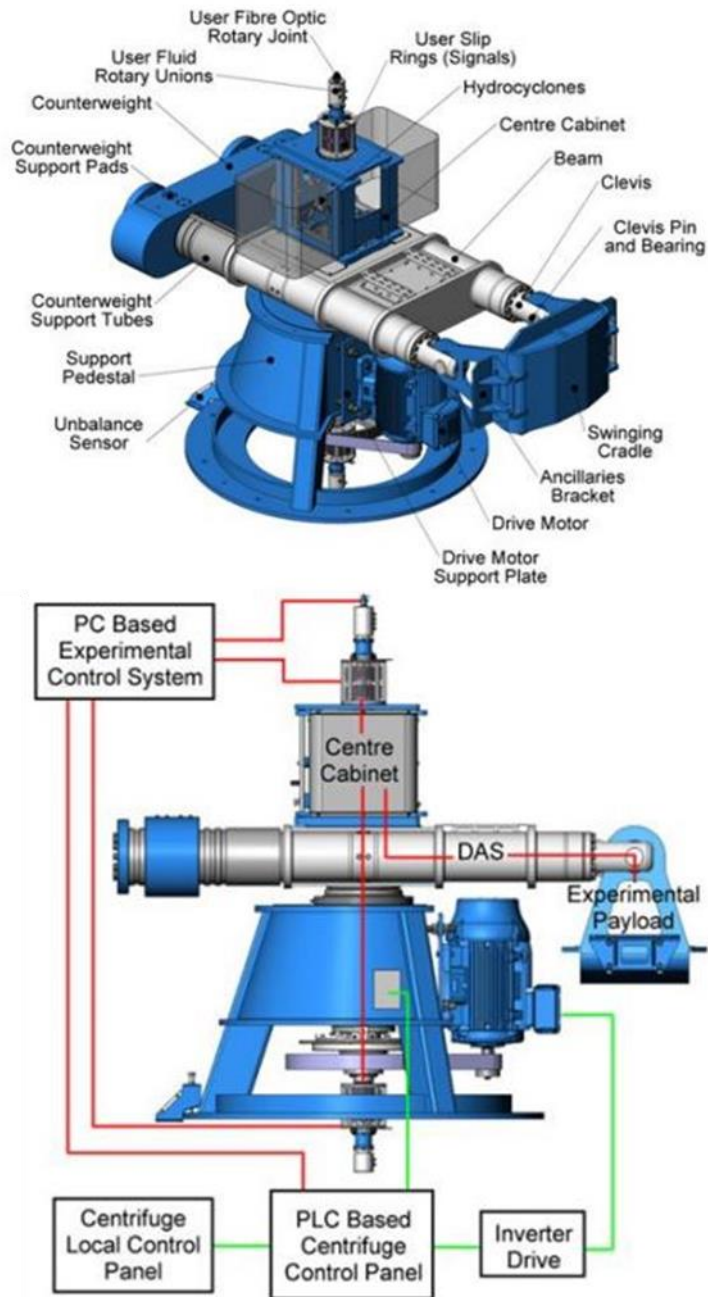


Figure 3-1 Centrifuge facility(UoS50gT) at CEIGR Sheffield University (Black J 2014)

Table 3-1 UoS50gT Centrifuge specification and performance (Black J 2014)

Description	Specification
Platform radius	2.0m
Effective radius	1.7m
Payload size	W=0.6m- circumferential L=0.8m-vertical in flight H=0.9m-radial in flight
Max Acceleration	500kg at 100g; 330 kg at 150g
In-flight balancing capability	From maximum of ± 45 kN to ± 1.5 kN at 280 RPM
Drive motor	55kW-4 pole-3 phase motor
Inverter	75 kW inverter with DC brake
Data cabinets	2 x 12 U high, interlocked to centrifuge control system
Hydraulic union	4 port, 10 bar g, 10 to 50 °C
Slip ring: Power	16 way 1000 RMS at 10A each
Communication	Fibre optic rotary joint, multimode, rated 1000 RPM to 1GB

3.3 Principles of Centrifuge Modelling

Taylor (1995) and Wood (2004) clarifies the mechanical theory of centrifuge modelling. The rotation of any mass (m) at constant radius (r) with a uniform circular motion (v) around axis (y) as illustrated in Figure 3-2 will experience a steady radial acceleration equal to v^2/r or $r\omega^2$ (ω is the circular velocity). The mass would be subjected to a centrifugal force equal to $mr\omega^2$ oriented towards the axis as a result of this acceleration. This acceleration of this mass can be determined by the acceleration of gravity (g) and therefore it can be said that this is equal to Ng , where N the scale factor and g with value of 9.81m/s^2 ($N = r\omega^2/g$). (Madabhushi, 2014).

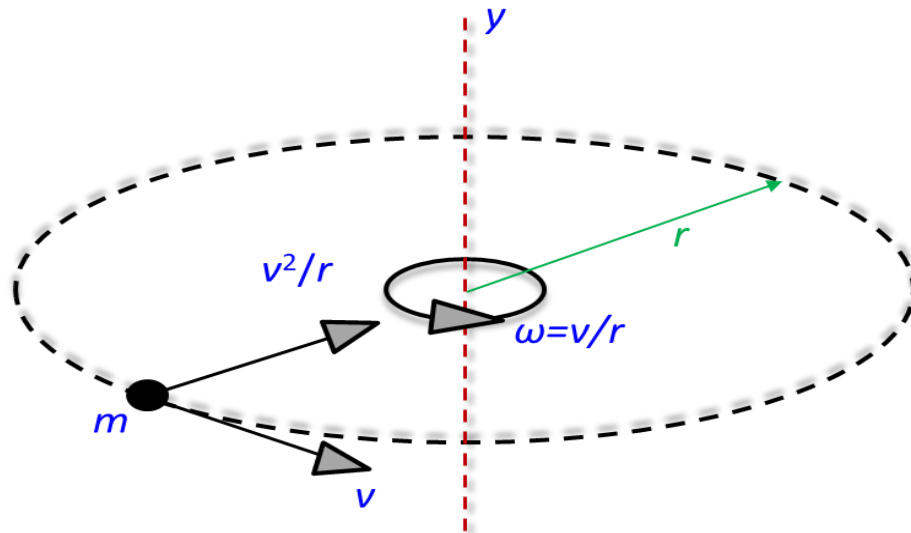


Figure 3-2 The basic concept of the centrifuge modelling (after Wood, 2004)

3.3.1 Scaling Laws

The fundamentals of centrifuge testing are that the prototype is scale down to a model geometry by a factor of N , for example a scale factor of 100 implies the experimental model is reduced in geometry by 100 times of the prototype. Gravitational forces must be increased by the same geometric factor (N) with respect to Earth's nominal gravity (g) field for compatibility of stress. An example of soil stress is Section (3.3.2) to confirm the how scaling laws are used to confirm the model stress experience is similar to the representative prototype values. The scale factor (N) must be applied within the centrifuge at an effective centrifuge radius (R_e) as shown in Equation 3-1.

$$N = R_t + \frac{\omega^2 R_e}{g} \quad \text{Equation 3-1}$$

Where N is scale factor, ω is the centrifugal angular velocity, R_e is the effective radius, R_t is the to the top-of-model radius and g is normal gravity field of the earth.

By considering the same stress-strain relationship at homologous points, Schofield (1980) derived most of the important scaling laws with the use of dimensional analysis. Table 3-2 describes some of the ideal parameters considered for centrifuge modelling with their metric units and the related scaling law. Therefore, it is important to interpret the data of small scale centrifuge tests and turn them into prototype dimensions.

Scaling laws enable the scale model observations to be related to the prototype conditions. It is essential that the relationship is carefully selected to ensure that the correct behaviour is captured and represented (Madabhushi, 2014). Some scaling aspects that are crucial to the current planned work are (i) how to correctly model a PVC pipe (ii) the load configuration and (iii) how to create or represent a void.

Table 3-2 Geotechnical centrifuge scaling laws (Taylor, 1995)

Parameter	Units	Field	Centrifuge model (Ng)
Length	m	l	$1/N$
Area	m^2	A	$1/N^2$
Mass	Kg	m	$1/N^3$
Stress	N/m^2	σ	σ
Strain	-	\mathcal{E}	\mathcal{E}
Force	N	F	$1/N^2$
Displacement	m	x	$1/N$
Bending Moment	Nm	M	$1/N^3$
Flexural stiffness	Nm^2	EI	$1/N^4$
Centrifugal acceleration	m/s^2	a	Na

Although scaling laws are useful in creating models in centrifuges, there are some errors due to variations in stress (non-linear stress distribution). This phenomenon is as a result of the uneven range between soil depths within the model and the centre of the centrifuge rotation. Another issue is the acceleration field over the depth of the model as point across the model on a horizontal plane do not have the same acceleration value (see Figure 3-3 & Figure 3-4). In order to minimize these errors, an effective radius (R_e), can be estimated by using Equation 3-2 (Taylor, 1995).

$$R_e = R_t + \frac{2H}{3} \quad \text{Equation 3-2}$$

Where H is the height of the model soil and R_t is the top-of-model radius.

The effective radius, R_e , which is the measured by the distance from the centre axis of the centrifuge to one-third above the surface of the model is utilized to give an exact relationship in stress between the model and prototype at two-thirds the model depth. The variance of the vertical model stress (σ_{vm}) with depth (z) can be determined for the specified values of ω , R_t , and soil density (ρ) as shown below in Equation 3-3 (Taylor, 1995) and the full scale prototype in Equation 3-4:

$$\sigma_{vm} = \sigma_{\omega^2 z} \left(R_t + \frac{z}{2} \right) \quad \text{Equation 3-3}$$

$$\sigma_{vp} = \rho N g z \quad \text{Equation 3-4}$$

Where the use of the m or p subscript denotes the model and prototype conditions respectively. Owing to the selection of a single point to reference the radius of the model, the effective radius, this gives rise to the condition of both under and over stress throughout the depth of the model compared to the prototype. This is due to the fact that the upper region of the model is subjected to a gravity less than Ng , while the lower region is higher.

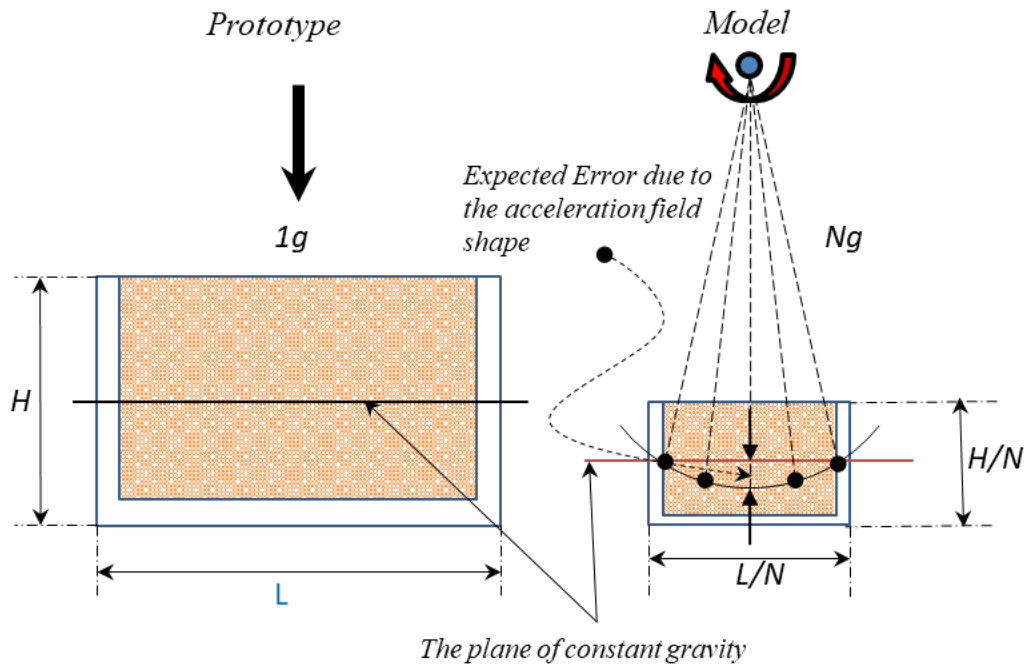


Figure 3-3 Prototype radial gravity field and model scale test (Madabhushi, 2017)

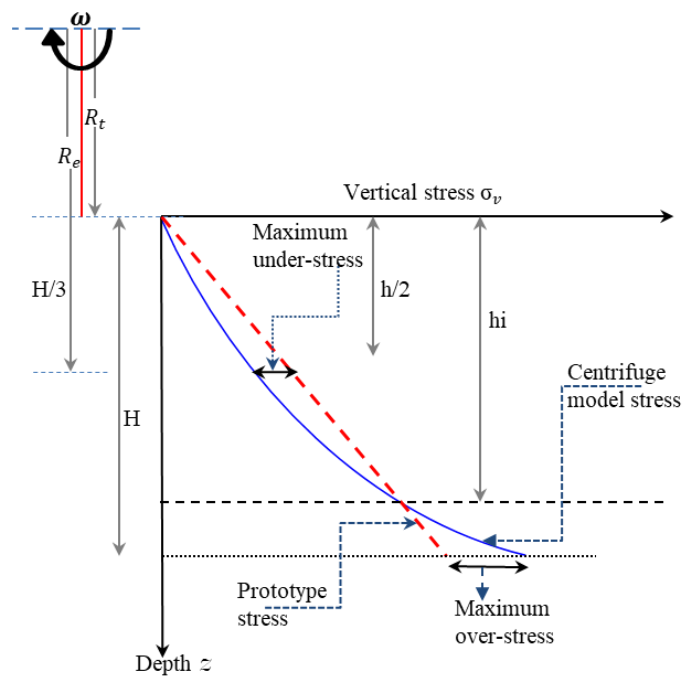


Figure 3-4 Under-stress and over stress in a centrifuge model (Madabhushi, 2017)

The centrifuge used in this research has a radius of 2.0m to the payload platform base in the fully raised position, and a payload strongbox depth of 400mm, resulting in a maximum error of 1.7%. This is small enough so that the effects can be ignored (Madabhushi, 2017).

3.3.2 Scaling Laws for Vertical Stress (σ_v)

The principle advantage of using the geotechnical centrifuge to model soil boundary value problems is the ability to correctly simulate the increase in soil stress with depth through the soil profile. At the prototype scale the vertical effective stress (σ_{vp}) can be calculated using Equation 3-5 and Figure 3-5 shows the comparison of vertical stress values in model and prototype scales using model scaling laws.

$$\sigma_{vp} = \rho g H \quad \text{Equation 3-5}$$

where ρ is the material, g is the earth's gravitation and H is the depth.

Consider a small scale model to be a reduced in scale ' N ' times from the prototype such that the length scale of the model will be l/N and depth H/N . Assuming the same material density is maintained and the model subject to an acceleration component N times greater than earth's gravity. Thus the vertical stress at the model scale σ_{vm} as shown in Equation 3-6.

$$\sigma_{vm} = \rho N g \frac{H}{N} = \rho g H \quad \text{Equation 3-6}$$

where H/N is equivalent to the model depth. It is observed that the stresses in the model and prototype are similar, i.e. $\sigma_{vp} = \sigma_{vm}$. The same concept applies to strain, which leads to a 1:1 scale for the soil stress-strain curve mobilised in the model, which will be identical to that of the prototype. Other basic centrifuge scaling relationships are discussed in detail by Garnier et al. (2007).

Even though scaling laws are helpful for creating models in the centrifuge, some concern may still arise regarding soil particle size effects relating to the pipe and footing contact interactions. Ovesen (1979) investigated the performance of circular foundations on sand by using different sized models at different g levels and reported the critical interaction ratio of 15-30 between the footing diameter and grain size

was required to prevent adverse interaction observations. Similar consideration is also given in the current study with respect to the particle scaling, pipe diameter and the vehicle load area.

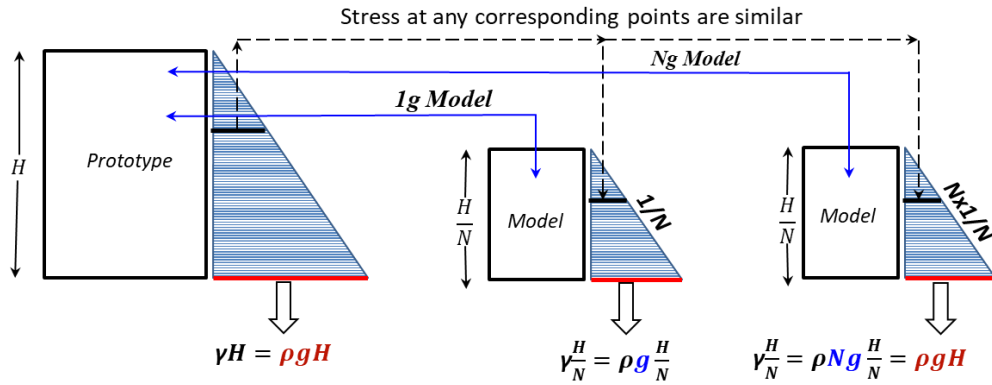


Figure 3-5 Concept of geotechnical centrifuge modelling (Abuhajar, 2013)

3.3.3 Scaling Laws for the Second Moment of Area (I)

The scaling law for the Second Moment of Area is obtained from the analysis of the Second Moment of Area for a circular hollow pipe. However, this method is applicable to any arbitrary cross-sectional area. Second Moment of Area (I) for a hollow circular pipe is calculated using Equation 3-7 and illustrated in Figure 3-6. The aim is to capture the correct bending response to maintain the bending stiffness relationship with scaling (E) or via geometry (I) of which will be explained in more detail later.

$$I = \frac{\pi}{64} * (D_{out}^4 - D_{in}^4) \tag{Equation 3-7}$$

Where D_{out} is the outer pipe diameter and D_{in} is the inner pipe diameter

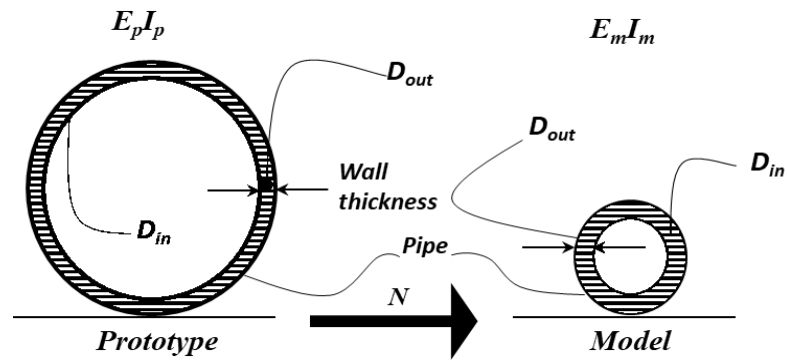


Figure 3-6 Scaling of prototype scale to model scale of the pipe

It can be seen that the equation is based on geometrical parameters only (diameter of the pipe), with a power of 4 for both inner and outer diameters. As the dimensional scaling law has already been established (See Table 3-2) to be a linear relationship (1: N), the scaling law for I is:

$$\left(\frac{1}{N}\right)^4 = \frac{1}{N^4} \quad \text{Equation 3-8}$$

3.3.4 Scaling Laws of Bending Moment (M)

The scaling law for the bending moment (M) has been determined by using the Flexural Formula

$$\frac{(M)}{I} = \frac{\sigma}{Y} \rightarrow M = \frac{\sigma}{Y} * I \quad \text{Equation 3-9}$$

Hence, the scaling relationship for the moment is based on the Second Moment of Area I and Y , the distance from the centre of the cross-sectional area to the point considered for the bending moment. Using the scaling relationships that are already established for these parameters it can be shown that

$$M_{mode} = \frac{\sigma_{prototype}}{Y_{prototype * \frac{1}{N}}} * I * \frac{1}{N^4} = \frac{\sigma_{prototype}}{Y_{prototype}} * I * \frac{1}{N^3} \quad \text{Equation 3-10}$$

Hence, the scaling relationship for the bending moment is: I/N^3

3.3.5 Scaling Laws for Bending Stiffness (EI)

To establish the scaling law for the bending stiffness, both the Young's modulus and the Second Moment of Area need to be considered. Young's modulus delivers a relationship between the stress and strain experienced by a material. As the purpose of the centrifugal modelling is to create the same level of stress in both the model and prototype environment, the scaling law for stress (and similarly to strain) is unity. This means that the scaling relationship of bending stiffness is only dependent on I , which was already determined as $I: N^4$. Therefore, the theoretical scaling law for bending stiffness is $I: N^4$. As the model dimensions have been scaled with the scaling law of $I: N$ as shown in Table 4-3 section 4.31 the geometry of the pipe is set. By knowing the geometry of the model and also of the prototype, the Second Moment of Area (I) can easily be calculated for both the model and the prototype using equation 3.7. The values for both the model and prototype materials are presented in Table 4-3 section 4.3.1. Now, the aim is to achieve a scaling relationship of $I: N^4$ for the flexural stiffness (EI). As the Second Moment of Area for the model and for the prototype is fixed, the Young's Modulus (E), which is dependent on the material of the pipe, had to be modified. It can be seen in Table 4-3 that PE100 was used for the material of the model and its properties of strength and stiffness, having the same Young's modulus of the HDPE. By using this material, the flexural stiffness (EI) of the model is in the correct scaling relation with respect to the prototypes flexural stiffness. The scaling law for the stiffness is presented in Equation 3-11

$$\frac{(EI)_m}{(EI)_p} = \frac{1}{N^4} \quad \longrightarrow \quad E_{model} = \frac{(EI)_p}{N^4 I_m} \quad \text{Equation 3-11}$$

where E is the Young's modulus of the material, I is the second moment of area per unit length of the material, (EI) is flexural stiffness, N is the scaling factor and m and p subscripts refer to model and prototype respectively.

3.3.6 Scaling Laws for the Applied Load

For the scaling relationship of the force, Newton's second law of motion was used

$$\text{Force} = \text{Mass} * \text{Acceleration} \quad \text{Equation 3-12}$$

Mass is the product of density and volume. The scaling relationship of density is unity, while the volume is based on the length, width and height of the model, each scaled with the relationship of $1:N$. This gives an overall scaling law of $1:N^3$. Acceleration is the gravitational acceleration, which was scaled with a factor of N . Therefore, the scaling law for the force is

$$F_{model} = \text{Mass}_{prototype} * \frac{1}{N^3} a_{prototype} * N \quad \text{Equation 3-13}$$

This provides a scaling relationship of

$$F_{model} = \frac{1}{N^2} F_{prototype} \quad \text{Equation 3-14}$$

CHAPTER 4

Experimental Methodology

4.1 Scope of chapter

This chapter describes the framework of the physical modelling experimental methodologies that has been used throughout the research period. The platform for testing was through the use of the University of Sheffield, UoS50gT geotechnical centrifuge facility. This has been explained in detail previously in Chapter 3. Nevertheless, centrifuge basics, individual test settings, test setup and data processing are summed up in detail. Additionally, preparatory test results are presented that provide insight into the effects of selected centrifuge modelling procedures and techniques that have not previously been documented. Further, this chapter also describes the experimental mechanical design of both surface loading system and the actuation apparatus for the axial force and modelling techniques that have been developed for the investigation of pipe performance subject to external loading. Key areas discussed relate to the material properties, the model pipes, the centrifuge test package with load simulation systems and instrumentation.

4.2 Experimental setup

The approach used in this research is to follow a physical modelling technique. As highlighted in the literature review, most previous research in the area of a buried pipe affect by a void in the surrounding area is numerical and few study the void effect with respect of bending moment at the pipe ring but not the longitudinal bending moment. Physical testing on buried pipes tend to lack the presence of a void. Therefore, this research is novel and covers an area that is previously unexplored.

As previously stated, physical modelling is extensive across all domains of geotechnical engineering. Theories are typically validated using a comparison with observed physical behaviours. In an ideal scenario, full-scale modelling would be used to test as these give a full representation of what is going on. However, this is not only an expensive technique but also costly in terms of time and impractical. Therefore, a small-scale representation of the problem is used in these experiments.

The set up for the experiments that are described in this thesis are outlined in detail for the centrifuge physical model set-up for plastic buried pipe. The tests were conducted in dry sand (fraction E) with relative density of 80%. The model setup procedures across the test matrix were varied in terms of preparation of the model according to the test scenario with regard to burial depth, load conditions and

presence of void (comprehensive test details are described subsequently in section 4-3). Furthermore, the sample then was laid on the centrifuge platform (payload). There were two phases of testing applied to each individual test, following the spin-up of the centrifuge. The first phase was a monotonic loading case of equivalent 6 tonnes applied to the model surface over a period of roughly 180 second. This was followed by a series of cyclic loading, where the load was applied 3600 times at regular intervals of 2 seconds. Both scenarios were performed at the targeted acceleration of 19g. Through this thesis, a total of 156 centrifuge tests were separately prepared and examined. The outcomes from some of these are not presented in this dissertation since these were purely for calibration and setup verification purposes. In addition, all material properties have been determined and instrumentation calibration have been conducted in advance, prior to the centrifuge test. All centrifuge tests were undertaken in a strong box with high- strength aluminium alloy 6061T6 of interior dimensions of 600Lx400Wx400H mm, which give a rigid boundary condition (appendix A).

4.2.1 Material Properties

4.2.1.1 Soil Properties

A fraction E silica sand (HST95) was selected for use in this investigation to form soil beds. This was selected particularly to ensure that there are sufficient particles around the pipe to obtain real soil-pipe interaction ((Figure 4-1). In order to further analyse the results, it was essential to classify the soil and determine its properties. Various laboratory tests including shear box, particle size distribution analysis and oedometer test, were carried out to get a full picture of the soil behaviour needed to complete the analysis and calculations following the centrifuge test. A target relative density in this research is 80% and was achieved by using 3D pluviation.

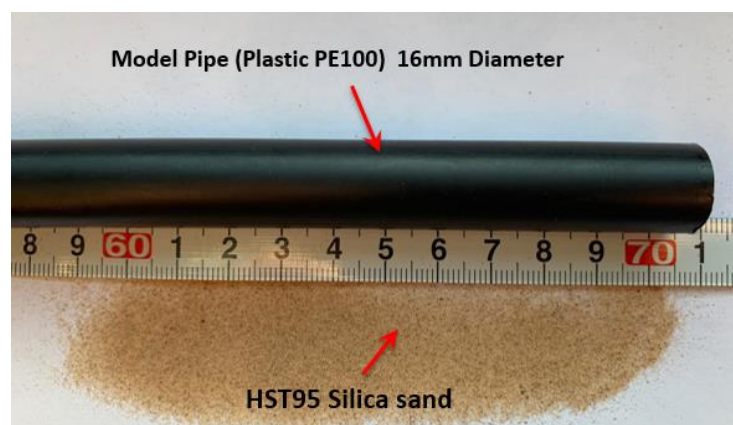


Figure 4-1 HST95 silica sand and model pipe (PE100)

4.2.1.1.1 Particle Size Distribution

The effect of particle size is one of the most important factors to consider. The dimension of the prototype scales down by the gravity scaling factor (N) in the centrifuge model. However, particle size is not scaled by the same factor. Taylor (1995) stated that one of the common issues in the field of geotechnical centrifuge modelling is whether particles should be included in scaling. If soil particle sizes were included in the scaling it is important that the chosen soil has the same granular structure so that it behaves in a similar way, which is impossible from a geotechnical engineer's perspective. It is wrong to assume that in soil mechanics a clay will behave similar to a sand. Therefore, it is essential to use a sand in the experiments in this project. To capture the true soil behaviour in a model, the same soil must be used in the prototype i.e. one with the same stress-strain relationship. The soil chosen in this research for the model is silica sand HST95 equivalent to fraction E with particle diameter 0.15mm (150 micron).

Particle size distribution (PSD) was tested to BSI (1990) and the soil classified as uniformly graded (Figure 4-2) having mean particle diameter D_{50} 0.147mm, D_{60} and D_{10} of 0.15mm and 0.098mm respectively. A details of HST95 sand properties are provided in Table 4-1. The coefficient of uniformity (C_u) was 1.5. In centrifuge model testing it is important to ensure that adequate scaling is applied a new value of D_{50} so that sufficient particle contacts are maintained at critical interfaces to adequately capture the correct soil-pipe response. According to Madabhushi (2014), as long as the ratio of pipe diameter to soil particle size is greater than 20, the relationship is valid. However, Iglesia et al. (2011) states that the scaling ratio, D_p , (pipe diameter to soil particle size) should be greater than 30. The scaling ratio here, preserved is in excess of 100 (D_p/D_{50}) thus no adverse interaction observations should occur.

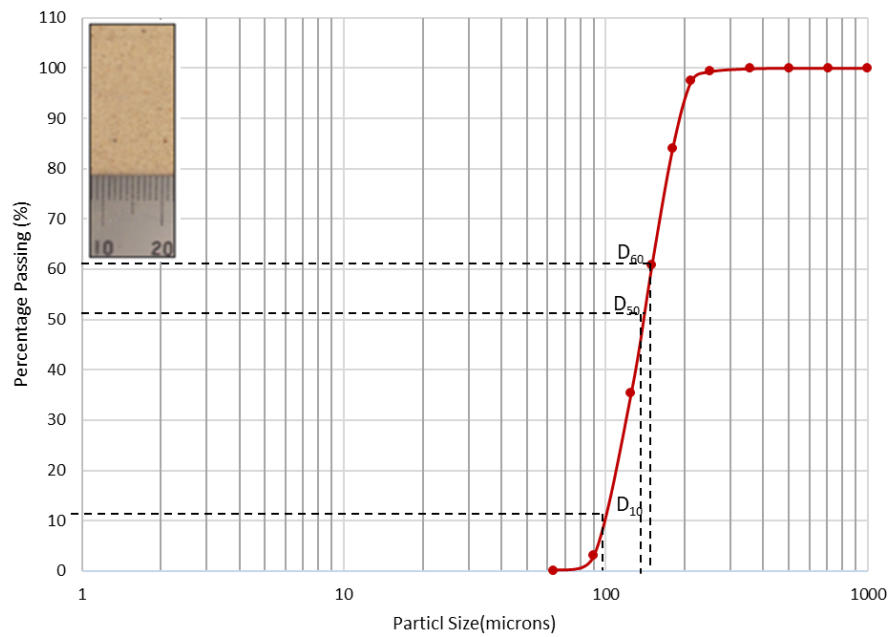


Figure 4-2 Particle size distribution curve of HST95 sand

4.2.1.1.2 Maximum and Minimum Void Ratio Test

It is standard practice to use a vibratory table to determine density characteristics of soils according to ASTM.D4253-16E1 (2006). This was used to find the maximum index density and unit weight of the HST95 sand. These tests were conducted in order to assess the density range of the sand to enable realistic pipe burial conditions to be simulated in the centrifuge experimental tests. The tests were conducted with the sand in a dry state thus only the minimum and maximum dry bulk density are reported that correspond to loose and dense placement conditions. Three repeated tests were conducted for both loose and dense conditions whereby average bulk densities of 1450 kg/m³ and 1750 kg/m³ were determined respectively. The specific gravity, G_s , of the HST95 silica sand is 2.65. This was also found to be the case in Bayton et al. (2018a). Likewise, the minimum and maximum void ratios, e_{min} and e_{max} respectively, are calculated using and was found to be 0.514 and 0.827 respectively.

Table 4-1 Properties of HST95 silica sand

<i>Property</i>	<i>Value</i>
<i>Particle size D_{10}</i>	<i>0.098</i>
<i>Particle size D_{50}</i>	<i>0.147</i>
<i>Particle size D_{60}</i>	<i>0.15</i>
<i>Specific gravity</i>	<i>2.65</i>
<i>Maximum void ratio</i>	<i>0.872</i>
<i>Minimum void ratio</i>	<i>0.514</i>
<i>Sand-Sand Peak angle of shear, φ_{peak}</i>	<i>37.5° (at $R_d=80\%$)</i>
<i>Sand-Pipe Peak angle of shear, φ_{peak}</i>	<i>19° (at $R_d=80\%$)</i>
<i>Maximum bulk density</i>	<i>1750kg/m³</i>
<i>Minimum bulk density</i>	<i>1450kg/m³</i>

4.2.1.1.3 Direct Shear Test

The shear strength characteristics were evaluated using direct shear tests in accordance with BSI (1990). The material was tested at a range of applied normal stresses and densities to simulate typical vertical stress conditions acting on the pipe in service. The experimental test, described later in this section and conceptually shown in Figure 4-3, considered a pipe burial depth of 1m in sand density of 1600 kg/m³, yielding a static vertical stress soil stress (σ_v) of 15.6 kN/m² acting at the pipe burial depth (Equation 4-1).

$$\sigma_v = \gamma * Z \rightarrow 1600 * 1.00 * 9.81 / 1000 = 15.6 \text{ kN/m}^2$$

Equation 4-1

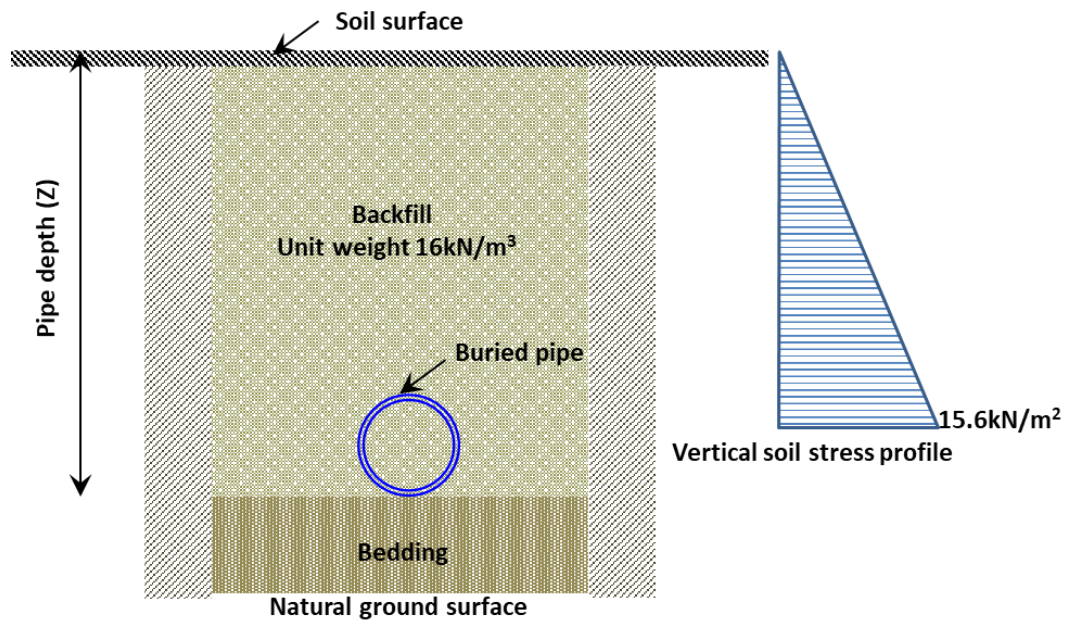


Figure 4-3 Idealised ground stress condition

A range of normal stresses of 7.5kN/m^2 to 100kN/m^2 was used to simulate a range of ground stress conditions reflecting the static stress (15.6kN/m^2) and up to a nominal traffic loading (100kN/m^2). The specimen was sheared at a rate of 1mm/min . Tests were also conducted as part of this investigation to determine the interface shear characteristics between the soil and pipe material. Interface tests were conducted by placing a square sheet of the pipe material into the lower section of the box while the granular material is sheared across the surface (Figure 4-4) to estimate a frictional interface coefficient. Measurements of force, horizontal and vertical displacement are recorded (Figure 4-5) and interpreted as shear stress, shear strain and vertical strain.

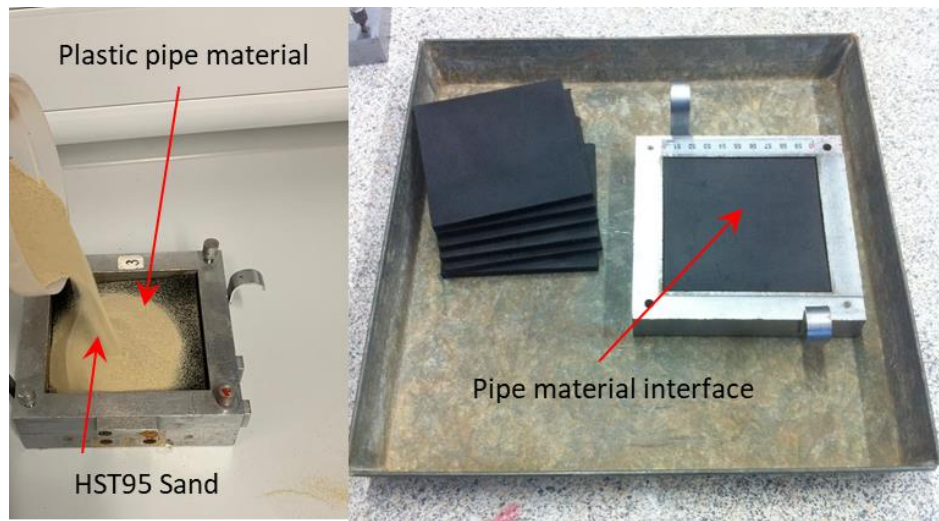


Figure 4-4 Soil-pipe interface shear test

Figure 4-5 and Figure 4-6 present the shear force to shear strain relationship and volumetric response for the HST95 sand shear tests at the stress range of normal stress 7kN/m^2 to 100kN/m^2 . Correlating the shear stress and applied normal stress enables the angle of shearing resistance to be evaluated. Figure 4-9 plots this relationship whereby a friction angle of 37.5° is found. This is consistent with shear angles reported for similar rounded HST95 sand (Bayton et al., 2018a).

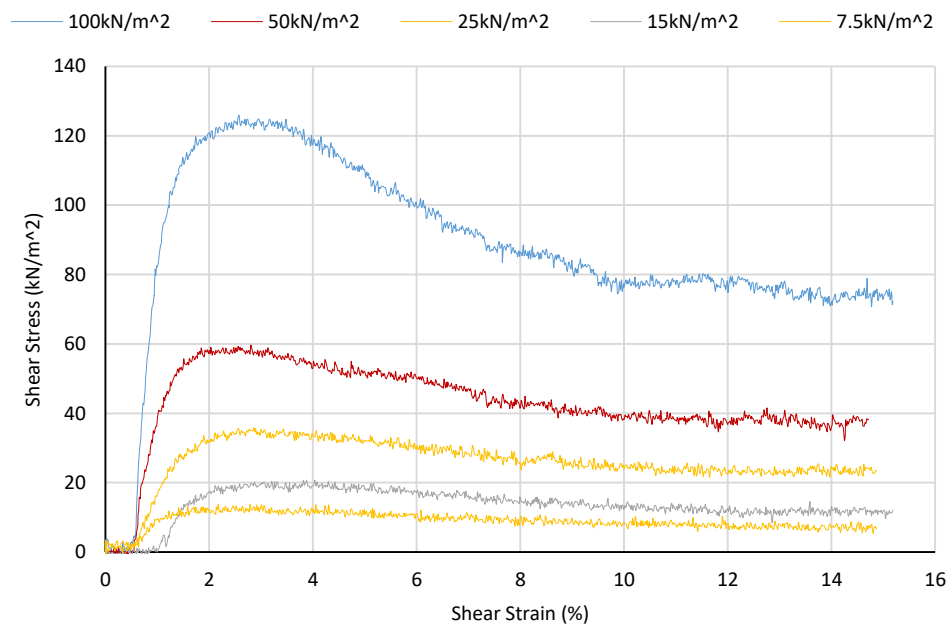


Figure 4-5 Shear stress- Shear strain response for sand-sand

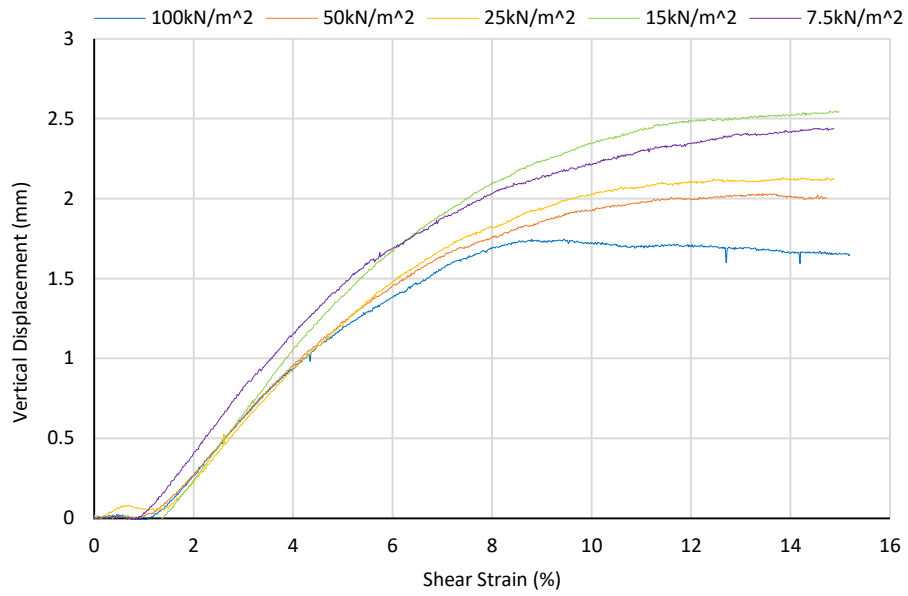


Figure 4-6 Volumetric response during sand- sand shearing

Figure 4-7 and Figure 4-8 present the shear force to shear strain relationship and volumetric response for the HST95 sand to pipe interface shear tests at the normal stress of 7.5 kN/m² to 100 kN/m².

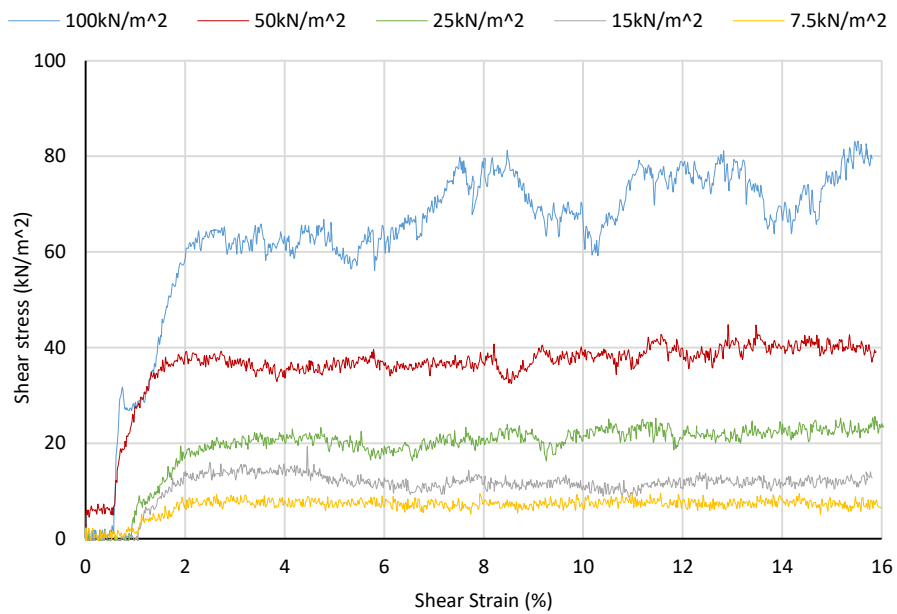


Figure 4-7 Shear stress- Shear strain response for sand-pipe

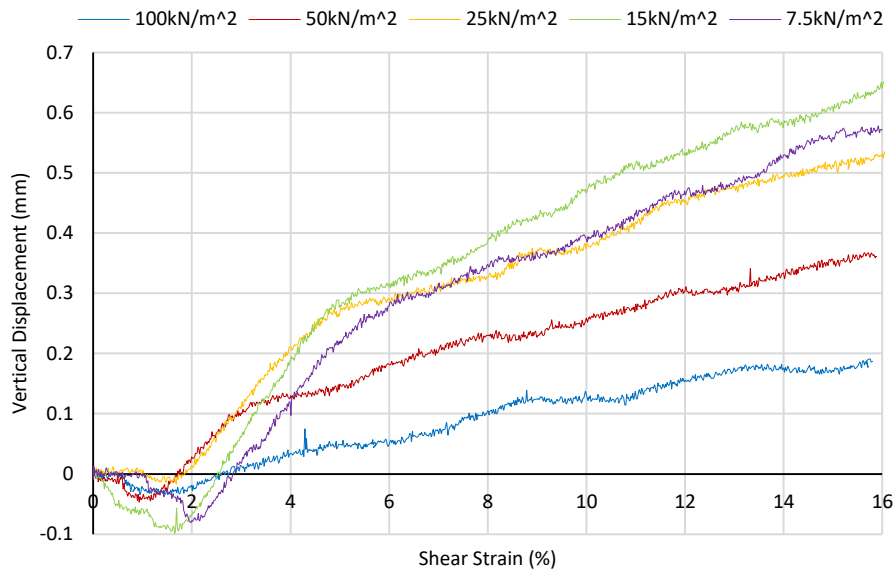


Figure 4-8 Volumetric response during sand-pipe shearing

The angle of friction from the shear stress and applied normal stress between the sand and pipe yields an angle of shearing resistance of 19° for a mobilised resistance of 1% strain. It is clear in Figure 4-9 that the friction angle is considerably lower for the soil-pipe interface compared to that of the soil on its own. This is due to sliding and lack of interlocking of sand particles in the shear zone along this rigid interface. This is consistent with shear interface angles reported by Negusse et al. (1989) and O'Rourke et al. (1990) in literature for other buried geotechnical structural interfaces.

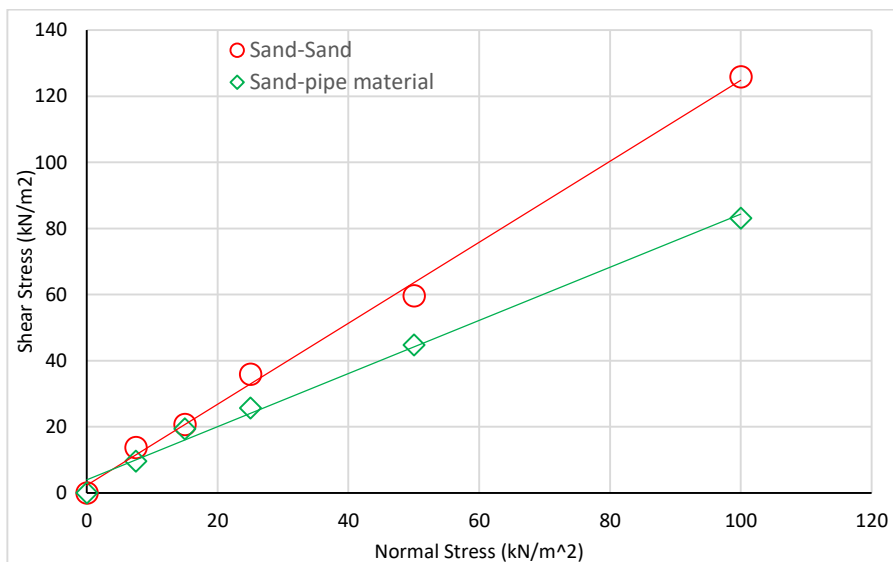


Figure 4-9 Sand-sand and sand-pipe friction angle

4.2.1.1.4 Oedometer Test

One dimensional compression tests were carried out in the oedometer according to BSI (2017), to examine the stiffness of the soil. Soil was placed at close to the target density as would be used in the model tests and subjected to increased vertical load to determine the compression characteristics. Loading and unloading were conducted. The specific volume against the natural logarithm of the stress during the test as shown in the Figure 4-10.

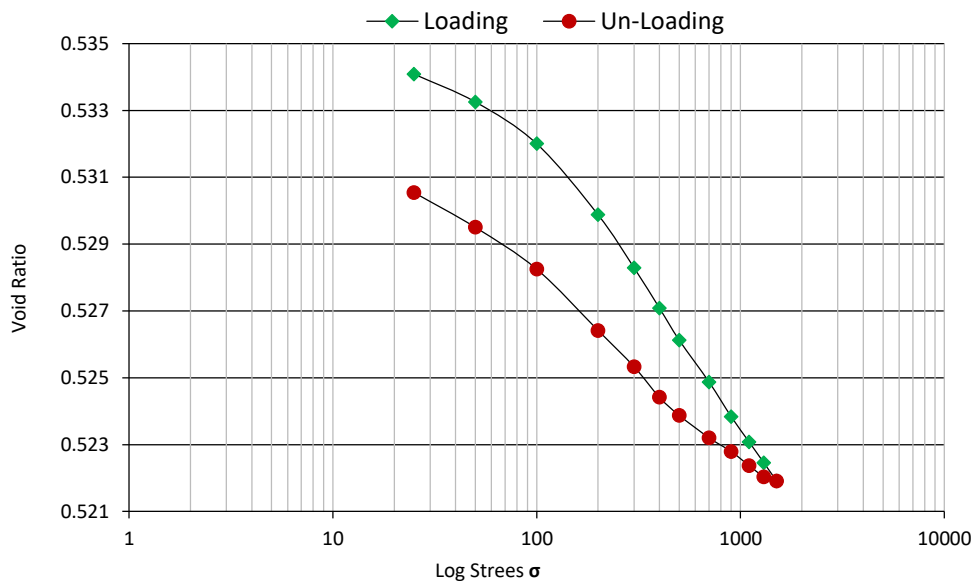


Figure 4-10 Oedometer test for HST95 silica sand

The Young’s Modulus (also known as the secant modulus) for the Oedometer test, E_{oed} , was calculated by determining the slope between the different points using Equation 4-2:

$$E = \frac{E_{Oed}(1+\nu)(1-2\nu)}{1-\nu} \rightarrow E_{Oed} = \frac{E(1-\nu)}{(1+\nu)(1-2\nu)} \tag{Equation 4-2}$$

Where ν is Poisson’s ratio, E is Young’s Modulus and E_{oed} is the Young’s Modulus based on the Oedometer test data.

4.2.1.2 Pipe Properties

A standard tensile test was used to determine the properties of PE100 pipe material, in particular the Young’s Modulus (E) of the pipe materials according ASTM.D638-02a (2002). Although a data sheet was provided from the manufactures, the accuracy of the wall thickness of the pipe was not 100% constant. For this reason, four lab tests were conducted in order to compare the manufacture properties with the lab result. A Shimadzu testing machine has been used for this purpose. Three test samples 420mm long were cut from the same PE100 plastic pipe as the modelled pipe. A groove was machined at the middle of the sample length around the outside of the sample so that the wall portion after machining was 60% of the initial nominal wall (see Figure 4-11). The ends of the pipe were threaded so that an aluminium end-piece could be attached to connect the sample to the testing rig, Figure 4-12.

Figure 4-13 presents the results of the tensile tests summarised in Table 4-2. The value of the Young’s Modulus (E) was found to be 877MPa, which is comparable to the manufacture’s specification (900MPa).

Table 4-2 Ultimate strength test results for PE100 plastic pipe

Test Number	Length of the Specimen L (mm)	Original Pipe Diameter D (mm)	Ultimate Tensile Strength E (MPa)
T_1	420	16	891
T_2	420	16	867
T_3	420	16	879
T_4	420	16	872
Average of Ultimate Tensile Strength (E_{avg}) 877 MPa and Standard deviation(DS) 12.9			

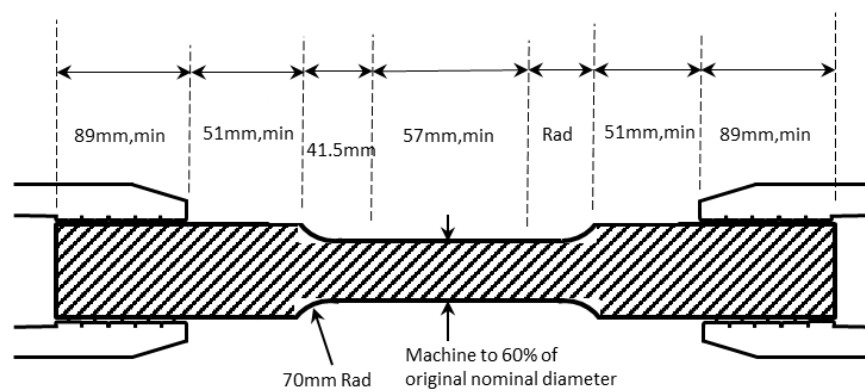


Figure 4-11 Dimensions of pipe specimens

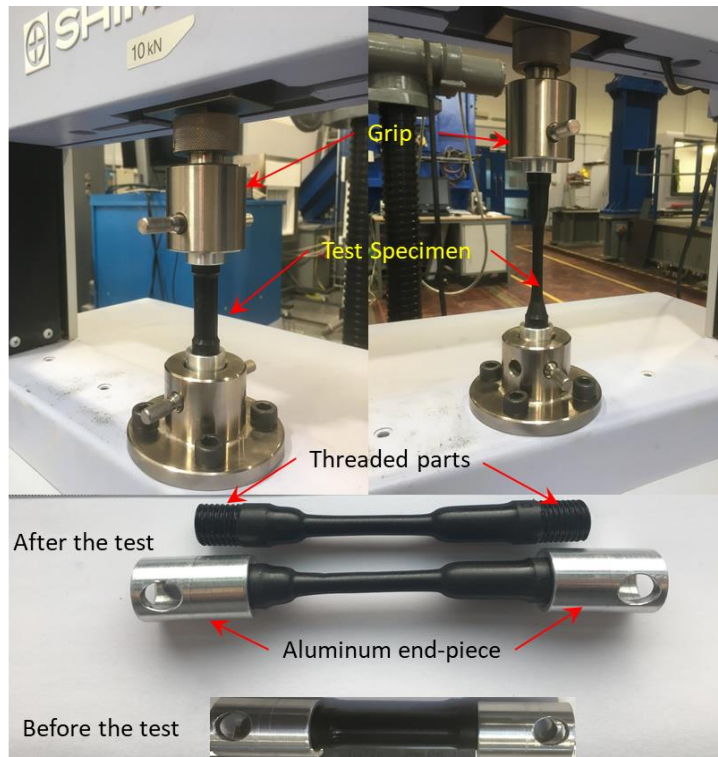


Figure 4-12 Test machine and sample shape

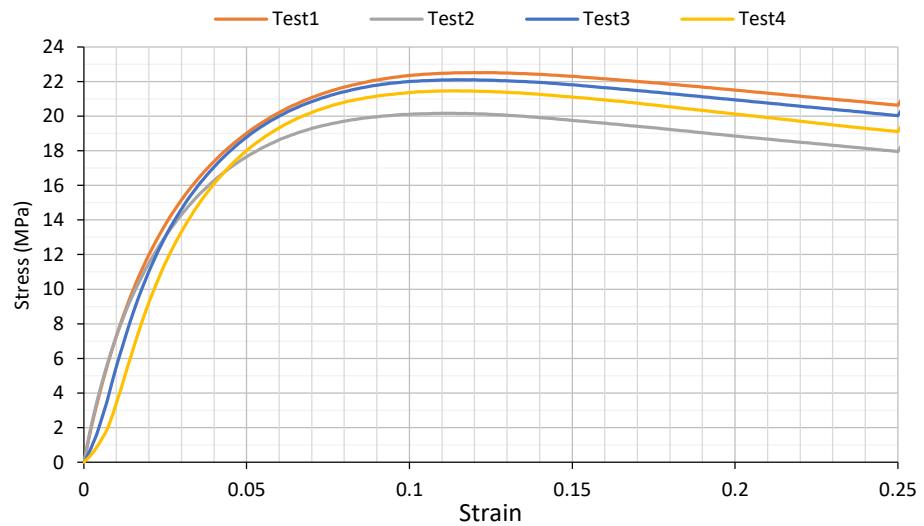


Figure 4-13 PE100 plastic pipe tensile test results

4.2.2 Model Design

4.2.2.1 Modelling of the Pipe

Water supply networks have undergone great development, especially in the second half of the 20th century when science and technology allowed the development and production of plastic, which became the main materials of the pipes used in water supply networks. High-density polyethylene (HDPE) is the most suitable and currently used plastic material for the production of pipes for water transmission in modern water supply systems. The obtained pipes and fittings are distinguished by a long service life, low maintenance costs, remarkable strength and low weight. HDPE pipes have many advantages over the classic pipes used so far (Vlase et al., 2020).

In this research the prototype (full size) pipe investigated was a 315 mm diameter (D_p) and 6 m length High Density Polyethylene (HDPE). These types of pipe are frequently used in the water utilities services for new network installations or renewals. This pipe is typical of a non-trunk water main deployed in the UK. However, the model pipe needed to be scaled down to mimic the prototype pipe. The scaled down model pipe, PE100, has diameter of 16.7 mm, based on smaller pipe section available commercially. This dictated the scaling– i.e. $315 / 16.7 = 18.9 \sim N$; hence, $N=19$ for the centrifuge tests.

In order to capture the appropriate pipe bending response, considerable effort has been focused on ensuring similitude between the observed model pipe and the flexural stiffness of the prototype. In practice, a 315 mm diameter HDPE has a nominal wall thickness of 28.6 mm, Young's Modulus (E) of 0.90 GPa and flexural stiffness of 26.7 kN.m². In order to establish similarity between the model pipe and prototype, representative-bending stiffness must be considered. As bending stiffness is a function of sectional area, the same material of prototype pipe sometimes cannot be used in the model as in practice and therefore it is typical to select an alternative material for the model. The alternative material may have different properties (strength and inertia) and therefore exhibit the same bending stiffness response. Sometimes the wall thickness of the pipe needs to be reduced down or machined in order to get the similar flexural stiffness of the prototype material by using scaling laws in Chapter 3. It was explained in Section 3.3 and Figure 3-6 how the pipe wall thickness differs between the prototype and model and shows how wall thickness can be different. The relationship between the diameter of the pipe and area moment of inertia is known. Hence flexural stiffness between the model and prototype is expressed as previously shown in Equation 3-11.

Since replication of the correct elastic response of the pipe is of importance, the model pipe using Poly Ethylene100 (PE100) had a different wall thickness to pipe diameter ratio than that of the prototype (HDPE). Referring to scaling laws presented in Table 4-3, bending stiffness of the prototype are related by $1/N^4$; hence, an appropriate model pipe geometry and material were selected to provide similitude. A comparison between both material properties of the pipe shows that there is a small error between the

prototype and replicated model due to the usage of scaling laws to non-accurate pipe wall thickness. This is reasonable as long as the $E_p I_p = E_m I_m$ (see Fig 4-14 and Equation 4-3). So it can be said that the model pipe sufficiently represents the behaviour that would be experienced by the prototype.

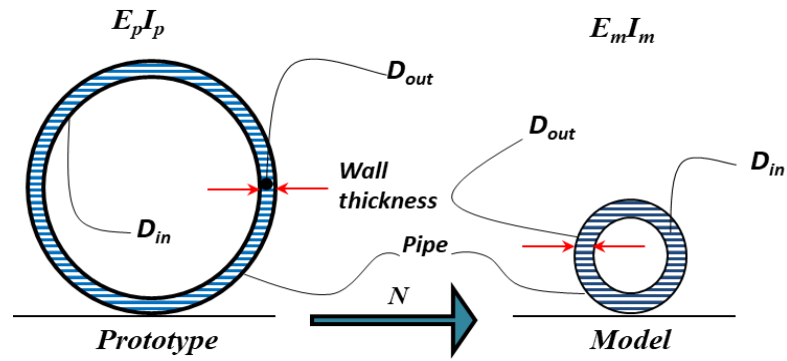


Figure 4-14 scaling concept for plastic pipe

$$\frac{(EI)_m}{(EI)_p} = \frac{1}{N^4} \longrightarrow E_{model} = \frac{(EI)_p}{N^4 I_m} \quad \text{Equation 4-3}$$

Table 4-3 Comparison of properties between prototype HDPE and the model for PE100

Setting	Prototype	Model required	Model available
<i>Material</i>	<i>HDPE</i>	<i>PE100</i>	<i>PE100</i>
<i>N</i>	<i>9.81g</i>	<i>19g</i>	<i>19g</i>
<i>E (MPa)</i>	<i>900</i>	<i>900</i>	<i>885.6</i>
<i>D_{outer} (mm)</i>	<i>315</i>	<i>16.58</i>	<i>16</i>
<i>D_{inner} (mm)</i>	<i>257.8</i>	<i>13.57</i>	<i>12.4</i>
<i>Wall_t (mm)</i>	<i>28.6</i>	<i>1.50</i>	<i>1.80</i>
<i>SDR=D_{outer}/wall thickness</i>	<i>11</i>	<i>11</i>	<i>9</i>
<i>I (mm⁴)</i>	<i>2.88e+8</i>	<i>2.04e+3</i>	<i>2.06e+3</i>
<i>EI (N.mm²)</i>	<i>2.40e+11</i>	<i>1.84e+06</i>	<i>1.85e+06</i>
<i>Scaling law for EI</i>	<i>1</i>	<i>1/19⁴</i>	<i>1/19⁴</i>

4.2.2.2 Road Surface

Pavement structures can either be rigid or flexible. The wearing surface of a rigid pavement is typically composed of Portland Cement Concrete (PCC). On the other hand, flexible pavements are made of asphalt (or bituminous). The large flexural strength of this material will allow the surface to act as a beam, bridging over any minor irregularities that may occur in the base or soil beneath. In the UK, roads are typically classified as flexible and fabricated from a tarmac surface (approx. 50mm thick) with multiple subgrade layers (up to 300mm thick); such that distortion or displacement occurring at the surface is reflected in the lower layers (Yoder and Witczak, 1991) .

According to Yoder and Witczak (1991), surface loads are spread over a wide area within the subgrade, and thus the stresses with depth are reduced. Hence, conventional flexible-pavement design, through which subgrade materials that have a low bearing capacity are covered with thick flexible-pavement structures, assumes a decreasing stress with depth. If real pavement or road surfaces are to be modelled, representing the bending stiffness of these materials may also need to be taken into account. Therefore, inclusion of a separation layer beneath the simulated load footprints was deemed necessary to minimise rutting/penetration of the ‘wheel’ into the sand, especially during cyclic tests.

Preliminary trials using Plaster-Of-Paris were attempted to model a road interface as if was felt this may be suitable as the stiffness properties can be tailored according to the binder content, however, cracking was observed in the miniature pavement and this was difficult to implement. Thus, it was decided to

use a thin rubber disk, of Shore resistance D to represent the road stiffness according to Equation 4-4. This was placed locally beneath the ‘wheel’ footprint area to replicate the transition pavement stiffness and prevent penetration into the soil in all tests and proved highly successful. The impact of a more stiff pavement was also considered in a limited number of tests whereby an additional rubber sheet (also Shore Resistance D) was placed between the ‘wheel’ and soil. Results of this are discussed in Section 6.3.1.5 and 6.3.1.6.

$$EI = \frac{bh^3}{12} \quad \text{Equation 4-4}$$

4.2.2.3 Modelling of the Void

In practice, voids can occur in the fill material owing to a number of possible processes, for instance washing out of fines through the process of suffusion, moisture changes from fluctuation of the ground water table and surface infiltration and pipe movements. Irrespective of the mechanism by which a void may form, if they occur in the vicinity of a pipe it will result in a localised loss of support which will only serve to increase the potential for pipe deformation under applied vertical surface loading.

The formation of a ‘real-time’ void in a centrifuge model by any of the above processes presents a considerable technical challenge. Mair (1979) pioneered the method of deflating a fluid filled “bladder” or membrane to simulate sub-surface volume loss in tunnelling applications. A similar approach of using suction to remove localised pockets of soil could also be feasible, but this was not guaranteed to leave a void, as soil would flow into the space. Sales et al. (2015a) conducted trial tests using ice in an attempt to provide an alternative means establishing a real-time propagating void in the soil. The hypothesis of this method was to build and spin the model in elevated gravity, with an ice block buried at the desired void location. The void would then then be formed by self-weight arching stresses aided by suction from residual water once the ice block melted. This method proved reasonably successful for small void sizes, however the formation of larger voids which were bigger than the pipe diameter, as frequently reported in practice, were not possible. Furthermore, a major challenge would be to complete construction and spinning of a larger model before the buried block of ice formed by self-weight arching stresses in the sand once the ice thawed.

A more representative approach would be to not model the complex process of void formation, but rather to recreate the conditions in the soil when a void is formed. Specifically, a void may be considered to be a region offering comparatively low (or zero) support to the pipe. Sales et al. (2015a) successfully

implemented a similar concept to fulfil these basic void criteria in the model tests by using a soft sponge (artificial polymers). The sponge was cut into different spheres or increasing geometry to simulate larger voids. This offered the ability to provide suitable support to hold back the sand material in a desired void geometry while providing a region of almost zero support in the proximity of pipe. Using this approach, spherical void geometries of 2 to 5 times the pipe diameter were created in the model that were representative of ‘wished-in-place’ conditions. This could be highly beneficial when compared to numerical model studies. A similar approach was adopted in this work, with the sponge being placed where voids were desired to be created. Different types of void were modelled in the experiment. The length that the void ran parallel with the pipe was kept constant at a size of $3D_p$ ($D_p=16\text{mm}$ model scale) where (D_p) is the diameter of the pipe, however the width was varied between $0.5D_p$, $1D_p$ and $2D_p$. Figure 4-15 shows an example of a rectangular prism (rectangular cuboid) of sponge used to replicate voids in the model and Figure 4-16 shows the sponge location.

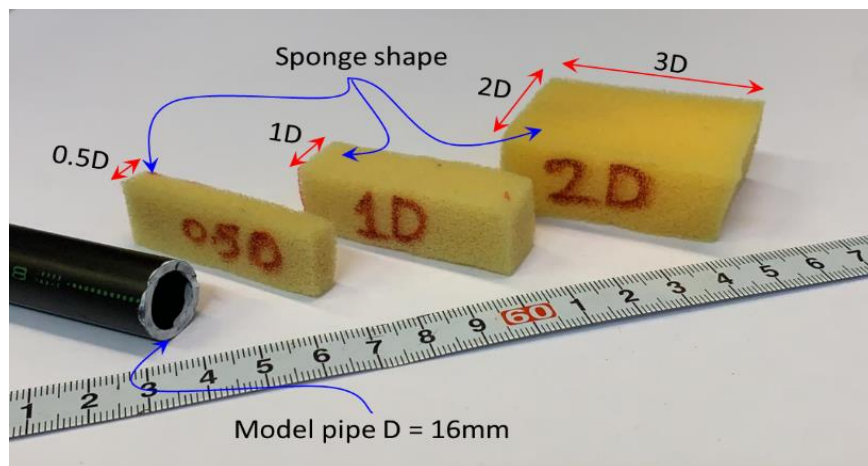


Figure 4-15 Rectangular prism of sponge used to replicate voids in the model

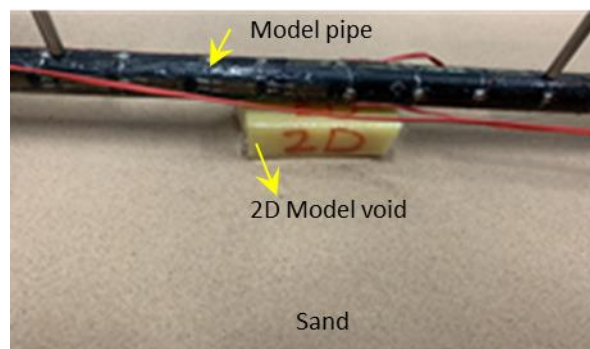


Figure 4-16 Model sponge location

4.2.3 Mechanical Design

4.2.3.1 Strong Box Design

In order to investigate the behaviour of the pipe-soil interaction in the model, and before embarking on any centrifuge experiments in CEIGR, a well-designed strong box (soil container) was required. Therefore, before designing a new model container, there are many aspects to consider. For example, there are accepted structural aspects of the container with a consideration of centrifuge flight. The soil container is very important to limit deflection and accommodate the high lateral stresses invoked by the increased acceleration field. Also, the model container (centrifuge modelling chamber) must withstand large soil and water pressures safely. To ensure the safe design, a hand calculation and numerical simulation has been done (see appendix A). The design of the strong box had sufficient dimensions to minimise boundary issues. In order to not induce any unwanted boundary effect which may affect the pipe-soil interaction, it was decided to place the pipe in a distance of not less than $14D$ from the base of the box and the internal face of the box.

The design of the strong box consisted of using high-strength aluminium alloy (Al-6061 T6); Proof Stress = 290 MPa; $E = 70$ GPA with an inner dimension of 600mm length (L), 400mm width (W), 400mm height (H) and 30mm wall thickness (t). Five plates were assembled to create the final shape of the strong box. The plates have been clamped together by using 46 M10 bolts. A 10mm diameter hole was machined in the top face of each plate to allow the loading frame to be fixed at the desired position as shown in Figure 4-17. The strong box itself was fixed by 4 M20 bolts from the box's base plate to a square mounting plate of dimensions of 800mm length (L), 800mm width (W) and 30mm thickness (t) that interfaced with the centrifuge platform. Figure 4-17 shows a photo of the designed model box.

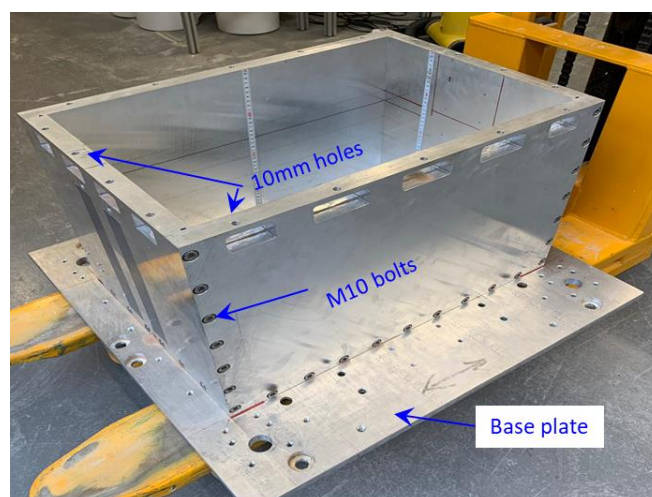


Figure 4-17 Strong box centrifuge model (CEIGR)

4.2.3.1.1 Influence of Boundaries

Another important factor that had to be considered were the boundary effects. By using a strongbox as a container, the area and depth for the soil layers were confined. This meant that if the increased stress field propagates to sides of the strongbox, the wall of the strongbox will modify the stress conditions of the soil due to their significantly higher stiffness. Vertical stress dissipates in the soil at an approximate ratio of 2V:1H (AASHTO, 2010) (see Equation 4-5) . Figure 4-18 shows that the area of the soil that experienced a change in stress is not near the wall of the strongbox, therefore the boundary effects are negligible. However, to avoid any boundary condition issues, the model pipe was placed 14D_p away from the base plate and proximately 12D_p away from each side wall (Schofield, 1980).

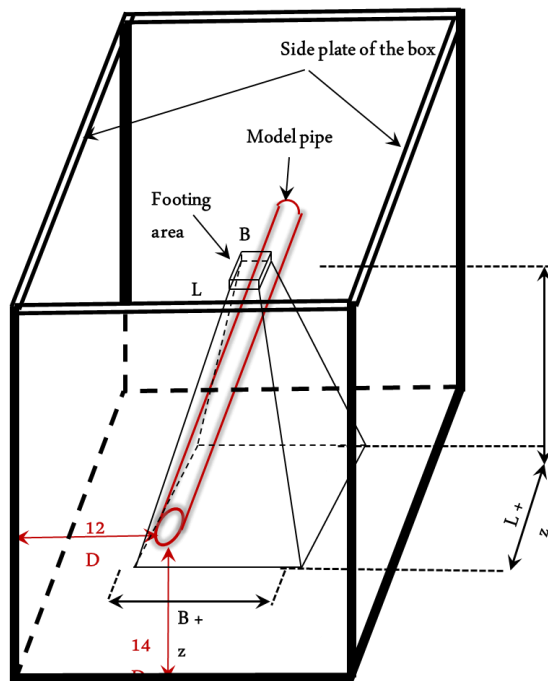


Figure 4-18 Approach used to show vertical stress increase in soil (2V:1H)

$$\Delta\sigma_z = \frac{Q}{(B + z)(L + z)} \quad \text{Equation 4-5}$$

where $\Delta\sigma_z$ is change in total vertical stress, Q is applied load, B is the footing width and L is the footing length.

4.2.3.2 Surface Loading System

Although the loads from vehicle wheels may be frequent, these loads typically have little effect on buried pipes underground compared to loading from trucks or other heavy vehicles that is less frequent but substantially heavier. Only the loading from these heavier vehicles is considered for the design of pipes under roads and highways. Therefore, the pressure that a vehicle transmits to a pipe depends on the depth of the pipe, the weight of the vehicle, the pressure of the tire and size of the tyre, the speed of the vehicle, the smoothness of the surface, the quantity and form of paving, the soil and the distance from the pipe to the loading point. Usually, vehicle loads are based on the American Association of State Highway and Transportation Officials (AASHTO) standard truck / lorry loadings or British Standards (BSI,1991-2). Using AASHTO standards, the loading is usually assumed to be a H20 (HS20) truck to estimate the soil pressure on the flexible pipe. Referring to Figure 4-19 the main wheel load is located at the rear axle(s) for these trucks and is equal to 40% of the truck's total weight. The monotonic load (static load) case is to confirm the capacity of the system. The load magnitude was applied according to AASHTO standards (6 tonnes, half-axial load or 12 tonnes, full-axial load) in the prototype scale which was sustained for a duration of approximately 180 seconds.

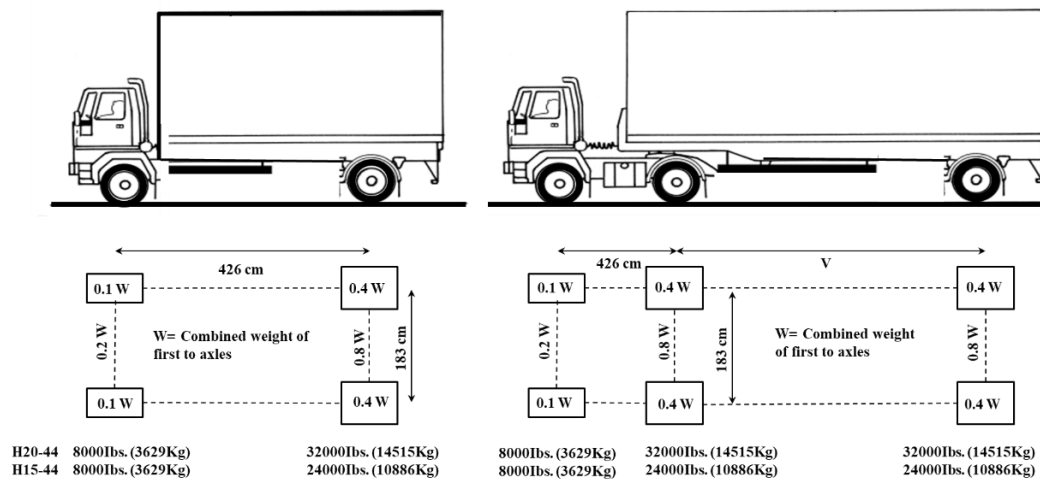


Figure 4-19 AASHTO H20 and HS20 wheel loads

The live load pressure is usually determined from the vehicle manufacturer's information on vehicle weight or wheel load, tyre contact area and wheel spacing. Additionally, the location of the wheels on the vehicle relative to the pipe is an important factor to determine how much load is transferred to the pipe (Smith and Dickson, 1990) . Two-wheel loads straddling a pipe can produce a higher pressure on

a pipe than direct load above the pipe from a single wheel. Timoshenko (1953) describes the soil pressure at a point directly under a distributed surface load, neglecting any pavement (see Figure 4-20), whereas Boussinesq gives the pressure under a concentrated surface load at any point in the soil mass as illustrated in Figure 4-21. Therefore, the Boussinesq equation can be used to find the transmitted pressure from a wheel load to a point that is not along the load's line of action. The impact of the pavement is neglected; see Figure 4-20 illustration of Boussinesq point loading (AASHTO, 2010).

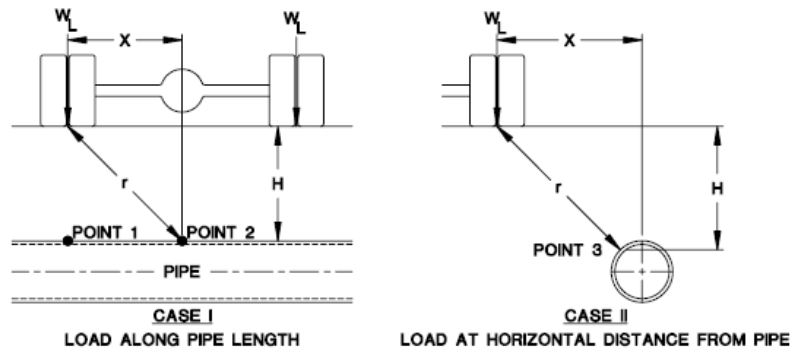


Figure 4-20 Illustration of Timoshenko soil pressure Timoshenko (1953)

Where is W_L wheel load (kN/m^2), H is cover depth (m), r is the distance from the point of load application to pipe crown (m).

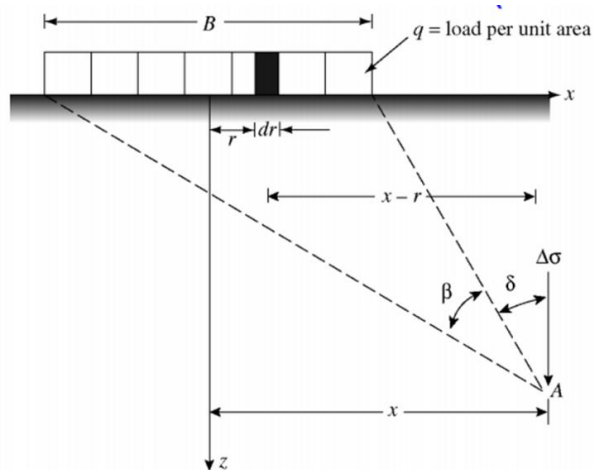


Figure 4-21 Illustration of Boussinesq strip loading (Boussinesq, 1885).

$$\Delta\sigma = \frac{q}{\pi} [\beta + \sin\beta(\beta + 2\delta)] \quad \text{Equation 4-6}$$

Where is $\Delta\sigma$ vertical soil pressure due to live load, q is load per unit area (kN/m^2), z is cover depth (m), x is distance from line load (m).

Since this research studied the aspects of soil-pipe interaction and performance of buried pipe infrastructure subjected to surface traffic loading, it was necessary to design the system which simulates an axle load from a typically articulated lorry with 44-ton load (12.5ton max permissible axle) AASHTO (2010). Surface loading conditions were via a rigid footing that had been manufactured using 6082 T6 aluminium material. The rigid footing parts were designed to be attached to the pneumatic compact cylinder’s pistons and create either dynamic loading or static loading. Figure 4-22 a & b show a single and double axle condition that have been used in the testing. The pneumatic compact cylinders were chosen carefully to simulate a single pair of axle wheels that represent the real lorry’s wheels according to the (AASHTO, 2010), article 3.30, based on assuming a single dual-tyre contact area of 500mm x 250mm and using the equivalent area method of load distribution. The real area was simulated as 13mm x 26mm at 19g. Figure 4-23 shows the typical articulated lorry and the wheel load surface contact area and the equivalent simulation wheels that have been designed specifically for this research.

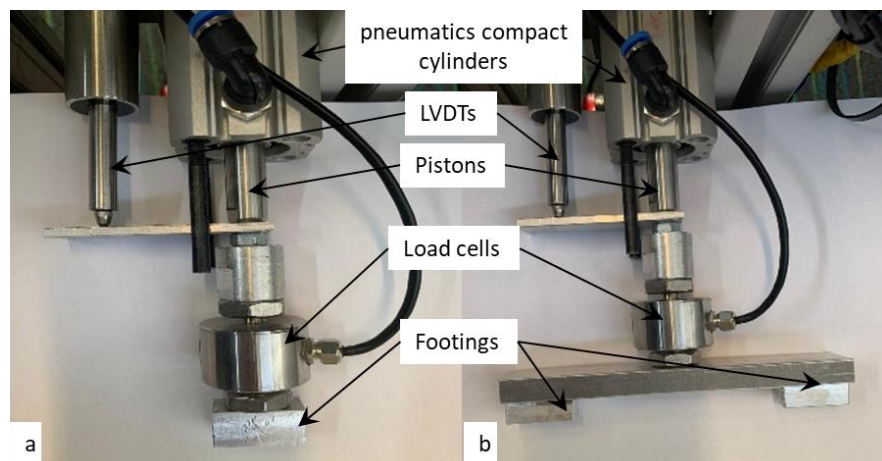


Figure 4-22 (a) Single axle footing (b) double axle footing

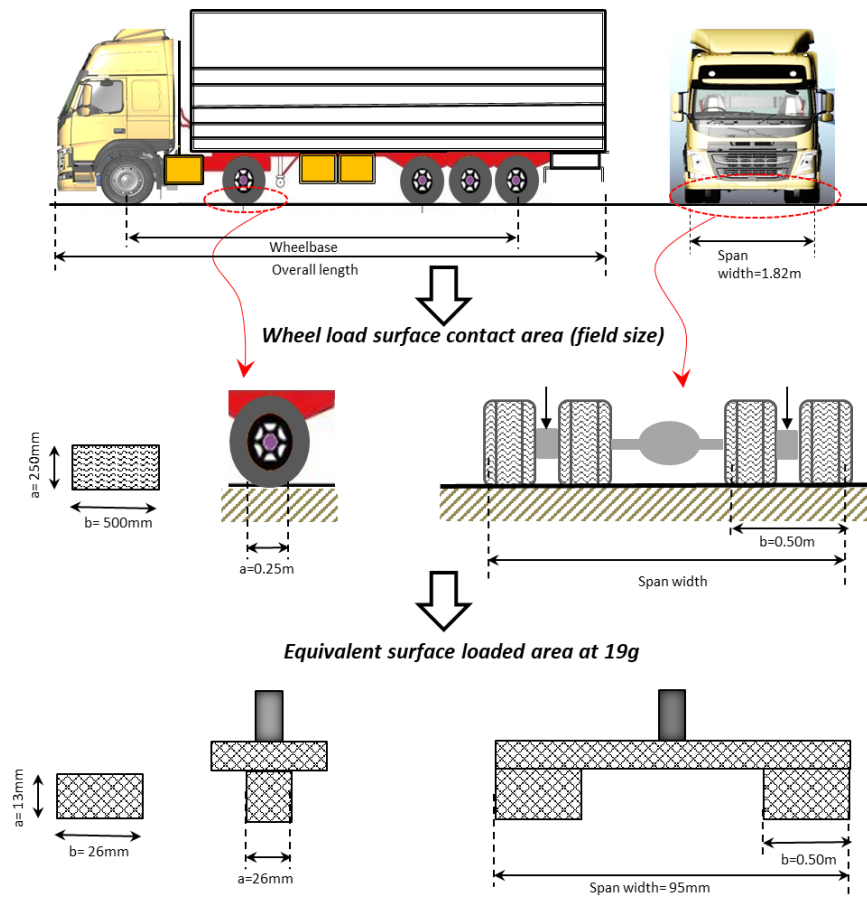


Figure 4-23 Wheel load surface contact area at 1g and 19g

An aluminium frame was designed to hold in place the instruments that are utilised to simulate the traffic loading, for instance, the pneumatic compact cylinder and the LVDTs which measure displacement. As a result of the high force generated from the pneumatic compact cylinder which represented frequent traffic loads, it was necessary to take into account the impact of these forces on the cross beam so that it was able to withstand these loads without any bending that might affect the results, especially the pipe settlements during the test. The aluminium frame is shown in Figure 4-24 and schematically in Figure 4-25, Figure 4-26 and Figure 4-27.

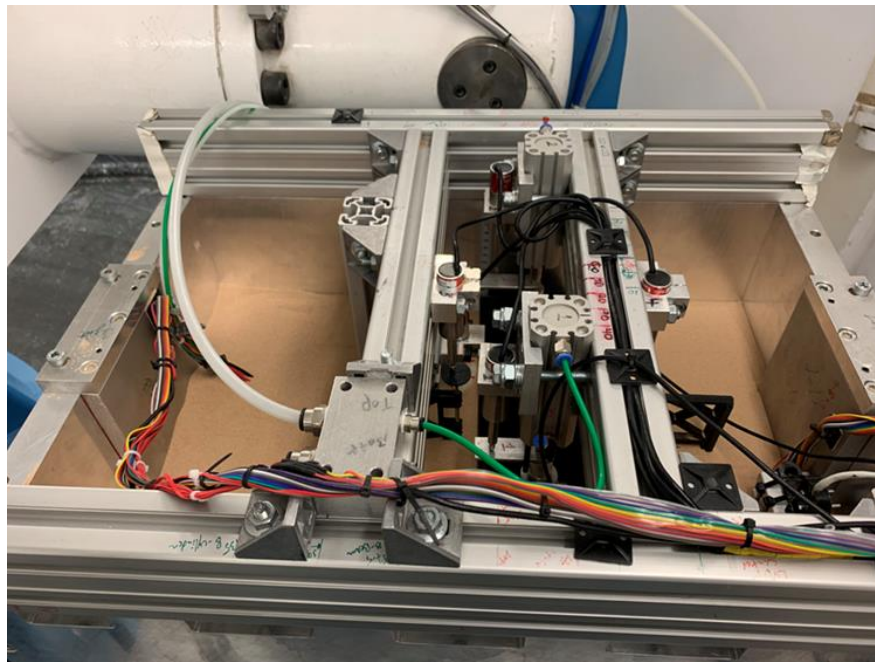
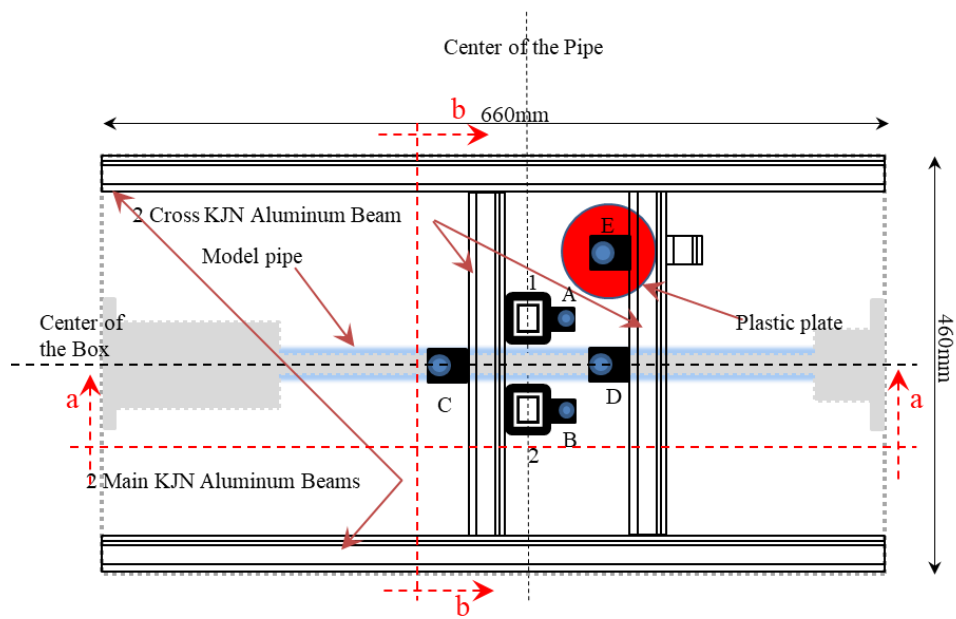


Figure 4-24 Aluminium frame mounted on the strong box



1&2 are the Pneumatics compact cylinder, A&B are the footing settlement LVDTs, D&C are the pipe settlement LVDTs and E is the soil settlement LVDT

Figure 4-25 Plan view schematic of the aluminium frame

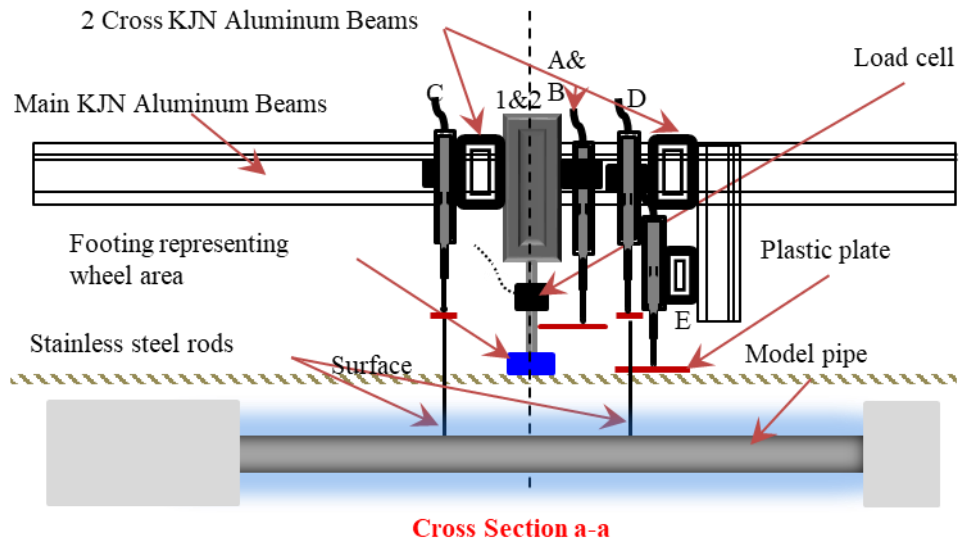


Figure 4-26 Cross section a-a schematic of the aluminium frame

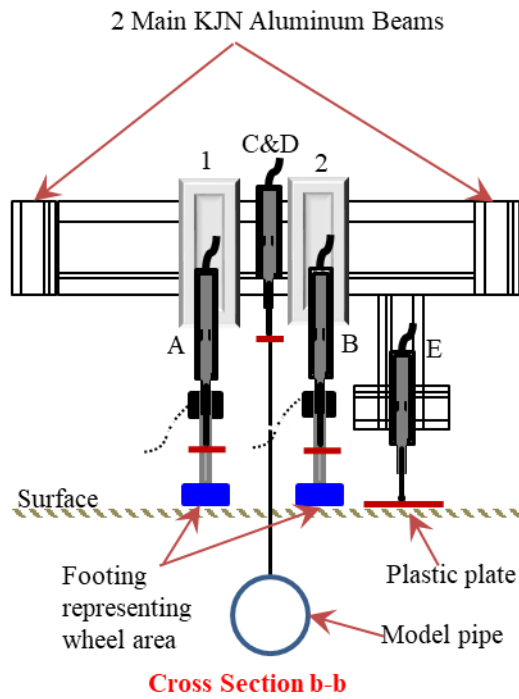


Figure 4-27 Cross section b-b schematic of the aluminium frame

4.2.3.3 Actuation Apparatus (internal water pressure)

It was necessary to design an apparatus capable of simulating the effects of internal pressurisation within pipe, and simulate the effect this physically has on the pipe. In the United Kingdom, water pressure in the distribution pipes ranges from 2 bar to 6 bar depending on the size of the pipe (Ofwat, 2020). Internal changes in pressure generate forces acting on the pipe circumference. As the pipe expands due to changes in internal pressure, axial forces are generated that generate changes in length due to the Poisson's ratio ν . This will give rise to tensile/compressive forces in the pipe if both ends are fixed, or the pipe is suitably restrained along its length by the soil backfill. The axial stress σ_z in the pipe with fixed ends are found using Equation 4-7 this is the same approach as shown in Figure 4-28. However, a different calculation was needed to obtain the hoop stress/ strain or the circumferential stress by using Equation 4-8. With consideration of an axial section of unit length, the force balance can be used in to determined how much force should be applied to the pipe using the new designed apparatus (Roylance, 2001).

$$p(\pi r^2) = \sigma_z(2\pi r)t \rightarrow \sigma_z = \frac{pr}{2t} \quad \text{Equation 4-7}$$

Where σ_z is stresses in the axial direction (N/mm²), p is Internal Pressure (N/mm²), t is wall thickness (mm), r is radius of the pipe (mm).

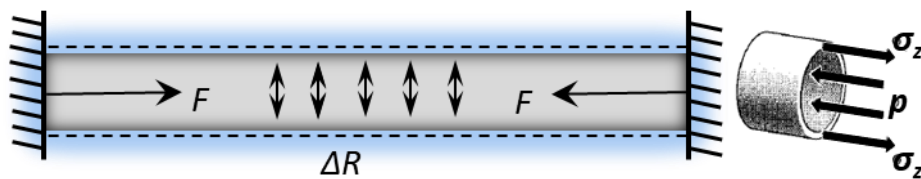


Figure 4-28 Axial stress end restraints on pipe

$$2\sigma_{\theta}(t.1) = p(2r.1) \rightarrow \sigma_{\theta} = \frac{pr}{t} \quad \text{Equation 4-8}$$

Where σ_{θ} is the hoop stress (N/mm²).

It can be seen from equations 4-7 and 4-8 that the circumferential or hoop stresses are twice the axial stresses. This difference of stress occurs more often than not in engineering structures, and shows one of the three compelling advantages for engineered material which can be made stronger in one direction than another (anisotropic property) (Roylance, 2001). The apparatus was designed to simulate the effect of changes in internal water pressure in the pipe by applying axial thrust force in the centrifuge tests. Appendix C shows the necessary calculation to have an optimum apparatus for water pressure simulation.

The axial loading system consists of two acrylic cylinders of 70mm diameter. Both cylinders were fixed by three bolts from end to end to two circle aluminium plates, each ends of the cylinders were mounted to a rectangular plate of aluminium which was located inside the strong box. The primary function of these two cylinders was to control the desired pipe boundary conditions and hold both ends of the pipe as well as to stop sand from getting inside the mechanism within the cylinders. The load apparatus, which were located inside the longer cylinder, consisted of a pneumatic compact cylinder with its piston connected to a steel rod passing through the pipe to its end. The steel rod worked by applying compression or tension to the pipe, according to the test scenario. Hence, its function simulated the the axial aspect of water pressure in the centrifuge experiments. Figure 4-29 shows a schematic of the actuation system apparatus and Figure 4-30 shows pictures of the device with details.

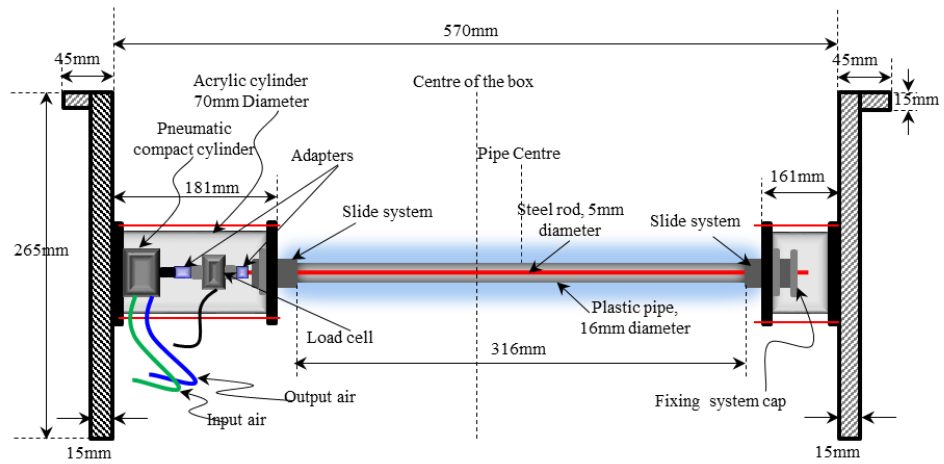


Figure 4-29 Schematic of the actuation system apparatus

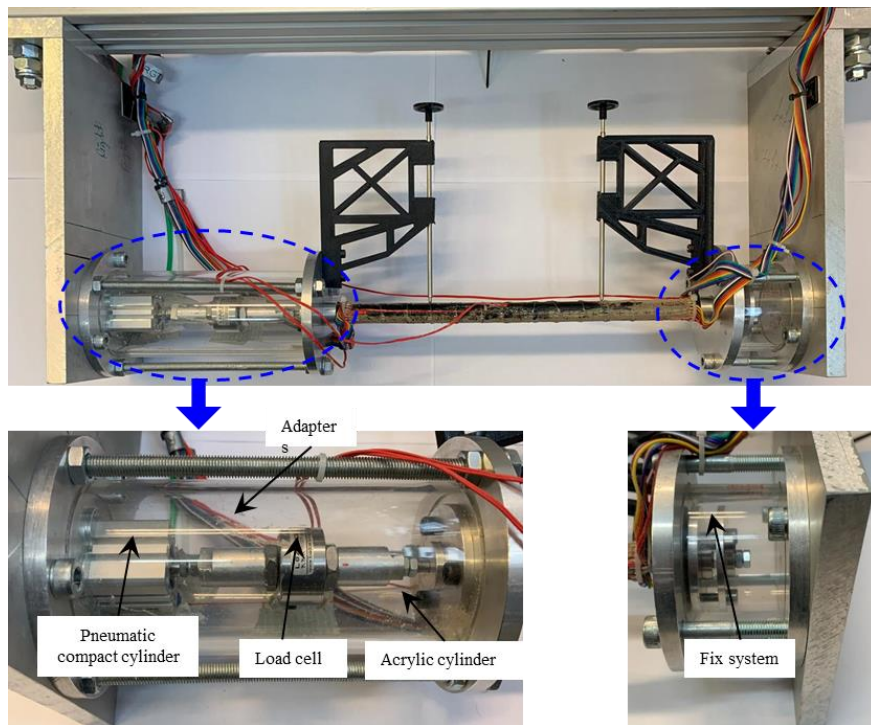


Figure 4-30 Actuation system apparatus

4.2.4 Instrumentation and Calibration

4.2.4.1 Displacement Measurement (LVDTs)

Five displacement sensors were used to record pipe deflection, footing displacement and soil settlement. The LVDT devices used in this research were a DCTH100AG with $\pm 0.25\text{mm}$ and sensitivity of 1950.9mV/mm supplied by RDP group. Calibrations were obtained using a LVDT calibration station with a typical calibration output shown in Figure 4-31. The sensors are highly linear and a summary of the 5 LVDTs are presented in Table 4-4.

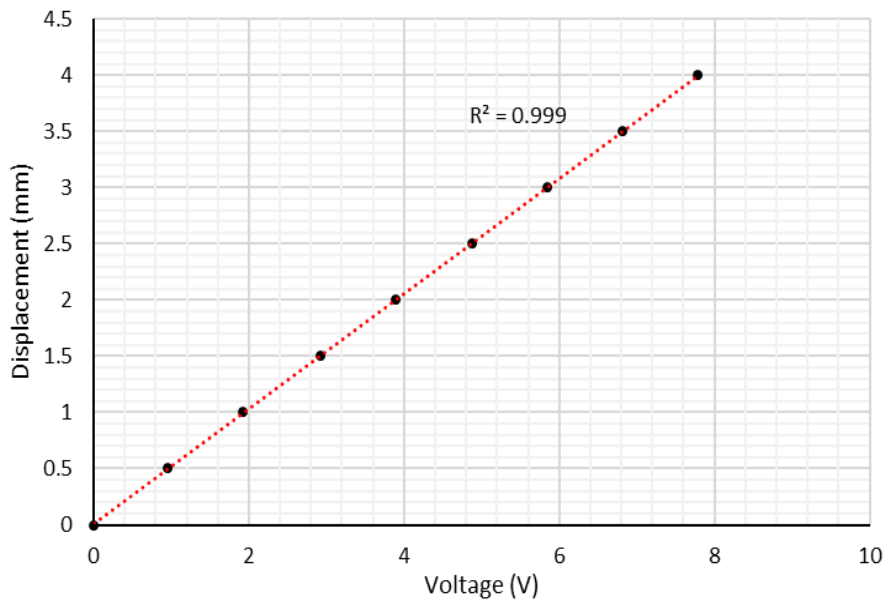


Figure 4-31 Graph showing line of best fit for LVDT calibration

Table 4-4 Summary of the LVDT calibration

LVDTs #	Calibration factor (mm/v)	Correlation coefficient, R ²
LVDT 1	-2.0861	0.976
LVDT 2	-2.0694	0.987
LVDT 3	-2.072	1
LVDT 4	-2.0905	0.999
LVDT 5	-2.0886	0.977

The LVDTs were mounted in five different locations using an aluminium holder that was fixed in a KJN aluminium profile frame on the top of the strong box. Two LVDT devices were installed at a distance of 1/3 of the pipe length and an extension from the head of the LVDT to the buried model pipe which allowed direct measurement of the buried pipe displacement. This extension had two parts, a steel feeler rod of length 150mm length and 2mm diameter topped with a flat circular cap, and hollow steel tube to allow the feeler rod to rest on the crown of the buried pipe.

Local soil settlement and simulated traffic settlement were also measured. A small circular footing was placed on the surface of the soil that ensured the LVDT tip did not penetrate the underlying soil, while the surcharge displacement sensors were connected to the pneumatic cylinders. The locations of the LVDTs are shown in Figure 4-32 shows more details of the location of the LVDTs.

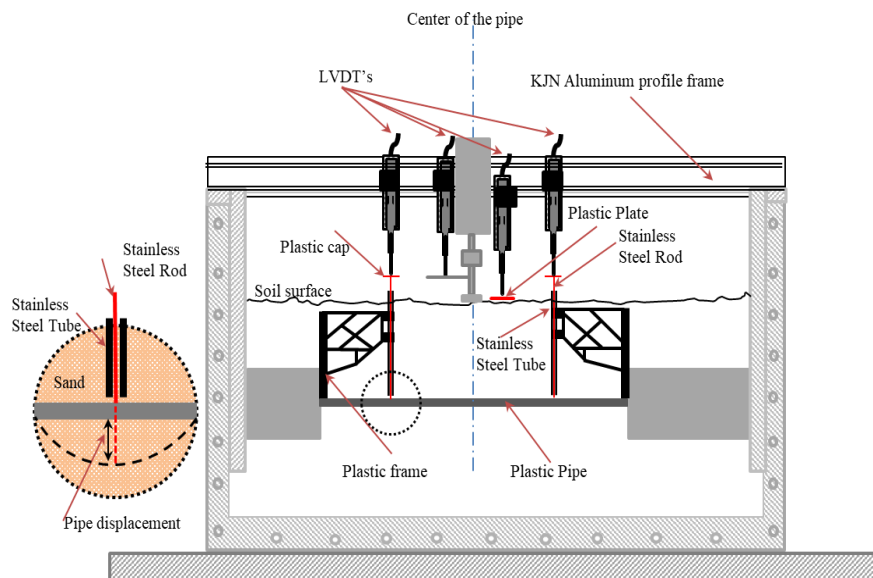


Figure 4-32 The LVDT's location

4.2.4.2 Force / Load Measurement

Three load cells were installed to measure the magnitude of the load being applied by the pneumatic cylinders to the soil surface and axially in the pipe. Two 500N load cells were used for the vertical load and a 250N load cell for the pipe axial loading see Figure 4-33. The locations of the load cells are shown in Figure 4-33. The load cell calibration consisted of three loading and unloading cycles using a Budenberg hydraulic machine. The voltage outputs were then plotted for load cell 1 (vertically positioned) as an example (see Figure 4-34) and calibration factor determined. The line of best fit for loading and unloading were very similar, and an average of the two was taken. It was found to be an R2 value of 0.9979 which demonstrated that the outputs from load cell can be relied upon to be very accurate. Table 4-5 shows the summary of the Load cell calibration.

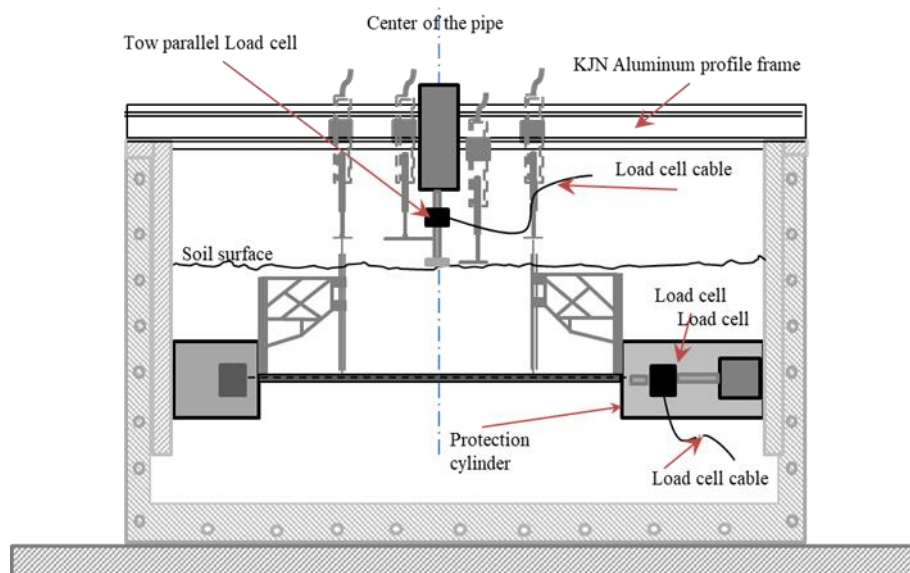


Figure 4-33 Schematic for the load cell layout

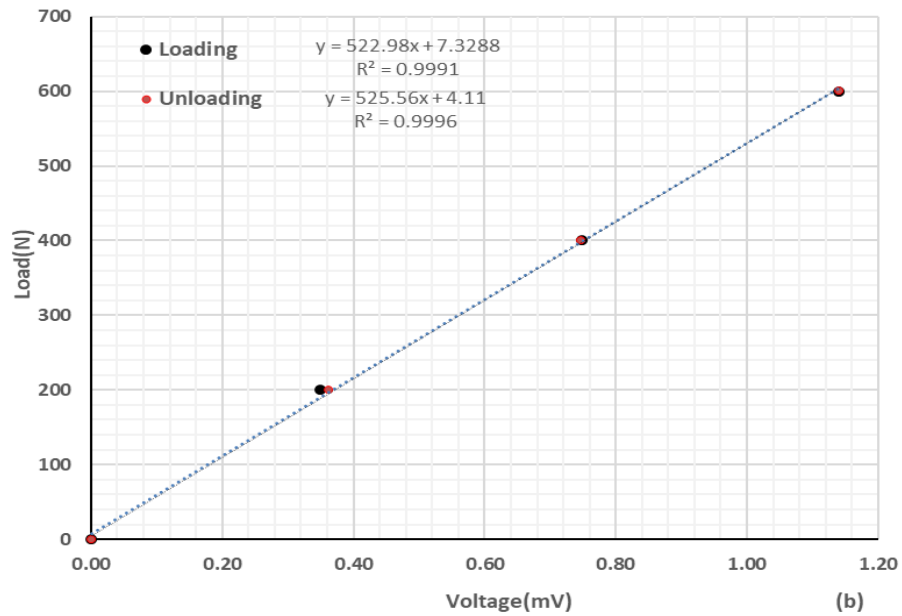


Figure 4-34 Example of load cell1 calibration graph

Table 4-5 Summary of load cells calibration

Load cell #	Calibration factor (mm/v)	Correlation coefficient, R ²
Load cell 1	5.161e+05	0.997
Load cell 2	5.369e+05	0.996
Load cell 3	1.26E+02	0.979

4.2.4.3 Bending Moment and Shear Force Measurement

In order to fully understand the pipe-soil interaction, the model pipes were instrumented with strain gauges, which were used to determine the bending and shear characteristics. KFP-5-120-C1-65 foil strain gauges with a typical resistance of about $120 \pm 0.5 \Omega$, and gauge length of 2.5mm were used in combinations of full and halfbridge to measure bending strain and axial strain of the pipe. The excitation voltage, V_{ex} , for these strain gauges was 5V, as was recommended.

Fourteen strain gauges were positioned as pairs on the major (vertical) axis (crown-invert) of the model pipe with constant spacing to measure strain on the major axis (Y-axis). Each pair of strain gauges were wired together to create a half-bridge configuration which yielded four times better output than using a

single strain gauge. Furthermore, the strain gauges were located diametrically opposite one another, thus responding in direct compression and tension, enable bending moments to be determined. To ensure that all the strain gauges were positioned in the exact location, a template created from paper were designed for this purpose as shown in Figure 4-35, with the locations of the strain gauges indicated.

Similarly, the same process was repeated for the minor (horizontal) axis of the model pipe except that the direction of the strain gauges was fixed on the X-axis. In additional 6 further strain gauges fixed in three different locations along the model pipe measured the applied axial force that represent internal water pressure. Figure 4-36 illustrates the exact strain gauge locations and more details are shown in Table 4-7.



Figure 4-35 Strain gauge insulation

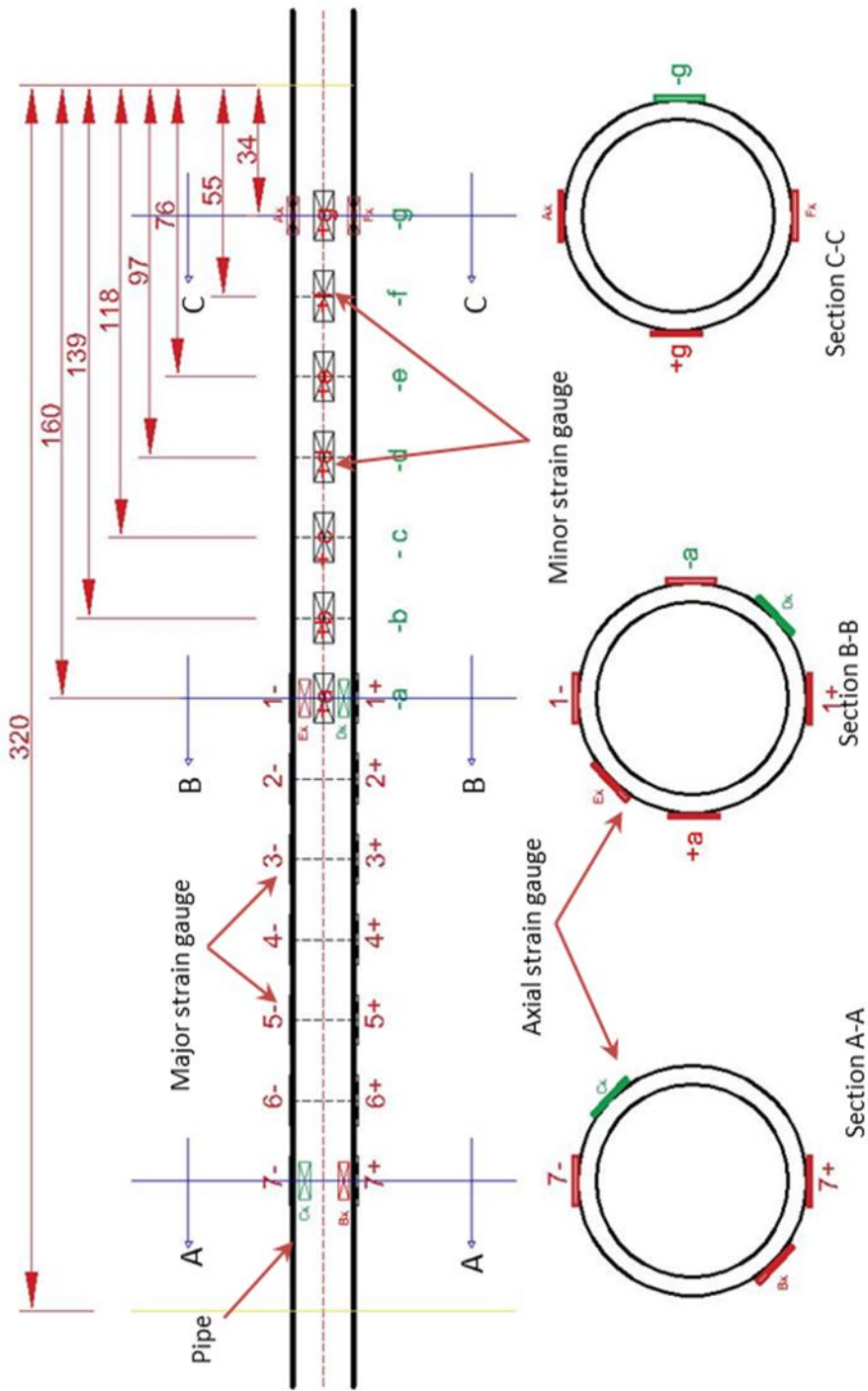
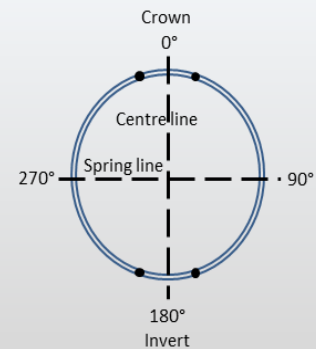


Figure 4-36 Schematic for the strain gauge locations

Table 4-6 Strain gauge locations

Major axis for bending moment			Minor axis for bending moment			Lateral load (Tensile)		
SG #	Location in y-axis Center line	Distance (mm)	SG #	Location in X-axis Spring line	Distance (mm)	SG #	Location	Distance (mm)
1 (+)	Crown (0°)	160 (pipe centre)	a (+)	270°	160 (pipe centre)	AX	Crown (0°)	34 (from right)
2 (+)	Crown (0°)	139 (from left)	b (+)	270°	139 (from left)	BX	210°	34 (from left)
3 (+)	Crown (0°)	118 (from left)	c (+)	270°	118 (from left)	CX	30°	34 (from left)
4 (+)	Crown (0°)	97 (from left)	d (+)	270°	97 (from left)	DX	150°	160 (pipe centre)
5 (+)	Crown (0°)	76 (from left)	e (+)	270°	76 (from left)	EX	330°	160 (pipe centre)
6 (+)	Crown (0°)	55 (from left)	f (+)	270°	55 (from left)	FX	Invert (180°)	34 (from right)
7 (+)	Crown (0°)	34 (from left)	g (+)	270°	34 (from left)			
1 (-)	Invert (180°)	160 (pipe centre)	a (-)	90°	160 (pipe centre)			
2 (-)	Invert (180°)	139 (from right)	b (-)	90°	139 (from right)			
3 (-)	Invert (180°)	118 (from right)	c (-)	90°	118 (from right)			
4 (-)	Invert (180°)	97 (from right)	d (-)	90°	97 (from right)			
5 (-)	Invert (180°)	76 (from right)	e (-)	90°	76 (from right)			
6 (-)	Invert (180°)	55 (from right)	f (-)	90°	55 (from right)			
7 (-)	Invert (180°)	34 (from right)	g (-)	90°	34 (from right)			



The calibration of the strain gauges in bending was a complex process and involved conducting a number of simply supported 3-point bending tests at mid-span and three other positions along the pipe for both the major (vertical) and minor (horizontal) axis of the plastic pipe. The theoretical bending moment induced by the applied forces was calculated using Equation 4-9 and plotted against the respective voltage outputs (see Figure 4-37), with the gradient of each line taken as the calibration factor. The theoretical bending moment calculated at the location was related to the strain readings obtained from the bending pipe.

$$M_{max}(\text{at point of load}) = \frac{pl}{4}$$

Equation 4-9

$$M_{max} \left(\text{when } x < \frac{l}{2} \right) = \frac{px}{2}$$

The axial strain gauges were calibrated by suspending the pipe vertically and applying a mass to apply load to the end of the pipe, extending it in tension. A summary of the calibration factor and the correlation coefficients are shown in Table 4-7.

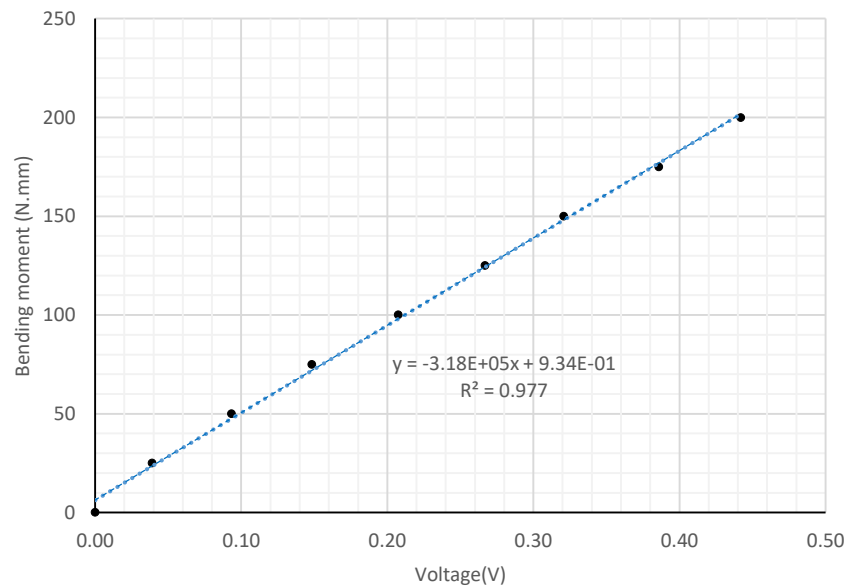


Figure 4-37 Example of strain gauges Calibration graph

Table 4-7 Summary of the strain gauge calibration

Strain gauge #	Calibration factor (mm/mv)	Correlation coefficient, R ²
SG 1	-2.33E+05	0.996
SG 2	-2.45E+05	0.976
SG 3	-2.55E+05	0.977
SG 4	-2.63E+05	0.989
SG 5	-2.77E+05	1
SG 6	-3.18E+05	0.977
SG 7	-3.86E+05	0.978
SG a	-2.22E+05	0.997
SG b	-2.53E+05	0.977
SG c	-2.50E+05	0.997
SG d	-2.81E+05	0.986
SG e	-3.29E+05	0.999
SG f	-3.85E+05	0.997
SG g	-4.11E+05	0.996
SG Ax	4.54E-01	1
SG Bx	1.33E-01	0.997
SG Cx	-1.22E-01	0.987
SG Dx	-2.29E-02	0.996
SG Ex	-4.48E-01	1
SG Fx	1.80E-01	0.998

4.2.5 Electronic/ Control Design

The in-flight computer is located in the centrifuge cabinet at the centre of rotation. The on-board data systems operate a National instrument (NI) PXIE-813 chassis and integrated controlled, power distribution board and data acquisition cards (see Figure 4-39). The flight computer in the rotational environment area connects to the external computer in the control room via optic fibre to facilitate the ability to log in remotely and control the on board test systems (load solenoid valves etc.) the data signals from the sensors are recorded using an NI cDAQ-9188 XT chassis that is equipped with six NI-9237 C Series modules that are dedicated for strain gauges and full bridge load cells (see Figure 4-38).

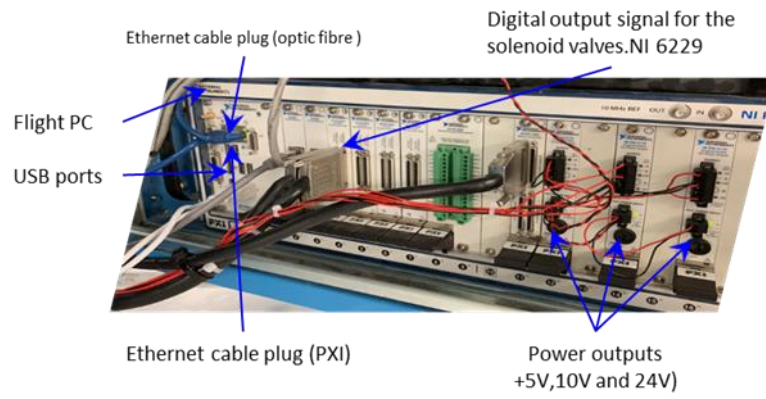


Figure 4-38 Centrifuge DAS cabinet (NI PIXe 1085)

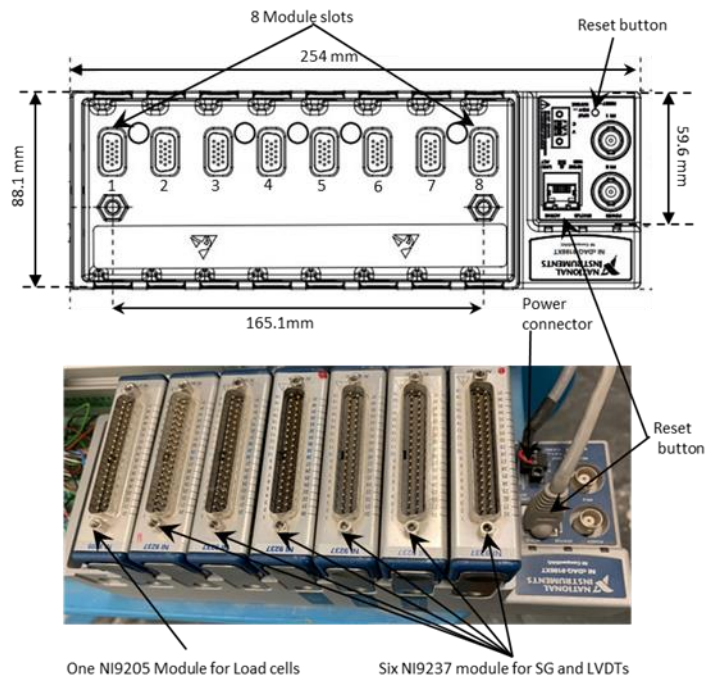


Figure 4-39 NI cDAQ-9188XT Chassis with two different modules

4.2.6 Sample Preparation Equipment

4.2.6.1 Point Pluviation of Sand Sample

The most established technique for preparation of dry sand samples is by sand pluviation. An automatic point pluviator with three degrees of freedom (Figure 4-40) was available and this was used to create uniform test beds in this research. A two-way direction path (x, y) was used with an overlapped pass to even out the surface level of each layer (Figure 4-41). Approximately 30kg of uniformly graded HST95 silica sand previously described was placed in the central hopper. The flow of sand from the hopper was controlled using a series of filter meshes and a pinch valve to open or close the exit orifice.

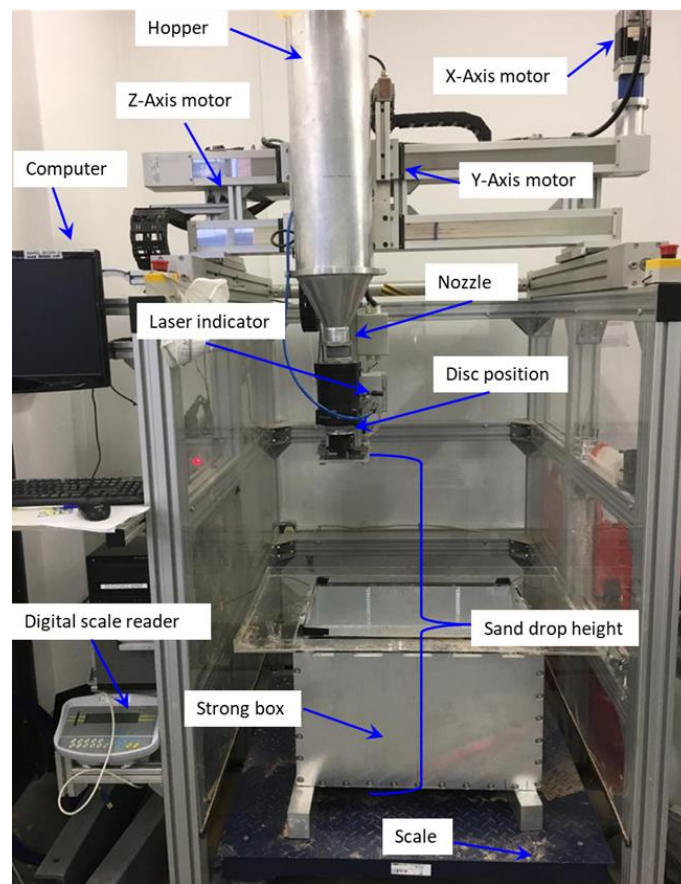


Figure 4-40 Sheffield University (CEIGR) automatic point pluviation.

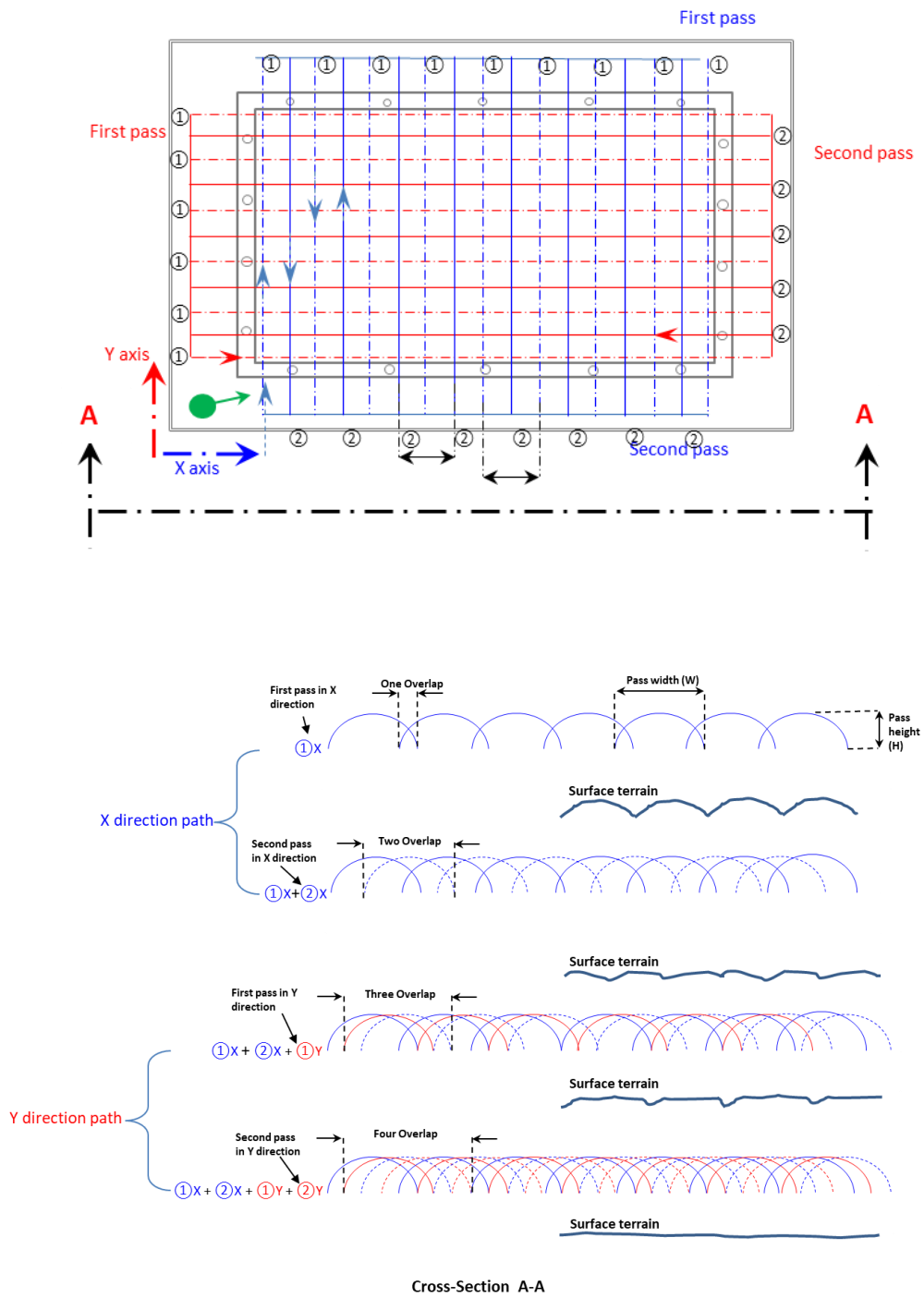


Figure 4-41 Schematic of the x, y paths of the automatic pluviator

The Z-axis controlled the sand free-fall drop height control, and the X and Y movements control the pluviation path. Each of the axes is operated by a LabVIEW program on the attached computer. A laser displacement sensor is attached adjacent the hopper nozzle to measure the sand height inside the strong box once each layer is finished. The increasing mass of the test chamber was recorded using the integrated mass balance which, enabled relative density to be calculated for each layer separately. The system was provided with flexible interface options program allowing the user to control movement and speed. For example, in this research a number of parameters have been set up in order to obtain targeted relative density of 80% in this research based on previous studies (Bayton et al., 2018a), these parameters for instance sand drop height of 110mm, an 85mm/s translation speed, 0.5-disc porosity and direction of (x, y). The ability to control these parameters precisely ensured that each test bed in the suite of experiments were controlled yielding a high degree of repeatability and able to achieve different relative densities of placed sand between 35% and 85%.

To ensure that sand is distributed over the whole area, it was essential to run the pluviator beyond the edges of the test chamber. Sand placed over the edges of the box collected in a catchment tray and removed from the layer calculations. In addition, when the pipe and the axial load apparatus were installed in the box two catchment boxes were placed on top of the cylinders are each end to prevent sand bounding off the cylindrical chamber and accumulating irregularly on either side. These were then removed once the level of the sand reached the height of the cylinders, ensuring that all the sand had a similar density in the whole system and a smooth surface. Figure 4-42 a and b shows both plastic tray and plastic boxes.

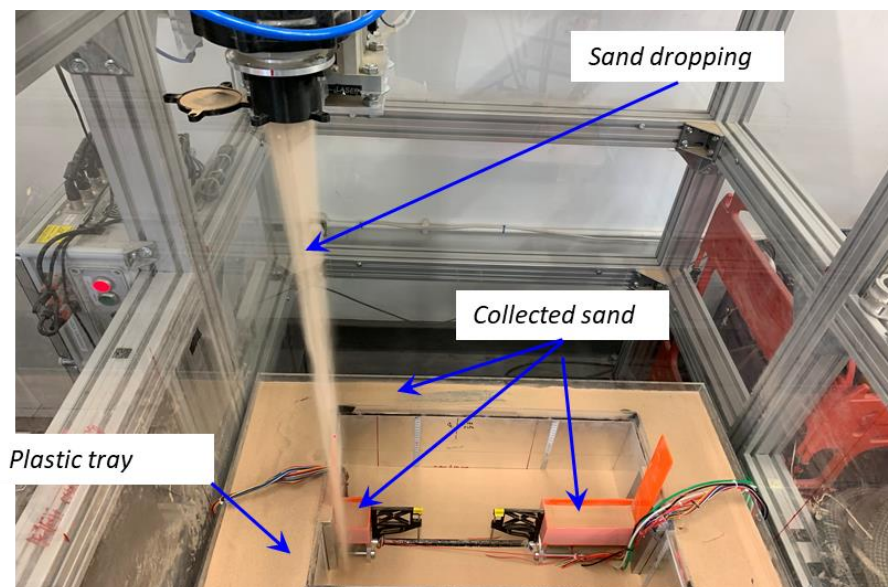


Figure 4-42 Sand collection tray and both boxes

As a result of the large weight of the model in the strong box, a system of a fork lift and four pistons hydraulic jack was utilised to lift the package into position at the centrifuge platform. This allowed for a stable lifting procedure to avoid disruption of the sample before testing could begin (see Figure 4-43)

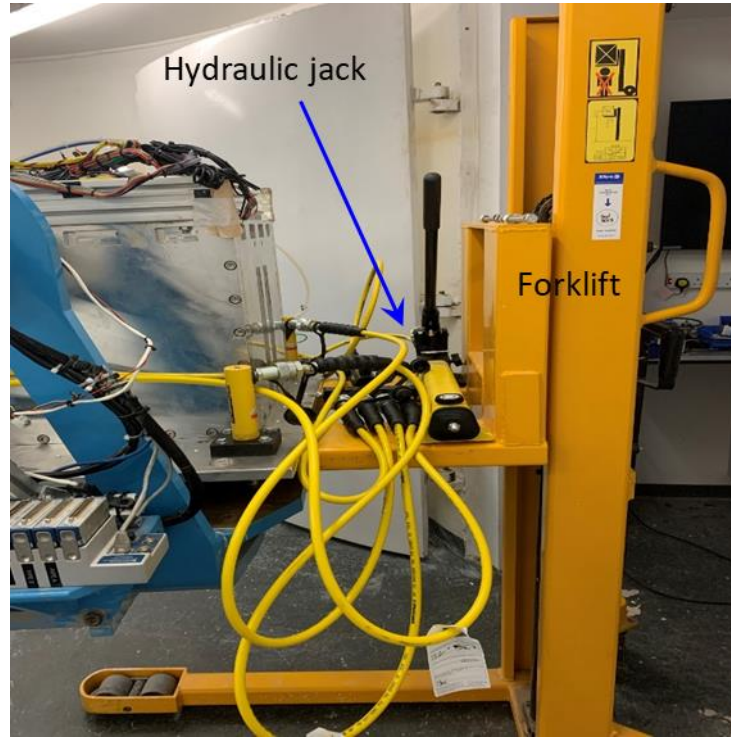


Figure 4-43 Hydraulic jack and forklift

4.2.7 Analysis of the test

4.2.8 Introduction to the Analysis

The aim of this section is to view the method utilised to analyse the performance of all the tests carried out in the centrifuge, highlighting of data processing steps and converting the output voltage data into understandable engineering units. This translation needs different steps using multiple computer programs like LabVIEW, MATLAB and Microsoft Excel. Each of those programs have specific mission for either collecting data or analysing it.

4.2.9 Data Processing

In order to interpret the data output by the sensors two main steps were involved that are referred to as pre and post-processing. These steps include a number of important sub-points as outlined below.

Data was collected at a rate of 100 samples per second (100Hz) and stored in '.txt' format. This file was exported to MATLAB (v2019b) where a script applied the necessary calibration factors for each sensor (converting the raw voltages to engineering units), converted it to prototype scale using the appropriate scale factors described in section 3.3, and removed the data offset. The final step in the data processing stage was filtering to reduce any electrical noise that impinged on the analogue signals. A Fast Fourier Transform, FFT, filtering was applied to all calibrated data, signal processing was utilised by using the low pass filter, with the frequency threshold selected after scrutiny of the Fast Fourier Transform (FFT) distribution. Typical lower band frequencies for 100Hz sampling frequencies in the region of 2 Hz for monotonic and cyclic loading. This was implemented using a MATLAB function tool to improve the quality of the signal.

For the cyclic load tests with 3600 loadings, a 'peakfinder' function was used to determine each cycle peak and trough position. This was used to ensure that data was being analysed and compared at the same load cycle. An example of the 'peakfinder' function graph presented in Figure 4-44.

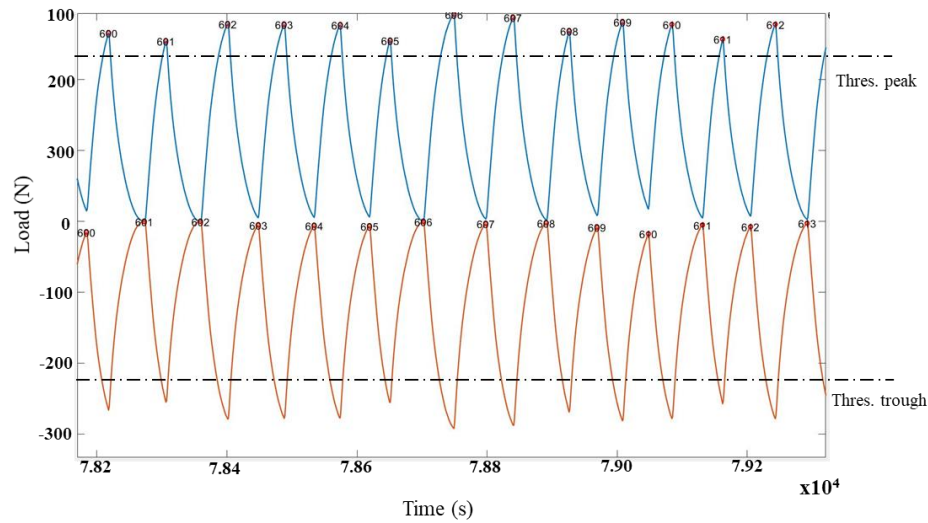


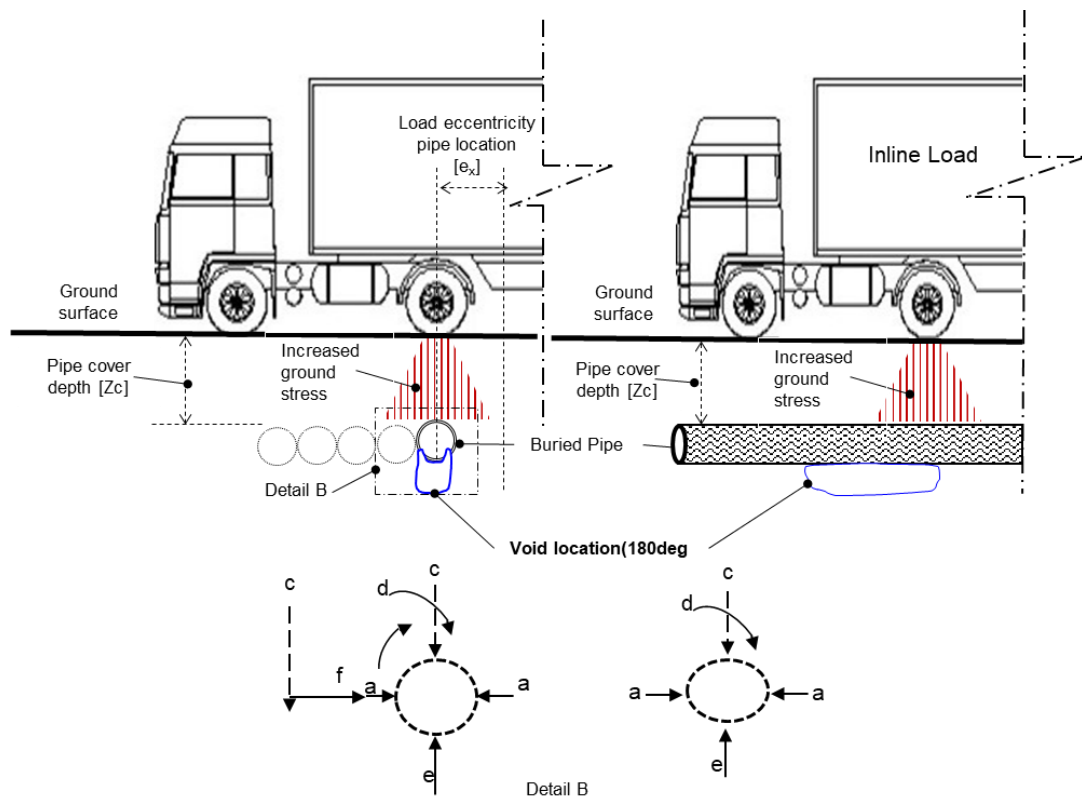
Figure 4-44 peakfinder threshold function graph

4.3 Model Configuration and Preparation

A total of 156 centrifuge tests at a centrifugal acceleration of 19 times Earth's gravity (19 g) were conducted to study the effects of burial depth and load condition on plastic pipe behaviour with and without the presence of the void. This study can be divided into two series, the response of the pipe to monotonic loading and the response of the pipe to cyclic loading behaviour, with the monotonic loading test results providing the backbone for cyclic normalisation. Table 4-8 presents the complete experimental plan. Different factors have been identified and have to be considered when the centrifuge tests are used in the investigation of pipe at prototype scale. The ideal non-void test was undertaken to capture the initial pipe behaviour and how the buried condition and load eccentricity affect the pipe. Accordingly, prior to any tests involving the buried pipe, a suite of 14 tests was conducted on the native virgin ground test to calibrate and understand the soil behaviour/response prior to introducing complexities, for instance pipes and voids. These tests provided the benchmark data as a point of reference and normalisation of the data. In addition, tests were conducted in two different scenarios specifically to determine the critical pipe position within certain area of depth and eccentric load position. This was to look at the effect of burial depth and the effect of the load eccentricity on the plastic pipe. Thus, results of these tests gave a strong basis to start with to understand the pipe behaviour then to build up an idea for further tests related to void existence. From this point of view, a set of tests was conducted related to the essence of the research topic, specifically to what extent are buried pipes affected by the presence of voids (size/location). The complete test matrix of all experiments conducted

regarding all scenarios is presented in Table 4-9. Figure 4-45 shows the general experimental schematic of the tests, and the test parameters considered in each test.

Each experimental model comprised a number of consecutive stages consisting of (i) spin up and equilibrium of stresses (ii) monotonic load up to the specific load requirements and (iii) a cyclic phase of 3600 cycles load applied at a frequency of 2Hz to observe the effects of repeated traffic load on the buried pipe (noting this was not the primary focus of the project and more cycles would be required in such a study). In phase (ii) and (iii) pipes could be subjected to axial tension at various magnitudes to simulate aspects of internal water pressurisation.



Where: (a) Lateral pressure of soil; (b) Minor axis bending; (c) Traffic load transferred to the buried pipe level; (d) major bending; (e) sup-port reaction from sand and (f) Load eccentricity.

Figure 4-45 General experimental schematic of the tests

The compilation of data analysis and presentation of the results required a long time. Thus, each group of tests to be compared to each other was classified separately and divided into 8 groups and a code was developed for each test to facilitate the analysis process and better show the results. Each group had its own aim and configuration. Table 4-8 presents the experimental matrix groups, schematic graph is later coupled with each related result in chapters 5 and 6.

Table 4-8 Experimental matrix of the groups

Group No.	Group name	Test code (ID) for each test with a different variable (X)
G1	Effect of Burial Depth (Zc)	Tx-Zc-L _m x-xe-xT-V _s x-V _L x ^{AM} -R _s [S/M/C]
G2	Effect of Eccentricity (e) Half Axle (6T)	
G3	Effect of Void Size Located @ 180deg	
G4	Effect of Void Size Located @270deg	
G5	Effect of internal water pressure	
G6	Effect of Road Surface (No void)	
G7	Effect of Road Surface (with 2D Void Located @180deg)	
G8	Effect of 2D Void Located @180deg(With Road surface)	

Note: Test code (ID) will refer to the data file captured during the centrifuge test.

Formatted as shown in above table 5th column; where

Tx= test number [T1-T156]; Z_c= soil cover depth [0.5m-0.75m-1.00m]; L_mx= load magnitude [6Ton =half axle12Ton= full axle];

xe= load eccentricity[1D-2D-3D-4D]; xT= axial tension [10N,20N,30N]; V_sx= void size [0.5D,1D,2D]; V_Lx= void location [6^{AM},9^{AM}];

R_s= Road surface; S/M/C= test stage [s=spin up/M= Monotonic loading/C= Cyclic loading].

Where x is different variable for each individual test, D is pipe diameter, N is axle force in newton.

Table 4-9 Test matrix

Test No.	Pipe Type	Cover Depth Z_c (m)	Load magnitude L_m (Ton)S/D	Eccentricity e	Internal pressure Bar	Void Size V_s	Void Location V_L	Road Surface R_s	Monotonic phase 1 (M)	Cycles (C) @2Hz freq
Test 1	PE100	1	6T- Single	4D	0	-	-	-	1	3600
Test 2	PE100	1	6T- Single	2D	0	-	-	-	1	3600
Test 3	PE100	1	6T- Single	0D	0	-	-	-	1	3600
Test 4	PE100	1	6T- Single	4D	1.5	-	-	-	1	3600
Test 5	PE100	1	6T- Single	2D	1.5	-	-	-	1	3600
Test 6	PE100	1	6T- Single	0D	1.5	-	-	-	1	3600
Test 7	PE100	1	6T- Single	4D	2.5	-	-	-	1	3600
Test 8	PE100	1	6T- Single	2D	2.5	-	-	-	1	3600
Test 9	PE100	1	6T- Single	0D	2.5	-	-	-	1	3600
Test 10	PE100	1	6T- Single	4D	5	-	-	-	1	3600
Test 11	PE100	1	6T- Single	2D	5	-	-	-	1	3600
Test 12	PE100	1	6T- Single	0D	5	-	-	-	1	3600
Test 13	PE100	1	6T- Single	3D	0	-	-	-	1	3600
Test 14	PE100	1	6T- Single	1D	0	-	-	-	1	3600
Test 15	PE100	1	6T- Single	0D	0	-	-	-	1	3600
Test 16	PE100	1	6T- Single	3D	1.5	-	-	-	1	3600
Test 17	PE100	1	6T- Single	1D	1.5	-	-	-	1	3600
Test 18	PE100	1	6T- Single	0D	1.5	-	-	-	1	3600
Test 19	PE100	1	6T- Single	3D	2.5	-	-	-	1	3600
Test 20	PE100	1	6T- Single	1D	2.5	-	-	-	1	3600
Test 21	PE100	1	6T- Single	0D	2.5	-	-	-	1	3600
Test 22	PE100	1	6T- Single	3D	5	-	-	-	1	3600
Test 23	PE100	1	6T- Single	1D	5	-	-	-	1	3600
Test 24	PE100	1	6T- Single	0D	5	-	-	-	1	3600
Test 25	PE100	1	6T-Double	Right&Left	0	-	-	-	1	3600
Test 26	PE100	1	6T-Double	Right&Left	1.5	-	-	-	1	3600
Test 27	PE100	1	6T-Double	Right&Left	2.5	-	-	-	1	3600
Test 28	PE100	1	6T-Double	Right&Left	5	-	-	-	1	3600
Test 29	PE100	1	6T-Double	0D	0	-	-	-	1	3600
Test 30	PE100	1	6T-Double	0D	1.5	-	-	-	1	3600
Test 31	PE100	1	6T-Double	0D	2.5	-	-	-	1	3600
Test 32	PE100	1	6T-Double	0D	5	-	-	-	1	3600
Test 33	PE100	1	6T-Double	2D	0	-	-	-	1	3600
Test 34	PE100	1	6T-Double	2D	1.5	-	-	-	1	3600
Test 35	PE100	1	6T-Double	2D	2.5	-	-	-	1	3600
Test 36	PE100	1	6T-Double	2D	5	-	-	-	1	3600
Test 37	PE100	1	6T-Double	4D	0	-	-	-	1	3600
Test 38	PE100	1	6T-Double	4D	1.5	-	-	-	1	3600
Test 39	PE100	1	6T-Double	4D	2.5	-	-	-	1	3600
Test 40	PE100	1	6T-Double	4D	5	-	-	-	1	3600
Test 41	No pip	0	6T- Single	0	0	-	-	-	1	0
Test 42	No pip	0	6T- Single	0	0	-	-	-	1	0
Test 43	No pip	0	6T- Single	0	0	-	-	-	1	0
Test 44	No pip	0	6T- Single	0	0	-	-	-	1	0
Test 45	No pipe	1	6T- Single	0D	0	0.5D	-	-	1	3600
Test 46	No pipe	1	6T- Single	1D	0	0.5D	-	-	1	3600
Test 47	No pipe	1	6T- Single	2D	0	0.5D	-	-	1	3600
Test 48	No pipe	1	6T- Single	4D	0	0.5D	-	-	1	3600
Test 49	No pipe	1	6T- Single	0D	0	1D	-	-	1	3600
Test 50	No pipe	1	6T- Single	1D	0	1D	-	-	1	3600
Test 51	No pipe	1	6T- Single	2D	0	1D	-	-	1	3600
Test 52	No pipe	1	6T- Single	4D	0	1D	-	-	1	3600
Test 53	No pipe	1	6T- Single	0D	0	2D	-	-	1	3600
Test 54	No pipe	1	6T- Single	1D	0	2D	-	-	1	3600
Test 55	No pipe	1	6T- Single	2D	0	2D	-	-	1	3600
Test 56	No pipe	1	6T- Single	4D	0	2D	-	-	1	3600

Test No.	Pipe Type	Cover Depth Z_c (m)	Load magnitude L_m (Ton)S/D	Eccentricity e (D)	Internal pressure Bar	Void Size V_s (D)	Void Location V_L	Road Surface R_s	Monotonic M	Cycles @2Hz freq C
Test 57	PE100	1	6T- Single	0D	0	0.5D	180deg	-	1	3600
Test 58	PE100	1	6T- Single	1D	0	0.5D	180deg	-	1	3600
Test 59	PE100	1	6T- Single	2D	0	0.5D	180deg	-	1	3600
Test 60	PE100	1	6T- Single	3D	0	0.5D	180deg	-	1	3600
Test 61	PE100	1	6T- Single	4D	0	0.5D	180deg	-	1	3600
Test 62	PE100	1	6T- Single	0D	5	0.5D	180deg	-	1	3600
Test 63	PE100	1	6T- Single	1D	5	0.5D	180deg	-	1	3600
Test 64	PE100	1	6T- Single	2D	5	0.5D	180deg	-	1	3600
Test 65	PE100	1	6T- Single	3D	5	0.5D	180deg	-	1	3600
Test 66	PE100	1	6T- Single	4D	5	0.5D	180deg	-	1	3600
Test 67	PE100	1	6T- Single	0D	0	1D	180deg	-	1	3600
Test 68	PE100	1	6T- Single	1D	0	1D	180deg	-	1	3600
Test 69	PE100	1	6T- Single	2D	0	1D	180deg	-	1	3600
Test 70	PE100	1	6T- Single	3D	0	1D	180deg	-	1	3600
Test 71	PE100	1	6T- Single	4D	0	1D	180deg	-	1	3600
Test 72	PE100	1	6T- Single	0D	5	1D	180deg	-	1	3600
Test 73	PE100	1	6T- Single	1D	5	1D	180deg	-	1	3600
Test 74	PE100	1	6T- Single	2D	5	1D	180deg	-	1	3600
Test 75	PE100	1	6T- Single	3D	5	1D	180deg	-	1	3600
Test 76	PE100	1	6T- Single	4D	5	1D	180deg	-	1	3600
Test 78	PE100	1	6T- Single	1D	0	2D	180deg	-	1	3600
Test 79	PE100	1	6T- Single	2D	0	2D	180deg	-	1	3600
Test 80	PE100	1	6T- Single	3D	0	2D	180deg	-	1	3600
Test 81	PE100	1	6T- Single	4D	0	2D	180deg	-	1	3600
Test 82	PE100	1	6T- Single	0D	5	2D	180deg	-	1	3600
Test 83	PE100	1	6T- Single	1D	5	2D	180deg	-	1	3600
Test 84	PE100	1	6T- Single	2D	5	2D	180deg	-	1	3600
Test 85	PE100	1	6T- Single	3D	5	2D	180deg	-	1	3600
Test 86	PE100	1	6T- Single	4D	5	2D	180deg	-	1	3600
Test 87	PE100	1	6T- Single	0D	0	0.5D	270deg	-	1	3600
Test 88	PE100	1	6T- Single	1D	0	0.5D	270deg	-	1	3600
Test 89	PE100	1	6T- Single	2D	0	0.5D	270deg	-	1	3600
Test 90	PE100	1	6T- Single	3D	0	0.5D	270deg	-	1	3600
Test 91	PE100	1	6T- Single	4D	0	0.5D	270deg	-	1	3600
Test 92	PE100	1	6T- Single	0D	30	0.5D	270deg	-	1	3600
Test 93	PE100	1	6T- Single	1D	5	0.5D	270deg	-	1	3600
Test 94	PE100	1	6T- Single	2D	5	0.5D	270deg	-	1	3600
Test 95	PE100	1	6T- Single	3D	5	0.5D	270deg	-	1	3600
Test 96	PE100	1	6T- Single	4D	5	0.5D	270deg	-	1	3600
Test 97	PE100	1	6T- Single	0D	0	1D	270deg	-	1	3600
Test 98	PE100	1	6T- Single	1D	0	1D	270deg	-	1	3600
Test 99	PE100	1	6T- Single	2D	0	1D	270deg	-	1	3600
Test 100	PE100	1	6T- Single	3D	0	1D	270deg	-	1	3600
Test 101	PE100	1	6T- Single	4D	0	1D	270deg	-	1	3600
Test 102	PE100	1	6T- Single	0D	5	1D	270deg	-	1	3600
Test 103	PE100	1	6T- Single	1D	5	1D	270deg	-	1	3600
Test 104	PE100	1	6T- Single	2D	5	1D	270deg	-	1	3600
Test 105	PE100	1	6T- Single	3D	5	1D	270deg	-	1	3600
Test 106	PE100	1	6T- Single	4D	5	1D	270deg	-	1	3600

Test No.	Pipe Type	Cover Depth Z_c (m)	Load magnitude L_m (Ton)S/D	Eccentricity e (D)	Internal pressure Bar	Void Size V_s (D)	Void Location V_L (AM)	Road Surface R_s	Monotonic M	Cycles @2Hz freq C
Test 107	PE100	1	6T- Single	0D	0	2D	270deg	-	1	3600
Test 108	PE100	1	6T- Single	1D	0	2D	270deg	-	1	3600
Test 109	PE100	1	6T- Single	2D	0	2D	270deg	-	1	3600
Test 110	PE100	1	6T- Single	3D	0	2D	270deg	-	1	3600
Test 111	PE100	1	6T- Single	4D	0	2D	270deg	-	1	3600
Test 112	PE100	1	6T- Single	0D	5	2D	270deg	-	1	3600
Test 113	PE100	1	6T- Single	1D	5	2D	270deg	-	1	3600
Test 114	PE100	1	6T- Single	2D	5	2D	270deg	-	1	3600
Test 115	PE100	1	6T- Single	3D	5	2D	270deg	-	1	3600
Test 116	PE100	1	6T- Single	4D	5	2D	270deg	-	1	3600
Test 117	PE100	0.5	6T- Single	0D	0	-	-	-	1	3600
Test 118	PE100	0.5	6T- Single	1D	0	-	-	-	1	3600
Test 119	PE100	0.5	6T- Single	2D	0	-	-	-	1	3600
Test 120	PE100	0.5	6T- Single	3D	0	-	-	-	1	3600
Test 121	PE100	0.5	6T- Single	4D	0	-	-	-	1	3600
Test 122	PE100	0.5	6T- Single	0D	5	-	-	-	1	3600
Test 123	PE100	0.5	6T- Single	1D	5	-	-	-	1	3600
Test 124	PE100	0.5	6T- Single	2D	5	-	-	-	1	3600
Test 125	PE100	0.5	6T- Single	3D	5	-	-	-	1	3600
Test 126	PE100	0.5	6T- Single	4D	5	-	-	-	1	3600
Test 127	PE100	1	6T- Single	0D	0	-	-	R_s	1	3600
Test 128	PE100	1	6T- Single	1D	0	-	-	R_s	1	3600
Test 129	PE100	1	6T- Single	2D	0	-	-	R_s	1	3600
Test 130	PE100	1	6T- Single	3D	0	-	-	R_s	1	3600
Test 131	PE100	1	6T- Single	4D	0	-	-	R_s	1	3600
Test 132	PE100	1	6T- Single	0D	5	-	-	R_s	1	3600
Test 133	PE100	1	6T- Single	1D	5	-	-	R_s	1	3600
Test 134	PE100	1	6T- Single	2D	5	-	-	R_s	1	3600
Test 135	PE100	1	6T- Single	3D	5	-	-	R_s	1	3600
Test 136	PE100	1	6T- Single	4D	5	-	-	R_s	1	3600
Test 137	PE100	1	6T- Single	0D	0	2D	180deg	R_s	1	3600
Test 138	PE100	1	6T- Single	1D	0	2D	180deg	R_s	1	3600
Test 139	PE100	1	6T- Single	2D	0	2D	180deg	R_s	1	3600
Test 140	PE100	1	6T- Single	3D	0	2D	180deg	R_s	1	3600
Test 141	PE100	1	6T- Single	4D	0	2D	180deg	R_s	1	3600
Test 142	PE100	1	6T- Single	0D	5	2D	180deg	R_s	1	3600
Test 143	PE100	1	6T- Single	1D	5	2D	180deg	R_s	1	3600
Test 144	PE100	1	6T- Single	2D	5	2D	180deg	R_s	1	3600
Test 145	PE100	1	6T- Single	3D	5	2D	180deg	R_s	1	3600
Test 146	PE100	1	6T- Single	4D	5	2D	180deg	R_s	1	3600
Test 147	PE100	0.75	6T- Single	0D	0	-	-	-	1	3600
Test 148	PE100	0.75	6T- Single	0D	5	-	-	-	1	3600
Test 149	PE100	0.75	6T- Single	1D	0	-	-	-	1	3600
Test 150	PE100	0.75	6T- Single	1D	5	-	-	-	1	3600
Test 151	PE100	0.75	6T- Single	2D	0	-	-	-	1	3600
Test 152	PE100	0.75	6T- Single	2D	5	-	-	-	1	3600
Test 153	PE100	0.75	6T- Single	3D	0	-	-	-	1	3600
Test 154	PE100	0.75	6T- Single	3D	5	-	-	-	1	3600
Test 155	PE100	0.75	6T- Single	4D	0	-	-	-	1	3600
Test 156	PE100	0.75	6T- Single	4D	5	-	-	-	1	3600

CHAPTER 5

Pipe-soil Behaviour Under Monotonic Loading

A total of 156 tests were carried out as described in Chapter 4. Since the volume of data was considerable, it is not feasible to present individual results for each test; hence, significant outcomes are reported based on a select number of tests that convey the trends and soil-pipe interaction behaviour observed. The methods of data analysis are described, results presented and comparisons made with the Winkler Spring method to verify the test observations.

5.1 Monotonic Loading

During the monotonic loading phase, the load was applied up to a maximum axial surface load condition of 6 tonnes in prototype scale, which was sustained for a duration of approximately 180 seconds. This was to represent half a HGV wheel axle acting on the surface. Thus, several tests have been divided into different subgroups, each having its own purpose for exploring aspects of the pipe-soil interaction. As previously outlined, each test consisted of three phases, spin-up, monotonic loading and cyclic loading, which was denoted in all tables as [S, M, C]. During the spin-up phase the rotational (*rpm*) speed of the centrifuge was increased to *25rpm*, *50rpm*, *75rpm* and *98rpm*, representing 1.3g, 5g, 11.5g and 19.2g respectively (at an effective radius of 1.742m). This ramp phase allowed bedding in of the pipe, which induced a small background bending stress within the pipe as observed in Figure 5-1. As the soil self-weight increased, some compression and 'flow' around the pipe occurred. Bending stresses occurred as the pipe was fixed at each end. The largest moments occurred at the centre span of the pipe. This data was reviewed during each spin up to ensure that the pipe sensors were functioning correctly. Similar effects may occur in practice during compaction of the fill material around a pipe thus this was not a grave concern. It was at this point the data was re-zeroed to observe only the impact of the additional wheel loading in either the monotonic or cyclic loading phase.

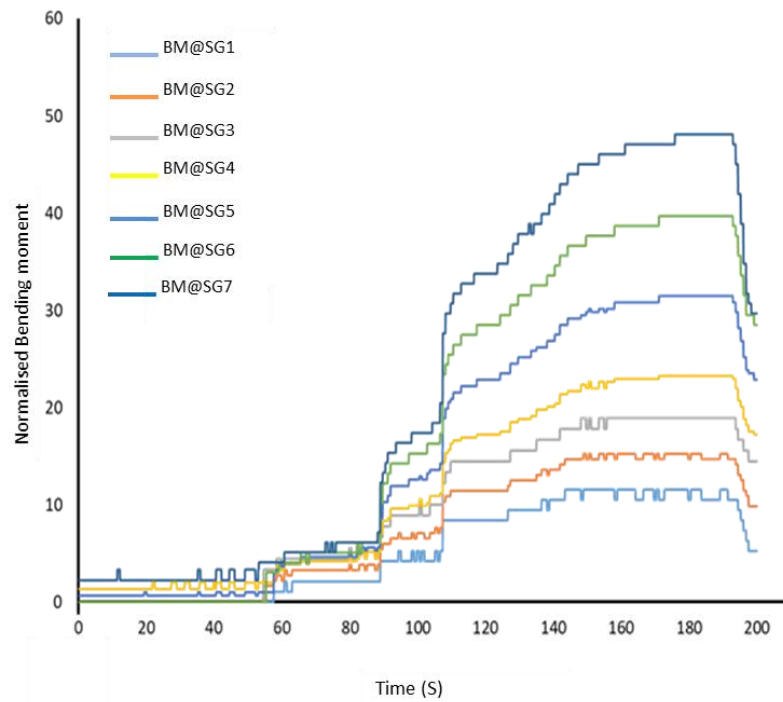


Figure 5-1 Spin-up stages and sand self-weight effect on the modelled pipe

In addition, note that all the pipe behaviour results are presented in dimensionless terms to allow direct comparison of the result between tests and to other modelling methodologies. Normalised parameters and dimensionless ratios used are shown in Table 5-1, and described in Figure 5-2. The non-dimensional parameters are: Bending moment (\widetilde{M}), Shear force (\widetilde{Q}), Pipe deflection (\widetilde{y}_p), Pressure (\widetilde{p}), Vertical applied load (\widetilde{F}), and the pipe length (\widetilde{L}_p).

Table 5-1 Non-dimensional ratio

$\bar{M} = \frac{M}{\gamma D_p^4}$	$\bar{Q} = \frac{Q}{\gamma D_p^3}$	$\bar{p} = \frac{p}{\gamma D_p}$	$\bar{y}_p = \frac{y_p}{D_p}$	$\bar{F} = \frac{F_p}{\gamma D_p^3}$	$\bar{L}_p = \frac{L_p}{D_p}$
------------------------------------	------------------------------------	----------------------------------	-------------------------------	--------------------------------------	-------------------------------

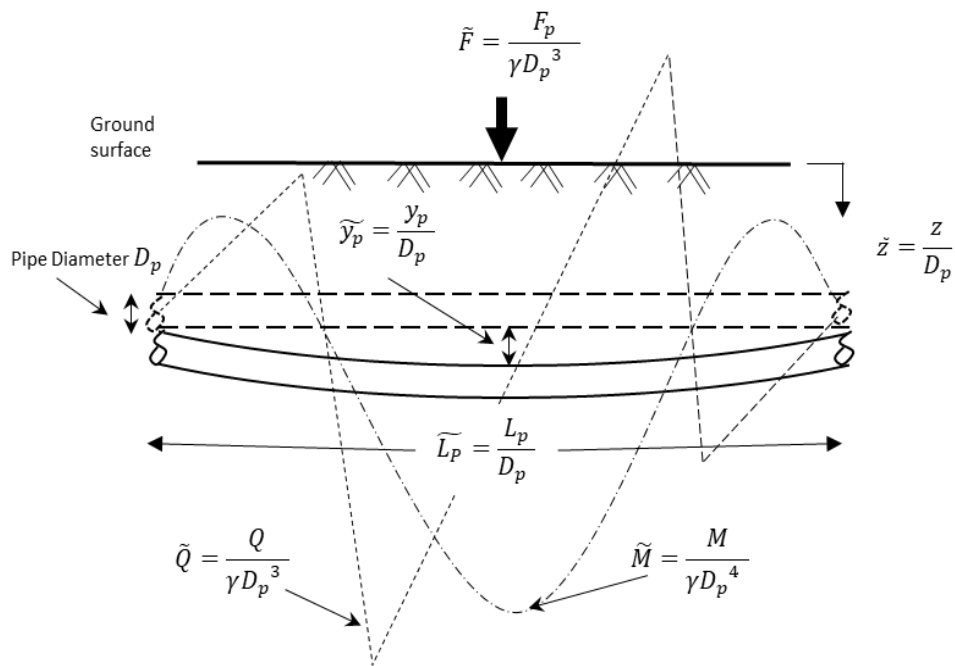


Figure 5-2 Schematic of the pipe behaviour and non-dimensional ratio

5.1.1 Effect of Burial Depth

The effect of burial depth is evaluated using the tests indicated in Table 5-2 and as shown in the schematic in Figure 5-3 for selected tests. During these experiments, the position of the traffic load relative to the pipe was directly on top of the pipe location (i.e. eccentricity = 0). The load applied simulated the 6T- single wheel loading. In order to obtain good results, it was necessary to repeat the same test scenario twice ensuring that all instrumentations had a similar outcome. Therefore, results were plotted and average of the bending moment has been taken for all tests. Thus, for the first graph these results shows bending moment obtained for three different burial depths (see Figure 5-5). It can be seen from the sup-plot from the same figure that there were only about 4% difference between similar tests. Therefore, results of average bending moment was plotted for all tests throughout this thesis as seen in Figure 5-5 .

Table 5-2 Effect of burial depth (Z_c)

	Test (#)	Test ID	Cover Depth (Z_c) m	Load magnitude L_m (Ton)	Load Eccentricity $e=D$	Internal pressure Bar	Void Size V_s	Void Location V_l (deg)	Roas Srfurface R_s	Monotonic Phase 1
Group 1	Test 3	T3- Z_c 1- L_m 6T _s -0e-0T[M]	1	6T- Single	0e	0	-	-	-	y
	Test 147	T147- Z_c 0.75- L_m 6T _s -0e-0T [M]	0.75	6T- Single	0e	0	-	-	-	y
	Test 117	T117- Z_c 0.5- L_m 6T _s -0e-0T[M]	0.5	6T- Single	0e	0	-	-	-	y

Note: Test code (ID) will refer to the data file captured during the centrifuge test.

Formatted as shown in above table 5th column; where

Tx= test number [T1-T156]; Z_c = soil cover depth [0.5m-0.75m-1.00m]; L_m x= load magnitude [6Ton =half axle12Ton= full axle];

xe= load eccentricity[1D-2D-3D-4D]; xT= axial tension [10N,20N,30N]; V_s x= void size [0.5D,1D,2D]; V_l x= void location [6^{AM},9^{AM}];

R_s = Road surface; S/M/C= test stage [s=spin up/M= Monotonic loading/C= Cyclic loading].

Where x is different variable for each individual test, D is pipe diameter, N is axle force in newton

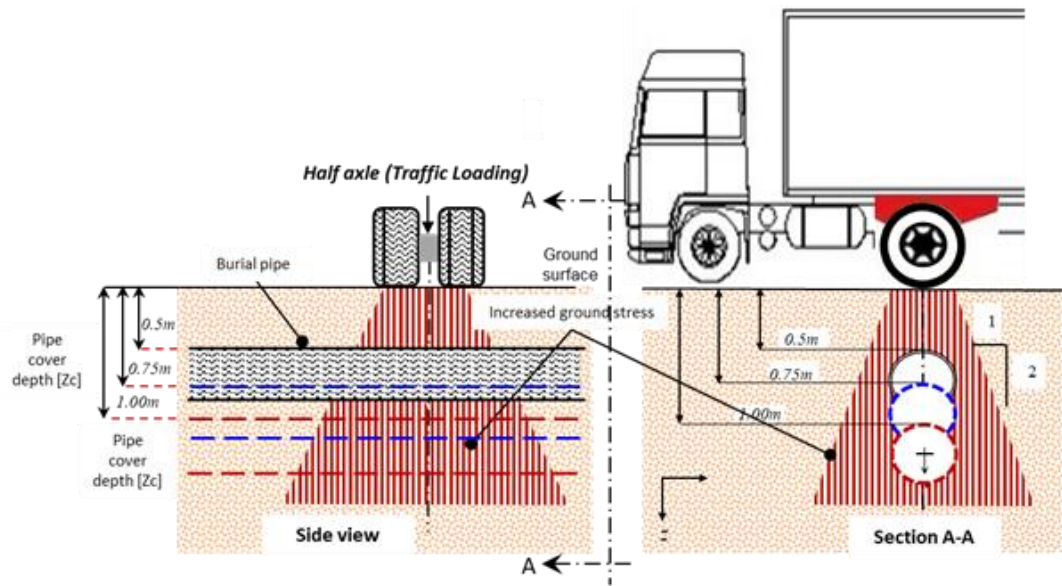


Figure 5-3 Schematic of pipe behaviour for different burial depths

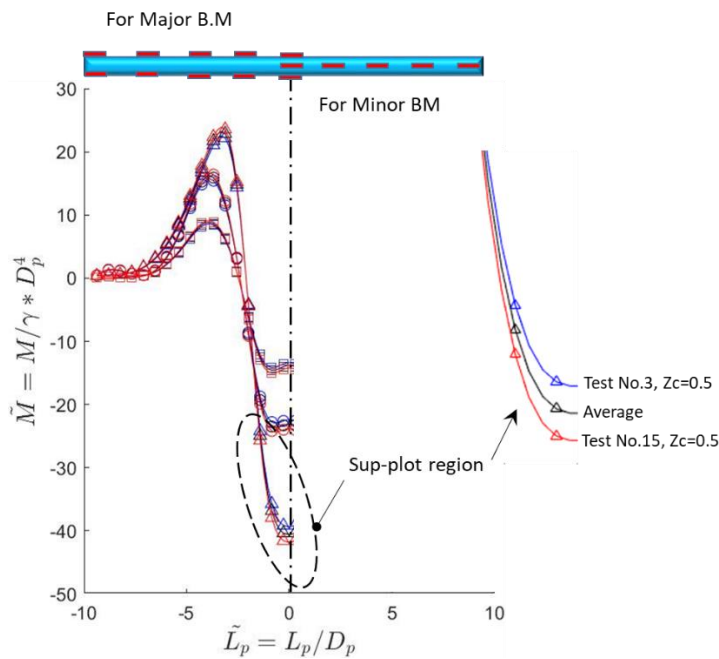


Figure 5-4 Maximum bending moment half pipe length for the major axis (repeated test)

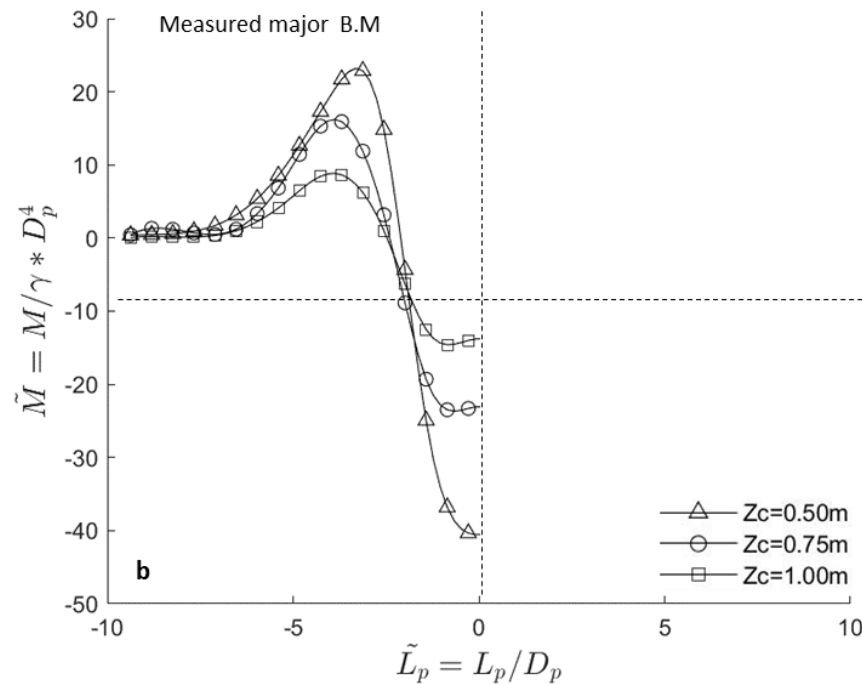


Figure 5-5 Maximum bending moment half pipe length for the major axis (average of repeated test)

The major (vertical) axis bending moment along the length of the pipe under monotonic loading is shown in Figure 5-5. The maximum sagging moment is observed at the mid-span of the pipe, which correlates to the position of the applied vertical load of 6T equivalent force. The observations in Figure 5-5 confirm that the magnitude of the maximum bending moment, either hogging (positive) or sagging (negative), of the pipe increases as the burial depth decreases. The shallower the pipe is buried, the steeper the gradient of the curve and the overall transition in bending moment is much larger. The analysis confirms that the traffic load contributes significantly to the bending of a pipe in the vertical axis (crown-invert) at shallow depths as the magnitude of bending observed in the pipe during spin up due to the soil cover self-weight contributed very little bending.

Interestingly the level of accuracy of the experiments was confirmed through observation of the minor axis. As the load was applied axially above the crown of the pipe, lateral bending would be unlikely to occur. Figure 5-6 confirms only a slight bending moment induced in the minor axis occurred, which does not exceed 3% of the major bending moment, thus the loading is confirmed as being vertically positioned above the pipe. Additional minor axis bending would be expected as the loading eccentricity increases such that lateral stresses are imparted to the pipe.

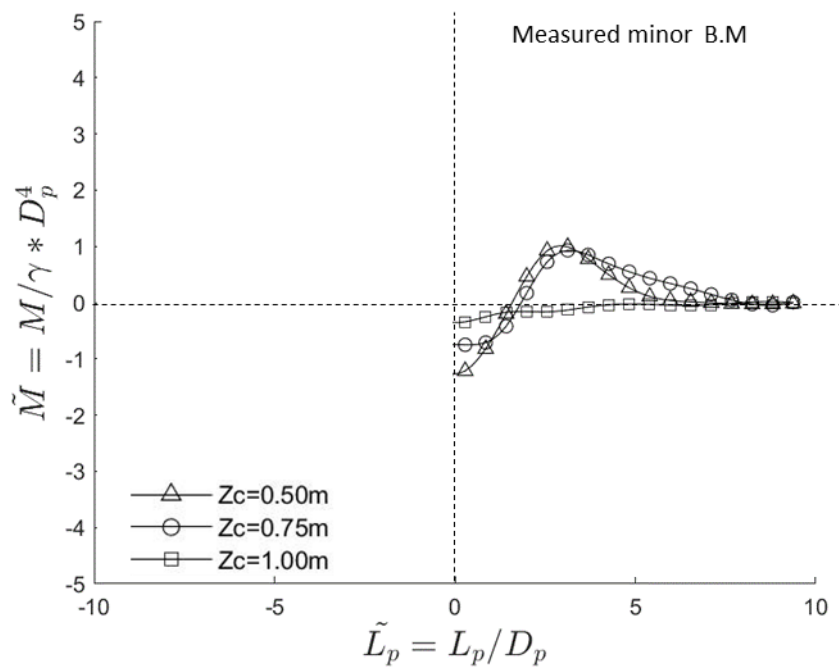


Figure 5-6 Maximum bending moment along the length of the pipe for the minor axis

The maximum resultant bending moment with the major and minor bending moment has been plotted together in a visual 3D graph (see Figure 5-7) to show the response for three different locations (subplot a, b and c) along the pipe length. It is clear that their resultant moment does not exceed 1.5° from the vertical, confirming the principle bending was in the vertical axis.

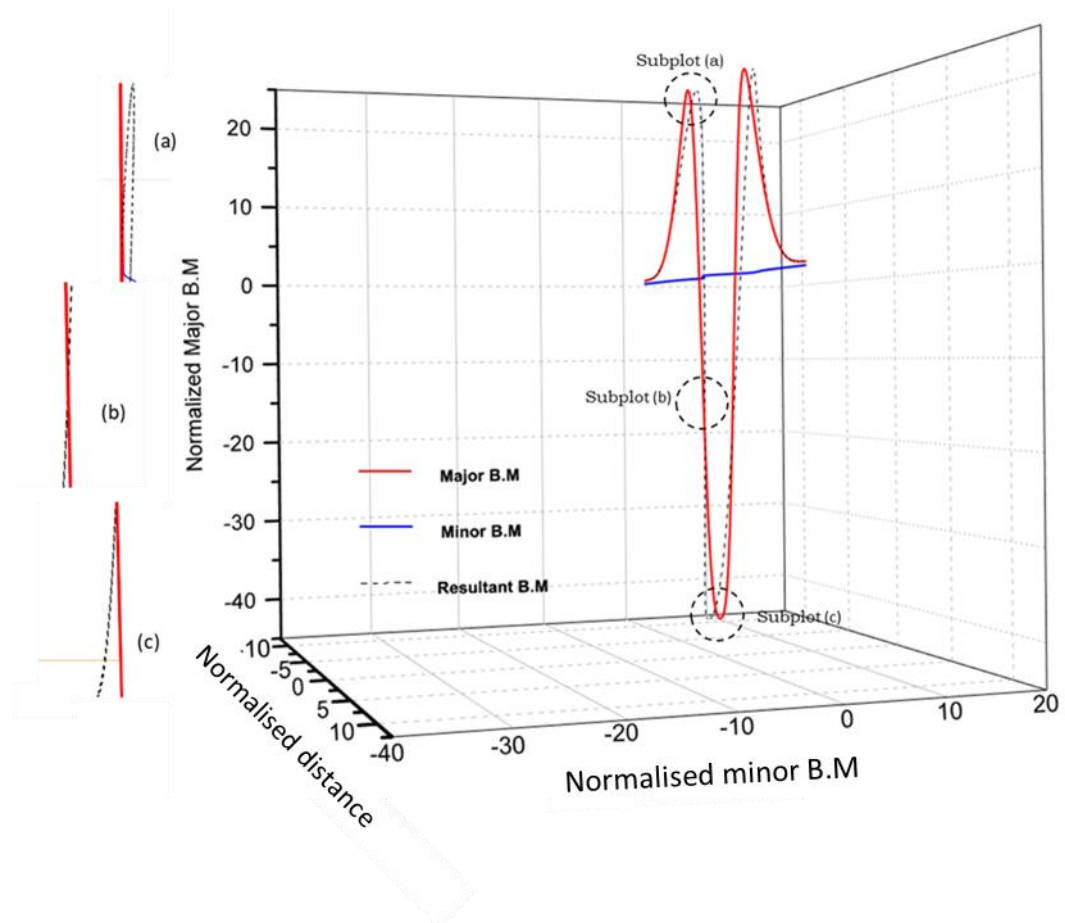


Figure 5-7 Resultant bending moment

An effective point load was calculated from the maximum bending moment to reflect the load each pipe experienced and this was used to calculate maximum shear force (Equation 5-1). Shear force diagrams were obtained by using the Euler-Bernoulli beam theory (Gere and Timoshenko, 1984):

$$Q = \frac{d}{dx} \left(EI \frac{d^2y}{dx^2} \right) \tag{Equation 5-1}$$

Q denotes the shear force and the term on right-hand side is the differentiation of the bending moment. Thus, the rate of change of the bending moment with respect to x (at any point) is equal to the shearing force, or the slope of the moment diagram at the given point is the shear at that point. (Figure 5-8). It is logical to assume that the variations of the shear force diagram are caused by the effect of soil pressure on the pipe as in the bending diagram. As the pipe modelled in the centrifuge was simply supported at the ends it is obvious that soil interaction causes positive shear at the ends of pipe at each case. The allowable shear strength of the pipe material is approximately 33MPa, which corresponds to an allowable shear force (less about 27%) found to be greater than the experimental shear force. Thus, the allowable shear strength of the pipe has not been exceeded.

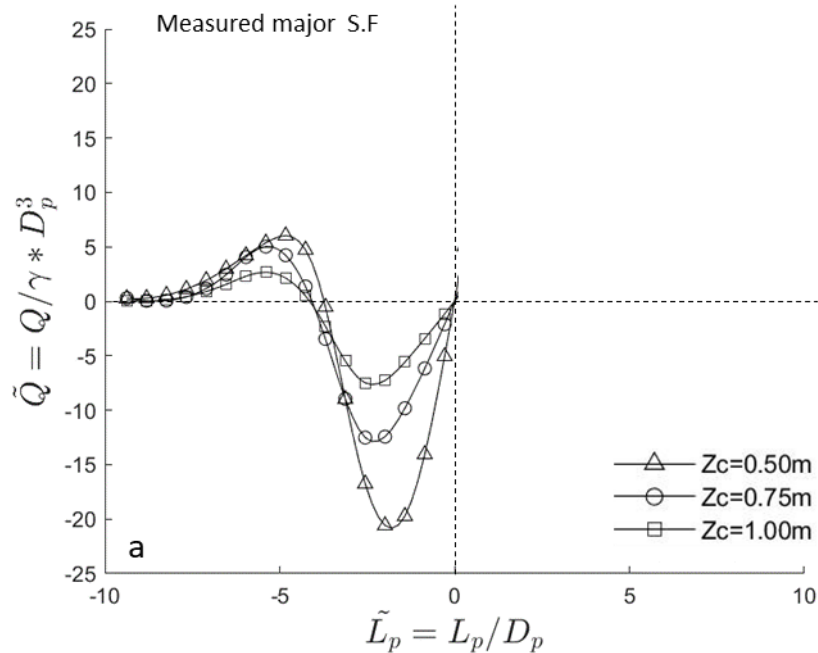


Figure 5-8 (a) Shear force along the length of the pipe for the major axis

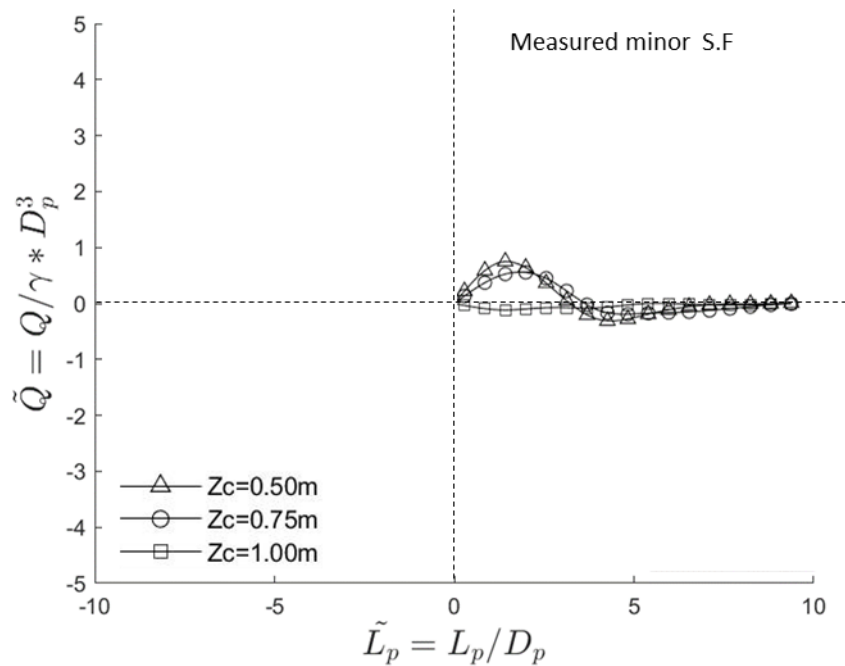


Figure 5-8 (b) Shear force along the length of the pipe for the minor axis

5.1.1.1 Change in soil stiffness

The response of the soil-pipe system to loading and unloading application investigated within the monotonic phase (Figure 5-9) shows a stiffer response when the pipe is present than without, and that the stiffness response is a function of the proximity of the pipe to the surface. The pipe is a stiffer element within the sub-surface, thus a greater proportion of load will be carried within the pipe, which yields the increased system stiffness observed. When the pipe is fully supported, these stresses are evenly distributed at the pipe invert, however if a loss of support were to occur then it could be hypothesised that greater pipe deflection and therefore higher bending will be highly likely as the stiffer pipe element will attract increased levels of surface loading. During unloading elastic rebound occurred in all cases. However, the level of recovery is more evident when the pipe is present, confirming the pipe initially absorbs a greater proportion of the applied surface loading, stores this elastically along its length and then ‘springs’ back once the load is removed. Settlements are not completely recorded during unloading, most likely because of compaction and sand grain redistribution that locks the pipe into place. However, it is noticeable that soil settlement recovery for the shallower pipe ($Z_c=0.50\text{m}$) is greater than with higher cover.

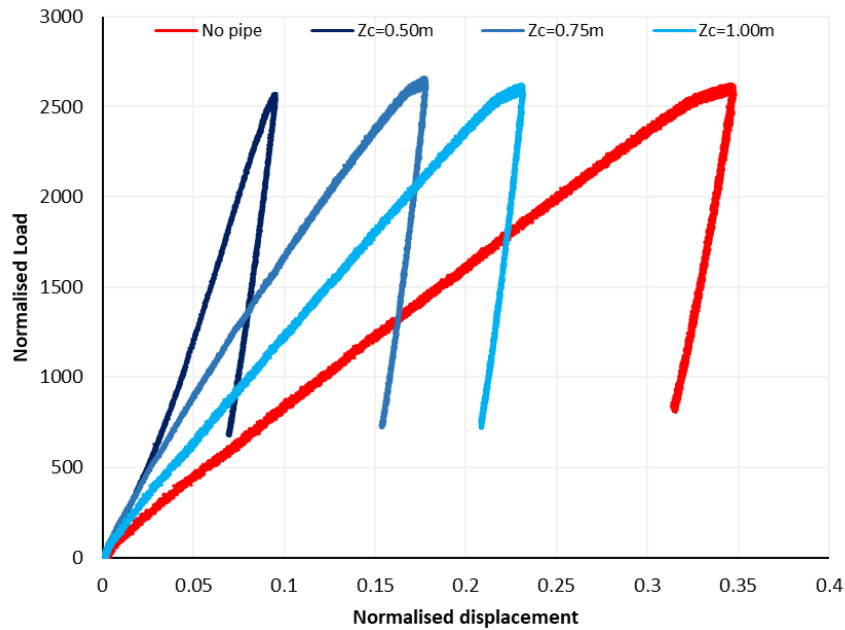


Figure 5-9 Variation in footing stiffness with pipe burial depth

Surface displacements were also recorded near to the wheel load application position within 2 metres radius (prototype scale) where a surface LVDT was located. It can be seen in Figure 5-10 that also the loaded area has an influence on the surrounding area extending to 2 metres. This is a result of soil particle re-arrangement due to soil compaction under the action of the surrounding applied load.

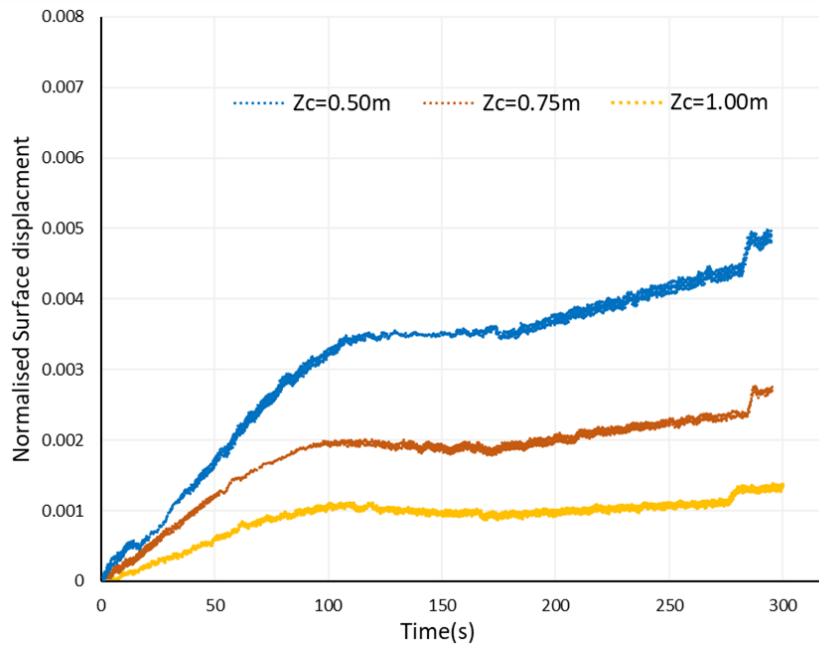


Figure 5-10 Soil surface settlements near the loading area.

As presented in Figure 5-11, the buried pipe is subjected two types of load, dissipated vertical load coming from the traffic load and uniform load coming from the soil self-weight. Therefore, the pipe deflection can be found by using Euler–Bernoulli (Equation 5-2) which describes the relationship between the pipe deflection and the applied load.

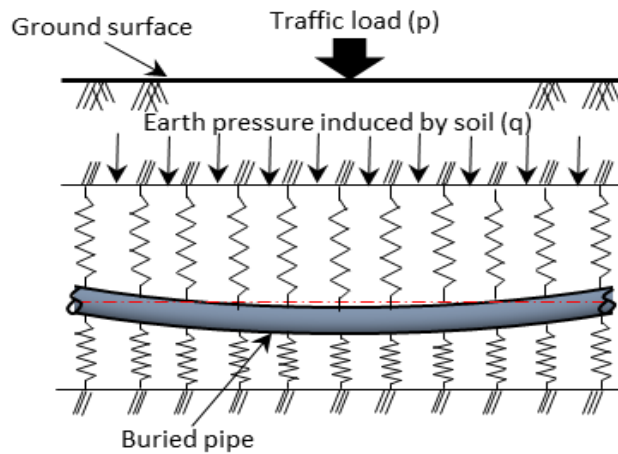


Figure 5-11 Schematic of the traffic load and soil self-weight load.

$$EI \frac{d^4y}{dx^4} - p(y) = 0 \tag{Equation 5-2}$$

Where EI is the flexural stiffness of the pipe, $p(y)$ -assumed = $y.k$ is the subgrade (soil) reaction force acting from the pipe and, k is the coefficient of the subgrade reaction.

To simplify the analysis, the finite difference method (FDM) is applied to Equation 5-2, yielding Equation 5-3 as described in Figure 5-12. This method was utilised herein to solve the differential equations of the fourth order derivative at any point along the pipe to determine deflection.

$$EI \left(\frac{y_{n-2} - 4y_{n-1} + 6y_n - 4y_{n+2} + y_{n+2}}{h^4} \right) - p = 0 \tag{Equation 5-3}$$

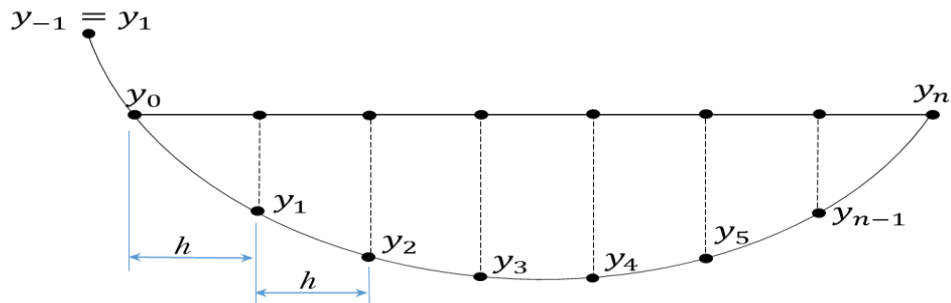


Figure 5-12 The technique of finite difference method depends on discretising a function on a grid

5.1.1.2 Pipe deflection response

On first inspection of Figure 5-13 it can be seen that higher deflections of the pipe are observed in shallower burial depths. This makes cover depth play an important role on the pipe deflection, which indicates surface load has a noticeable effect on shallower pipes. Highest deflections are also obtained for loads applied directly over the pipe burial depth. The result for the cover depth $Z_c=0.50\text{m}$ shows more deflection in comparison to the cover depth $Z_c=1.00\text{m}$, whereas the deflection of the cover depth $Z_c=0.50\text{m}$ is 38% higher than the maximum deflection value obtained for $Z_c=1.00\text{m}$; unlike the small deflection observed in the minor direction which is negligible compared to the major axis. Since the deflections on the minor axis were negligible, these results are only valid for deflections about the major axis. Therefore, it is worth mentioning that pipe burial depth has a significant effect on the pipe deflection on the major axis when load is applied directly above the pipe crown. The load near the pipe, produced maximum deflection in the centre of pipe, with maximum deflections observed from centre and emphasizing that deeper cover produces smallest values. This clearly shows that the pipe-soil interaction not only depends on vertical load but also on burial depth and the boundary condition of the pipe.

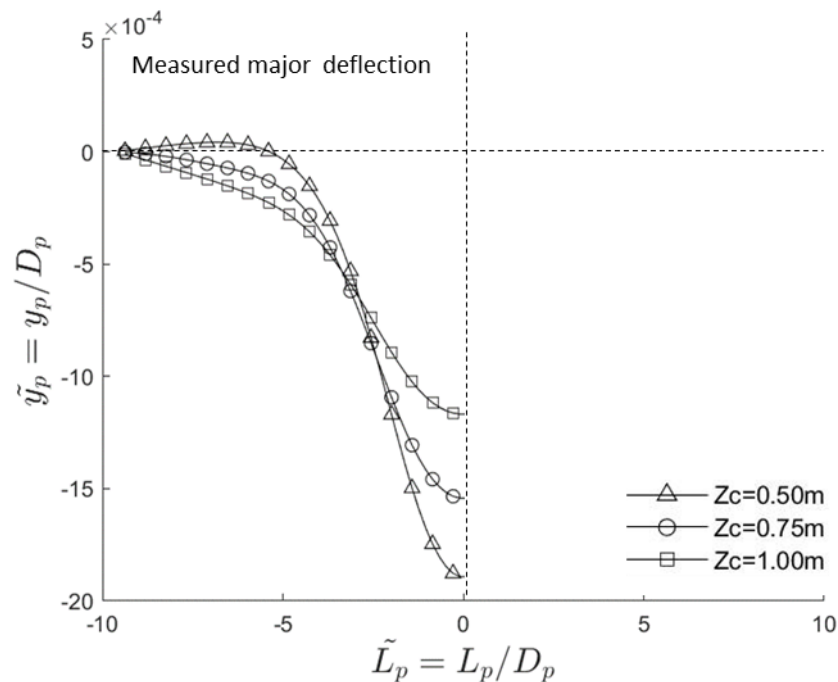


Figure 5-13 Pipe deflection under monotonic load at various burial depths

5.1.2 Effect of Eccentricity

The position of the traffic load relative to the pipe will influence the amount of stress that is transferred to the pipe. In this grouping the soil cover was set at 1.0 m in order to study the effect of load eccentricity. Eccentricities of $0D_p$, $1D_p$, $2D_p$, $3D_p$ and $4D_p$ of the pipe diameter were considered, as in Table 5-3 and Figure 5-14, with the loads being applied to the mid-length of the pipe.

Table 5-3 Effect of eccentricity (e) half axle (6Tonnes)

	Test (#)	Test ID	Cover Depth (Z_c) pro- Mod- m	Load magnitude L_m (Ton)	Eccentricity e (D)	Internal pressure Bar	Void Size V_s	Void Location V_l (deg)	Roas Sruface R_s	Monotonic
Group 3	Test 3	T3-Z _c 1-L _m 6T _s 0e-0T[M]	1	6T- Single	0e	0	-	-	-	y
	Test 14	T14-Z _c 1-L _m 6T _s 1e-0T[M]	1	6T- Single	1e	0	-	-	-	y
	Test 2	T2-Z _c 1-L _m 6T _s 2e-0T[M]	1	6T- Single	2e	0	-	-	-	y
	Test 13	T13-Z _c 1-L _m 6T _s 3e-0T[M]	1	6T- Single	3e	0	-	-	-	y
	Test 1	T1-Z _c 1-L _m 6T _s 4e-0T[M]	1	6T- Single	4e	0	-	-	-	y

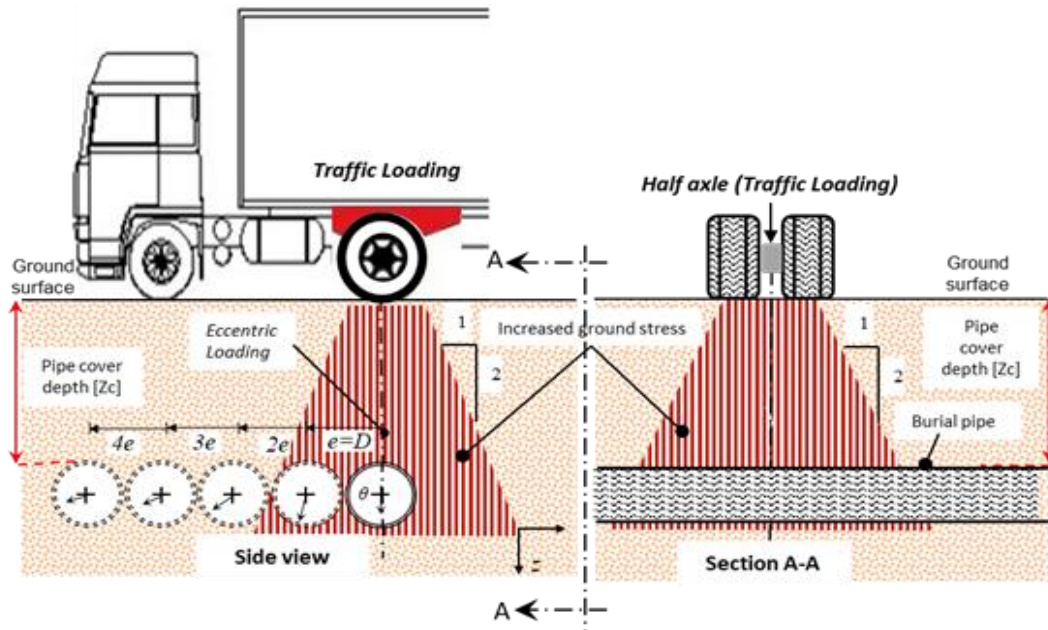


Figure 5-14 Schematic of the pipe behaviour under 6tonnes eccentric load

Unlike the case where the pipe was loaded directly over the crown position, the introduction of eccentric loading is expected to induce increased lateral bending in the pipe that will be observed in the minor axis of bending (springline). As described in Figure 5-14, the load spread from the wheel contact is expected to dissipate at the ratio 2V:1H, thus the zone of influence can be estimated as in

Figure 5-15. It is observed that the pipe at $e=1D$ with 1 m deep is well within the bounds of the influence zone, unlike $e=2D$ case where 75% of the pipe is within the loaded zone and 25% of the pipe on the zone edge.

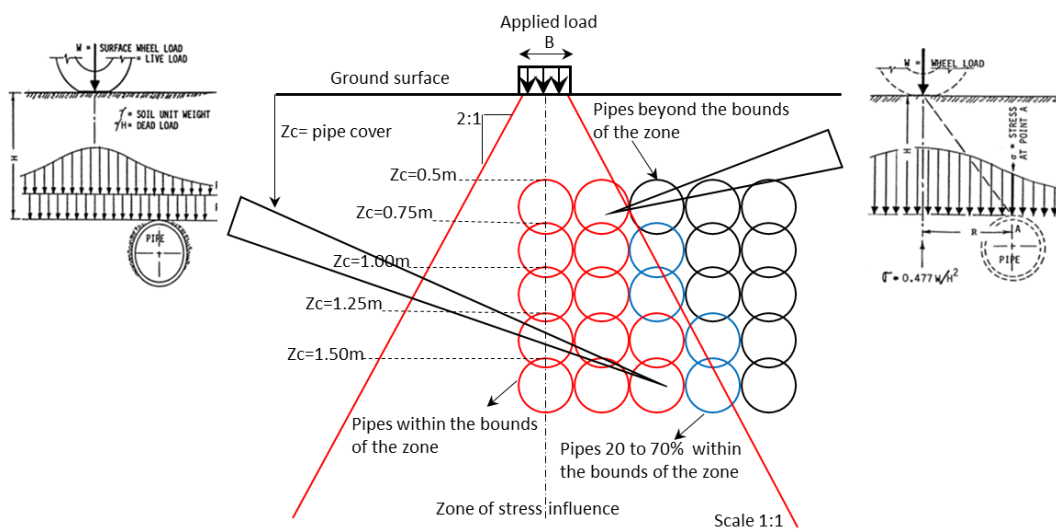


Figure 5-15 Schematic of the zone of stress influence.

Figure 5-16 presents the bending moments recorded on the major and minor axis (vertical and horizontal) with variation in load eccentricity. Reflecting on the vertical axis, it is clearly observed that as the load eccentricity increases, the maximum hogging and sagging bending of the pipe are reduced. Conversely, in the horizontal axis increased bending moments occur as the load position varies, with the critical case being when the load is positioned at an eccentricity of 1D. A summary of the individual and resultant major and minor bending is provided in Table 5-4. While clearly the highest bending occurs in $e=0D$ condition, the $e=1D$ has a similar resultant magnitude, which is almost twice that of $e=2D$.

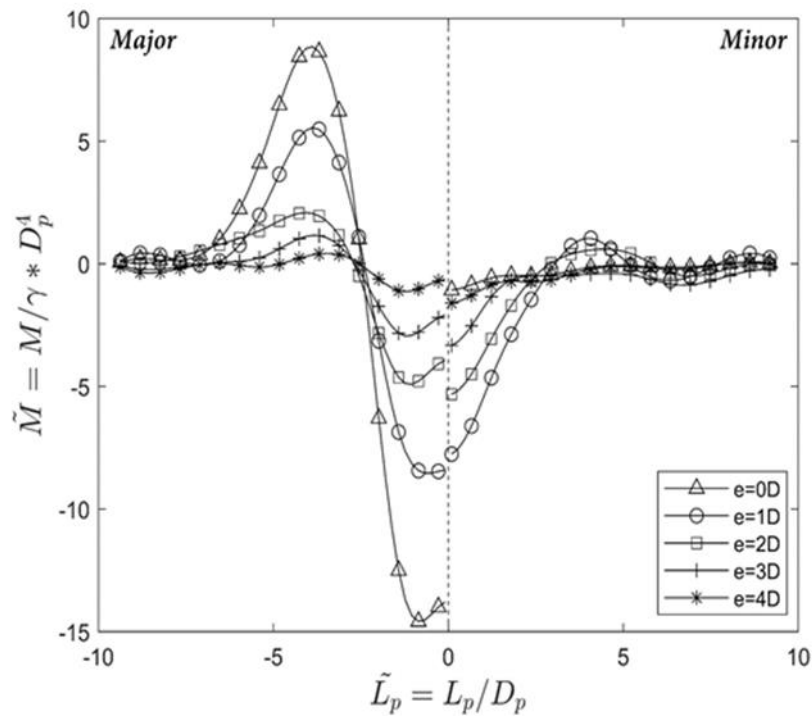


Figure 5-16 Variation in bending moment with load eccentricity at burial depth of $Z_c=1.00\text{m}$ and applied load of 6 tonnes.

Table 5-4 Pipe bending moment magnitude and direction due to eccentricity of load

ECCENTRICITY (e)	NORMALISED BENDING MOMENT				
	Major	Minor	Resultant	angle (°)	RATIO
0D	14.58	0.4	14.59	1.57	0.027
1D	8.4	7.7	11.39	42.5	0.91
2D	4.9	5.3	6.58	58	1.08
3D	2.1	3	3.66	55	1.43
4D	0.64	1.5	1.63	66.9	2.34

It is evident that there is a large difference in behaviour of the pipe, depending on whether the pipe is within or outside the boundaries of the main stress influence zone. For instance, a pipe at depth $Z_c = 1$ and eccentricity $e = 2D$ is completely within the zone of stress influence and exhibits bending increases in both major and minor axis. Whereas, when the pipe is located beyond the zone of the stress influence, there is a negligible bending moment in both major and minor axis, as illustrated in Figure 5-17. Similarly, bending moment reductions for the effect of eccentric load were observed by Hosseini and Tafreshi (2000).

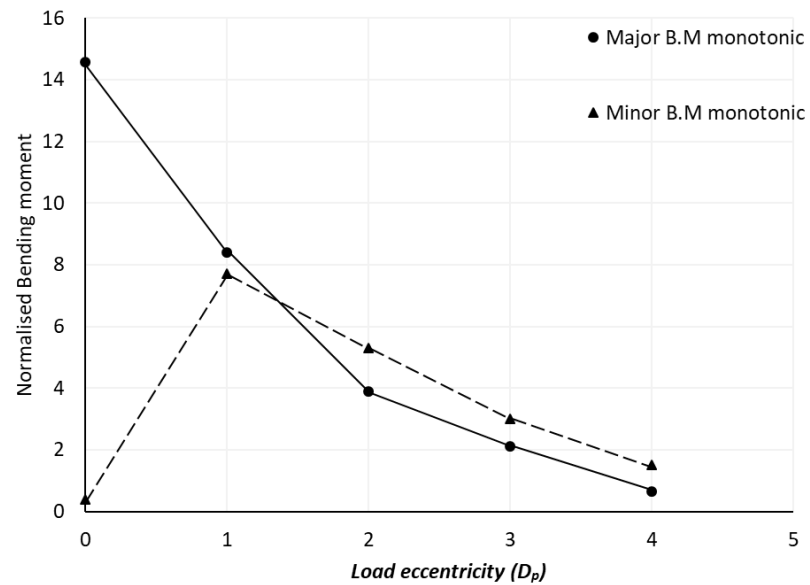


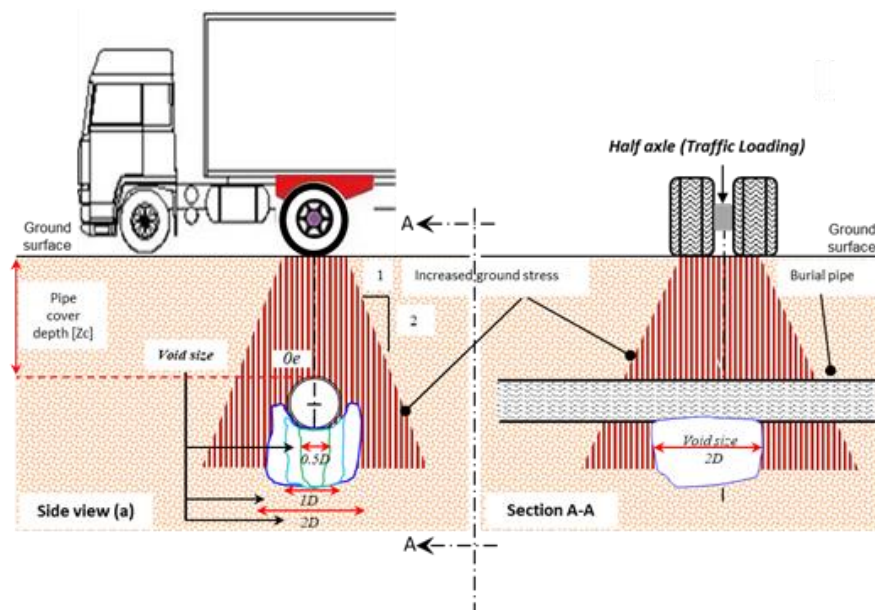
Figure 5-17 Identification of load eccentricity for a 1 m deep pipe.

5.1.3 Effect of void size at the pipe invert (180deg)

In this subgroup pipe deflection and bending response when a void is present are reported. The void configuration was a rectangular prism void shape of length $3D_p$ with widths of $0.5D_p$, $1D_p$, and $2D_p$. As before, the reference case of 1m burial depth is considered to demonstrate the impact of voids on the pipe performance. Two void locations are considered, beneath the invert (180deg) and also along the side of the pipe along the spring line (270deg). This section will show the tests considered in the subgroup are reported in Table 5-5 and also schematically shown in Figure 5-18. The next section shows the results related to the void located at the pipe springline (270deg).

Table 5-5 Effect of void size at the pipe invert (180deg).

Group	Test (#)	Test ID	Cover Depth (Z_c) m	Load magnitude L_m (Ton)	Load Eccentricity $e=D$	Internal pressure Bar	Void Size V_s	Void Location V_l (deg)	Roas Sruface R_s	Monotonic
Group 4a	Test 57	T57- $Z_c1-L_m6T_s-0e-0T-V_s0.5D-V_l180deg$ [M]	1	6T- Single	0e	0	0.5D	180deg	-	y
	Test 67	T67- $Z_c1-L_m6T_s-0e-0T-V_s1D-V_l180deg$ [M]	1	6T- Single	0e	0	1D	180deg	-	y
	Test 77	T77- $Z_c1-L_m6T_s-0e-0T-V_s2D-V_l180deg$ [M]	1	6T- Single	0e	0	2D	180deg	-	y



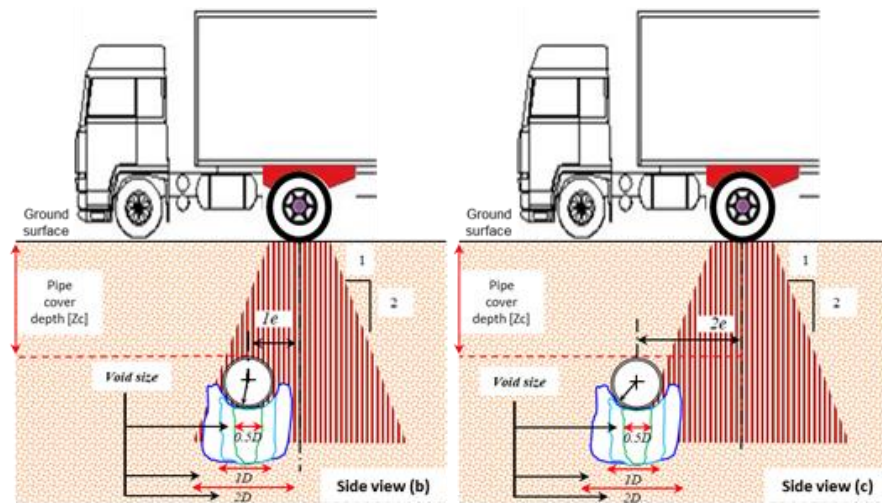


Figure 5-18 Schematic of the pipe behaviour with eccentricity of load and in the presence of different void size at the pipe invert (180deg)

In practice voids might occur around the pipe at any location, however for simplicity, the springline and invert locations are considered herein. This decision is supported by observations of Spasojevic et al. (2007) who observed that voids occurring at the pipe's invert are filled by the soil that moves down from the springline thus resulted in loss of support beneath and to the side of the pipe. The void was located at the mid-span of the pipe in each case.

It is clear from Figure 5-19 that a void located beneath the invert has a significant influence on the pipe performance whereby the bending and deflection increases considerably from the no-void condition. Further increases occur as the void size increased from $1D_p$ to $2D_p$. The maximum bending moments and pipe deflection observed at the major axis when the void was only $0.5D_p$ represented a 5-fold increase in bending. Despite the reduced support beneath the pipe invert, observation confirmed that for the case $e=0D_p$, the lateral bending of the pipe remained small. Further, the relevant pipe deflection for voids bigger than that exceeding the permissible deflection criteria of 5% of pipe diameter during the installation whereas the allowable deflection of the buried pipe should not exceed 2% of the pipe diameter, resulting in significant drooping and hogging moments in the pipe at the point of inflection. Additionally, insignificant bending moment and deflection was observed on the minor axis as expected (also shown in the previous tests).

The observations of surface settlement of the wheel loading also confirmed the loss of stiffness in the pipe-soil system with the introduction of the void and the increased mobility of the load area. Figure 5-20 shows the comparison between the no-void and void condition for different sizes. It is interesting

to note that in each of the cases where the void is present, the stiffness and elastic rebound are similar in magnitude, confirming the critical role a void of any geometry has on the mobility of the pipe.

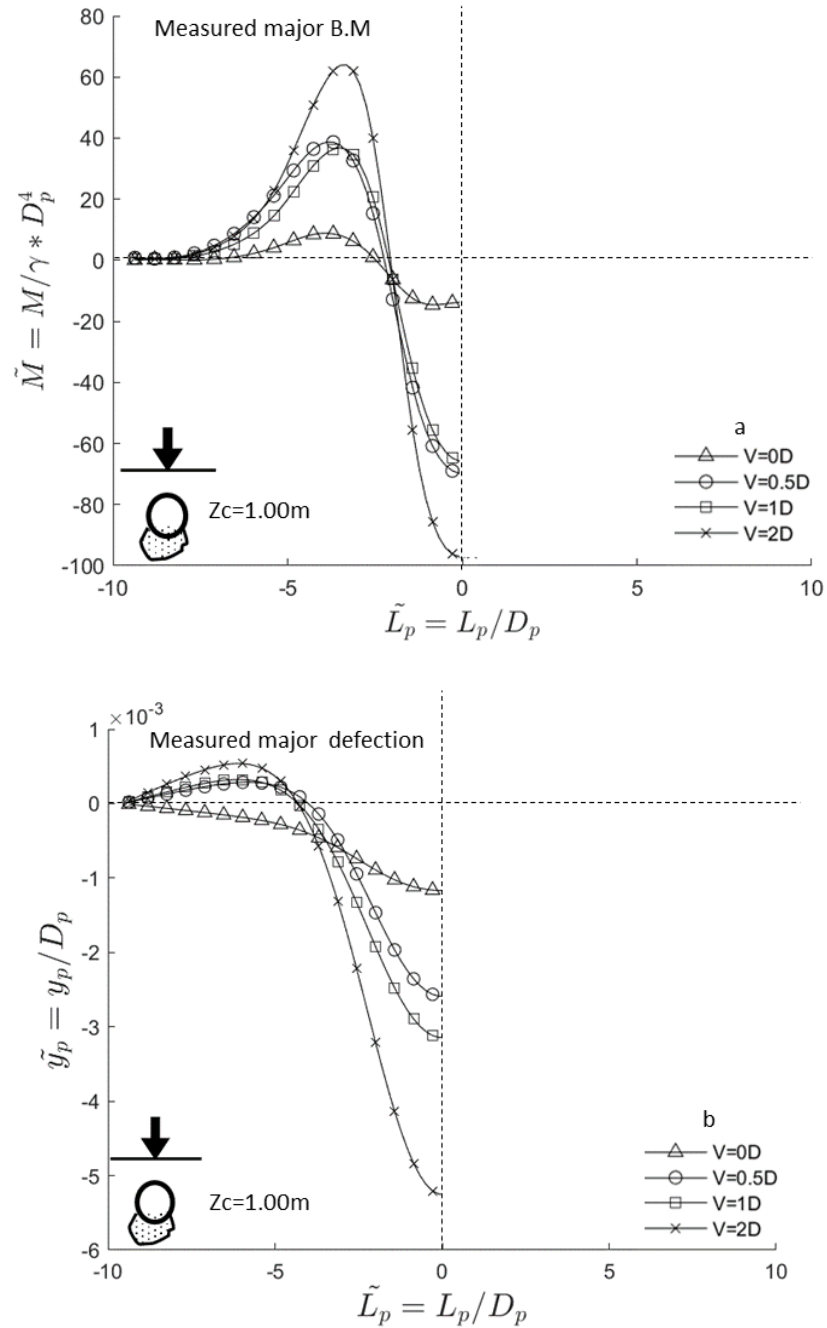


Figure 5-19 Pipe monotonic response with the presence of a void; (a) Bending moment; (b) Pipe deflection

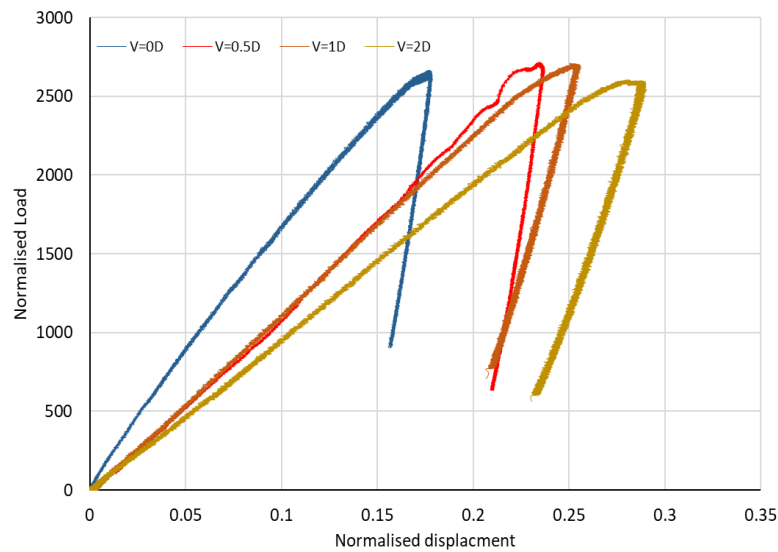


Figure 5-20 Variation in footing stiffness with different void size

5.1.4 Effect of a void at the pipe springline (270deg)

The effect of the void location was evaluated using the tests indicated in Table 5-6 and as shown in the schematic diagram in Figure 5-21. It can be seen from the results that when void is located at the springline (270deg) with an eccentricity load $2D_p$, and 1m depth, the bending moment and pipe deflection are increased in the minor (horizontal) axis of the pipe. However, it was noticed that a slight increase occurred in the bending moment value compared to the test when no void was present – see Figure 5-22a. Thus, it can be concluded that there is a remarkable change in bending moment and pipe deflection associated with the size and location of the void as shown in Figure 5-22b. This indicates that the voids have a very large effect on the pipes. Similarly, the influence of void on buried pipe has been studied by Sales et al. (2015a) who found pipe relative deflection exceeded the allowable design criteria. Flexible pipe design criteria specify that the allowable performance limit for deflection is 5% of the pipe diameter and a factor of safety of 2.5 is used on the allowable buckling pressure (Association, 1998).

Table 5-6 Effect of Void Size at the pipe springline (270deg).

	Test (#)	Test ID	Cover Depth (Z_c) m	Load magnitude L_m (Ton)	Load Eccentricity $e=D$	Internal pressure Bar	Void Size V_s	Void Location V_l (deg)	Roas Surface R_s	Monotonic
Group 4b	Test 87	T87-Z _c 1-L _m 6T _s -0e-0T-V _s 0.5D-V _l 270deg[M]	1	6T- Single	0e	0	0.5D	270deg	-	y
	Test 97	T97-Z _c 1-L _m 6T _s -0e-0T-V _s 1D-V _l 270deg[M]	1	6T- Single	0e	0	1D	270deg	-	y
	Test 107	T107-Z _c 1-L _m 6T _s -0e-0T-V _s 2D-V _l 270deg[M]	1	6T- Single	0e	0	2D	270deg	-	y

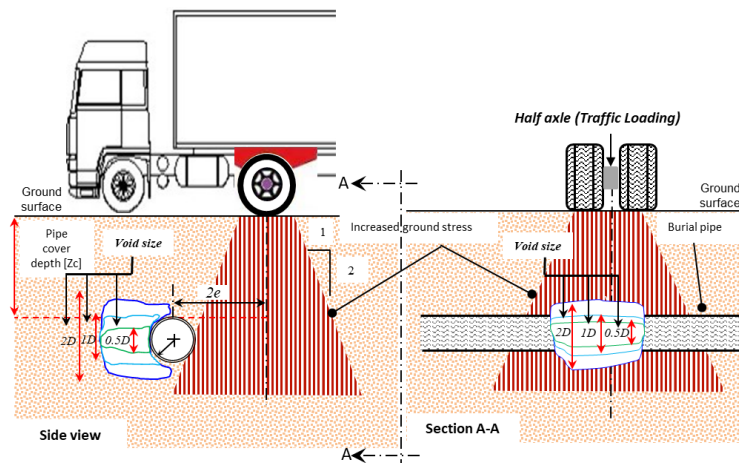


Figure 5-21 Schematic of the pipe behaviour with an eccentricity load ($2D_p$) and void size of $0.5D_p$, $1D_p$ and $2D_p$ at the pipe springline (270deg)

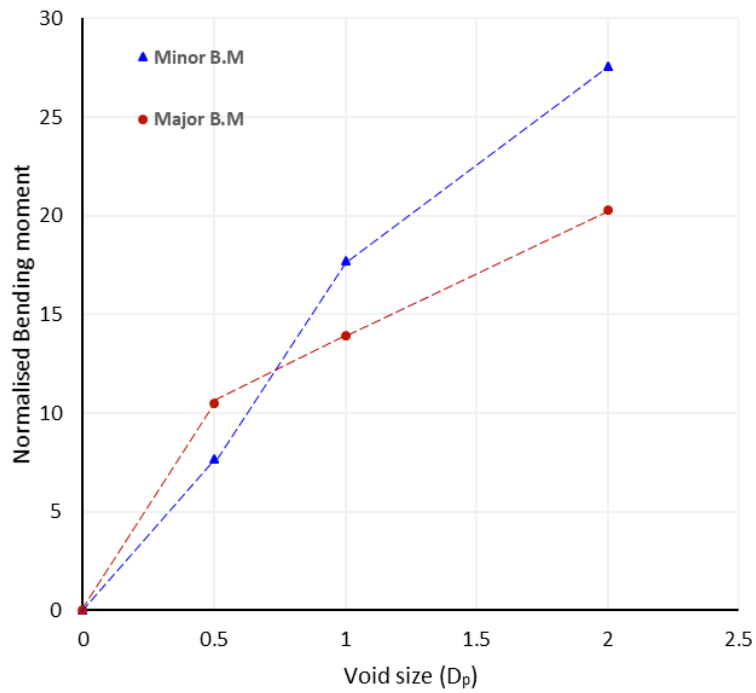
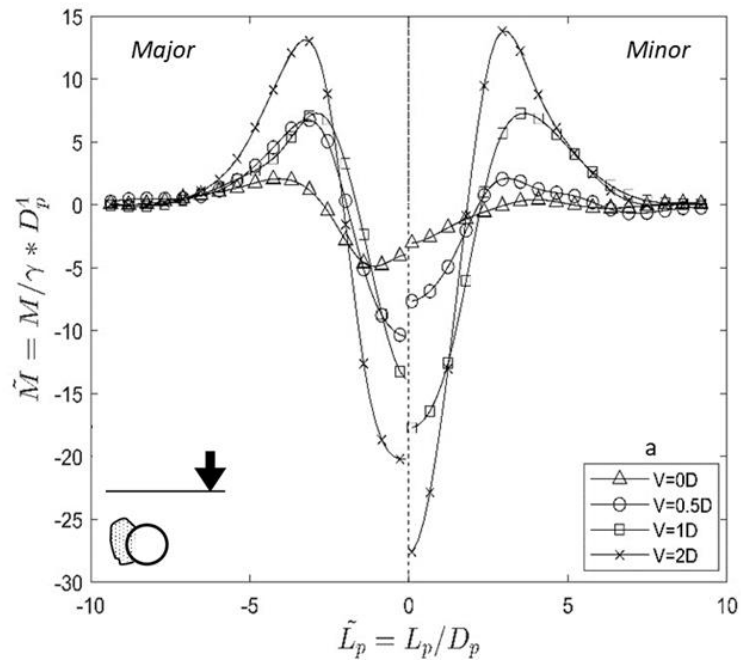


Figure 5-22 Void size and location effect at $e=2$; (a) Major and minor bending moment;

(b) void size effect

5.1.5 Effect of internal water pressure via axial force

A set of centrifuge tests was undertaken to evaluate the effect of an axial force along the pipe under vertical load that is representative of an in-service condition. Circumferential expansion due to pressurisation leads to a reduction in pipe length giving rise to an internal tension force along the cross section of the pipe if both ends are fixed. The internal water pressure simulated in T6, T9 and T12 was 1.5 bar, 2.5 bar and 5 bar respectively and applied as an equivalent force to the pipe using the end loading systems previously described. Table 5-7 reports the tests presented and Figure 5-23 portrays this visually. T3 is also considered as this represented an unpressurised (or empty) pipe condition.

Table 5-7 Effect of Axial Load “from internal pressure”

	Test (#)	Test ID	Cover Depth (Z_c) m	Load magnitude L_m (Ton)	Load Eccentricity $e=D$	Internal pressure Bar	Void Size V_s	Void Location V_l (deg)	Roas Sruface R_s	Monotonic
Group 2	Test 3	T3-Z _c 1-L _m 6T _s 0e-0T[M]	1	6T- Single	0e	0	-	-	-	y
	Test 6	T6-Z _c 1-L _m 6T _s 0e-10T[M]	1	6T- Single	0e	1.5	-	-	-	y
	Test 9	T9-Z _c 1-L _m 6T _s 0e-20T[M]	1	6T- Single	0e	2.5	-	-	-	y
	Test 12	T12-ZC1-Lm6Ts-0e-30T[M]	1	6T- Single	0e	5	-	-	-	y

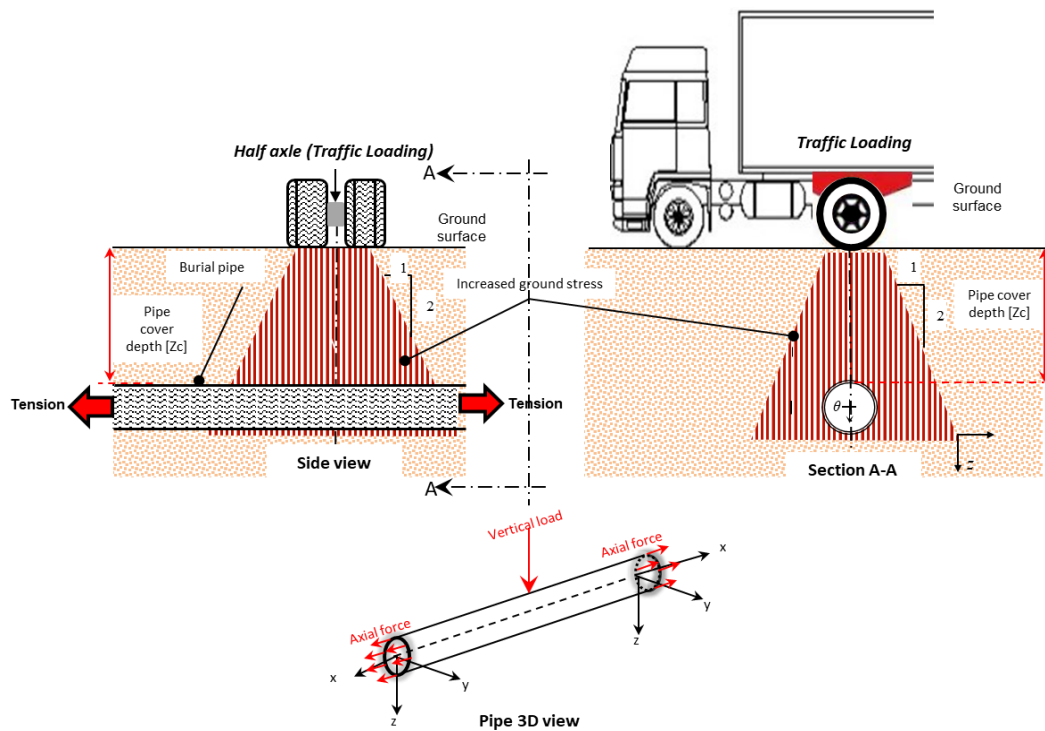


Figure 5-23 Schematic illustration of pipe behaviour due to axial load

Upon completing the centrifuge testing exploring the effect of the internal water pressure, the resulting outputs for bending moment and shear force were measured and plotted, this is shown in Figure 5-24 a & b. These indicate axial force has a noticeable effect on reducing both bending moment and shear force compared to when the pipe is unloaded. This can be explained by the concept of a pre-stressed concrete beam whereby the pre-stress, or in this case the axial stress, limits the deflection of the pipe which in turn reduces the bending and shear components. The reduction in maximum bending is approximately 30% when the pipe is pressured by an equivalent of 5 bar pressure compared to when no pressure is applied. This raises several questions about the impact of service and whether leaks within the network actually contribute to further failures by operating at lower internal pressures. In contrast, practically a high water pressure may lead to pipe explosions and pipe failure, especially in the UK pipeline system, which was built 100 years ago during the industrial revolution.

Furthermore, during service work, should adjoining pipes in the network not be pressurised but a road remains in service overhead, this increases the risk for increased levels of deterioration and damage from increased bending stresses and shear. This message is further reinforced when the pipe deflections are considered (Figure 5-25) where a clear difference in performance is observed for the un-pressurised case. Interestingly, even a small internal pressure provides some additional benefit to reduce pipe deflections theoretically so far. Thus it could be stated that during maintenance or renewal works, it would be beneficial to maintain a nominal allowable fluid head (depending on BSI standards) to restrict uncontrolled deformations. The effect of the axially-modelled internal water pressure is illustrated in Figure 5-26.

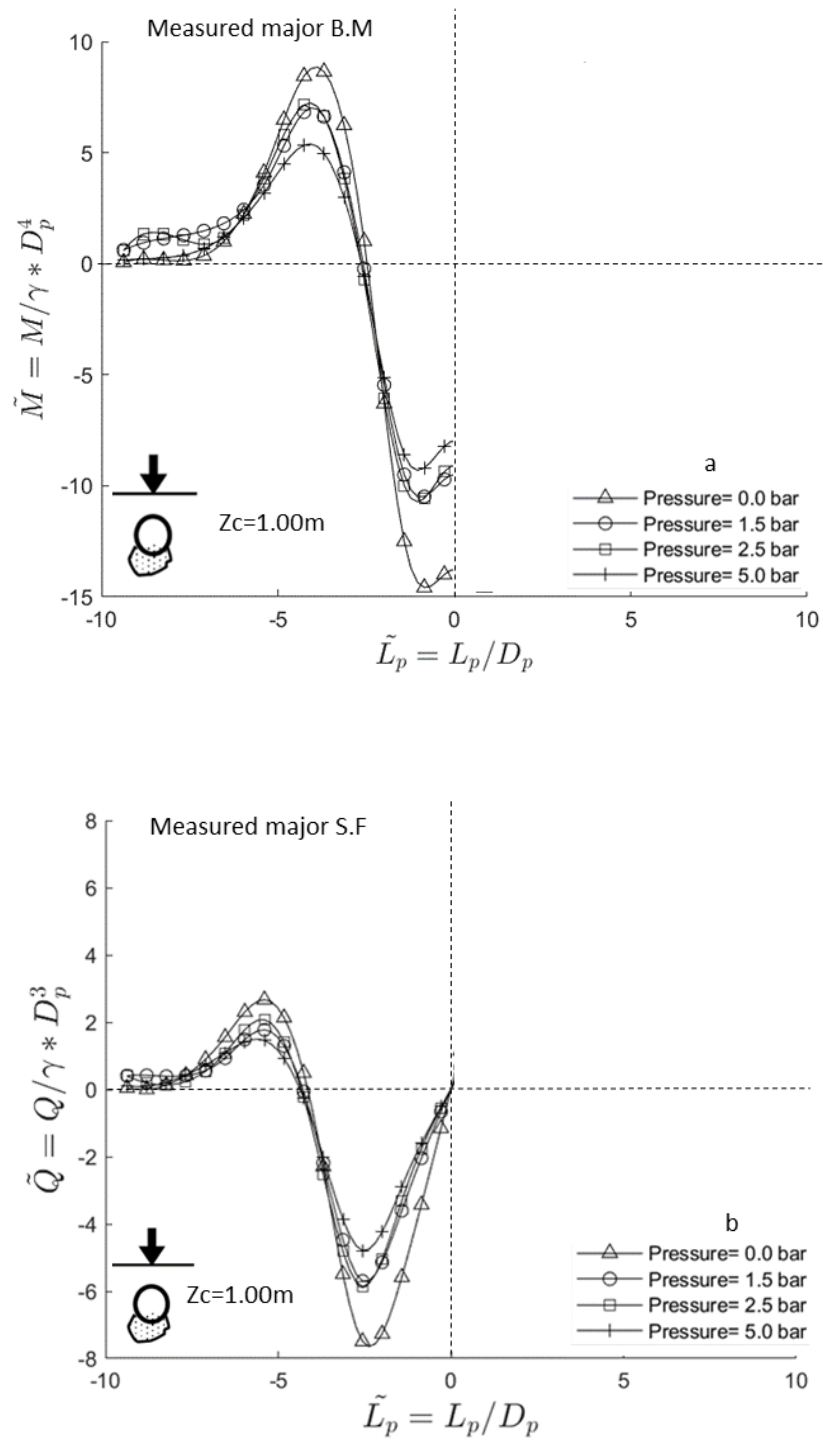


Figure 5-24 Pipe behaviour under axial force; (a) bending moment; (b) shear force

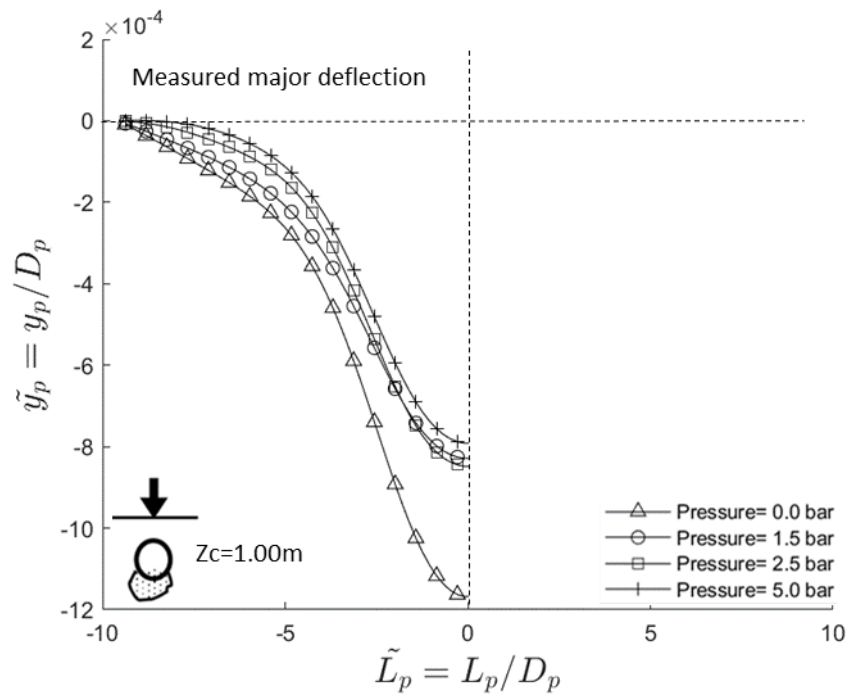


Figure 5-25 Pipe deflection no-axial force compared with axial force applied to the pipe.

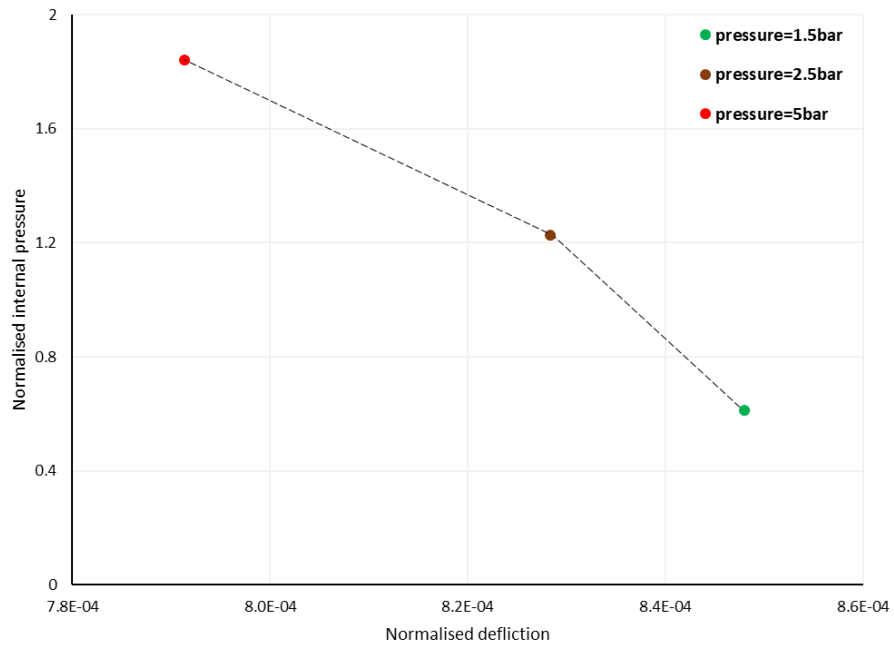


Figure 5-26 Inverse correlation between internal pressure and pipe deflection.

5.1.6 Effect of Road Surface

A series of experiments was performed in this research to investigate to what extent the pavement layers might have an influence on the behaviour of buried pipes under monotonic loading. Therefore, a rubber piece to represent the roadway pavement was placed under the wheel model. It is noted that the rubber does not mimic the real pavement 100% but serves to mitigate the stresses distributed to the pipe. Hence, further study is required regarding more realistic materials to represent the pavement layers. Thus, across the experimental matrix, a total of 20 tests were carried out, to evaluate the effect of the road surface with and without the presence of void, as per the tests in subgroup Table 5-8, Table 5-9 and Table 5-10 and illustrated in Figure 5-27, Figure 5-28 and Figure 5-29. These tests were divided into groups in order to compare the results with others that have no road surface applied to the test scenario. The test configuration has been documented in Chapter 4.

Table 5-8 Effect of Road Surface (No Void Presence).

Group	Test (#)	Test ID	Cover Depth (Z_c) m	Load magnitude L_m (Ton)	Load Eccentricity $e=D$	Internal pressure Bar	Void Size V_s	Void Location V_l (deg)	Road Surface R_s	Monotonic
Group 5a	Test 15	T15- $Z_c1-L_m6T_s-0e-0T[M]$	1	6T- Single	0e	0	-	-	-	y
	Test 127	T127- $Z_c1-L_m6T_s-0e-0T-R_s[M]$	1	6T- Single	0e	0	-	-	R_s	y

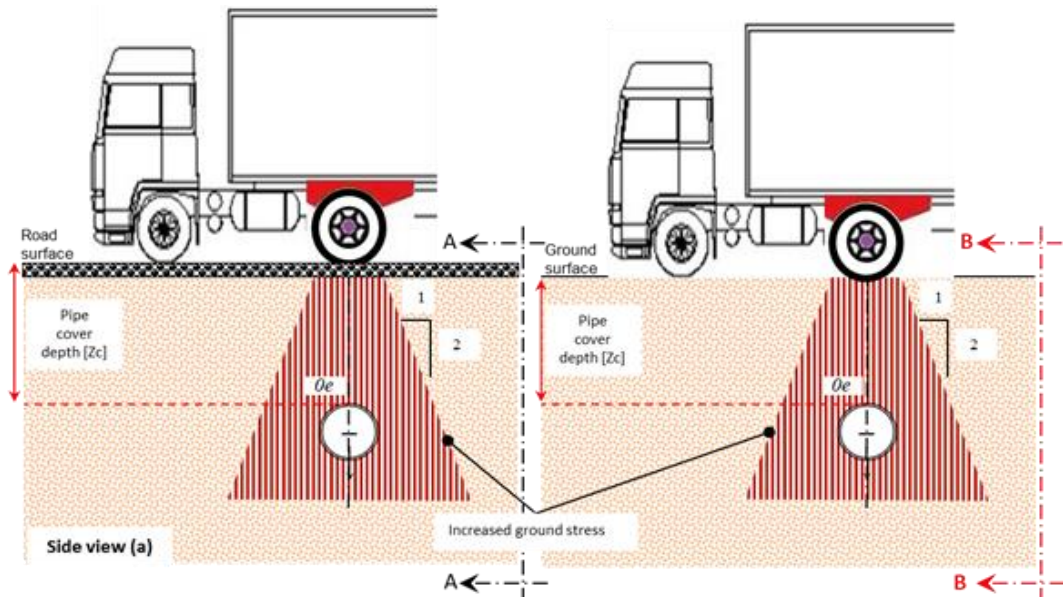


Figure 5-27 Schematic of the pipe behaviour: (a) with road surface; (b) without road surface

Table 5-9 Effect of road surface with the presence of a $2D_p$ void located at the pipe invert (180deg).

Group	Test (#)	Test ID	Cover Depth (Z_c) m	Load magnitude L_m (Ton)S/D	Load Eccentricity $e=D$	Internal pressure Bar	Void Size V_s	Void Location V_l (deg)	Roas Surface R_s	Monotonic
5b	Test 77	T77- $Z_c1-L_m6T_s-0e-0T-V_s2D-V_l180deg$ [M]	1	6T- Single	0e	0	2D	180deg	-	y
	Test 137	T137- $Z_c1-L_m6T_s-0e-0T-V_s2D-V_l180deg-R_s$ [M]	1	6T- Single	0e	0	2D	180deg	R_s	y

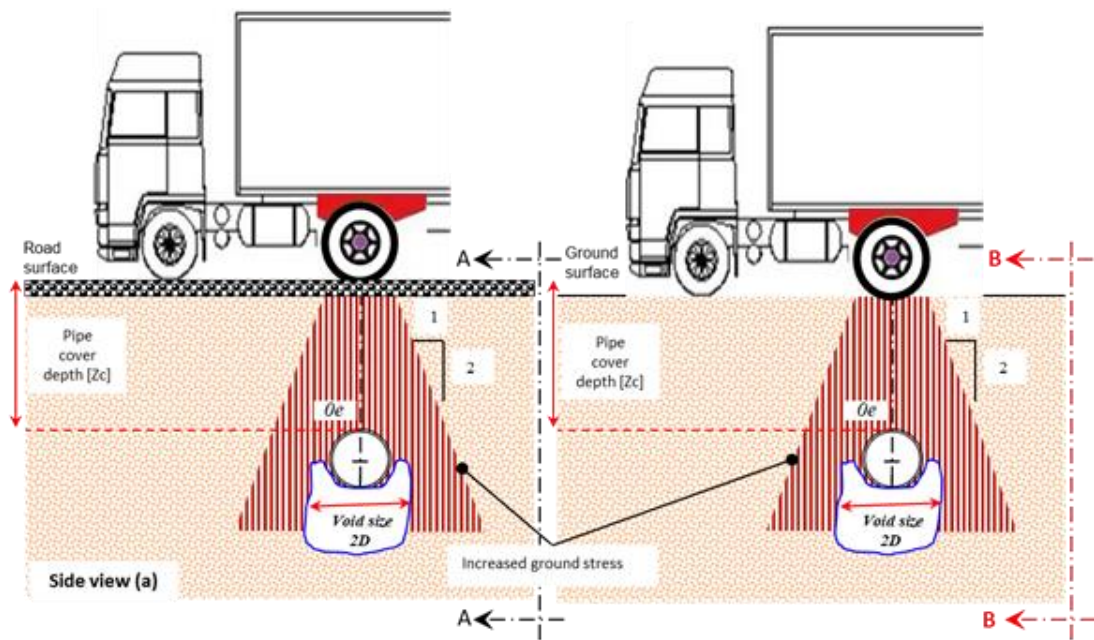


Figure 5-28 Schematic of the pipe behaviour in the presence of a $2D_p$ void located at pipe invert (180deg): (a) with road surface; (b) without road surface.

Table 5-10 Effect of a $2D_p$ void located at the pipe invert (180deg) with presence of a road surface.

Group	Test (#)	Test ID	Cover Depth (Z_c) m	Load magnitude L_m (Ton)	Load Eccentricity $e=D$	Internal pressure Bar	Void Size V_s	Void Location V_l (deg)	Roas Sruface R_s	Monotonic
9c	Test 127	T127-Z _c 1-L _m 6T _s -0e-0T-R _s [M]	1	6T- Single	0e	0	-	-	R _s	1
	Test 137	T137-Z _c 1-L _m 6T _s -0e-0T-VS2D-V _l 180deg-R _s [M]	1	6T- Single	0e	0	2D	180deg	R _s	1

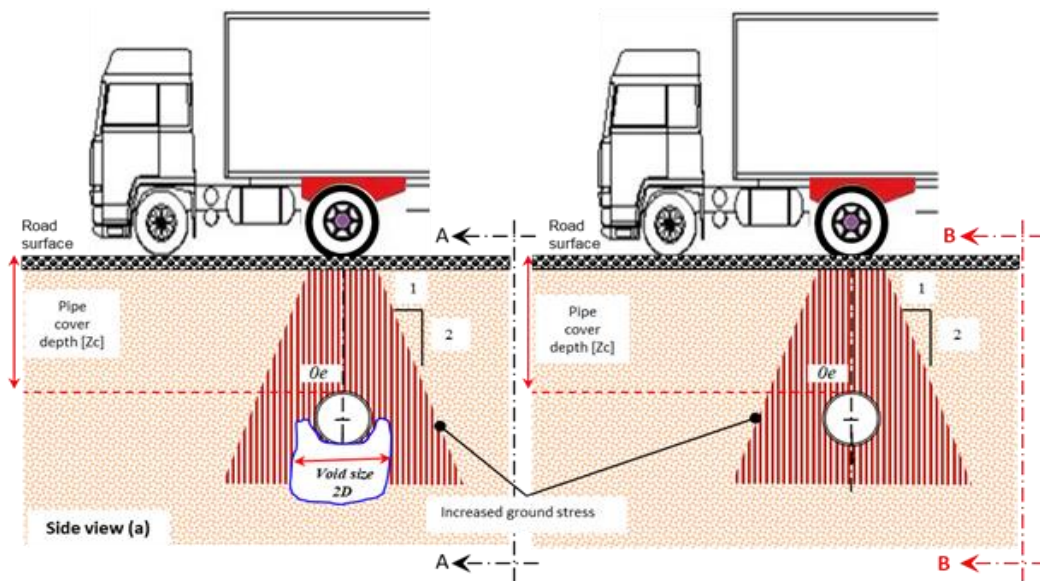


Figure 5-29 Schematic of the pipe behaviour with road surface: (a) with $2D_p$ void located at pipe invert (180deg) ; (b) without void

The results obtained from the tests related to road surface impact are presented in Figure 5-30 a and b. Based on the observations of bending moment, deflection and shear force, limited differences are evident for the comparative tests when no void is present. The largest differences is in the stiffness of the system, which is reduced due to the presence of a void. A decrease in bending moment of approximately 15% occurs for the $2D_p$ void case which indicates that the road stiffness helps to shelf the void and minimise the stress concentration in this region. Shear forces were reduced as well by 20% compared to the previous test that had no road surface applied (see Figure 5-31). Thus, for optimum performance of the pipe it is clear that the road integrity must be maintained to mitigate the stress directly to the pipe. While the road surface was not 100% modelled, results show that loss of support beneath the road surface will also serve to increase the bending stress in the road surface that may lead to increased deterioration in potholing.

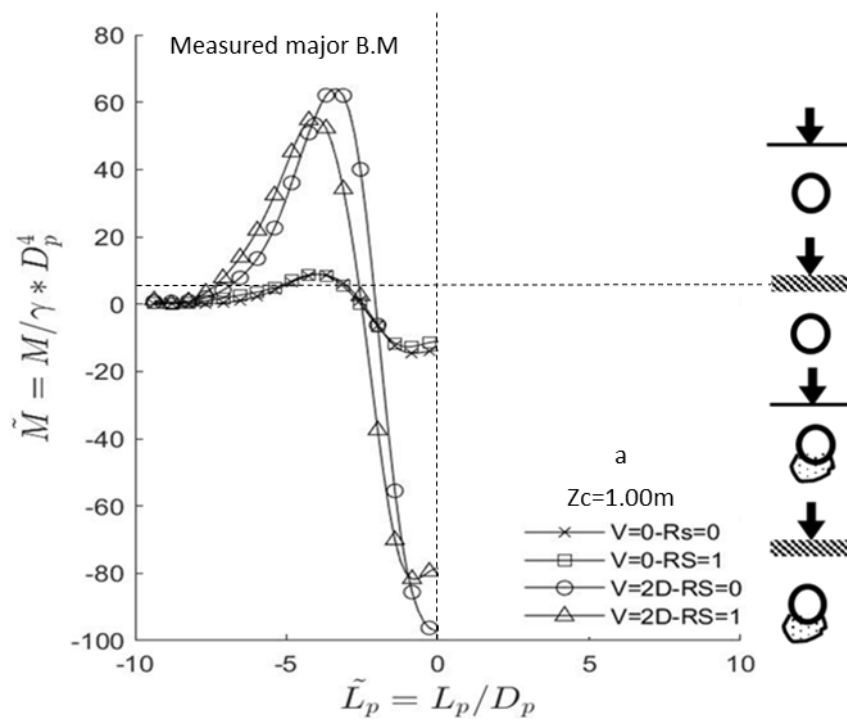


Figure 5-30: (a) bending moment. Where is V is void and Rs is road surface

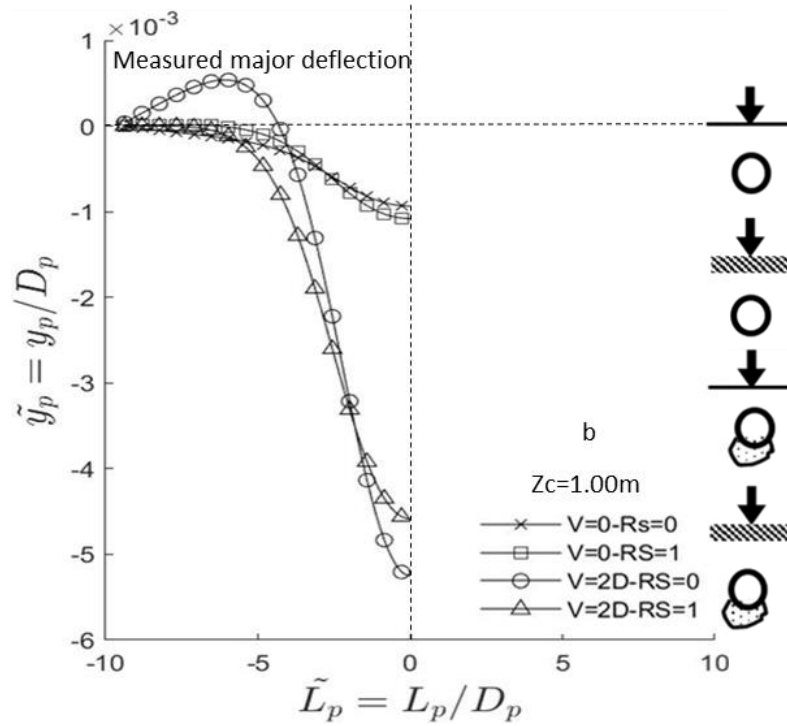


Figure 5-30 (b) pipe deflection where is V is void and Rs is road surface

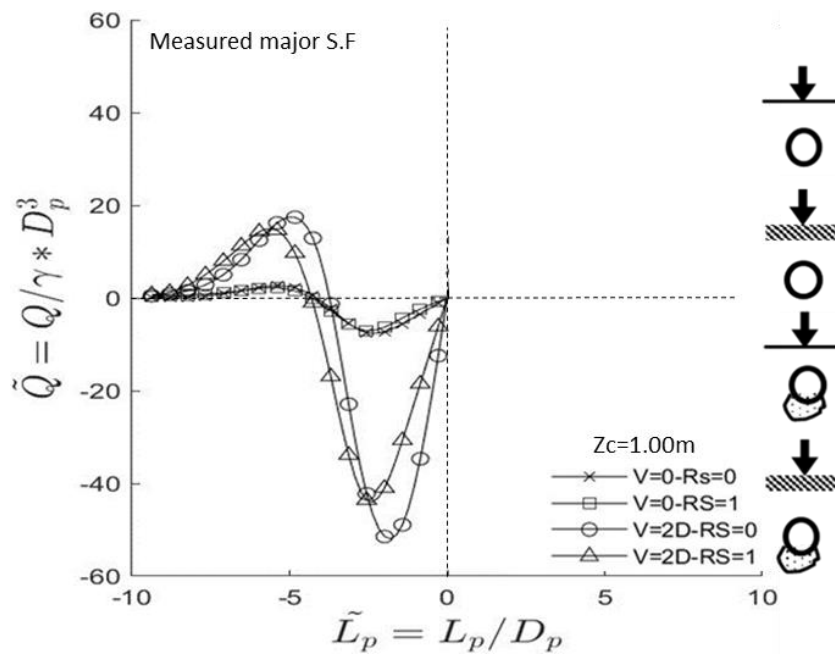


Figure 5-31 Shear force diagram of the pipe with and with presence of road surface/ void

5.1.7 Model Verification

In an attempt to validate the results from the centrifuge test, a finite difference method (FDM) was implemented using MATLAB (v2019b), which generated output in accordance with Boussinesq theory for soil stress distribution and displacements. This has been shown to be an accurate method for calculating the vertical stress at any point below the surface of an elastic, homogeneous and isotropic half space (Boussinesq, 1885). However, before the FDM could be used to support the result of the centrifuge test, the validity of this method had to be confirmed by simple hand calculation using the Boussinesq method with Fadum's chart and bulbs for vertical stress diagram are performed to compare results and assess their reliability.

The results for the pipe deflection from centrifuge model, and FDM model (test T117) were compared (Figure 5-32). The result for pipe deflection show the FDM is capable of capturing the general trend of the pipe deformation, although a 12% difference is noted. This is due to different conditions of the pipe used in the centrifuge model investigation to that used in the theoretical FDM approach. Though the values differ slightly, the deflection diagram of the centrifuge model and the FDM model do follow similar trends as highlighted in Figure 5-32. More details are presented in appendix A.

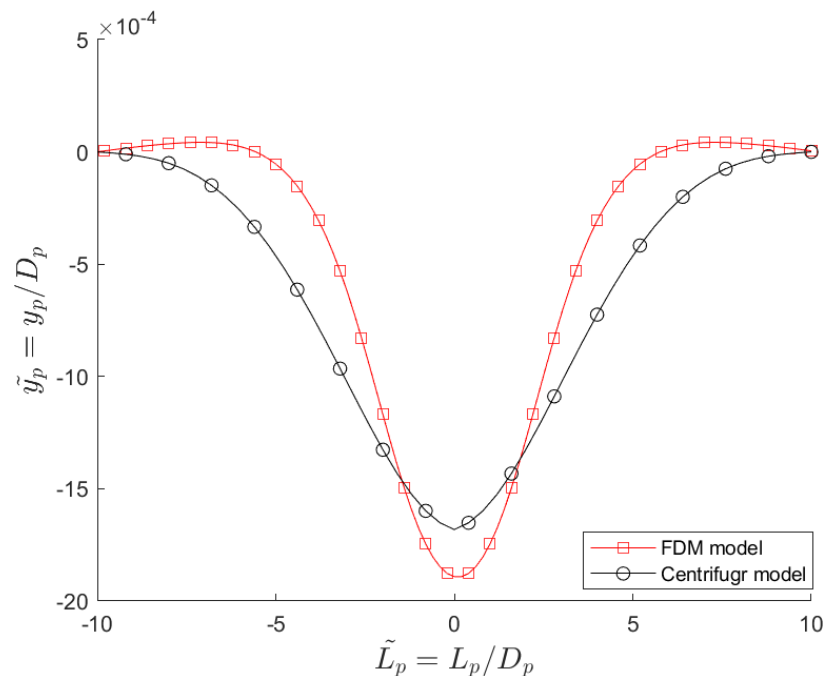


Figure 5-32 Comparison of deflection of pipe from centrifuge test and FDM model

CHAPTER 6

Discussion and Interpretation of Monotonic Loading Results

The impact of the void on the pipe performance was apparent with the evolution of the void size beneath the pipe. In order to investigate the response of HDPE pipes to different burial and loading condition with the presence of a void, a series of experiments has been conducted utilising centrifuge modelling enabling insights into the soil-pipe interaction. 156 tests relevant to soil-pipe interaction were carried out with different full-scale burial depths of 0.5 m, 0.75 m and 1 m, as well as with varying eccentric loading conditions of $0D_p$, $1D_p$, $2D_p$, $3D_p$ and $4D_p$. The main objective of these tests was not only to investigate the state of loading and burial, but also to explore the effect of the presence of voids through this variation of pipe burial depth and loading conditions (vertical and axial).

From a burial condition perspective, the bending moment and pipe deflection decreased with the increase of burial depth. Comparison of pipes buried at different depths ranging from 0.5 m to 1 m shows that shallower pipes experience significantly greater bending moments. The pipe would experience the most unfavourable conditions when the load is applied above the pipe crown, with minimal soil cover (0.5 m). At this position, the pipe experiences a significant bending moment at mid-span, resulting in a significant deflection. This increase in bending moment was also seen by previous authors (Bayton et al., 2018b) among others) and has been expanded by examining the behaviour under varying burial conditions in the current work.

It was also noted that the settlement of the footing was the lowest for pipes buried at 0.5 m for the conditions tested (range of pipe burial depths of 0.5, 0.75 and 1 m) suggesting the importance of the pipe in the development of overall stiffness at shallower depths. The most notable aspect of the results is that the maximum sagging bending moment was observed at the mid span of the pipe, which correlates to the position of the applied vertical load above the pipe. However, it is observed that, increases in the hogging and sagging moments occur irrespective of the burial depth. In each case there is a clear increase in bending moment from the monotonic loading. These results are in good agreement with previous research of (Cao et al., 2016).

One of the key pipe design parameters is to ensure that large variations in bending moment over short distances are minimised. Account should also be taken of sudden points of inflexion as these have large

shear stresses associated with them. As presented, the selection of a greater burial depth facilitates this reduction in pipe stress and could extend the life of the pipe.

Eccentric loads of $0D_p$, $1D_p$, $2D_p$, $3D_p$ and $4D_p$ were inspected, each describing the pipe position relative to the traffic applied, i.e. eccentricity, is a critical parameter for performance of buried plastic pipe along with burial depth. During the test when $e=0D_p$, loading was applied directly above the pipe crown with no eccentricity. This was carried out in order to allow the eccentric test result to be benchmarked against a control test. As expected, as a result of the eccentric load, the pipe is exposed to additional lateral soil pressure and therefore subject to horizontal bending moments and deflection as well as vertical. However, the stress dissipation into the soil depth can be considered to be classical 2V:1H zone of influence. As was seen, the pipe at $1D_p$ is well within the zone of stress influence, whereas the pipe at $2D_p$ transcends boundaries the edges of the zone of stress influence. The results revealed that there is an evident distinction in the behaviour of the pipe according to whether the pipe within or beyond the boundaries of the zone of stress influence. For instance, for two pipes fully inside this zone, the value of the resultant bending moment is comparable. In the case of the pipe eccentrically loaded at $e=1D_p$, the bending moment at the major axis is reduced and the bending moment at the minor axis increased. This would imply the same increase in resultant stress acting on the pipe, but with lateral and vertical components of differing magnitudes. It was noticed that there is a significant reduction in the resultant bending moment when the pipe is positioned just on the outside border of the zone of stress influence, with both the main and minor moments reducing in parallel. The lateral stress is greater than the vertical at this position, and the values do not drop to zero. Hosseini and Tafreshi (2000) found similar observations of bending moment decreases for eccentric loads. The transitional stress states produced on the underground pipe in serviceable circumstances under transient loads associated with traffic loading are reflected in the measurements of maximum and minimum bending moments occurring in the major (vertical) and minor (horizontal) planes.

Regarding the pipe behaviour with the presence of the void beneath the pipe at the invert, the result of the tests showed that the presence of the void significantly increased the sagging and hogging bending moment, deflection and shear. This increase of the bending moment is linked with the increase of void size. Hence, the buried pipe with presence of void ($3D_p$) that located at pipe invert recorded the highest bending moment among other smaller void sizes. The result of these tests showed a direct link between the bending moment and the void size ($0.5D_p$, $1D_p$ and $2D_p$) with maximum increase about 15% ($2D_p$) compared to the pipe response when no void was present. In contrast, it was shown that the bending moment increased at the minor axis with the pipe loaded eccentrically and with void presence at the springline. However, it was noticed that a slight bending moment occurred at the major axis.

Using rubber material to represent the road surface to investigate the influence of the road surface on an underground pipe was an option to enable insight into the impact of the road surface in underground pipes. Although the modelled material does not mimic the real road pavement entirely, it should be

noted that a remarkable change in bending moment was observed, with the road surface offering some improvement in pipe performance when a void was present at the invert. Thus, road surface contribution has a significant impact in reducing load transfer to the pipe, which in turn reduces the bending moment by an average of 20% when compared to the test that had no road surface present. These results are consistent with the findings of other researchers (Cao et al., 2016) among others) which stated that road surface has significant influence on underground pipes, although different materials was used to mimic the rigid pavement.

CHAPTER 7

Pipe-soil Behaviour Under Cyclic Loading

7.1 Introduction

The cyclic loading stage was implemented to offer some understanding of pipe behaviour under a more realistic load case scenario of multiple vehicle passes over the pipe. Over the lifetime of the buried pipe system and its existence in service, it is subjected to thousands of cyclic loading every day, varying in load magnitude and load eccentricity. This has a notable influence on pipe performance that must be taken into account (Mehrjardi and Tafreshi, 2008); (Tafreshi and Khalaj, 2008). While the present work only considered load packages up to 3600 cycles, the onset of loading and the initial evolution of performance that takes place beyond the single monotonic loading is still interesting to explore.

7.2 Cyclic Loading Response

During the cyclic loading stage of the experimental test, a 6 tonnes load was applied and removed in a cycle 3600 times, on order to simulate multiple vehicles travelling over the pipe, as would be in the case of major road. Hence, the increases of level of stress on a pipe due to a repetitive cyclic load could result in accelerated level of fatigue failure. Most fatigue failures are caused by cyclic loads significantly below the loads that would result in yielding of the material; accordingly, the tests reported offer an insight of the changes in pipe performance that develop and thus draw comparisons with the monotonic load configurations. A key consideration in understanding the soil-pipe interaction behaviour under cyclic loading is how realistically the centrifuge model represents the passing vehicles. While there are dynamic impulse load effects arising from the load being transient, this limitation is not considered detrimental as there is a lack of studies, experimental or numerical, in the literature that consider such effects (Bayton et al., 2018b).

Data processing was similar to that for the monotonic condition with the deployment of the ‘peakfinder’ script to aid the identification of cyclic number so temporal data could be extracted. A trace of load with time for a typical example is presented in Figure 7-1, with zoomed section that shows 50 cycles. The monotonic load is evident up to 180 seconds, followed by the 3600 load cycles taking up to 30min to complete.

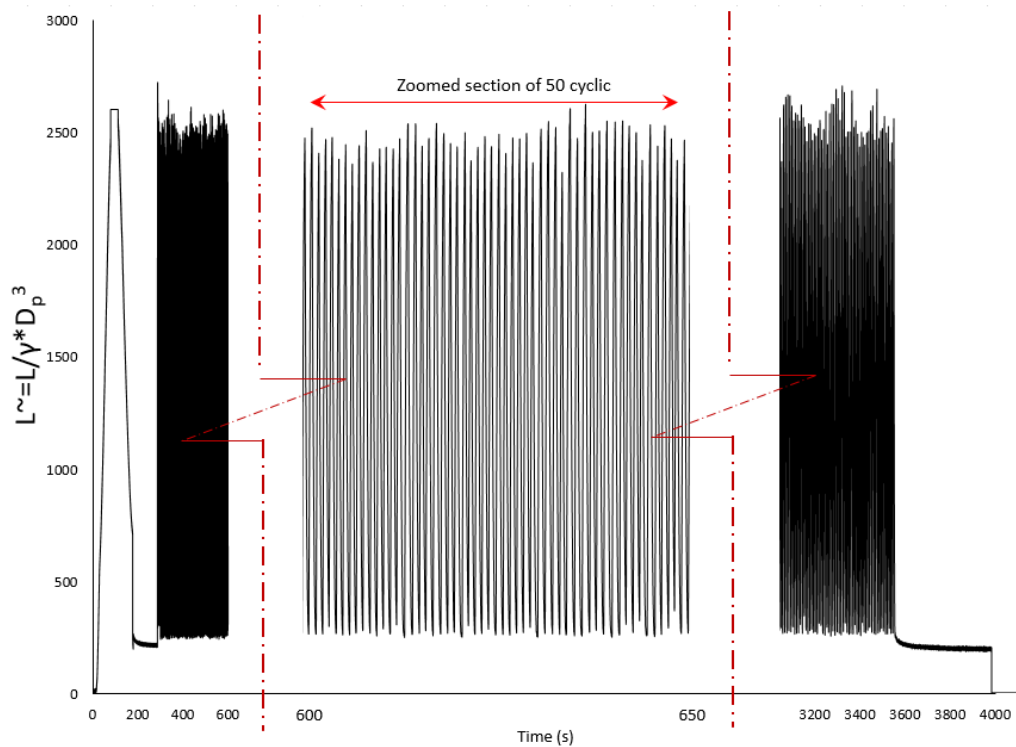


Figure 7-1 Example of the cyclic load time history.

7.2.1 Effect of surface loading on soil stiffness

Four baseline tests (no buried pipe) were performed to benchmark the performance objectives of this investigation. All tests were conducted on sand with average relative density ranging from 78% to 80%. Isolating the influence of the pipe allowed the performance of the void only to be observed. Samples were tested without void ($V=0D_p$) and with a void ($V=0.5D_p$, $V=1D_p$ and $V=2D_p$). The response of sand subjected to loading and unloading was also investigated, with the initial prediction suggesting a relatively fast response upon application of the load. These expectations were matched as seen in fig 4 where sand displacement increased at a slower rate in comparison to the loading condition, which is a typical behaviour for granular soil. It was evident from the results when no void was present the settlement of the simulated wheel progressed gradually in the initial loading cycles, then reached a steady condition until the end of the experiment from around 200 cycles. When a void was present the rate of settlement increased more rapidly in the initial 10 cycles, reaching higher levels of settlement, before also stabilising at approximately the 200th cycle. This was due to the gradual compaction of the soil as the test progressed, as illustrated in Figure 7-2. Also, it can be noticed that the soil density tends to increase by approximately 4% beyond 200th cycle. This has been measured manually by knowing the difference in sample height after the test and compared with the LVDT measurements which were mounted for this purpose.

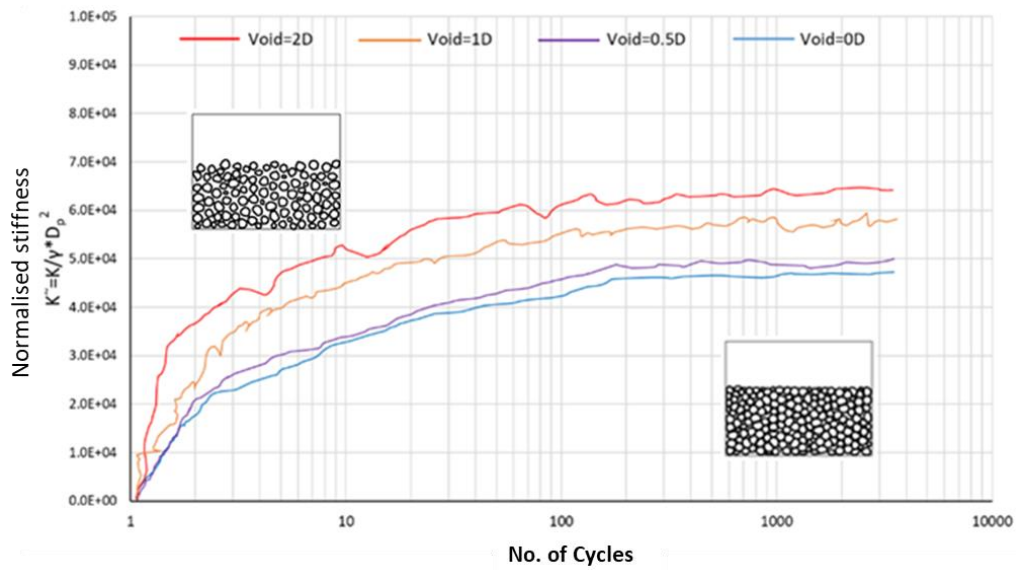


Figure 7-2 Soil stiffness comparison with number of cycles at 6 tonne load per cycle

7.2.2 Effect of Burial Depth

Tests that evaluated the effect of burial depth, with no void, in this subgroup were T3, T147 and T117 as presented in Table 7-1. Data was extracted and analysed using the same steps outlined in Chapter 5. The evolution of the bending moment is shown with respect to burial depth in Figure 7-3 (a, b and c) for 3 different pipe burial depths of 0.5m, 0.75m and 1m, respectively. Interestingly the maximum bending moments increase during the first cycles and decrease slightly towards the end of the test. The increase is more apparent in early cycles with the increase becoming lesser between later cycles. This suggests that residual moments in the pipes will eventually plateau after a certain number of cycles. It further confirms that the residual moments are thought to be the result of the pipe not being able to revert to its un-deformed shape due to the displaced soil essentially pinning it in position, in that vertical displacement increases with each cycle as do residual bending moments. Following the trend of the monotonic tests, the bending moment experienced by the pipe is markedly reduced, by a factor of 3 approximately, as the burial depth approaches 1m. This confirms the significance of burial depth to protect pipes from excessive traffic load interaction.

Table 7-1 Effect of burial depth (Z_c).

	Test (#)	Test ID	Cover Depth (Z_c) m	Load magnitude L_m (Ton)	Load Eccentricity $e=D$	Internal pressure Bar	Void Size V_s	Void Location V_L (deg)	Roas Sruface R_s	Cycles @2Hz freq
Group 1	Test 3	T3- Z_c 1- L_m 6T _s -0e-0T[C]	1	6T- Single	0e	0	-	-	-	3600
	Test 147	T147- Z_c 0.75- L_m 6T _s -0e-0T [C]	0.75	6T- Single	0e	0	-	-	-	3600
	Test 117	T117- Z_c 0.5- L_m 6T _s -0e-0T[C]	0.5	6T- Single	0e	0	-	-	-	3600

Note: Test code (ID) will refer to the data file captured during the centrifuge test.

Formatted as shown in above table 5th column; where

Tx= test number [T1-T156]; Z_c = soil cover depth [0.5m-0.75m-1.00m]; L_m x= load magnitude [6Ton =half axle12Ton= full axle];

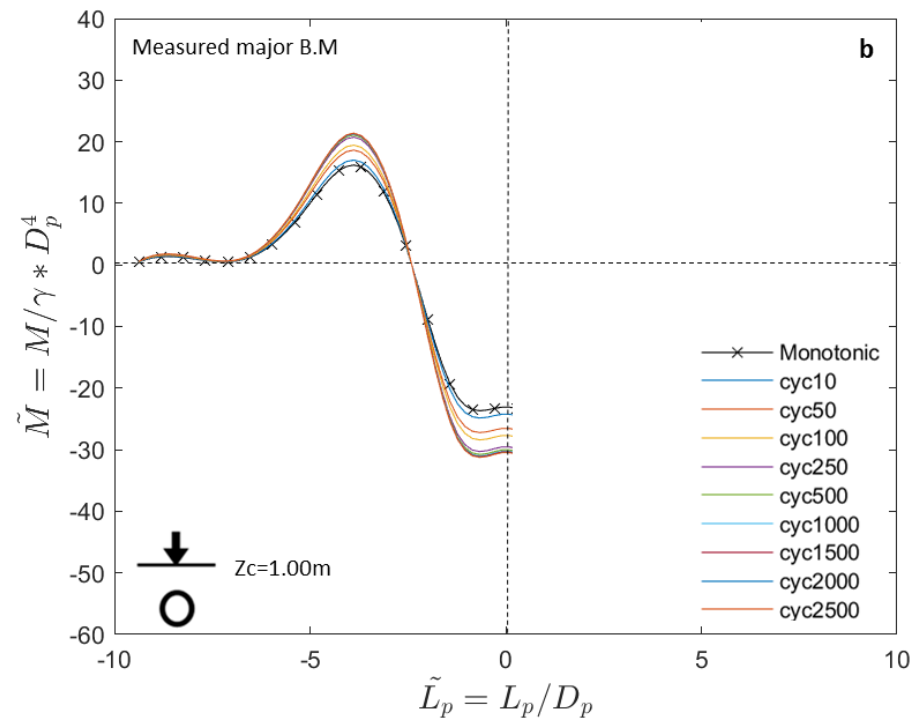
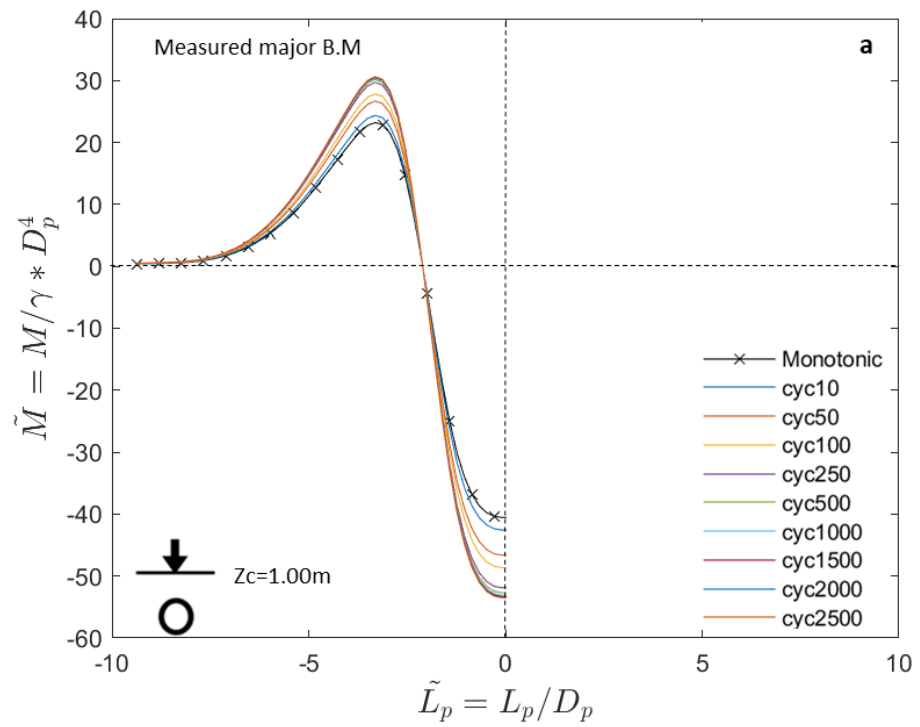
xe= load eccentricity[1D-2D-3D-4D]; xT= axial tension [10N,20N,30N]; V_s x= void size [0.5D,1D,2D]; V_L x= void location [6^{AM} , 9^{AM}];

R_s = Road surface; S/M/C= test stage [s=spin up/M= Monotonic loading/C= Cyclic loading].

Where x is different variable for each individual test, D is pipe diameter, N is axle force in newton

Reflecting on the transition from monotonic to the cyclic loading at each burial depth, it is observed that increases in the hogging and sagging moments occur irrespective of the burial depth. In each case there is a clear increase in bending moment from the monotonic loading up to the 10th cycle where the behaviour is similar to that of the static loading as seen in Figure 7-3 (a, b and c). Further increases are observed with a group of cyclic responses (50th to 100th) having similar performance. Beyond this there is a further increase up to 250 cycles after which there is little change and the bending moment stabilises. A steady bending moment was observed once the number of cycles reached 2500, where a new soil regime, either with dilation and local shear taking place, or the soil being critical state, means that the bending moment remains constant. This confirms that the most critical evolution of performance follows immediately after the pipe burial, and thus indicates that ensuring correct burial conditions during a pipe replacement or renewal scheme is critical. It is uncertain whether this stabilisation would continue for cycles beyond those tested here, but nevertheless it still confirms that repeat loading of a pipe, even in optimal burial conditions still yields greater bending than a static case.

In contrast, when the load was removed, the bending moment did not return to zero and residual 'locked-in' bending moment was observed. The phenomenon is clearly more pronounced for the shallower buried pipes. For instance, for pipe with cover depth 0.5 m, the increase in residual bending moment is over 40% beyond 250 cycles, which is a significant design consideration. This can be attributed to localised changes in sand grain distribution and density, and therefore new soil-structure interaction regimes on each cycle. Hosseini and Tafreshi (2000) suggest a reason evolving bending moments due to the residual bending moments being locked into the pipe as the soil around is compacted, before the next cyclic load application. The evolution of maximum bending moment is shown in Figure 7-4.



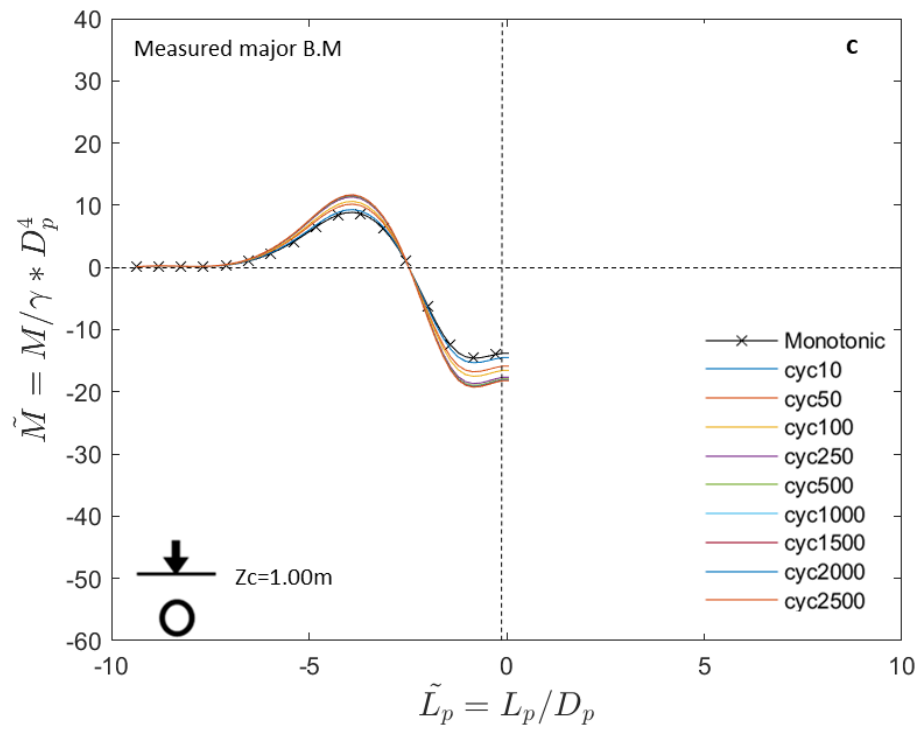


Figure 7-3 Bending moment under cyclic load with different burial depth (a) $Z=0.5m$ (b) $Z=0.75m$; (c) $Z=1m$

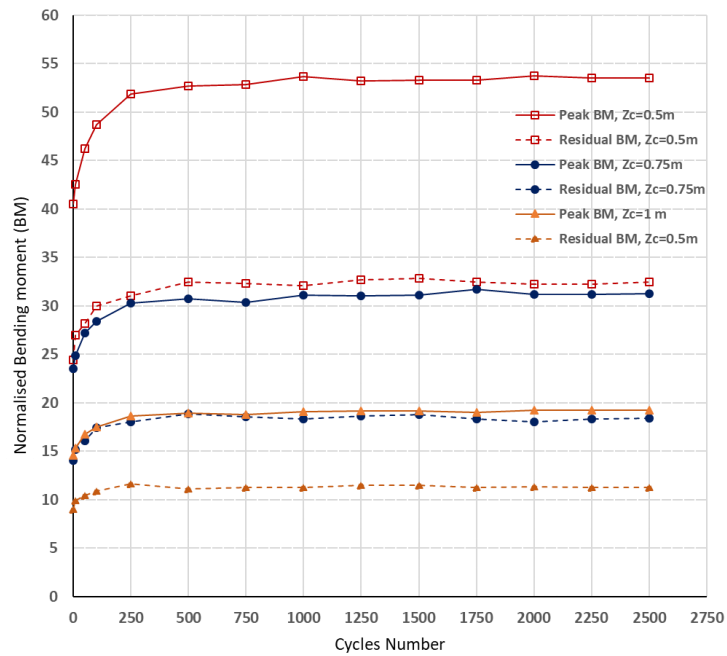
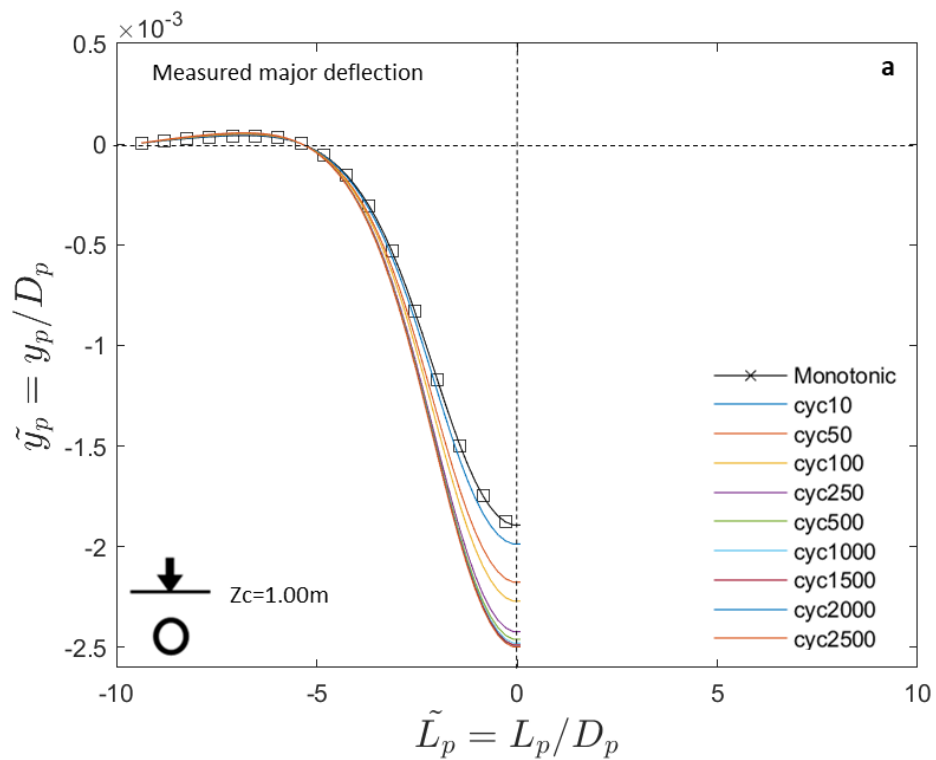


Figure 7-4 Peak and residual major bending moment with increases in cycles

It is expected that there will be minimal bending moments in the minor axis due to the load application with zero eccentricity. This was investigated earlier in the previous chapter. Similarly, there is a noticeable decrease in the total displacement from the 0.5m depth to the 1m depth. Again this reduction follows the expected trend as the increased depth reduces the total moment on the pipe and therefore the deflection produced. On the other hand, the trend in the displacements is that under each cycle the displacement shows a slight increase, which then contributes to an overall pipe displacement. Finally, there is a difference in pipe deflection between the outputs displayed previously for the monotonic loading and the outputs displayed for the cyclic loading, which exhibits a higher deflection due to the cyclic loading. In contrast, advanced cyclic load results in less compaction and deflection, whereas bending moment remains constant (see Figure 7-5 (a, b and c)).



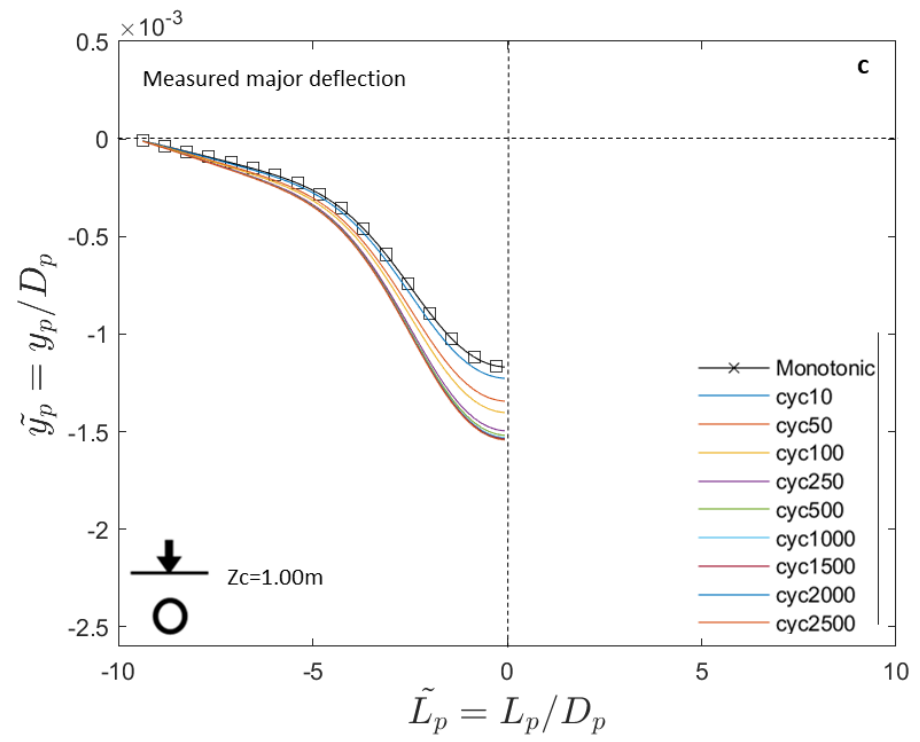
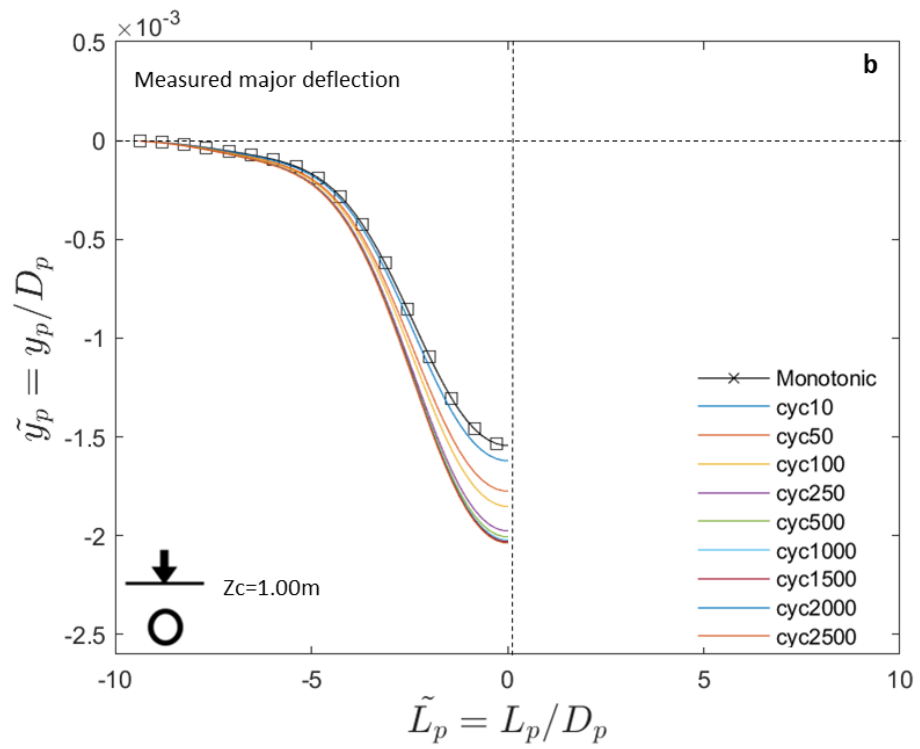


Figure 7-5 Pipe deflection under cyclic loading; (a) $Z=0.5\text{m}$; (b) $Z=0.75\text{m}$; (c) $Z=1\text{m}$.

7.2.3 Effect of Eccentricity

Eccentric loading combined with cyclic loading was considered for a pipe at a burial depth of 1m depth with eccentricities of $0D_p$, $1D_p$, $2D_p$, $3D_p$ and $4D_p$. These conditions correspond to the tests numbers presented in Table 7-2.

Table 7-2 Effect of eccentricity (e) half axle (6Ton).

	Test (#)	Test ID	Cover Depth (Z_c) pro-Mod-m	Load magnitude L_m (Ton)	Eccentricity e (D)	Internal pressure Bar	Void Size V_s	Void Location V_l (deg)	Roas Sruface R_s	Cycles @2Hz freq
Group 3	Test 3	T3-Z _c 1-L _m 6T _s -0e-0T[C]	1	6T- Single	0e	0	-	-	-	3600
	Test 14	T14-Z _c 1-L _m 6T _s -1e-0T[C]	1	6T- Single	1e	0	-	-	-	3600
	Test 2	T2-Z _c 1-L _m 6T _s -2e-0T[C]	1	6T- Single	2e	0	-	-	-	3600
	Test 13	T13-Z _c 1-L _m 6T _s -3e-0T[C]	1	6T- Single	3e	0	-	-	-	3600
	Test 1	T1-Z _c 1-L _m 6T _s -4e-0T[C]	1	6T- Single	4e	0	-	-	-	3600

Based on the outcome from physical model tests, it is clear that the zero eccentric loading $e=0D_p$ has greater impact on the major axial and negligible impact on the minor axis. In contrast, in case of eccentric load of $e=1D_p, 2D_p, 3D_p$ and $4D_p$, the impact of the load increases on the minor axis rather than the major axis to some extent, not exceeding zone of stress influence. Figure 7-6 presents the change in bending moment due to a variety of load eccentricities under a maximum number 2500 cycles. A similar trend of bending moments has been observed when monotonic loading was applied (Section 5.2). Table 7-3 presents the effect of the cyclic load with variation of eccentric load and 1m cover depth on major and minor bending moments and, also the corresponding resultant vector direction.

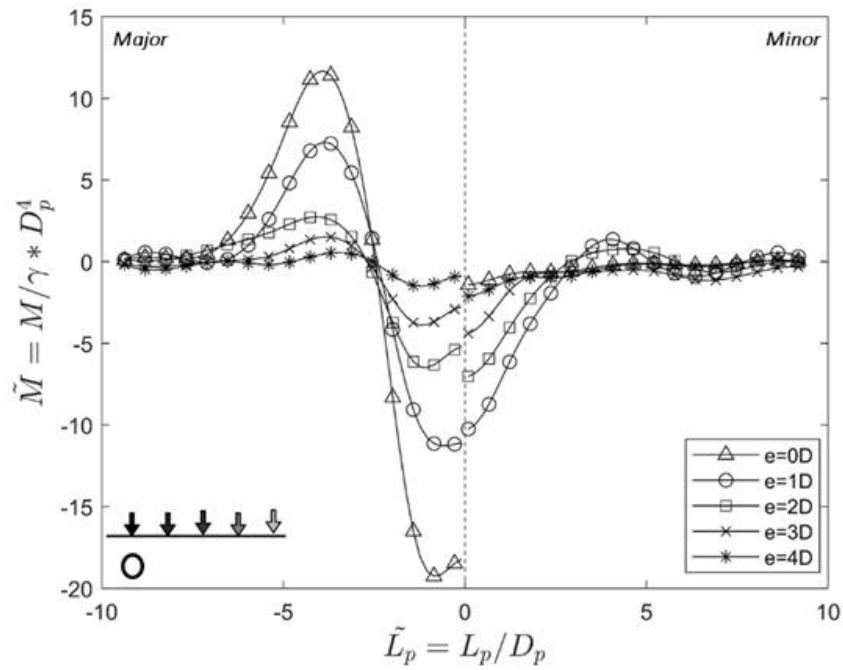


Figure 7-6 Variation in bending moment with load eccentricity at a burial depth of $Z_c=1m$ and applied load of 6tonns

Table 7-3 Pipe bending moment magnitude and direction due to eccentricity of load.

ECCENTRICITY (e)	NORMALIZED BENDING MOMENT@2500CYCLES			angle (°)	RATIO
	Major	Minor	Resultant		
0D	19.16	0.52	14.59	1.55	0.027
1D	11.25	10.13	15.13	42	0.90
2D	5.19	6.97	6.69	53	1.34
3D	2.75	3.94	4.80	55.1	1.43
4D	0.84	1.98	2.15	67	2.36

It can also be seen in Figure 7-7 that a range of magnitudes of cyclic loading has an influence on pipe eccentricity, this impact being greater in both major and minor axis, when the pipe located at the zone of stress influence. This has been outlined across the literature.

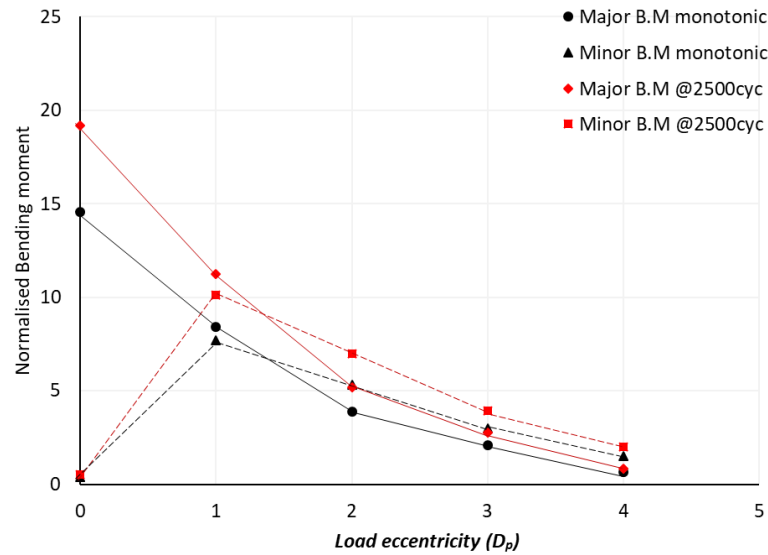


Figure 7-7 Identification of load eccentricity monotonic and cyclic (2500cycles) loading for 1m deep pipe.

It can be seen that a reasonable duration of cyclic load creates a larger contribution to the pipe deflection compared with monotonic load only, with a more than 30% increase of pipe deflection at the end of 2500 cycles. Although, there were 3600 cycles applied, as the soil structure regime changed and soil dilation and shear took place, the soil reached the critical state and the pipe showed no further increase in deflection to this point. It is also notable that during the initial period of cycles, from cycle 1 to cycle 300, in particular, the sand particles were still rearranging and compacting each cycle. This led to a clear change in deflection for the first 300 cycles, followed by a gradual rise in value of the deflection until it stabilized at 2500 cycles. This behaviour was observed during all scenarios for $e = 1D_p, 2D_p, 3D_p,$ and $4D_p$. Figure 7-8 (a, b, c, d and e) shows the normalised major axis of pipe deflection of centrifuge experiments.

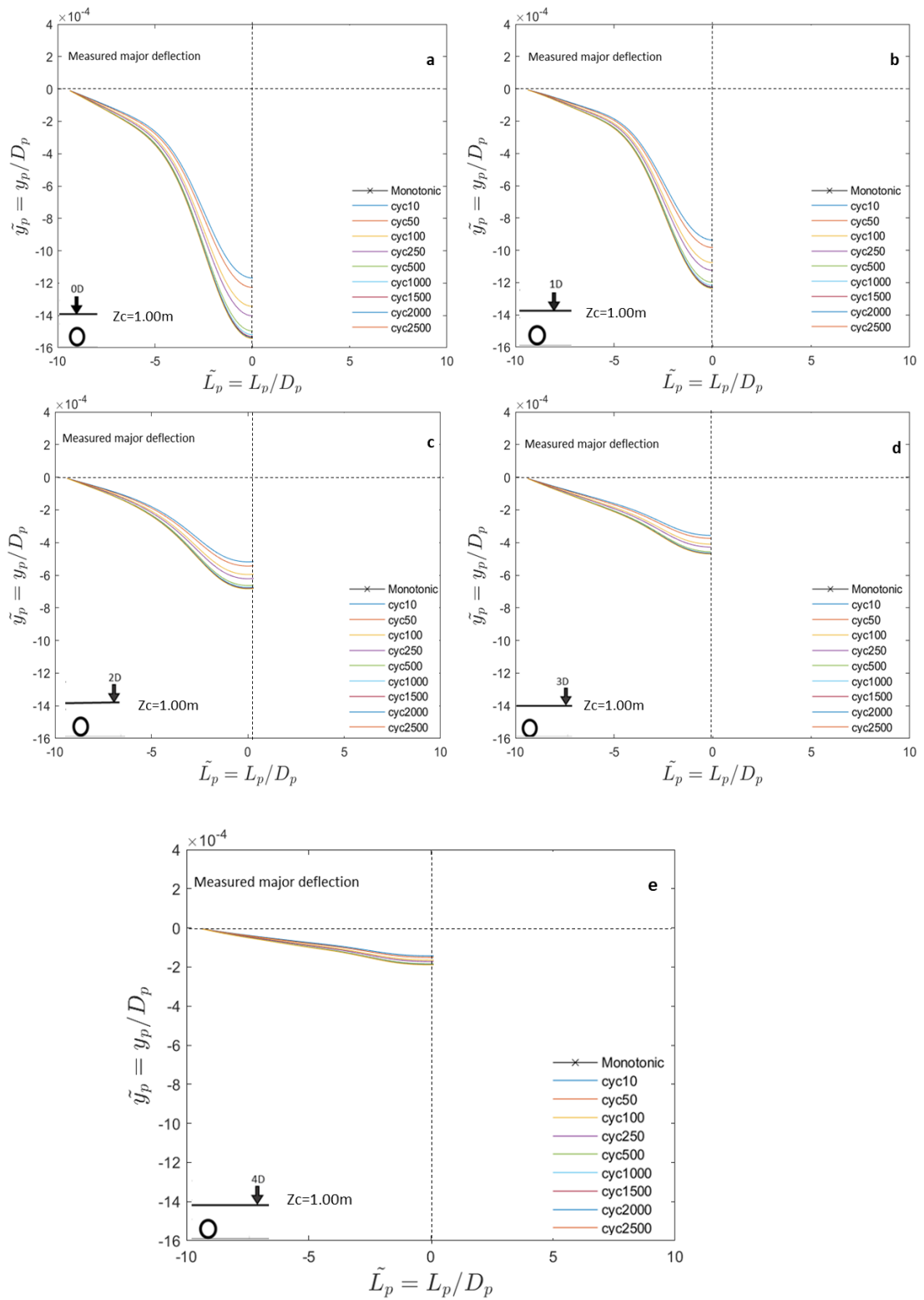


Figure 7-8 Variation in pipe deflection with load eccentricity at burial depth of $Z_c=1.00\text{m}$ and applied load of 6 tonnes (a, b, c, d and e).

7.2.4 Effect of Void Size and Location

The effect of voids was determined to be significant on pipe performance in the monotonic case. A void of $2D_p$ was determined to have a considerable detrimental effect especially when formed beneath the invert for vertically aligned loading, and more pronounced with eccentricity on the springline axis. As before, the case of a 1 m buried pipe is examined for the cyclic loading case. More details of the test configuration are given in Table 7-4 and Table 7-5.

Table 7-4 Effect of void size at the pipe invert (180deg).

	Test (#)	Test ID	Cover Depth (Z_c) m	Load magnitude L_m (Ton)	Load Eccentricity $e=D$	Internal pressure Bar	Void Size V_s	Void Location V_l (deg)	Roas Ssurface R_s	Cycles @2Hz freq
Group 4a	Test 57	T57- $Z_c1-L_m6T_s0e-0T-V_s0.5D-V_l180deg$ [C]	1	6T- Single	0e	0	0.5D	180deg	-	3600
	Test 67	T67- $Z_c1-L_m6T_s0e-0T-V_s1D-V_l180deg$ [C]	1	6T- Single	0e	0	1D	180deg	-	3600
	Test 77	T77- $Z_c1-L_m6T_s0e-0T-V_s2D-V_l180deg$ [C]	1	6T- Single	0e	0	2D	180deg	-	3600

Table 7-5 Effect of Void Size at the pipe springline (270deg).

	Test (#)	Test ID	Cover Depth (Z_c) m	Load magnitude L_m (Ton)	Load Eccentricity $e=D$	Internal pressure Bar	Void Size V_s	Void Location V_l (deg)	Roas Ssurface R_s	Cycles @2Hz freq
Group 4b	Test 87	T87- $Z_c1-L_m6T_s0e-0T-V_s0.5D-V_l270deg$ [C]	1	6T- Single	0e	0	0.5D	270deg	-	3600
	Test 97	T97- $Z_c1-L_m6T_s0e-0T-V_s1D-V_l270deg$ [C]	1	6T- Single	0e	0	1D	270deg	-	3600
	Test 107	T107- $Z_c1-L_m6T_s0e-0T-V_s2D-V_l270deg$ [C]	1	6T- Single	0e	0	2D	270deg	-	3600

The results for cyclic loading with the presence of a void at the pipe invert and pipe springline are presented in in Figure 7-9 and Figure 7-10. Both test scenarios were performed while the load was located directly above the pipe crown ($e=0D$). This kind of experimental test was conducted to explore the impact of the void on pipe behaviour under cyclic loading. As anticipated, in both cases of void location, cyclic loading had a continued negative impact on the pipe performance such that increased bending moments are apparent. Thus, it was observed during the higher number of cycles (2500), the value of sagging and hogging bending moment in the major axis increased by 25% when void was located at the pipe invert. For the pipe buried at 1 m, it can be seen that residual bending moment in increases by 15% after each 250 cycle up to almost 40% with an advance cycle which is a significant design consideration. These results were compared with the results of the similar scenario except that the load being applied monotonically. The minor axis showed negligible bending which is due to the axial load being applied directly above the pipe. The displacement of the soil also shows similar behaviour under cyclic loading, where the soil displaces more with each loading cycle. This is due to the compaction of the soil surface at regular intervals. Hence more and more pressure is applied to the pipe after every cycle, and can be attributed to localised change in the distribution of sand grains and increase in soil density, and therefore new soil structure interaction regimes on each cycle. Contrary to

the above statement, a bigger value of bending moment was observed at the minor axis in the case of a void located at the springline and load eccentricity $e=2D_p$ (distance from the pipe centre). However, it is still clear that a bending moment occurred in the major axis although the load was applied $2D_p$ distance from the pipe crown. Thus, it is clear that the pipe was exposed to a high resultant bending moment. Figure 7-11 show the effect of void size on maximum bending moment of both cases of void location.

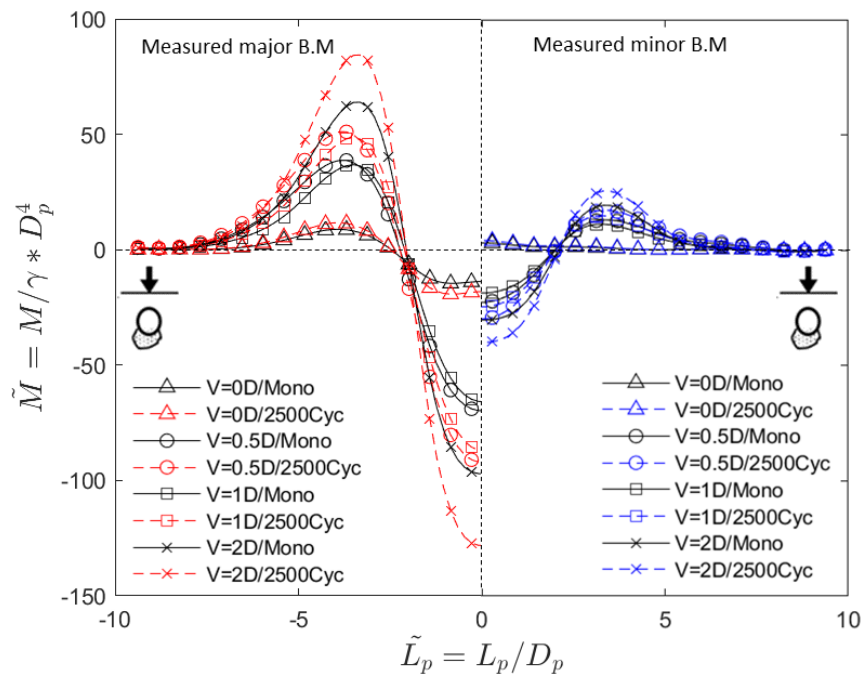


Figure 7-9 Major and minor bending moment for $2D_p$ void located at pipe invert(180deg)

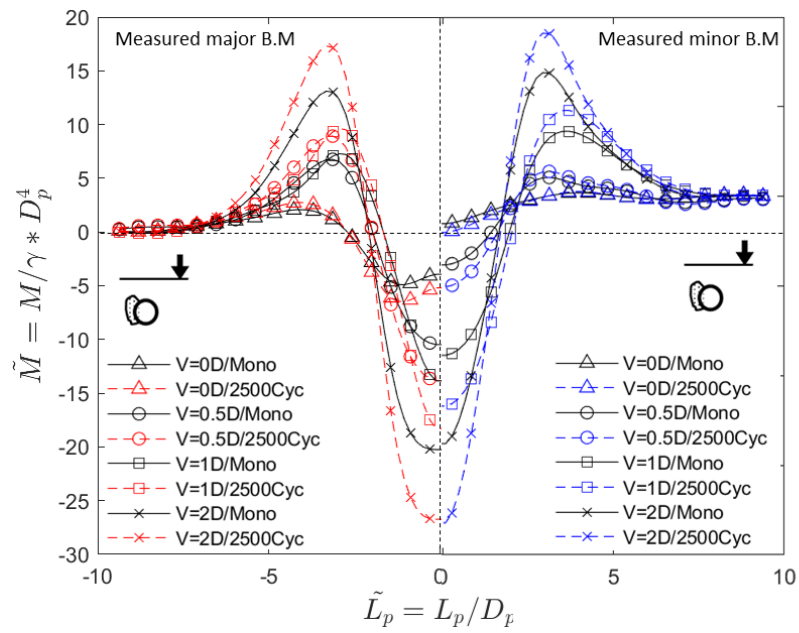


Figure 7-10 Major and minor bending moment for $2D_p$ void located at pipe springline ($270deg$)

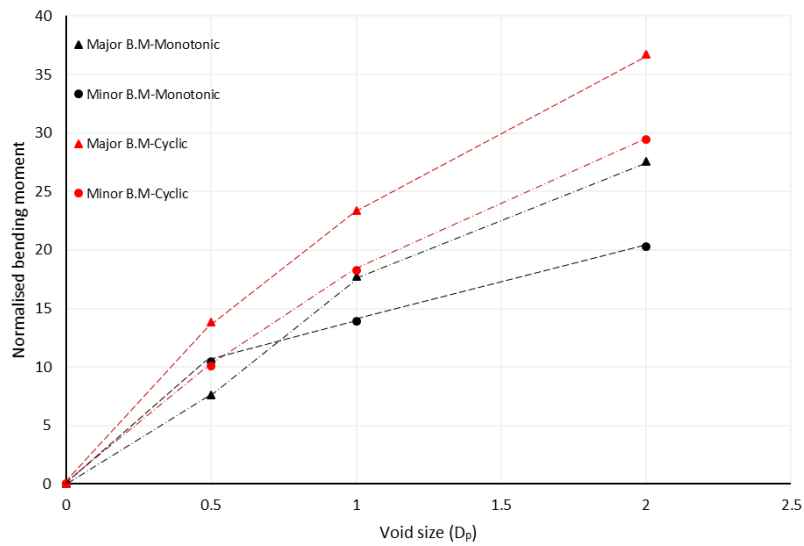


Figure 7-11 Effect of void size on the maximum bending moment

The extent of the pipe movement downward or sideward is directly related to the void location and load eccentricity as observed in Figure 7-12 a and b, where greater vertical displacement occurs when a void is located at the bottom of the pipe (invert) and load is directly above the pipe. As the deflection is correlated with the bending moment magnitude, unsurprisingly a bending moment transition from major (vertical) axis to minor (horizontal) axis, occurs when the void is at the springline when combined with eccentric loading started with $1D_p$, $2D_p$, $3D_p$ and $4D_p$. In this case, the cyclic loading scenario has a greater value exceeding 30% compared to that to which the pipe is subjected to a monotonic load. This presents a very complex condition in reality owing to the transient nature of the wheel loadings that will occur that is not incorporated in the load scenario within the experimental test. The experiment only considered the extreme conditions of loading in-line with the pipe directly; however, if the load were to be moving orthogonal (across) the pipe then the presence of a void would have significant influence. In this situation where the loading moves from eccentric to overhead (directly above the pipe crown), it is highly likely the pipe would experience a torsional shear as the wheel approached and rolled over the pipe location. This could have considerable effect on the fatigue life of the pipe, then this would be more critical to the pipe design criteria.

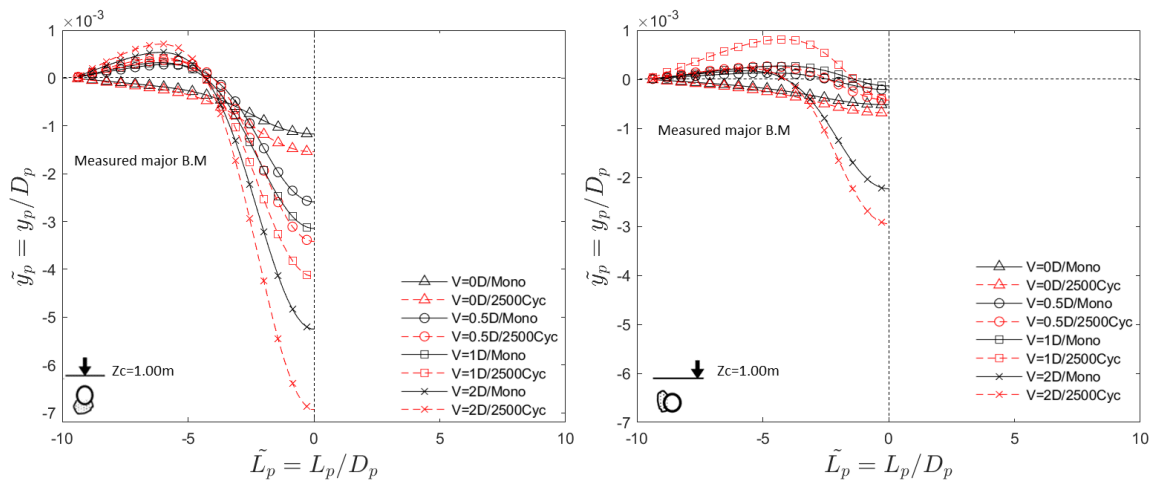


Figure 7-12 Major pipe deflection: (a) void located at 180deg; (b) void located at pipe springline (270deg).

Figure 7-13 illustrates the soil behaviour under the wheel loading area with increased cycles. It can be seen there is a clear effect of cyclic loading on the soil surface and this evolves with increases of cycle count. It is noteworthy that the surface settlement when the void size is $0.5D_p$ increases by almost 30%, and about 30% more when void size is $2D_p$. While the relative density of the soil has gradually increased due to the external repeated load applied by the footing, resulting in stiffer soil as a result of soil compaction and leading to more stress being transferred to the pipe ring, no pipe ring deflection was observed as the pipe was stiffer than the soil material.

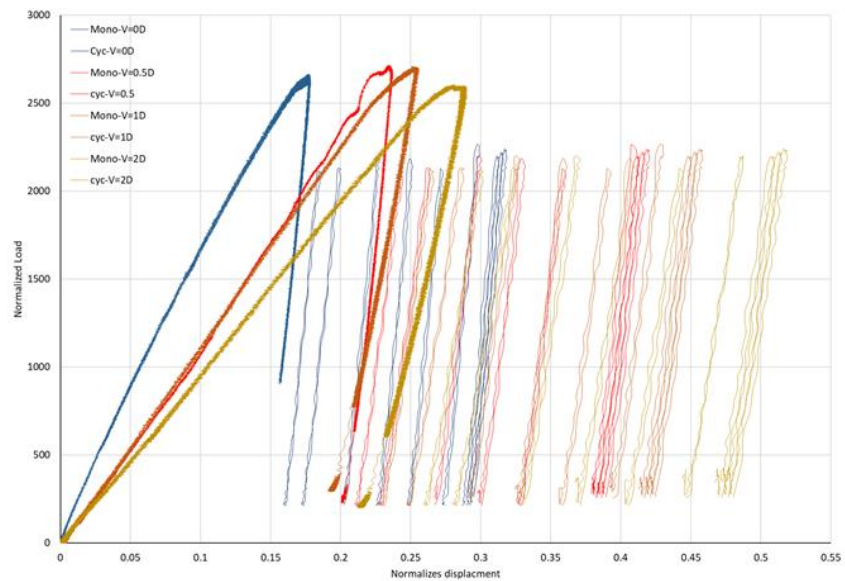


Figure 7-13 Variation in footing stiffness with presence of different void size

$V=0D$, $V=0.5D$, $V=1D$ and $V=2D$.

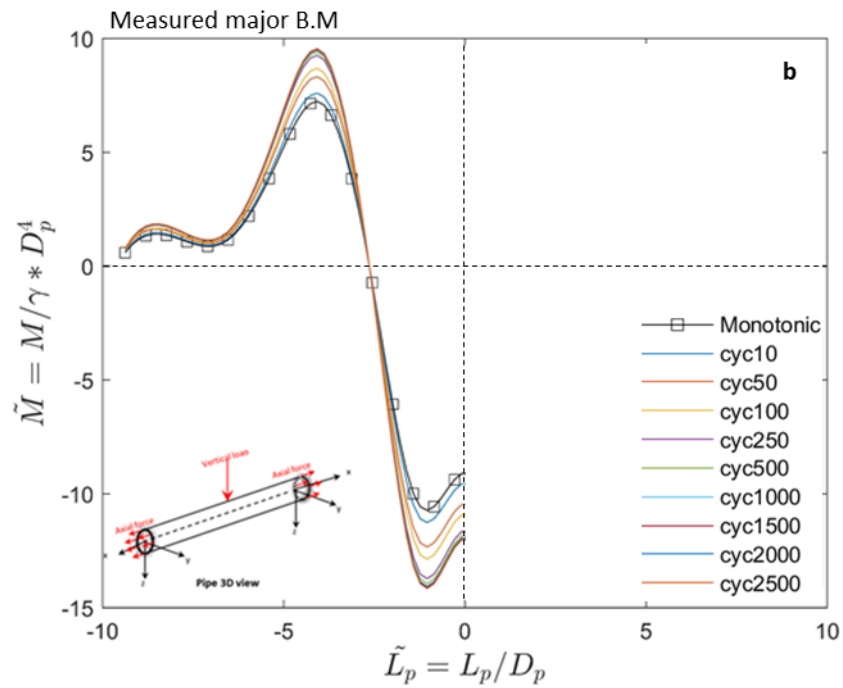
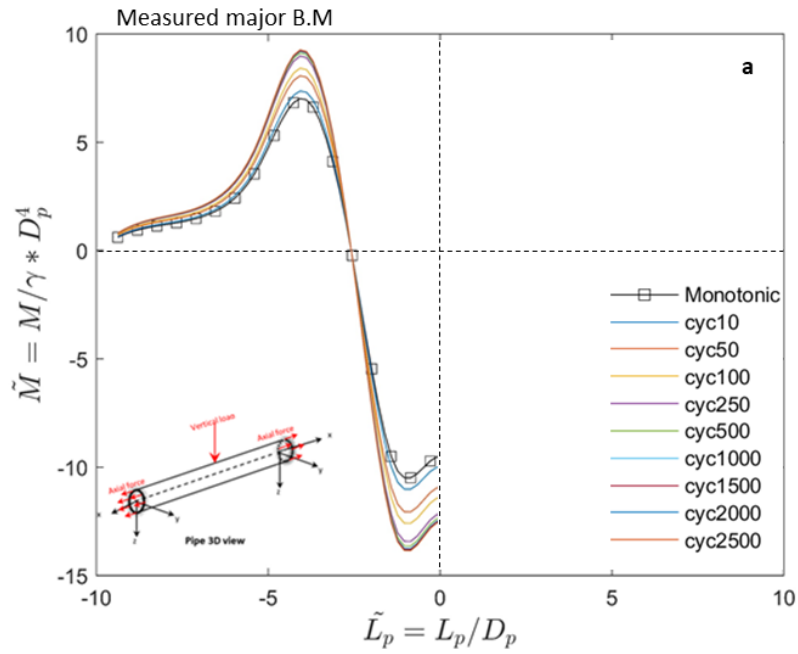
7.2.5 Influence of internal water pressure via axial load modelling

Similar to the monotonic tests, the effect of axial tension simulating the internal pressurisation of the pipe (1.5 bar, 2.5 bar and 5 bar), was examined under cyclic loading (see Table 7-6).

Table 7-6 Effect of internal pressure

	Test (#)	Test ID	Cover Depth (Z_c) m	Load magnitude L_m (Ton)	Load Eccentricity $e=D$	Internal pressure Bar	Void Size V_s	Void Location V_L (deg)	Roas Sruface R_s	Cycles @2Hz freq
Group 2	Test 3	T3-Zc1-Lm6Ts-0e-0T[C]	1	6T- Single	0e	0	-	-	-	3600
	Test 6	T6-Zc1-Lm6Ts-0e-10T[C]	1	6T- Single	0e	1.5	-	-	-	3600
	Test 9	T9-Zc1-Lm6Ts-0e-20T[C]	1	6T- Single	0e	2.5	-	-	-	3600
	Test 12	T12-ZC1-Lm6Ts-0e-30T[C]	1	6T- Single	0e	5	-	-	-	3600

The analysis of the cyclic data indicates that similar increases occur in bending moment due to increased cyclic loading, but as in the monotonic case, the magnitudes of bending are considerably reduced due to the axial tensile force (internal pressure) for cover depth of 1m. Again the largest effect of the cyclic loading is during the early cycles with stability being observed after the 250th cycle, Figure 7-14 (a, b and c). An internal pressure of 5 bar has a considerable impact in reducing the bending compared to the unpressurised case. The impact of the cyclic loading is reduced considerably when axial load is applied, such that even after the maximum cycle count at 5 bar modelled load, the pipe bending performance is still considerably below the monotonic case. The reduction in bending moment is confirmed in Figure 7-15 and this verifies the individual pipe deflection responses in (Figure 7-16 a, b and c). Therefore, the assumption of an internal pressure of 1.5 bar, 2.5 bar and 5 bar is suggested to have a significant effect on reducing both the bending moment and deflection on the pipe. This reduction depends on the internal pressure applied to the pipe. It is clear, the greater the axial force, the greater reduction in bending moment.



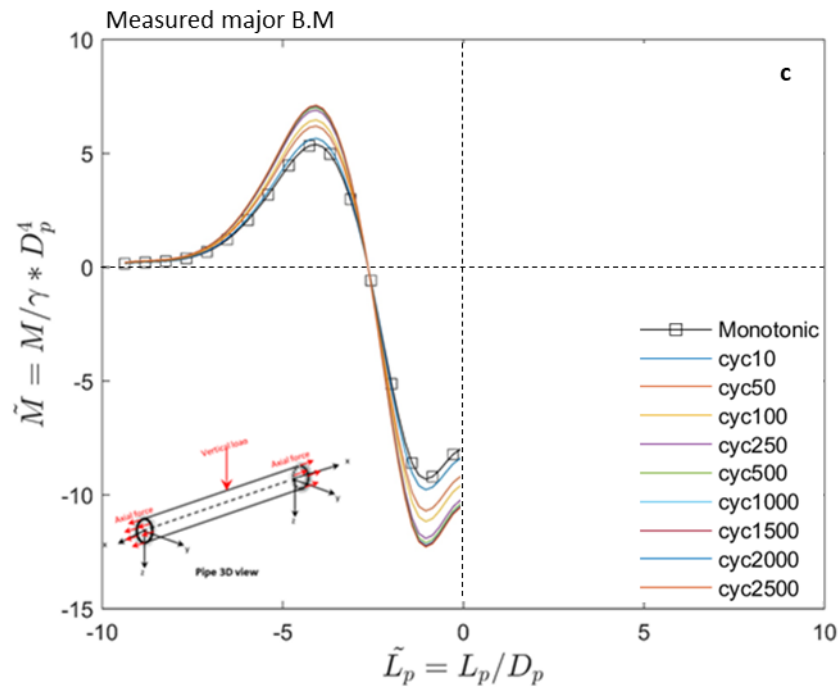


Figure 7-14 Bending moment under cyclic loading with internal pressure; (a) $p=1.5\text{bar}$; (b) $p=2.5\text{bar}$; (c) $p=5\text{bar}$

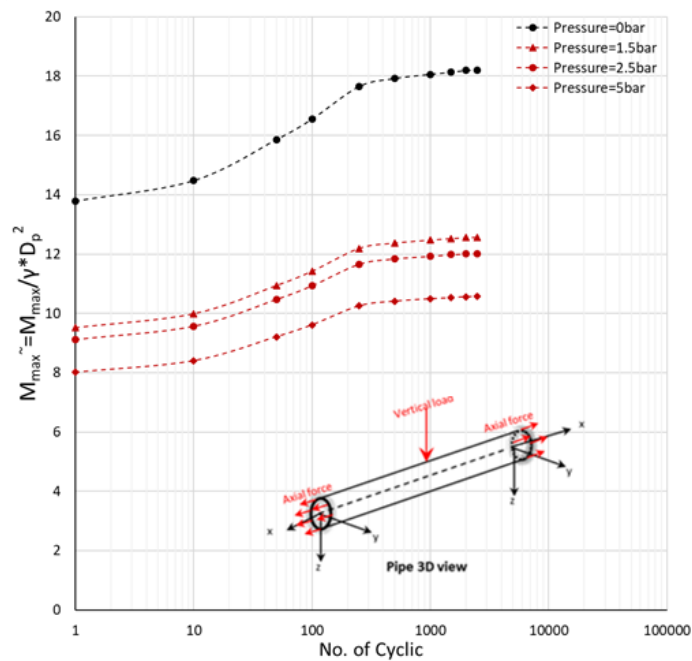
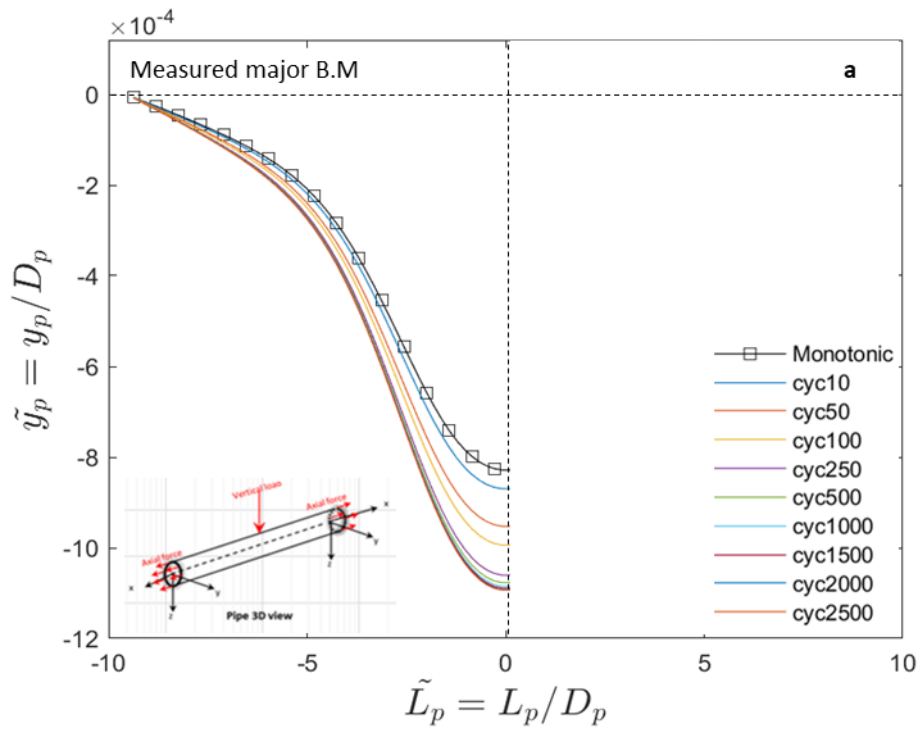
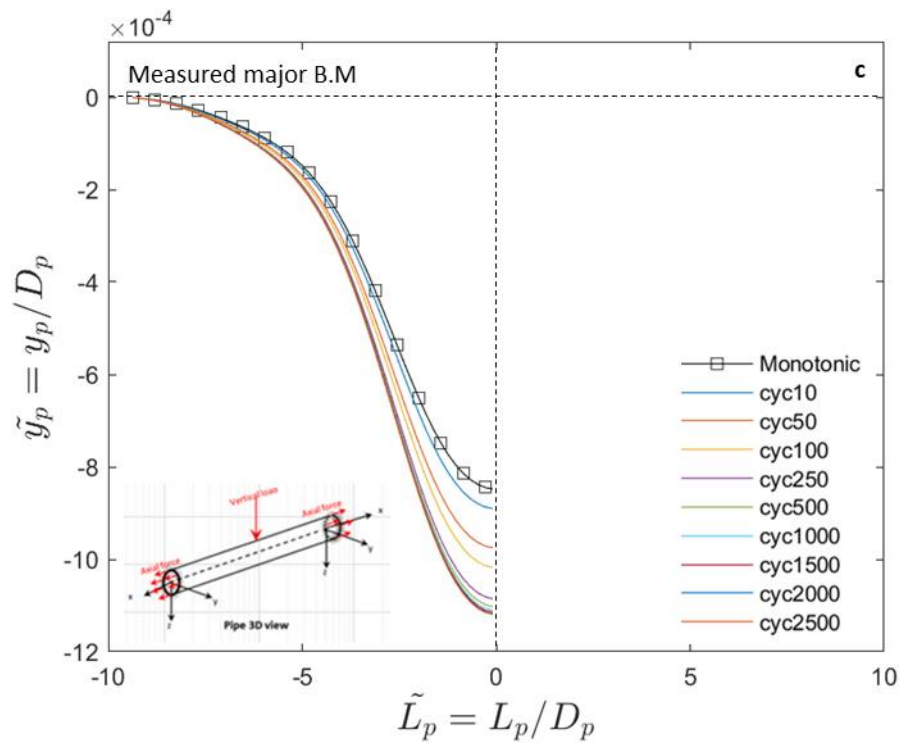


Figure 7-15 Maximum bending moment under internal pressure; i, monotonic loading ii, cyclic loading



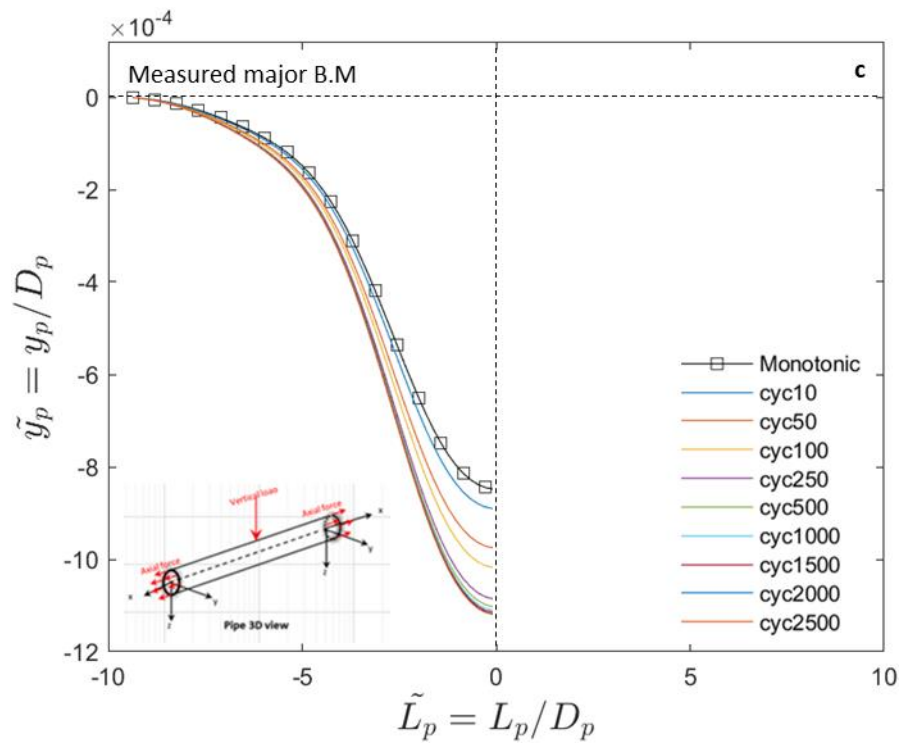


Figure 7-16 Pipe deflection under cyclic loading with internal pressure; (a) $p=1.5\text{bar}$; (b) $p=2.5\text{bar}$; (c) $p=5\text{bar}$

For comparison of pipe deflections under monotonic and cyclic loading, see Figure 7-17. It is clear that the pipe exhibits greater deflection resistance with an increase internal pressure, as modelled by axial load, with a reduction of 15 to 20% pipe deflection compared to with no axial load case. However, it can be seen that cyclic loading has significant effect on the buried pipe in both cases (pressurised pipe/unpressurised pipe).

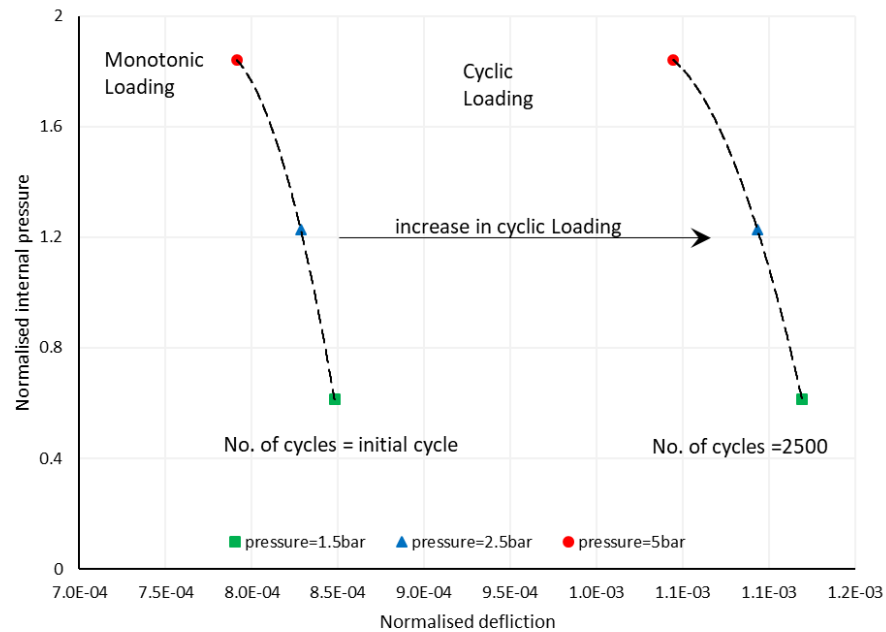


Figure 7-17 Comparison between monotonic and cyclic loading under axial force.

7.2.6 Effect of Road Surface

The placement of an equivalent road during cyclic conditions also mitigates the stresses on the pipe for both cases of buried pipe condition. The first case is of the buried pipe with no void. The second case is the buried pipe with the presence of a void either at the invert or at the springline (see test configuration presented in Table 7-7, Table 7-8 and Table 7-9), as observed in Figure 7-18 (a, b, c and d). The existence of the modelled road surface at the top of the sand seems to have prominent impact on the pipe bending moment, such that the pipe bending moment reduces by 20 to 30% compared to the bending moment where no road surface was applied. Maximum sagging bending moment was observed at the mid-span of the pipe and maximum hogging bending moment. This bending increases with the increase of the void size, which corresponds to the variable pipe support conditions a result of the void size. This observation is in agreement with an early study by Sales et al. (2015a) who conducted similar tests to explore only the effect of voids in buried pipes without consideration of the road surface.

Table 7-7 Effect of road surface (No void Present).

	Test (#)	Test ID	Cover Depth (Z_c) m	Load magnitude L_m (Ton)	Load Eccentricity $e=D$	Internal pressure Bar	Void Size V_s	Void Location V_L (deg)	Roas Srurface R_s	Cycles @2Hz freq
Group 5a	Test 15	T15- $Z_c1-L_m6T_s-0e-0T[C]$	1	6T- Single	0e	0	-	-	-	3600
	Test 127	T127- $Z_c1-L_m6T_s-0e-0T-R_s[C]$	1	6T- Single	0e	0	-	-	R_s	3600

Table 7-8 Effect of a road surface with the presence of a $2D_p$ void located at the pipe invert (180deg).

	Test (#)	Test ID	Cover Depth (Z_c) m	Load magnitude L_m (Ton)S/D	Load Eccentricity $e=D$	Internal pressure Bar	Void Size V_s	Void Location V_L (deg)	Roas Srurface R_s	Cycles @2Hz freq
Group 5b	Test 77	T77- $Z_c1-L_m6T_s-0e-0T-V_s2D-V_L180deg[C]$	1	6T- Single	0e	0	2D	180deg	-	3600
	Test 137	T137- $Z_c1-L_m6T_s-0e-0T-VS2D-V_L180deg-R_s[C]$	1	6T- Single	0e	0	2D	180deg	R_s	3600

Table 7-9 Effect of a $2D_p$ void located at the pipe invert (180deg) with the presence of a road surface.

	Test (#)	Test ID	Cover Depth (Z_c) m	Load magnitude L_m (Ton)	Load Eccentricity $e=D$	Internal pressure Bar	Void Size V_s	Void Location V_L (deg)	Roas Srurface R_s	Cycles @2Hz freq
Group 9c	Test 127	T127- $Z_c1-L_m6T_s-0e-0T-R_s[C]$	1	6T- Single	0e	0	-	-	R_s	3600
	Test 137	T137- $Z_c1-L_m6T_s-0e-0T-VS2D-V_L180deg-R_s[C]$	1	6T- Single	0e	0	2D	180deg	R_s	3600

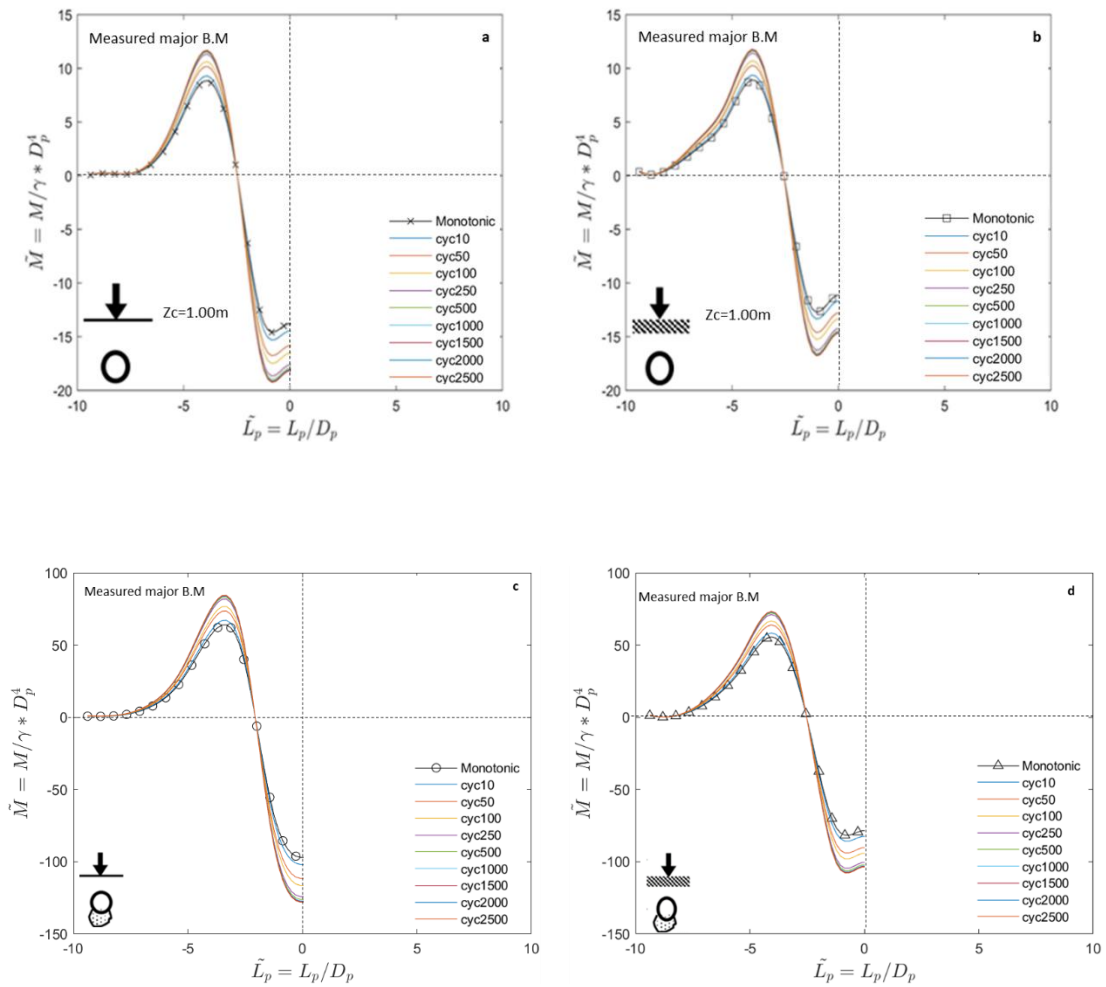


Figure 7-18 Bending moments: (a) no void no road surface ;

(b) no void with road surface; (c) 2D void no road surface; (d) 2D void with road surface

Pipe behaviour under the progress of cyclic loading showed increases in pipe deflection ranging between 15% to 30% depending on buried condition, location and void size – see Figure 7-19 (a, b, c and d) (a, b, c and d). Likewise, the pipe deflections are seen to take place for the first 200 cycles, then a rapid increase in deflection from cycle 200 to cycle 1500 can be observed. Whereby, steady deflection was observed once the cyclic loading number reached 2500 cycles. This was not observed in later cycles as a result of the increase of soil density due to the compaction that was caused by load cycling. This was also explained in Section 5.2.1.6.

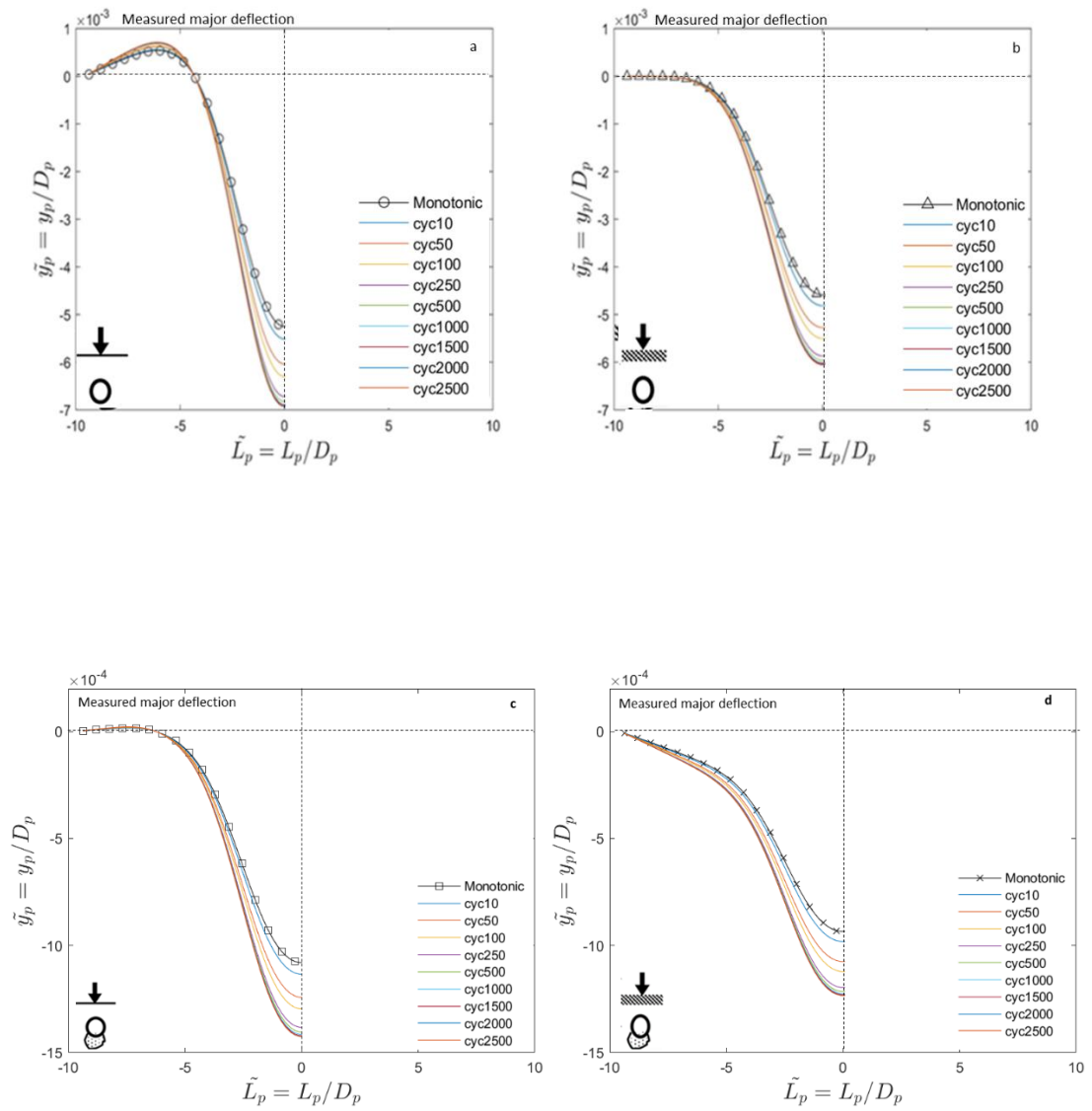


Figure 7-19 Pipe deflection: (a) no void, no road surface ;

(b) no void with road surface; (c) 2D void, no road surface; (d) 2D void with road surface

CHAPTER 8

Discussion and Interpretation of Cyclic Loading

Results

To evaluate and monitor the influence of cyclic loading on underground pipes, preliminary centrifuge tests were first conducted in order to determine the influence of repetitive loading and understand the soil response to this load. Therefore, to develop a benchmark, four tests were conducted in dense sand ($R_d=80\%$), without a buried pipe. This was done for four different scenarios, without void ($V=0D_p$) and with presence of various size of voids ($V=0.5D_p$, $V=1D_p$ and $V=2D_p$). The centrifuge modelling results showed that cyclic loading from HGV traffic stiffens the soil surrounding the pipe. The soil shows an inverse relationship between void size and final stiffness attained with the with $V=0D_p$ showing the greatest stiffness.

The results can be used in practice to inform designers of the effective forces on a pipe at a specific burial depth. The centrifuge results can also be used to determine after how many load cycles are required to attain the ultimate stiffness of the soil in order to calculate long-term soil-structure interaction. Once the benchmark tests were completed, a subsequent series of experiments consisting of 156 centrifuge tests related to the topic research were performed to evaluate the impact of the void on buried plastic pipe. Similar scenarios of burial depth (0.5, 0.75 and 1m) and load conditions ($e=0D_p$, $1D_p$, $2D_p$, $3D_p$ and $4D_p$), which was applied for the monotonic loading tests in chapter 5 except that load was applied and removed 3600 times to simulate the traffic loading (cyclic loading).

The effect of cyclic loading with varying burial depth (0.5, 0.75 and 1.0m) was one of the important parameters to investigate the effect of repeated traffic loading and therefore all aspects of the load-unload response were captured for each of the tests. The results demonstrate a range in performance for moment response across the different depths. It was found that the increase of the maximum bending moment is about 30% higher when load was applied directly above the pipe crown compared with other result from monotonic loading case. Shallow buried pipes in the first 10 cycles show similar pipe behaviour observed due to the monotonic loading. The bending moment increased by ~15% between the 50th and 100th cycles. Further increases are noted between 250 cycles and 1500 cycles, which shows a continued increase in bending moment by approximately 30%, where a slight change in performance and the bending moment stabilise. This reveals that the most crucial evolution of performance occurs just after the pipe is buried, implying that proper burial conditions are critical throughout a pipe replacement or renewal plan. Although it is unsure if this stabilisation would last for longer than the

cycles investigated here, it does demonstrate that recurrent loading of a pipe, even under ideal burial conditions, results in higher bending than a monotonic situation. The change in bending moment on both the load-unload phase appeared to increase upon each cyclic application of load. It was noticed that the maximum moment experienced within the pipe does not vary greatly with cycles. In contrast, when the load was removed the bending moment did not return to zero and residual 'locked-in' bending moment was observed. The phenomenon is clearly more pronounced for the shallower buried pipes. For instance, pipe with cover depth 0.5 m, the increase in residual bending moment is over 40% once the number of cycle beyond 250 cycles, which is a significant design consideration. This can be attributed to localised changes in sand grain distribution and density, and therefore new soil-structure interaction regimes on each cycle. The rationale for developing bending moments, according to Hosseini and Tafreshi (2000), is that residual bending moments are locked into the pipe when the soil around it is compacted before the next cyclic load application.

From the research conducted, an extensive insight of the effects of eccentric loads on buried plastic pipelines was acquired. Series of experiments conducted highlighted the impacts on bending moments in the major (vertical) and minor (horizontal) axes when subject to cyclic loading scenarios. Forces directly above the pipe ($e=0D_p$) were examined and as were eccentric loads ($e=1D_p$, $2D_p$, $3D_p$, and $4D_p$). Not only were load positions adjusted, but also the type of loading, from monotonic loading as reported previously to cyclic loads. The eccentrically applied load induces not only vertical stresses on the pipe, but also applies a lateral earth pressure on the pipe, deforming it in its minor axis. Hence, due to the eccentricity of the applied load in related test, it was expected that the minor axis bending moments was significant because of the way load spreads out from a point on the surface as explained by Boussinesq (1885). Largely the data supports this theoretical expectation with the maximum minor axis moment being recorded in the mid-span of the pipe. Therefore, eccentric load leads to a decrease in bending moment on major axis and increase of bending moment in the minor axis. Thus, the pipe experienced high bending moments during the cyclic loading with increase by approximately 30% (more than was observed in the monotonic loading). From previous research (Bayton et al., 2018b), the centrifuge tests seem to be in agreement with the findings of full scale testing. It has been found that the greater distance from the pipe crown, the lower the influence of traffic on major axis and increase on the minor axis.

Analysing the effect of void size/location across the test matrix, all tests experienced a significant increase in bending moment, in the presence of voids either at the pipe invert or pipe springline. Similar trends were found in the monotonic and cyclically loaded tests except that the bending moment was higher by 30% with the increase of number of cycles in the cyclic cases. It is clear that pipe deflection increases with increase in void size with a similar percentage. Under loading-unloading residual moments in the pipe have also been compared to peak moments in both major and minor axis. It is well observed that the residual major axis moments are a percentage of the peak major axis moments, which approached 40% as the maximum cyclic loading was applied. This relationship is more difficult to

observe in the minor axis, particularly where load is applied directly above the pipe crown. The results of cyclic testing showed a negative relationship between void size and bending moment, this indicates that soil structure behaviour is depending on void size, with the results showing that small void size seems to semi-collapse leading to stiffer soil around the pipe circumference.

A series of tests with similar scenarios coupled with axial load application that simulates internal water pressure was performed to explore the impact of the internal water pressure on buried pipes under cyclic loading. The result of the cyclic loading application found a significant decrease in bending moment with the increase in internal pressure as modelled by axial load. The percentage of bending moment decrease ranged between 15% and 20% once the pipe experienced 5 bar internal pressure. Furthermore, testing was conducted to investigate the influence of a road surface. The presence of an equivalent road surface during cyclic conditions also mitigates the stress concentrations whether a void is present or not. This reduction of the stresses ranged between 20% and 30% compared to the situation where no road surface was applied. Thus, results indicated that the road surface model has a direct effect of both stress reductions to the pipe and surface settlement under and around the footing area.

CHAPTER 9

Conclusions and Recommendations for Future Work

In recent years, the failure of underground pipes has come under increasing scrutiny. In a world of growing populations and decreasing resources, sustainability is an agenda of utmost importance and is essential to meet the growing demands of our natural resources. The failure of these underground networks leads to the depletion of the most valuable resource, potable water. At present up to 22% of potable water can be lost from source to tap, due to inefficiencies in the UK pipe network. Therefore, pipeline water leakage leads to void forming at the pipe circumference owing of pipe deterioration whether due to aged pipe or being exposed to greater magnitude of traffic loads.

The experiments performed in this research serve to highlight and understand the pipe-soil-void behaviour and number of current design methodologies for a HDPE buried pipeline set out in the Winkler spring model, as well as a number of mentioned concerns through the physical modelling of both monotonic and cyclic vertical loading scenarios coupled with axial force that simulate internal water pressure. Centrifuge modelling has proven to be a successful way to replicate the prototype conditions and the data obtained can be used with confidence. The main research findings of this thesis are summarised in the following sections.

9.1 Major and minor contributions

Water leakage and pipe deterioration were the reasons many researchers explored the behaviour of buried pipelines subjected to external vertical loading. Two important factors which may have direct impact on underground pipe system failure were considered here. The first major contribution in this study included the impact of voids on buried utility pipes subjected to surface traffic loading, both under monotonic and cyclic loading. Thus, geometrical shape/size and location of the void at the circumferences of the pipe were considered as being important factors. The second major contribution was to look at the effect of the internal water pressure via modelling an axial pipe load for all test scenarios of the void size/location. While the influence of road surface was a minor contribution, results showed that the road surface has a significant effect on buried pipes. Details are given below:

- The influence of void size/location on a buried plastic pipe was investigated for the first time with respect to longitudinal bending moment, where previous studies were looking at only pipe deformation.

In these study, the void been chosen to be with restricted length of 3 pipe diameters ($3D_p$), where the void width was changed three times $0.5D_p$, $1D_p$ and $2D_p$. Soft sponge was used to mimic the prototype void, which provide opportunity for the soil to create and keep that cavity. This research provided a valuable initial insight into the behaviour of HDPE pipes with presence of voids, which was exposed to surface traffic loading.

- For the first time, the effect of the internal water pressure was studied under three different internal pressure ranging from 1.5 bar to 5 bar. This was performed by applying axial force to both ends of the pipe during the test for each chosen scenario utilising a new designed apparatus of the axial load simulator. The apparatus is one-of-a-kind, in that it can provide axial tension or compression to the pipe, which is a novel feature of the experimental setup.
- The impact of the road surface on buried pipe was investigated. Although, the issue of the road surface simulation has been studied as a minor contribution, the results from conducted experiments with the existence of the modelled road surface has indicated that there is a reduction of approximately 20% of pipe deflection compared to other tests where no road surface was applied on the top of the sample.

9.2 Conclusions

Through physical modelling of both monotonic and cyclic surface loading scenarios, the work presented in this thesis aimed to address a number of these concerns related to the effect of void size and locations relative to the buried plastic pipe. Therefore, series of tests were carried out on buried plastic pipe in dense sand in order to investigate pipe-soil-void response to the vertical load and axial force, which simulate traffic load and internal pressure respectively. In this study, several parameters have been considered to offer insight into the impact of void on buried utility pipes subjected to surface traffic loading. The parameters were chosen carefully to fill the gap in literature and have better understanding. Therefore, beside the cover depth and load condition it was important to present void size and location throughout the test program. Thus, this research studied the role of void and its effect on underground pipe system. The key findings of this study are summarised as follows.

- The contribution of the impact of the void size/ location on buried pipe exposed to external loading was investigated. The results of the investigation revealed that the void size and location plays a significant role on the bending moment and pipe deflection, where a bigger void size beneath the pipe located on pipe invert (180deg) leads to an increase in the major bending moment about 25% compared to the result of non-void test. Hence, the pipe deflection increased considerably with increasing void size to an extent that it exceeded the allowable deflection criteria of 2% pipe diameter. It was also seen that when load is removed (unloading) the bending moment does not return to the original and progressively

increases in bending moment rate with accumulative of cyclic loading, leaving some residual bending moment as a result of new soil- structure regimes obtained. For the buried pipes at deeper depths, this phenomenon is much less pronounced suggesting less interaction. The difference between the peak and residual bending moment increases by 15% after 250 cycle up to almost 40% with an advance cycle (2500 cycles), whereas any further cyclic loading shows reduction of the residual bending moment, which is a significant design consideration. Additional to that, when the void was located at the springline (270deg), the results showed significant increases of bending moment in the minor axis. In contrast, results showed decrease of bending moment in the major axis. The results of the bending moment, deflection and shear were compared to the result when was no presence of the void. it can be seen that pipe deflection increases in the minor axis with increasing void size located at the pipe springline.

- Analysing all tests related to the influence of the internal water pressure it was found that, simulating hoop stress as a result of the internal force caused by the water pressure plays a significant role in the magnitude of the major and minor bending moment as well on the pipe deflection. The test results revealed a direct inverse relationship between the magnitude of the internal pressure and the value of the bending moment/ pipe deflection. Therefore, the assumption of an internal pressure of 1.5 bar, 2.5 bar and 5 bar has proven to have a significant effect on reducing both bending moment and deflection on the pipe. This value range between 15% to 20% of the bending moment reduction with a maximum internal water pressure of 5 bar. It would be beneficial to maintain a nominal allowable fluid head (depends on BSI standards) to restrict uncontrolled deformations. Although this is novel and interesting conclusions and discussion that Pressure is often associated with reduced pipe lifetime in stats modelling.
- Comparison of pipes buried at different depths presents that shallow buried pipes are experienced to significantly greater bending moments. However, shallower pipes show that not much change in bending moment at the first 10 cycles but, remarkable increase about 15% occurred between cycle ranging 50th to 100th. This was observed when pipe cover is 0. 5Dp. Further increases are noted beyond this cyclic up to 250 cycles to 1500 cycles which shows a rapid increase in bending moment approximately about 30%, where a slight change in performance and the bending moment stabilise. Footing displacement was also the lowest for the shallowest pipe proposing that increased stiffness of the system due to the pipe structure. On the other hand, a negligible bending moment was recorded at the minor axis when the load is over the crown.
- Eccentric loads were also applied to the buried pipes. The magnitude of the resulting bending moment remained comparable to that of the pipe loaded on the centreline when the pipe remained within the eccentric load's zone of stress influence. The magnitude of the resultant bending moment decreases dramatically as the pipe is beyond this zone. Therefore, the pipe experienced high value of bending

moment during the cyclic loading with increase by approximately 30% (more than the one was observed on the monotonic loading). The pipe experiences the most unfavourable conditions when loading is applied at an eccentricity of two pipe diameter from the crown of the pipe. Whereby, the bending moment in minor axis were significantly increased but, also it can be noticed that major axis exposed to external load that occurred slight increase in bending compared to the one when load was directly applied above the pipe crown. therefore, combined bending would lead to increases shear acting on the pipe.

- To conclude the experimental test matrix, series of tests were performed relevant to soil-pipe interaction. Thus, several factors were investigated during the centrifuge tests study. among of these the equivalent road surface layer of them and its effect on pipe system beneath it. Although the modelled material does not mimic the real road pavement 100% but, it is to be noted that a remarkable change in bending, where the road surface offered some improves in pipe performance with presence of void at the invert. Thus, road surface contribution has a significant impact in reducing load dissipation to the pipe, which in turn reduce bending moment. This reduction of the stresses ranging between 20% to 30 % compared to the one where no road surface was applied. Thus, results indicated that the road surface model has direct effect of both stress reductions to the pipe and surface settlement under and around the footing area.

9.3 Recommendation for future work

The centrifuge experiments have been shown to be very useful in the comprehension of buried pipe system behaviour when exposed to both monotonic and cyclic loading scenarios. Nevertheless, there are still many challenges surrounding pipeline design which are outside the framework of this PhD thesis. This study included too many variables between tests for a direct comparison of the different buried pipe conditions. As a result, major recommendation for further research would be restrict these variable in turn, to enable a detailed analysis of the influences in soil-pipe interaction. Therefore, if a future study were undertaken, it is recommended to focus on the most effective variables that would have a great impact on pipes performance during their service life. A summary of a key selection of these are identified below:

- The centrifuge experimental tests of buried plastic pipe subjected to external loading conducted in different scenarios revealed fresh insights into the role played by void size/location. However, the research restricted to limited size of void ($0.5D_p$, $1D_p$ and $2D_p$). Hence, it is important to explore the influence of this factor with different void sizes perhaps start with smaller void size of $0.25D_p$ and double it up to $3D_p$ void size while, void width can be restricted to $2D_p$, to examine the effect of the void size evaluation under the cyclic loading. The challenge in using the small void size is to keep the void cavity constant while test samples are being prepared, and hence a consideration of the proper material would be needed to mimic the void.
- In terms of cyclic loading, observation of pipe behaviour response for long period of cyclic loading would be also very useful to examine the effect of High cycle fatigue.
- A hypothesis has been proposed in this study regarding the influence of internal water pressure inside the pipe to a maximum of 5 bars. The outcome of the tests strongly supports future search in this area to investigate the effect of the internal water pressure on buried plastic pipe. Thus, it would be interesting to conduct similar tests on plastic pipes with higher internal pressure.
- The soil used in the research was dry sand with different densities. It would be interesting to investigate the effect of saturated and partially saturated sand, since these are more realistic materials available during the construction of box culverts. Also, investigating different types of soil, for instance clay or mixed soils would give a broader prospective of their effects on the behaviour of box culverts under monotonic and seismic loads. On a practical level, the foundation soil under the box culvert may be different than the soil used as the backfill on the side walls and above the top slab, and therefore investigating layered soils that have different properties may be useful to investigate the response of the box culvert and the soil culvert interaction under the effect of different soil configurations.

- Finally, road surface contribution was one of the minor parameters included in this study. However, model the road layers with the same real material would have been over complicated. Instead, an alternative material (rubber) was used to simulate the road surface and offer insight for the influence of the surface on the behaviour of a buried pipeline. Thus, future related research is recommended in which a material that mimics a real pavement bending stiffness is used.

References

AASHTO, L. 2010. Bridge design specifications. American Association of State Highway and Transportation Officials

ABUHAJAR, O. S. A. 2013. Static and seismic soil culvert interaction.

AL-DEFAE, A. & KNAPPETT, J. Stiffness matching of model reinforced concrete for centrifuge modelling of soil-structure interaction. 8th International Conference on Physical Modelling in Geotechnics, ICPMG 2014, 2014. CRC Press, 1067-1072.

ALZABEEBEE, S., CHAPMAN, D. & FARAMARZI, A. 2018. A comparative study of the response of buried pipes under static and moving loads. *Transp Geotech* 15: 39–46.

AMERICAN WATER WORKS ASSOCIATION MANUAL M23 2002. *PVC Pipe--design and Installation*, American Water Works Association.

ARIYARATHNE, P., LIYANAPATHIRANA, D. & LEO, C. J. 2013. Comparison of different two-dimensional idealizations for a geosynthetic-reinforced pile-supported embankment. *International Journal of Geomechanics*, 13, 754-768.

AROCKIASAMY, M., CHAALLAL, O. & LIMPETEEPRAKARN, T. 2006. Full-scale field tests on flexible pipes under live load application. *Journal of performance of constructed facilities*, 20, 21-27.

ARON, C. & JONAS, E. 2012. Structural element approaches for soil-structure interaction. *Structural Engineering and Building Performance Design, Chalmers University of Technology. Master of Science.*

ASSOCIATION, A. W. W. 1998. *Distribution system requirements for fire protection*, American Water Works Association.

ASTM.D638-02A 2002. D638-02a. 2002. *Standard test method for tensile properties of plastics.*

ASTM.D4253-16E1 2006. Standard test methods for maximum index density and unit weight of soils using a vibratory table.

ATTEWELL, P. B., YEATES, J. & SELBY, A. R. 1986. Soil movements induced by tunnelling and their effects on pipelines and structures. United States: N. p., 1986. Web.

AUDIBERT, J. M. & NYMAN, K. J. 1977. Soil restraint against horizontal motion of pipes. *Journal of the Geotechnical Engineering Division*, 103, 1119-1142.

BALKAYA, M. & MOORE, I. D. 2009. Analysis of a gasketed polyvinyl chloride pipe joint. *Transportation Research Record*, 2131, 113-122.

References

- BALKAYA, M., MOORE, I. D. & SAĞLAMER, A. 2012. Study of non-uniform bedding due to voids under jointed PVC water distribution pipes. *Geotextiles and Geomembranes*, 34, 39-50.
- BAYTON, S. 2020. *Centrifuge Modelling of Monopiles in Sand Subject to Lateral Loading*. University of Sheffield.
- BAYTON, S., BLACK, J. & KLINKVORT, R. 2018a. Centrifuge modelling of long term cyclic lateral loading on monopiles. *Physical Modelling in Geotechnics, Volume 1*. CRC Press.
- BAYTON, S., ELMROM, T. & BLACK, J. Centrifuge modelling utility pipe behaviour subject to vehicular loading. *Physical Modelling in Geotechnics, Volume 1: Proceedings of the 9th International Conference on Physical Modelling in Geotechnics (ICPMG 2018)*, July 17-20, 2018, London, United Kingdom, 2018b. CRC Press, 163.
- BLACK, J., BAKER, N. & AINSWORTH, A. 2014. Establishing a 50 g-ton geotechnical centrifuge at the University of Sheffield.
- BOUSSINESQ, J. 1885. *Application des potentiels à l'étude de l'équilibre et du mouvement des solides élastiques: principalement au calcul des déformations et des pressions que produisent, dans ces solides, des efforts quelconques exercés sur une petite partie de leur surface ou de leur intérieur: mémoire suivi de notes étendues sur divers points de physique, mathématique et d'analyse*, Gauthier-Villars.
- BRACHMAN, R. W. & KRUSHELNITZKY, R. 2005. Response of a landfill drainage pipe buried in a trench. *Canadian geotechnical journal*, 42, 752-762.
- BSI 1990. Methods of test for soils for civil engineering purposes. *BS1377*.
- BSI 1997. BS EN 1295-1:1997 Structural design of buried pipelines under various conditions of loading. Part 1. General requirements Categories: Pipelines. Part 1. British Standards Institution (BSI). London: BSI.
- BSI 2004. NA+ A1: 2014 to BS EN 1997-1: 2004+ A1: 2013. UK National Annex to Eurocode 7. Geotechnical design. General rules. BSI London, UK.
- BSI 2017. BS. EN. ISO 17892-5: Geotechnical investigation and testing- Laboratory testing of soil: Incremental loading oedometer test. London: BSI.
- BSI 2020. BS. 9295 2020. BS 9295: 2020, Guide to the structural design of buried pipelines. London: BSI.
- BURLAND, J. 1987. The teaching of soil mechanics-a personal view. *Proc. 9th ERCSMFE, Dublin, 1987*, 1, 1427-1447.
- BURNS, J. Q. & RICHARD, R. M. Attenuation of stresses for buried cylinders. *Proceedings of the Symposium on Soil-Structure Interaction, September 1974.*, 1964. American Society for Testing and Materials, West Conshohocken, Pa.: 379-392.

References

- CAO, Z., HAN, J., XU, C., KHATRI, D. K., COREY, R. & CAI, Y. 2016. Road surface permanent deformations with a shallowly buried steel-reinforced high-density polyethylene pipe under cyclic loading. *Geotextiles and Geomembranes*, 44, 28-38.
- CARDER, D., LAWRENCE, G. & TAYLOR, M. 1984. Behaviour of a shallow buried pipeline under impact and abnormal loads.
- CARDER, D., NATH, P. & TAYLOR, M. 1981. A method of modelling the effect of traffic on undermined buried pipelines.
- CASELUNGHE, A. & ERIKSSON, J. 2012. Structural element approaches for soil-structure interaction.
- CHAPMAN, D., ALZABEEBEE, S., JEFFERSON, I. & FARAMARZI, A. Investigating the maximum soil pressure on a concrete pipe with poor haunch support subjected to traffic live load using numerical modelling. 11th Pipeline Technology Conference, 2016.
- CHINA, P. 2010. Ministry of Housing and Urban-rural Development. *Unified Design Standard for Reliability of Engineering Structure*.
- CLAYTON, C. R., XU, M., WHITER, J. T., HAM, A. & RUST, M. Stresses in cast-iron pipes due to seasonal shrink-swell of clay soils. Proceedings of the Institution of Civil Engineers-Water Management, 2010. Thomas Telford Ltd, 157-162.
- COHEN, B. R. 2012. Fixing America's crumbling underground water infrastructure. *Issue Anal*, 4.
- DAIYAN, N., KENNY, S., PHILLIPS, R. & POPESCU, R. Numerical investigation of oblique pipeline/soil interaction in sand. 2010 8th International Pipeline Conference, 2010. American Society of Mechanical Engineers, 157-164.
- DAS, B. M. & SEELEY, G. R. 1975. Load-displacement relationship for vertical anchor plates. *Journal of Geotechnical and Geoenvironmental Engineering*, 101.
- DAVIES, J., CLARKE, B., WHITER, J. & CUNNINGHAM, R. 2001. Factors influencing the structural deterioration and collapse of rigid sewer pipes. *Urban water*, 3, 73-89.
- DFT 2018. Road Traffic Forecasts 2018. Department for Transport London.
- DISCOVERWATER. 2019. *Leaking pipes* [Online]. Available: <https://discoverwater.co.uk/leaking-pipes> [Accessed].
- FARSHAD, M. 2011. *Plastic pipe systems: Failure investigation and diagnosis*, Elsevier.
- FERNANDO, M. E. 1992. *Field performance of corrugated plastic pipes under simulated high soil cover*. Ohio University.
- GARNIER, J., GAUDIN, C., SPRINGMAN, S. M., CULLIGAN, P., GOODINGS, D., KONIG, D., KUTTER, B., PHILLIPS, R., RANDOLPH, M. & THOREL, L. 2007. Catalogue of scaling laws and

References

similitude questions in geotechnical centrifuge modelling. *International Journal of Physical Modelling in Geotechnics*, 7, 1.

GERE, J. M. & TIMOSHENKO, S. 1984. Mechanics of Materials 2e. *Brooks/Cole Engineering*, 198.

GLOVER, M. & SHANE, B. A. 1983. Results from Axle Weight Surveys at Lichfield and Barham.

GUMBEL, J., SPASOJEVIC, A. & MAIR, R. 2003. Centrifuge modelling of soil load transfer to flexible sewer liners. *New Pipeline Technologies, Security, and Safety* (pp.352-362).

GUMBEL, J. E. 1983. *Analysis and Design of Buried Flexible Pipes*. University of Surrey.

HETÉNYI, M. 1971. *Beams on elastic foundation: theory with applications in the fields of civil and mechanical engineering*, University of Michigan.

HETÉNYI, M. & HETBENYI, M. I. 1946. *Beams on elastic foundation: theory with applications in the fields of civil and mechanical engineering*, University of Michigan press Ann Arbor, MI.

HOSSEINI, S. & TAFRESHI, S. 2000. Soil-structure interaction of buried pipes under cyclic loading conditions. *WIT Transactions on the built environment*, 48.

HSU, T.-W. 1993. Rate effect on lateral soil restraint of pipelines. *Soils and foundations*, 33, 159-169.

HSU, T.-W., CHEN, Y.-J. & WU, C.-Y. 2001. Soil friction restraint of oblique pipelines in loose sand. *Journal of transportation engineering*, 127, 82-87.

HSU, T., CHEN, Y. & HUNG, W. 2006. Soil friction restraint of oblique pipelines in dense sand. *J. Transp. Eng.*, 132, 175-181.

IGLESIA, G. R., EINSTEIN, H. H. & WHITMAN, R. V. 2011. Validation of centrifuge model scaling for soil systems via trapdoor tests. *Journal of Geotechnical and Geoenvironmental Engineering*, 137, 1075-1089.

INDUSTRY, U. W. 2014. Water industry information & guidance note. *Code of practice: In situ resin lining of water mains*. *Water UK Standards Board*, 1-30.

JONES, G. M. A. 1984. The Structural deterioration of sewers. *International conference on the planning, construction, maintenance & operation of sewerage systems*,. Reading, UK, September 1984. .

KATONA, M. G. & MCGRATH, T. J. 2007. Guideline for Interpreting AASHTO Specifications to Design or Evaluate Buried Structures with Comprehensive Solution Methods. *Transportation Research Record*, 2028, 211-217.

KAVITHA, P., NARAYANAN, K. & BEENA, K. A review of soil constitutive models for soil structure interaction analysis. *Proceedings of Indian Geotechnical Conference*, 2011. 903-906.

References

- KLAR, A., VORSTER, T., SOGA, K. & MAIR, R. 2005. Soil-pipe interaction due to tunnelling: comparison between Winkler and elastic continuum solutions. *Geotechnique*, 55, 461-466.
- KONUK, I., PHILLIPS, R., HURLEY, S. & PAULIN, M. 1999. Preliminary ovalisation of buried pipeline subjected to lateral loading. *OMAE99/PIPE*, -5023.
- LASPIDOU, C. 2014. ICT and stakeholder participation for improved urban water management in the cities of the future. *Water Utility Journal*, 8, 79-85.
- LESTER, J. & FARRAR, D. 1979. An examination of the defects observed in 6 km of sewers. *TRRL Supplementary Report*, 531.
- MADABHUSHI, G. 2014. *Centrifuge modelling for civil engineers*, CRC Press.
- MADABHUSHI, G. 2017. *Centrifuge modelling for civil engineers*, CRC Press.
- MAIR, R. 1979. Centrifugal modelling of tunnel construction in soft clay.
- MARSTON, A. 1913. The theory of loads on pipe in ditches and tests of cement and clay drain tile and sewer pipe. *Bulletin*, 31.
- MATYAS, E. L. & DAVIS, J. B. 1983. Prediction of vertical earth loads on rigid pipes. *Journal of Geotechnical Engineering*, 109, 190-201.
- MCGRATH, T. 2005. Performance of Thermoplastic Pipe Under Highway Vehicle Loading.
- MCGRATH, T. J., CHAMBERS, R. E. & SHARFF, P. 1990. Recent trends in installation standards for plastic pipe. *Buried plastic pipe technology. ASTM STP*, 1093, 281-293.
- MEHRJARDI, G. T. & TAFRESHI, S. Buried pipes analysis in reinforced sand under repeated loading. Proceedings of the Second BGA International Conference on Foundations, ICOF2008, Dundee, UK, 2008. 1103-1110.
- MOHAMED, H. S. & MOGHADAS, T. S. 2002. Soil-structure interaction of buried pipes under cyclic loading conditions.
- MOORE, I., BECERRIL GARCIA, D., SEZEN, H. & SHELDON, T. 2012. Structural design requirements for culvert joints. NCHRP Web-only document 190, Contractor's Final Report for NCHRP Project 15-38, April 2012. *Transportation Research Board, Washington, DC*.
- MOSER, A. P. & FOLKMAN, S. 2008. *Buried pipe design*, McGraw-Hill Education.
- NEGUSSEY, D., WIJEWICKREME, W. & VAID, Y. 1989. Geomembrane interface friction. *Canadian Geotechnical Journal*, 26, 165-169.
- NG, P. C. F. 1994. *Behaviour of buried pipelines subjected to external loading*. University of Sheffield.
- NIELSEN, D., JACKSON, R., CARY, J., EVANS, D., BOERSMA, L., EVANS, D., FERGUSON, A., GARDNER, W., HANKS, R. & KEMPER, W. 1972. Soil Water.

References

- O'REILLY, M., ROSBROOK, R., COX, G. & MCCLOSKEY, A. 1989. Analysis of defects in 180km of pipe sewers in Southern Water Authority.
- O'ROURKE, T., DRUSCHEL, S. & NETRAVALI, A. 1990. Shear strength characteristics of sand-polymer interfaces. *Journal of geotechnical engineering*, 116, 451-469.
- OFWAT. 2020. *The economic regulator of the water sector in England and Wales* [Online]. Available: <https://www.ofwat.gov.uk/> [Accessed].
- OVESEN, N. K. The scaling law relationship-panel discussion. Proc. 7th European Conference on Soil Mechanics and Foundation Engineering, 1979, 1979. 319-323.
- PAULIN, M. J., PHILLIPS, R. & BOIVIN, R. 1995. Centrifuge modelling of lateral pipeline/soil interaction--Phase 2. American Society of Mechanical Engineers, New York, NY (United States).
- PENG, Y., DING, X., ZHANG, Y., WANG, C. & WANG, C. 2021. Evaluation of the particle breakage of calcareous sand based on the detailed probability of grain survival: an application of repeated low-energy impacts. *Soil Dynamics and Earthquake Engineering*, 141, 106497.
- PETER, J. M., CHAPMAN, D., MOORE, I. D. & HOULT, N. 2018. Impact of soil erosion voids on reinforced concrete pipe responses to surface loads. *Tunnelling and Underground Space Technology*, 82, 111-124.
- POCOCK, R., LAWRENCE, G. & TAYLOR, M. 1980. Behaviour of a shallow buried pipeline under static and rolling wheel loads.
- POKROVSKY, G. 1936. Studies of soil pressures and soil deformations by means of a centrifuge. *Proc. of 1st ICSMFE*, 1, 70-71.
- RAHMAN, S. & BIRD, W. 2006. PVC Pipe Jointing: The Rieber System in North America. *Plastic Pipes XII. CD-ROM. Transportation Research Board of the National Academies, Washington, DC.*
- RAJAH, S., SHUMAKER, S., BARDAKJIAN, H., BOTTEICHER, B., BUSHDIECKER, K., CONNER, R., COX, A., FISHER, C., LEBLANC, J. & MCCABE, M. 2014. Soil parameters for assessing axial and transverse behavior of restrained pipelines—Part 2: Transverse behavior. *Pipelines 2014: From Underground to the Forefront of Innovation and Sustainability*, 3-6.
- RAKITIN, B. & XU, M. 2013. Centrifuge modeling of large-diameter underground pipes subjected to heavy traffic loads. *Canadian Geotechnical Journal*, 51, 353-368.
- RAKITIN, B. & XU, M. 2014. Centrifuge modeling of large-diameter underground pipes subjected to heavy traffic loads. *Canadian Geotechnical Journal*, 51, 353-368.
- ROYLANCE, D. 2001. Pressure vessels. *Department of Materials Science and Engineering, Massachusetts Institute of Technology, Cambridge.*

References

- SALES, H., BLACK, J. A. & COLLINS, R. P. Effect of voids on the bending response of buried flexible utility pipes. Proceedings of GéoQuébec 2015, 2015a. GEOQuébec2015.
- SALES, H., BLACK, J. A. & COLLINS, R. P. Effect of voids on the bending response of buried flexible utility pipes. 2015b.
- SCHOFIELD, A. N. 1980. Cambridge geotechnical centrifuge operations. *Geotechnique*, 30, 227-268.
- SMITH, C. C. 1991. *Thaw induced settlement of pipelines in centrifuge model tests*. University of Cambridge.
- SMITH, D. & DICKSON, J. 1990. Contributions of vehicle weight and ground pressure to soil compaction. *Journal of Agricultural Engineering Research*, 46, 13-29.
- SPANGLER, M. G. & SHAFER, G. The structural design of flexible pipe culverts. Highway Research Board Proceedings, 1938.
- SPASOJEVIC, A., MAIR, R. & GUMBEL, J. 2007. Centrifuge modelling of the effects of soil loading on flexible sewer liners. *Géotechnique*, 57, 331-341.
- SRIVASTAVA, A., GOYAL, C. R. & RAGHUVANSHI, A. 2012. Load settlement response of footing placed over buried flexible pipe through a model plate load test. *International Journal of Geomechanics*, 13, 477-481.
- TAFRESHI, S. M. & KHALAJ, O. 2008. Laboratory tests of small-diameter HDPE pipes buried in reinforced sand under repeated-load. *Geotextiles and Geomembranes*, 26, 145-163.
- TAN, Z. & MOORE, I. D. 2007. Effect of backfill erosion on moments in buried rigid pipes.
- TAYLOR, M., LAWRENCE, G. & CARDER, D. 1984. Behaviour of a shallow buried pipeline under impact and abnormal loads.
- TAYLOR, R. 1995. Centrifuges in modelling: principles and scale effects. *Geotechnical centrifuge technology*, 19-33.
- TIMOSHENKO, S. 1953. History of strength of materials McGraw-Hill book company. *Inc., New York/Toronto/London*.
- TIMOSHENKO, S. 1983. *History of strength of materials: with a brief account of the history of theory of elasticity and theory of structures*, Courier Corporation.
- TRAUTMANN, C. H. 1983. Behavior of pipe in dry sand under lateral and uplift loading.
- VLASE, S., MARIN, M., SCUTARU, M. L., SCĂRLĂTESCU, D. D. & CSATLOS, C. 2020. Study on the Mechanical Responses of Plastic Pipes Made of High Density Polyethylene (HDPE) in Water Supply Network. *Applied Sciences*, 10, 1658.

References

VORSTER, T., KLAR, A., SOGA, K. & MAIR, R. 2005. Estimating the effects of tunneling on existing pipelines. *Journal of Geotechnical and Geoenvironmental Engineering*, 131, 1399-1410.

WATER, U. 2000. Water Industry Specification 4-35-01. *Water UK*, 7, 13-16.

WINKLER, E. 1867a. *Die Lehre von der Elasticitaet und Festigkeit: mit besonderer Rücksicht auf ihre Anwendung in der Technik für polytechnische Schulen, Bauakademien, Ingenieure, Maschinenbauer, Architekten, etc*, Dominicus.

WINKLER, E. 1867b. *Theory of Elasticity and Strength*, (H. Dominicus). *Prague, Czech Republic*.

WOOD, D. M. 2004. *Geotechnical modelling*, CRC press.

YANG, C. & LI, S. 2021. Theoretical analysis and finite element simulation of pipeline structure in liquefied soil. *Heliyon*, 7, e07480.

YODER, E. J. & WITCZAK, M. W. 1991. *Principles of pavement design*, John Wiley & Sons.

YOUNG, O. C. & O'REILLY, M. 1983. *A guide to design loadings for buried rigid pipes*.

YOUNG, O. C. & O'REILLY, M. 1983. *A guide to design loadings for buried rigid pipes*.

ZHAN, C. & RAJANI, B. 1997. Load transfer analyses of buried pipe in different backfills. *Journal of transportation engineering*, 123, 447-453.

Appendix A

Preliminary pipe interaction model tests

A number of preliminary tests have been conducted to investigate the soil-pipe interaction behaviour and provide initial insight of the expected data and factors to consider for the main test programme. The total number of the experiment were 18 tests, 11 of them were tested flexible pipe and the other 7 were tested rigid pipe. The centrifuge was used to model scaled down vertical stresses which represented the appropriate forces from a real size prototype model. When the centrifuge is spun to 25g, the loads applied to the top of the soil simulate half axle 6T and full axle 12T of HGV passing over the top of the pipe. Two different pipes material were laid on layer of sand with requested depth, orientation, and eccentricity (Figure a-1 shows test set up schematic). An aluminium pipe was used to represent the cast-iron pipe, and a plastic pipe was used to represent the HDPE pipe in the centrifuge test. Both model pipes aluminium and plastic had an outer diameter of 13.35, 14.2mm and inner diameter of 8, 10mm with a Young's modulus (E) of 70 GPa 2.6 GPa. This pipes represents a prototype pipe with a Young's modulus of 200 GPa 1.0 GPa with outer and inner diameter of 355,333.75mm and 305.82, 288.10mm respectively. It is important to note that only the outer diameter scales were used as the pipe thickness does not scale. This is because the second moment of area (I) has been chosen to ensure that the bending stiffness (EI) of the pipe scales to the prototype allowing the pipes mechanical behaviour to remain realistic.

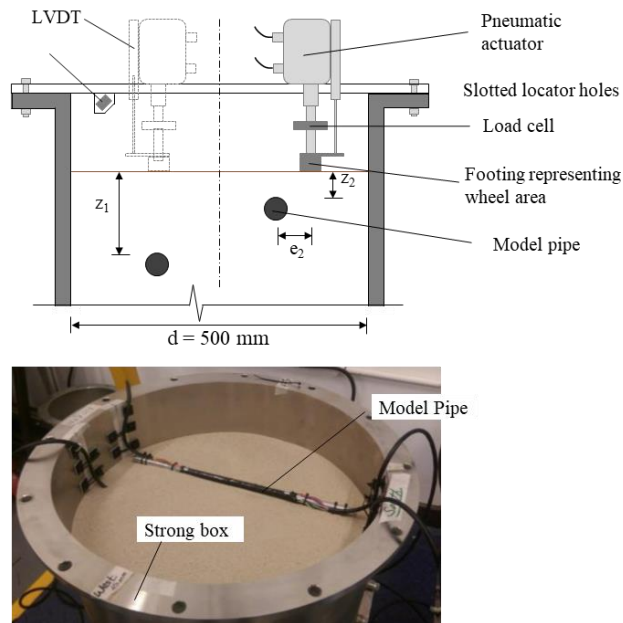


Figure (a-1). test set up schematic

A total of eight strain gauges; four in the major axis and four in the minor axis, were attached to the respective axes using electrical tape (with near zero stiffness ensuring no contribution to the stiffness of the pipe). As the buried pipe is subject to external loads, strain gauges recorded measurements of pipe deformations in both minor and major axes. The payload container to be tested in the centrifuge was filled with the chosen sand material in layers, consisting of a base soil sand bed layer, then two different pipes were laid in their respective positions, then a further sand layer representing the topsoil cover. A dry pluviation method was performed to create the dense soil sand bed. The depth at which the pipe had to be buried meant that three different layers of soil with varying relative densities were required.

The load was applied over an area of 0.5m x 0.25m onto the surface of the sand. An aluminium footing, designed to represent the contact area of a HGV on a road was used. The load represents the maximum UK haulage limit per axle 12T for a HGV. The other test only modelled the force from a single wheel, therefore transferring only 6T to the footing. An LVDT was set up above the footing to record its displacement into the soil surface. Voltage outputs were related to displacements of the sand surface/footing, which was calibrated to give the displacement in mm.

Three type of experimental were conducted to investigate the following on soil-pipe interaction:

- The effect of burial depth and load eccentricity on buried HDPE and Cast Iron pipes.
- The effect of load orientation on buried HDPE and Cast Iron pipes.
- The effect of pipe stiffness on the bending moment response of the pipe.
- The behaviour of HDPE and Cast Iron pipes under a range of load magnitude.

Figure a-2 below shows the response of the pipes to the above mentioned points in the centrifuge for (a) different burial depths ranging from 0.5m to 1.5m at full prototype conditions. The effect of pipe burial depth is clear whereby it is observed that deeper pipes are less affected by the applied surface load such that the stress concentrations are considerably lower and hence the bending moments are greatly reduced. This provides confidence in the experimental methodology, sensors etc. as a suitable means to develop a compressive study to evaluate the effect of voids in close proximity to buried pipes.

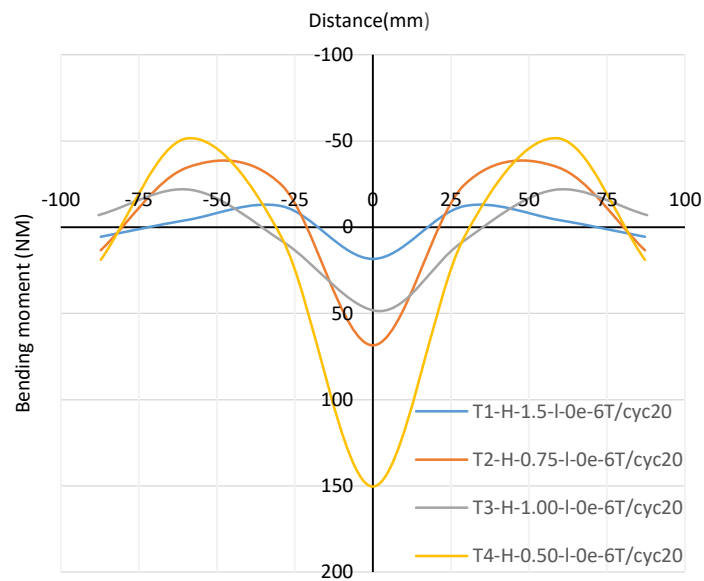


Figure (a2). Pipe bending moment diagram for burial depth

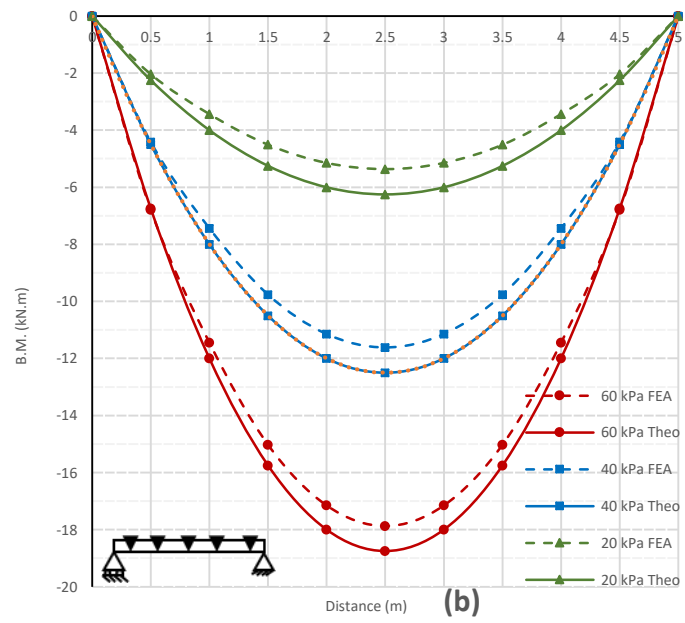
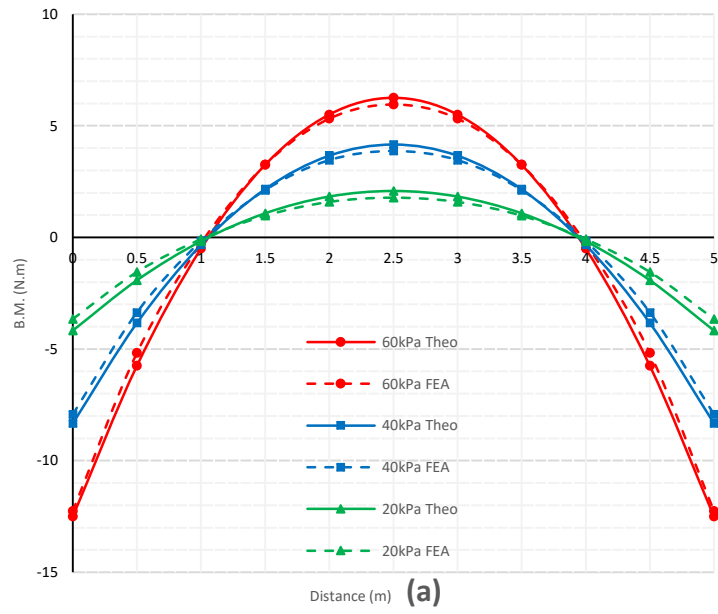
Modelling of pipe as a beam (validation)

Numerical analysis has been carried out using ABAQUS/Standard version 6.4 to investigate the effect of various static loading on beams with different boundary condition. These numerical models have been conducted to validate basic understanding of the program and individual key elements of what will become the complex pipe-soil interaction problem. Hand calculations using basic structural analysis has also been conducted to verify the bending moment output. Three assumptions were considered to represent the real buried pipe cases. Table a-1 below shows each case individually.

Table a-1. Assumption of the real buried pipe.

case	ABAQUS Model	Real pipe situation and boundary condition
1-	Simple Beam with UDL semi-fixed at the end.	Buried pipe placed on non-uniform bedding between two pipe segment.
2-	Simple Beam with UDL Fixed at the end.	Buried pipe physically restrained between manholes.
3-	Continues Beam with Fixed End and /different load magnitude.	Buried pipe placed on uniform beading physically restrained between manholes.

The bending moment of different load magnitude and boundary condition for mentioned cases above of hand calculation was compared with ABAQUS models of similar assumption and graphs of the results is plotted as shown in Figure a-3 (a, b, and c). The shapes of the curve of bending moment obtained in ABAQUS are quite similar to those obtained by hand calculations. Different mesh size was used to improve the output accuracy. Mesh sensitivity of the model was compared against the theoretical analysis which confirmed that a medium or fine mesh provided suitable accuracy.



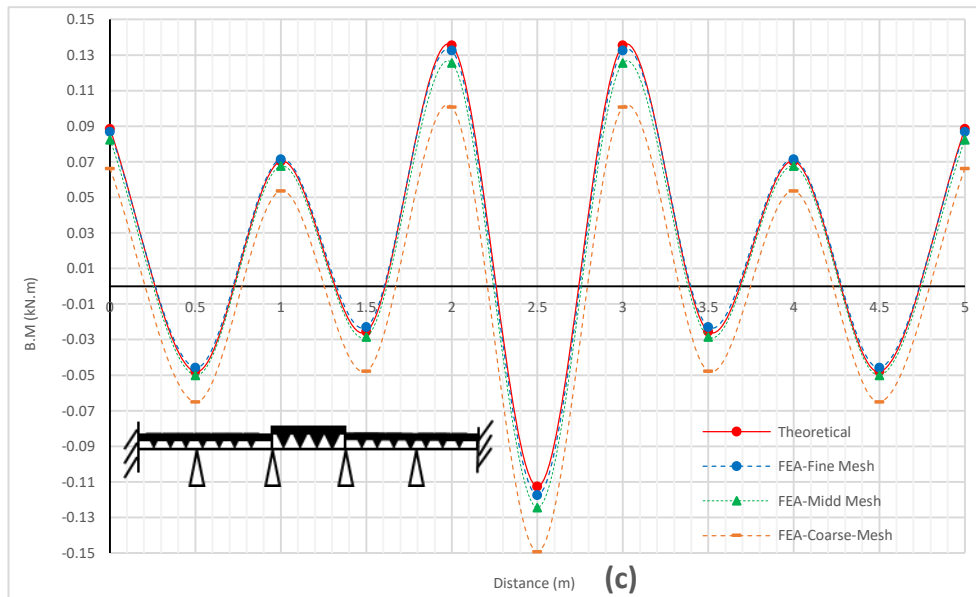


Figure a-3. Comparison between hand calculation and ABAQUS result for (a) Simple Beam with UDL Fixed at the end. (b) Simple Beam with UDL semi-fixed at the end(c) Continues Beam with Fixed End.

Modelling of a shallow foundation

In order to simulate similar situation of traffic load onto ground, a series of 2-D & 3-D FE analyses of a typical shallow foundation has been considered as a simple case to represent an aspects theorem, which is the load been applied from the vertical traffic loads as uniform contact pressure on the top of the surface of the soil. The surface loading used was simulating whether is a single or double axel HGV wheel load; according to AASHTO (2010).

Boussinesq (1885) devised a method that allowed for the determination of stresses in an isotropic, homogeneous, elastic half-space under a strip loading Powrie (2004). Fadum (1948) later presented a chart-based solution to the Boussinesq method, allowing for the vertical stresses to be determined underneath a rectangular footing with uniform surcharge. Given that the HGV load can be simplified by uniformly loading an equivalent surface area

Figure a-4 The simple hand calculations were needed in an attempt to validate the result from ABAQUS output and good correlation was observed Figure a-5.

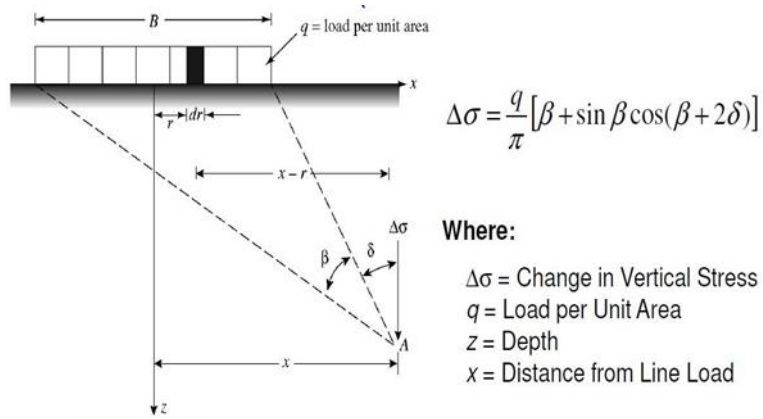


Figure a-4. Vertical stress increase in soil (strip loading).

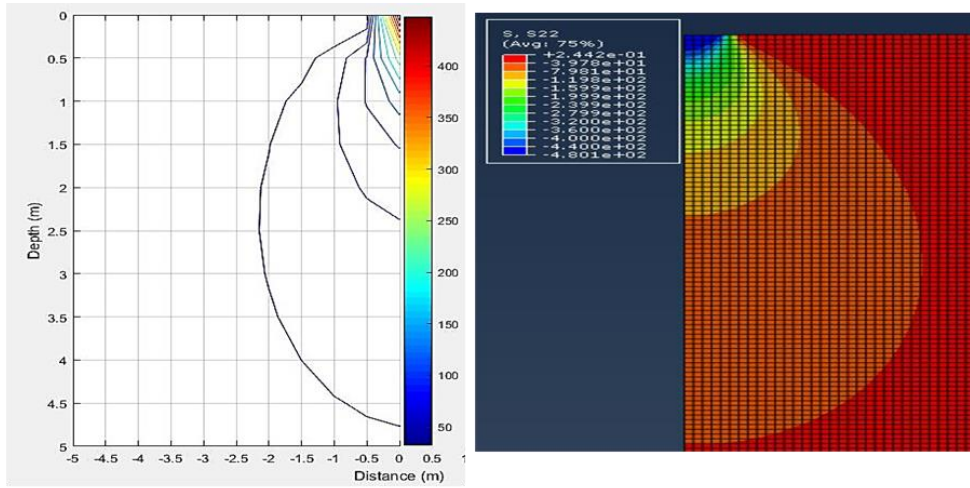


Figure a-5. Comparison of FEA and hand calculations using MATLAB

Appendix B

Design of strong box

The report relates to the design of a new strong box for use in geotechnical centrifuge testing at University of Sheffield Centre for Energy & Infrastructure Ground Research (CEIGR). The purpose of the strongbox is to do experimental studies of soil pipe interaction while being spun at centrifugal acceleration up to a maximum of 50g. Several assumptions are outlined regarding the applied loads/stresses and are outlined herein; for example, assuming that the lateral stress acting on the side plates is a uniform load as a worst case scenario. The box is designed by using high-strength aluminium alloy 6061T6. The box plates are attached to each other by bolts, and the box itself suitably fixed to the platform of the centrifuge. The box has two additional plates attached to the side of the internal plates in order to mount the actuation apparatus. A schematic diagram of the strong box with the apparatus shown in Figure b-1 and photo b-2.

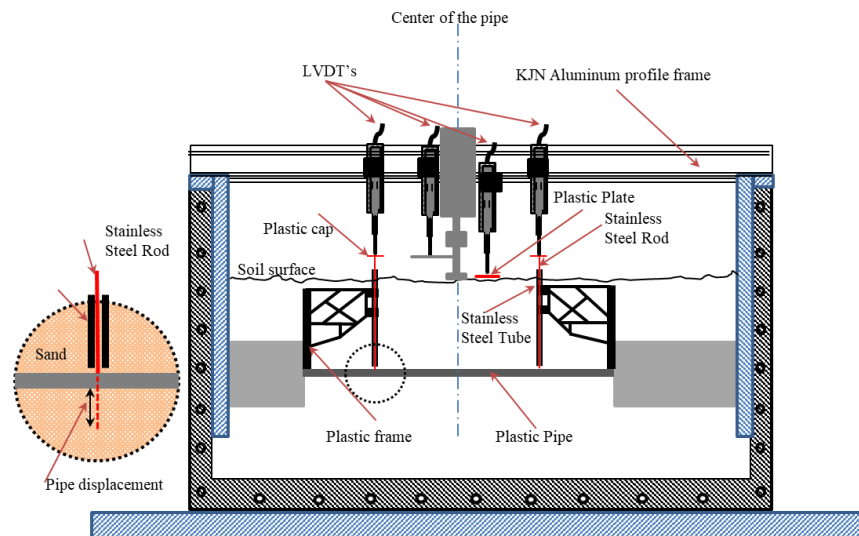


Figure b-1 Schematic diagram of the strong box.

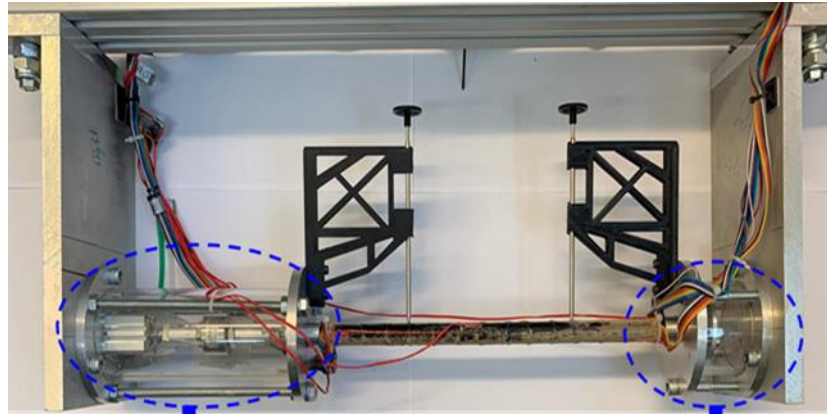


Figure b-2 Photo of the strong box.

Design summary

The external overall dimensions of the strongbox is proposed to be 600x x 425, all dimensions in mm see **Error! Reference source not found.** The box has 5 parts made from high-strength aluminium alloy 6061T6 , each part has different dimensions as shown in the Tableb-1 below.

Table b-1. Strongbox parts dimensions and weights.

Parts name	Dimension “mm”	Quantity	Wight “Kg”
Full box “Interior dimensions”	600 L x 400 W x 400 H	-	-
Bottom plate	600 L x 400 W x 25 t	1	18.37
Front or Back plates	650 L x 425 W x 25 t	2	42.52
Side plates	425 L x 400 W x 25 t	2	22.58
platform	800 L x 800 W x 25 t	1	41.10
Bolts M10* ¹	50 L , T 20, Di 10	100	3.900
Bolts M14* ¹	14 Di	8	0.680
Standard Washers	10 Di	100	0.770
Standard Washers	14 Di	8	0.1
Full box “Overall dimensions”	750 L x 450 W x 425 H	-	130.11

Material specification

The strongbox plates and the platform are made from aluminium 6061 T6 and these materials have properties as shown in the Table b-2.

Table b-2. Material properties (ASTM-B209-14- standard specification for aluminium and aluminium alloy sheet and plate).

Property	Value	Units
Elastic modulus	69000	N/mm ²
Poisson's Ratio	0.33	N/A
Tensile Strength	310	N/mm ²
Yield Strength	275	N/mm ²
Thermal Expansion Coefficient	2.4e-005	/k
Mass Density	2700	Kg/m ³
Hardening Factor	0.85	N/A

Hand calculation

Soil loading assumption

The purpose of the strongbox or the container is to enable an experimental study of soil pipe interaction such that the container will be filled by soil to a required density. The inner surfaces of the box will be subjected to complex loading conditions (i) static/active/passive ground stresses, (ii) water pressure Figure b-3, and (iii) surface loading **Error! Reference source not found.**, thus the box is designed to accommodate this range of applied stresses.

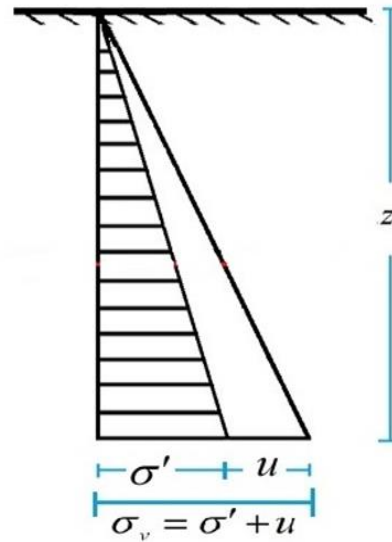


Figure b-3. Total, effective and neutral stress in the soil

This strongbox has been designed for an assumption of worst scenario of the static ground stresses on the inner surfaces of each vertical component Figure b-4. For example, increasing ground lateral stress is represented as a uniform pressure distribution for the maximum value of soil height. Active state occurs due to the latera pressure; it is the case when plastic equilibrium with lateral expansion takes place (wall moves outward from the soil). In this case the load cause only very small strain, because the plates are rigid and does not yield, as the worst scenario has been assumed and the value of k_a is negligible. k_o value is been used for the calculation” horizontal soil pressures are said to be at-rest pressure or K_o state” and the horizontal stress is calculated as shown below. K_p limit state has not been considered as the worst case, since it is assumed that the plate never moves into the soil, thus developing a passive state. Table b-3 shows approximate magnitudes of movements required to reach minimum active and maximum passive earth pressure condition.

Table b-3. Deformation (Δx) Corresponding to Active and Passive Earth Pressure, as a Function of Wall Height, H

Soil Type	Δ_x/H	
	Active	Passive
Dense sand	0.001	0.01
Medium-dense sand	0.002	0.02
Loose sand	0.004	0.04
Compacted silt	0.002	0.02
Compacted clay	0.01	0.05

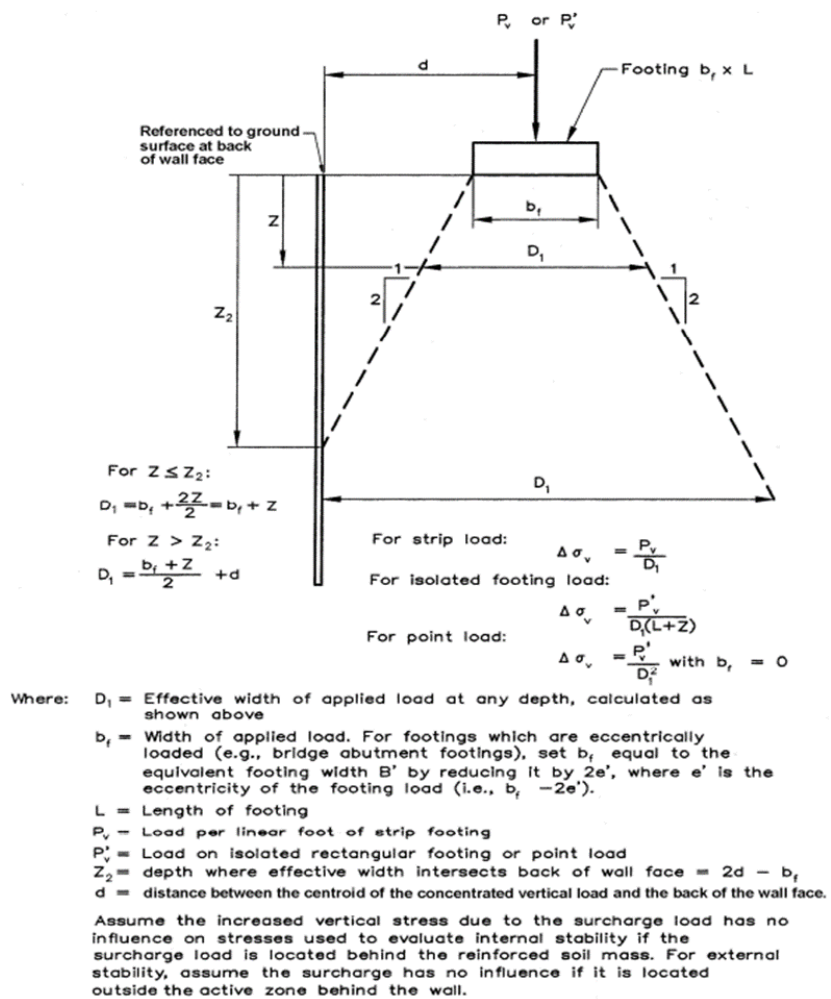


Figure b-4. Increase of vertical stress due to surface load (AASHTO 2010).

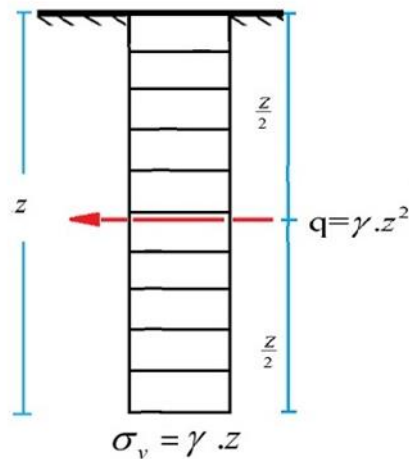


Figure b-5. Lateral pressure "Uniform load".

Vertical total stress

$$\sigma_v = \gamma_{soil} \cdot z_{soil}$$

$$\sigma_v = 20 * 0.4 = 8kPa$$

porewater pressure

$$u = \gamma_w \cdot z_w$$

$$u = 9.81 * 0.4 = 3.92kPa$$

Vertical effective stress

$$\sigma'_v = \sigma - u$$

$$\sigma'_v = 8 - 3.92 = 4.08kPa$$

Horizontal effective stress

$$\sigma'_h = k_o * \sigma'_v$$

$$k_o = 1 - \sin \phi'_c \rightarrow 1 - \sin 30 = 0.5 \rightarrow \text{case of sand only}$$

$$\sigma'_h = 0.5 * 4.08 = 2.04kPa$$

Horizontal total stress

$$\sigma_h = \sigma'_h + u$$

$$\sigma_h = 2.04 + 3.92 = 5.92kPa$$

Horizontal total stress @ 50g

$$\sigma_{h50} = 5.92 * 50 = 289kPa$$

Surface pressure that increase vertical stress in soil

rectangular area(footing)see eq.from fig 5

Load assumption

Full load

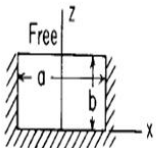
where : –

- σ_v – Vertical total stress (kPa), u – porewater pressure ,
- σ'_v – Vertical effective stress(kPa), σ'_h – Horizontal effective stress(kPa)
- σ_h – Horizontal total stress(kPa), k_0 – coefficient of earth pressure
- ϕ'_c = critical angle of friction, k_0 value for dense sand is =0.5
- σ_v – Vertical stress(kPa), γ – specific weight of soil(N / m^3)
- z – soil depth(m), N – centrifugal acceleration = 50g

Strongbox plates–stress analysis

The assumption of the plates’ boundary conditions is very important for the calculation of the max stress and deflection at certain point and, for this reason Roark’s formulas Table b-4 and the theory of plates and shells have been used for rectangular plates with three edges built in and the fourth edge free see the table below.

Table b-4. Formula for flat plates with straight boundaries and constant thickness.

Rectangular plate; three edges fixed, one edge (a) free 	10a. Uniform over entire plate	$(\text{At } x = 0, z = 0) (\sigma_b)_{\max} = \frac{-\beta_1 qb^2}{t^2} \text{ and } R = \gamma_1 qb$							
		$(\text{At } x = 0, z = b) \sigma_a = \frac{\beta_2 qb^2}{t^2}$							
		$(\text{At } x = \pm \frac{a}{2}, z = b) \sigma_a = \frac{-\beta_3 qb^2}{t^2} \text{ and } R = \gamma_2 qb$							
		a/b	0.25	0.50	0.75	1.0	1.5	2.0	3.0
		β_1	0.020	0.081	0.173	0.321	0.727	1.226	2.105
		β_2	0.016	0.066	0.148	0.259	0.484	0.605	0.519
		β_3	0.031	0.126	0.286	0.511	1.073	1.568	1.982
		γ_1	0.114	0.230	0.341	0.457	0.673	0.845	1.012
		γ_2	0.125	0.248	0.371	0.510	0.859	1.212	1.627

where : –

σ_a = stress at $x = 0, z = b$

β_2 = value from the table depend on the value of $\frac{a}{b}$

$q = \sigma_h$ = horizontal effective stress

b = plate height

a = plate width

t = plate thickness

*Max stress calculation for the front and back plates 0.7m*0.4m*0.025m*

$$\sigma_a = \frac{((5.65 * 10^{-1}) * 298280 * 0.4^2)}{0.025^2} = 4.3 * 10^7 (N / m^2) \rightarrow 43(N / mm^2)$$

Summary Outcome:

Yield Stress = 43 N/mm2 which represents 17% of the total proportion of the maximum material yield stress = 275N/mm2. Typical graph shows the stress strain curve for aluminium 6061 T6 Figure b-6.

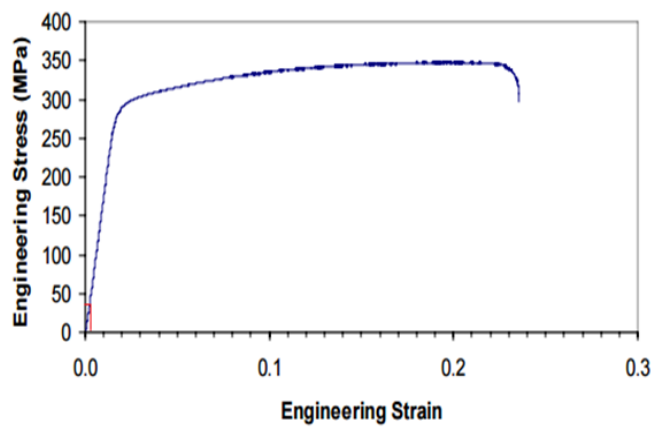


Figure b-6. Typical stress strain curve for Aluminium 6061 T

Therefore, all the proposed parameters for this design is appropriate design and it is ideal to be used for maximum 50 g.

Table b-5. Deflections, bending moments, and reaction of uniformly load.

$\frac{b}{a}$	$x = 0, y = b$		$x = 0, y = b/2$			$x = a/2, y = b$		$x = a/2, y = b/2$		$x = 0, y = 0$	
	w	M_x	w	M_x	M_y	M_x	V_x	M_x	V_x	M_y	V_y
	$= \alpha_1 \frac{qa^4}{D}$	$= \beta_1 qa^2$	$= \alpha_2 \frac{qa^4}{D}$	$= \beta_2 qa^2$	$= \beta_2' qa^2$	$= \beta_3 qa^2$	$= \gamma_3 qa$	$= \beta_4 qa^2$	$= \gamma_4 qa$	$= \beta_5 qa^2$	$= \gamma_5 qa$
	α_1	β_1	α_2	β_2	β_2'	β_3	γ_3	β_4	γ_4	β_5	γ_5
0.6	0.00069	0.0089	0.00044	0.0060	0.0062	-0.0179	0.093	-0.0131	0.136	-0.0242	0.248
0.7	0.00069	0.0093	0.00058	0.0080	0.0074	-0.0172	0.081	-0.0170	0.158	-0.0261	0.262
0.8	0.00068	0.0096	0.00072	0.0100	0.0083	-0.0164	0.069	-0.0206	0.177	-0.0278	0.275
0.9	0.00067	0.0096	0.00085	0.0118	0.0090	-0.0156	0.057	-0.0239	0.194	-0.0290	0.286
1.0	0.00065	0.0095	0.00097	0.0135	0.0094	-0.0146	0.045	-0.0269	0.209	-0.0299	0.295
1.25	0.00056	0.0085	0.00121	0.0169	0.0092	-0.0119	0.018	-0.0327	0.234	-0.0306	0.309
1.5	0.00042	0.0065	0.00138	0.0191	0.0075	-0.0087	-0.006	-0.0364	0.245	-0.0291	0.311

where :-

ω = deflection at $x = 0, y = b$

α_1 = the value from the table depend on the value of $\frac{b}{a}$

$q = \sigma_h$ = horizontal effective stress

b = plate height

a = plate width

$$D = \frac{Et^3}{12(1-\nu^2)}$$

E = Young's modulus of elasticity

t = plate thickness

ν = Poisson's ratio

Deflection at $x = 0, y = b$

$$\omega = \alpha_1 \frac{qa^4}{D}$$

$$D = \frac{Et^3}{12(1-\nu^2)}$$

$$D = \frac{(6.9 * 10^7)(N / m^2) * 0.025^3 (m)}{12(1-0.33^2)} = 134 N.m$$

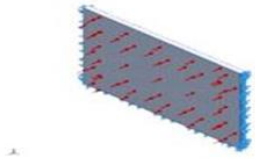
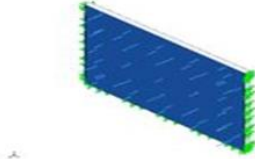
Deflection calculation for the front and back plates $0.7m * 0.4m * 0.025m$

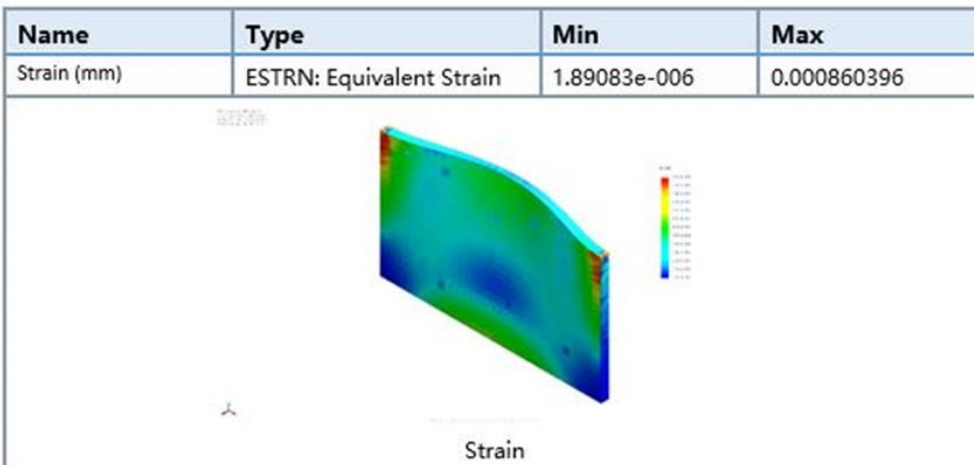
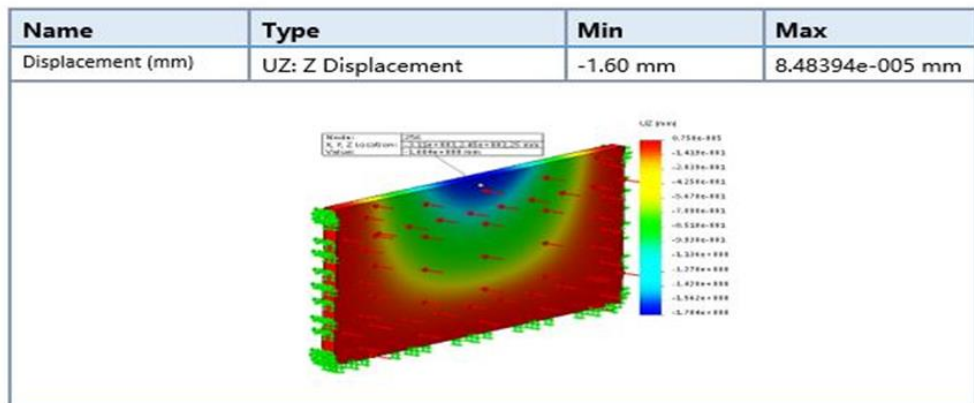
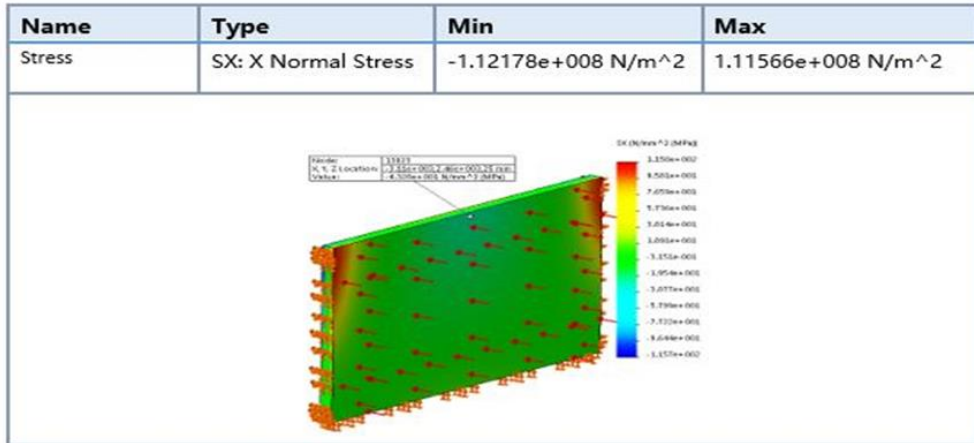
$$\omega = (2.66 * 10^{-3}) \frac{298.28(KN / m^2) * 0.7^4 (m)}{134 N.m} = 0.0014(m) \rightarrow 1.4(mm)$$

Summary plate deflection:

The impact of the horizontal total stress on the proposed plate causes deflection in free edge of the plate as has been calculated according to the theory of plate and shells, hand calculation and finite element results shows that the deflection is very small especially that the design assumption has been taken as the worst case scenario and to ensure that safety factors has been considered.

FEA / Finite Element Analysis summary (Solidwork software)

Fixture name	Fixture Image	Fixture Details		
Fixed-1		Entities: 3 face(s) Type: Fixed Geo		
Resultant Forces				
Components	X	Y	Z	Resultant
Reaction force(N)	-2.51367	0.990814	80922.5	80922.5
Reaction Moment(N.m)	0	0	0	0
Load name	Load Image	Load Details		
Pressure		Entities: 1 face(s) Type: Normal to selected face Value: 0.289 Units: N/mm^2 (MPa)		



Comparison between hand calculation and Finite Element Analysis

In all hand calculation and FEA using Solidworks software the assumption has taken into consideration the worst case scenario. Hand calculation where used to ensure that the results from FEA are logical, Based on Roark’s formula for stress and strain, and the theory of plates and shell. Table b-6 shows both results.

Table b-6. Comparison between hand calculation and FEA (solidworks)

Calculation method	Displacement(mm)	Stress (N/mm ²)
Hand calculation	1.40	43
FEA	1.6	43.28

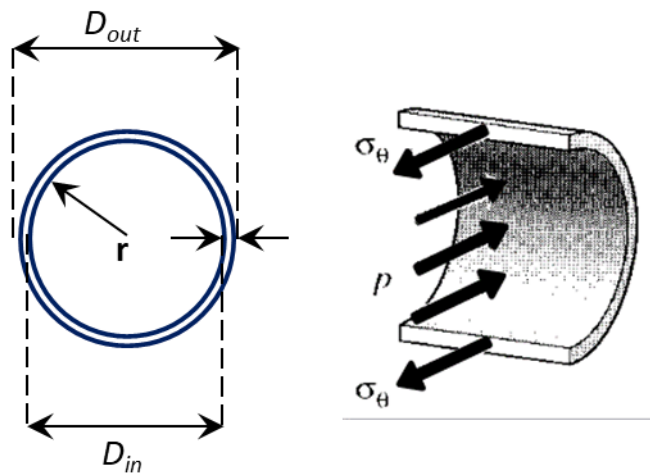
Appendix C

Hoop stress/strain for open end pipe problem

In order to simulate the internal water pressure and design the apparatus for this purpose, it was necessary to understand the working mechanism of the internal water pressure on the pipes then to implement this concept for the centrifuge experiments. From the assumption of that if the pipe expands from internal pressure, it will want to reduce in length due to Poisson's ratio ν . This will give a tensile force in the pipe if both ends are fixed therefore, the calculation of hoop stress/strain is presented in detail below.

Assuming that: -

$$\sigma_{\theta} = \frac{pr}{t}$$

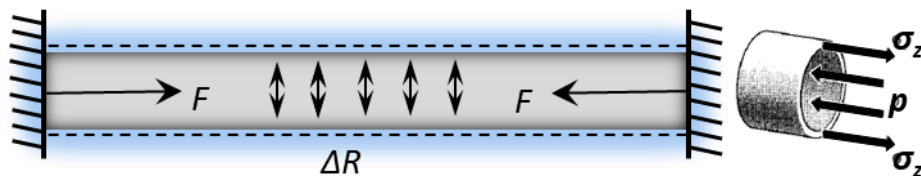
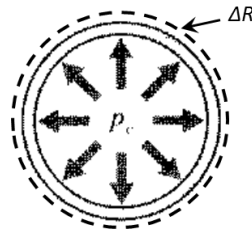


Where σ_{θ} is the hoop stresses, maximum internal water pressure $p = 0.5 \text{ N/mm}^2$ (5 bar), outer pipe diameter $D_{out} = 16\text{mm}$, inner pipe diameter $D_{in} = 12.4\text{mm}$, pipe radius $r = 6.2$, pipe wall thickness $t = 1.8\text{mm}$, Poisson's ratio $\nu = 0.4$ and pipe module of elasticity $E = 885 \text{ MPa}$.

$$\sigma_{\theta} = \frac{500 * 6.2}{1.8} = 1667 \text{ kPa or } 1.667 \text{ MPa}$$

$$\sigma_{\varepsilon} = \frac{\sigma_{\theta}}{E} = \frac{1.667}{885} = 0.0018824$$

- Change in radius



$$\Delta R = \frac{PR^2}{tE} = \frac{500 * 0.0062^2}{0.0018824 * 885 * 10^3} = 0.0018824$$

Publications

- Change in length ϵ_L

$$\epsilon_L = \nu \epsilon_\theta 0.45 * 0.0018824 = 0.0008495$$

Total pipe length 315mm

$$315 * 0.0008495 = 0.2675925 \text{mm}$$

- Force to resist

$$F = A \sigma_L = A \epsilon_L E$$

$$F = \pi \frac{D_{out}^2 - D_{in}^2}{4} * \epsilon_L * E$$

$$F = \pi \frac{0.016^2 - 0.0124^2}{4} * 0.0008495 * 885 * 10^3 = 60N$$

Publications

Part I

Physical Modelling in Geotechnics – McNamara et al. (Eds)
© 2018 Taylor & Francis Group, London, ISBN 978-1-138-34419-8

Centrifuge modelling utility pipe behaviour subject to vehicular loading

S.M. Bayton, T. Elmrom & J.A. Black

Centre for Energy and Infrastructure Ground Research (CEIGR), University of Sheffield, Sheffield, UK

ABSTRACT: Centrifuge model tests of buried flexible pipes in dry sand subjected to surface traffic loads are presented. Model pipe tests were performed at 25 gravities (25g) of a prototype pipe 355 mm in diameter. Pipe behaviour was observed for different burial depths of 0.5, 0.75, 1.0 and 1.5 m; and load eccentricities of 1 and 2 pipe diameters. Results show that pipes buried at shallower depths are subjected to significantly greater bending moments and corresponding shear stresses. When the load is applied at an eccentricity, if the pipe remains within the zone of stress influence, a comparable magnitude of maximum moment is anticipated. An initial series of 20 cycles were also carried out. Results indicate an amount of 'locked-in' bending moment upon unload; a phenomenon more evident for the shallower buried pipe.

1 INTRODUCTION

The integrity and performance of buried pipe infrastructure plays a significant role in modern society; providing the safe distribution of potable water, transportation of sewage and connection of communication services, amongst other applications. For this purpose, a diverse range of buried pipes are deployed such as large diameter concrete sewer pipes to small diameter plastic fresh water pipes. Municipal water distribution and wastewater infrastructure systems are of national importance and the aspect of water leakage, coupled with water scarcity, has become a serious problem in many countries. In England and Wales alone, over 3 billion litres of water is lost through leakage every day (DiscoverWater 2017), representing up to 30 per cent loss of the potable water from source to the consumers tap.

Typically, utility pipes are located beneath the surface of road networks to simplify installation, distribution and maintenance. Owing to the shallow burial depth of these critical infrastructure assets they are highly vulnerable from a number of factors that may influence their performance and deterioration; for example, the impact of heavy surface traffic loading and changeable burial conditions. A summary of the complexities surrounding buried utility pipes and the challenges faced by the water industry is illustrated in Figure 1.

Boussinesq (1883) developed a solution for the stress at any point in a homogeneous, elastic, and isotropic medium, caused by a point load applied on the surface of an infinitely large half-space. Based on these Boussinesq equations, Young & O'Reilly (1983) established a method for estimating the

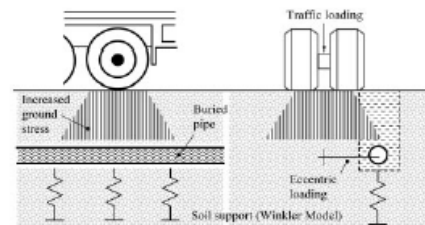


Figure 1. Buried pipe infrastructure and its challenges.

vertical stress on an underground pipe caused by traffic wheel loading. Various charts based on the Boussinesq method were developed, which are still in use in BS EN 1295-1 (BSI 1998). Other researchers, like Marston & Anderson (1913) and Burns & Richard (1964), introduced their theories about influence of loads on underground pipelines. Pocock et al. (1980) measured the bending strain developed in a shallow buried pipeline comprising eight cast iron pipes; while Taylor & Lawrence (1985) noticed that the response of a cast iron pipeline to heavy vehicles depended on structure of the pavement, backfill height, and pipe bedding.

Given the high leakages, combined with increased traffic loading, there is a high motivation to understand the behavior of buried shallow pipe networks to increase future resilience. At present however, there exists relatively little available literature with experimental results, in particular relating to these pressing challenges surrounding pipe-soil interaction. This is despite considerable uncertainties remaining.

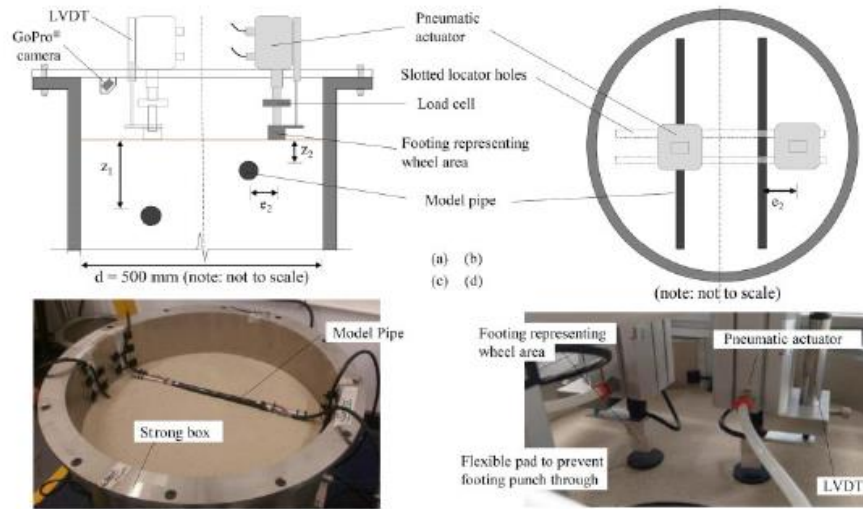


Figure 2. Test setup: schematic (a) elevation and; (b) plan view; (c) photo of pipe placement and; (d) actuator and LVDT setup.

This paper presents the results from a suite of small-scale buried pipe experiments performed in a geotechnical centrifuge at elevated gravity to simulate prototype stresses. The aim of the current research is to investigate the effect of pipe burial depth and load eccentricity on the behaviour of flexible HDPE pipes in sand with the view of providing an insight of the role of these external factors in the pipe-soil interaction.

2 CENTRIFUGE EXPERIMENTAL SETUP

A series of centrifuge model tests, at a centrifugal acceleration of 25 times Earth's gravity ($25g$) was conducted using the University of Sheffield's 4 m diameter 50g-tonne geotechnical beam centrifuge (Black et al., 2014). The centrifuge allows for the replication of prototype stress conditions to adequately capture the small-strain stiffness and dilation responses associated with the pipe-soil interaction problem.

A medium-fine grain sand commercially known as CH30 sand (see Table 1) was dry pluviated into a cylindrical strong box to an average relative density, R_d , over the test matrix of 81.0%. The model chamber had internal diameter and height of both 500 mm and provided a rigid boundary. The pluviating continued until reaching the desired level to the base of the buried pipe (i.e. burial depth). See Figure 2(a) for an illustrative diagram of the experimental setup; noting Figure 2(a) and (b) are not to scale.

The two acetal pipes were placed in parallel at a distance of 100 mm apart at the required burial depth. Further sand was pluviated on top until the desired cover above the respective pipes was achieved.

Table 1. CH30 sand properties.

Property	Value
Particle size, d_{10}	0.355 mm
d_{50}	0.450 mm
Specific gravity, G_s	2.67
Maximum void ratio, e_{max}	0.756
Minimum void ratio, e_{min}	0.508
Peak angle of shear, ϕ_{peak}	37° (at $R_d = 80\%$)

Table 2. Flexible HDPE pipe properties.

Description	Prototype Dimension	Model Dimension
Gravity (g)	1	25
Material	HDPE	Acetal
Young's Modulus (E)	1.5 GPa	2.6 GPa
Diameter (D)	355 mm	14.2 mm
Thickness (t)	33.5 mm	2.1 mm
Flexural Stiffness (EI)	661 Nm ²	3.91×10^{-3} Nm ²
Scaling law of EI	1	$1/25^4$
Ratio of $EI_{model/prot}$	1	2.3

The model pipe material was selected to replicate prototype HDPE and can be considered to be flexible. Pipe and scaling properties are presented in Table 2. Using the bending stiffness scaling law of $1:N^4$, the model pipe's scaled bending stiffness provides an adequate representation of the prototype given that it is

in the same order of magnitude and flexible behaviour should still be captured.

Eight pairs of strain gauges (KFG type) in half bridge configurations (four in the major axis from the mid-span along one half of the pipe, and four from the mid-span in the minor axis along the other half) were positioned on the pipe length at 30 mm intervals. This allowed the bending response captured to be mirrored at the mid-span given the load application was at this point. Bending moment calibration of the strain gauges was performed on each 90 degree orientation. The proportion of out-of-plane bending was recorded to be a maximum of just 7% of the respective in-plane bending. The pipe, and respective strain gauges, was then protected with a thin covering of electrical tape (with near zero stiffness ensuring no contribution to the stiffness of the pipe). Figure 2(c) presents the arrangement of the model pipes at different burial depths.

Additional scaling aspects considered were the sand-pipe particle interaction. In the present study, the pipe circumference, C , was 44.5 mm yielding a $C/d_{50} \approx 100$ and $D/d_{50} \approx 31$; conforming to the particle contact relationship outlined by Bolton et al (1999).

A bespoke loading frame was assembled from machined aluminium plate with specific locator slotted holes for the positioning of load actuation systems at any desired eccentricity across the width of the pipe (Figure 2(b)). The load application was achieved by the use of a 50 mm diameter dual acting pneumatic cylinder actuator, with a maximum load capacity of 1.3 kN. A positive pressure was supplied to the reverse action side during spin-up to prevent the piston from contacting the surface under increased self-weight. The opposing pressure line was then increased to apply load to the surface. A load cell was calibrated over the loading range and attached between the actuator and the model aluminium footing representing the lorry wheel load. The footing had dimensions of 10 mm \times 20 mm to replicate a wheel contact area of 0.25 m \times 0.5 m at prototype scale. The settlement of the footing was measured using one LVDT located directly on the footing. A flexible rubber mat was positioned on the sand surface to prevent the aluminium footing from punching directly through the sand since there is no restraint on the sand surface. Note, future tests have utilised sculpting plaster to model the contact road bending stiffness, which also plays an important role in dissipating the applied surface loading. Hence, it is likely that the observed load-displacement and bending moments reported herein reflect upper bound interaction levels.

3 TEST MATRIX

Six centrifuge tests were performed to study the effects of burial depth and load eccentricity on the pipe-soil behaviour. After the initial monotonic load, a further 20 load cycles were applied to observe the effects of repetitive traffic load. Table 3 presents the full test matrix.

Table 3. Experimental test matrix [prototype dimension in square brackets].

Test (#)	R_d (%)	Burial depth (z)		Load eccentricity (e)	
		(mm)	[m]	(mm)	[m]
1	80.1	60	[1.5]	0	[0]
2	79.6	40	[1.0]	0	[0]
3	84.8	30	[0.75]	0	[0]
4	81.9	20	[0.5]	0	[0]
5	80.1	40	[1.0]	14.2	[0.355]
6	79.6	40	[1.0]	28.4	[0.710]

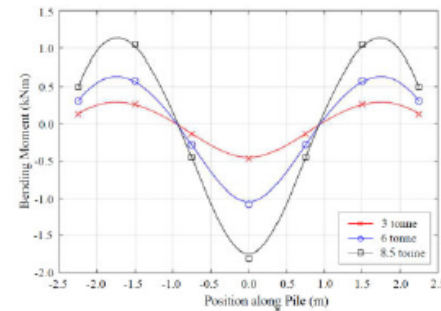


Figure 3. Evolution of bending moment with load for pipe embedded at $z = 1.0$ m.

The magnitude of the model load was selected to represent one half of a wheel axle of a 44 tonne articulated lorry at prototype scale (this equates to the largest permissible load on UK roads). This equals to a vertical load of 6 tonnes per wheel base. This is in accordance with monotonic and cyclic loading recommendations in AASHTO (2010).

4 RESULTS & DISCUSSION

Load was applied in stages and footing displacement and pipe bending moment were measured. Figure 3 presents the evolution of moment with load for the pipe buried at 1.0 m depth. All measurements are expressed in prototype dimensions. As expected, the greater the load on the footing, the greater the moment experienced within the pipe. It can also be seen that the point of zero moment remains in the same location throughout the load increments.

4.1 Effect of burial depth

For a footing loaded along the centreline and at mid-span of the pipe, settlement behaviour was observed for the range of pipe burial depths (sand cover of 0.5, 0.75 and 1.0 and 1.5 m) (Figure 4). It can clearly be

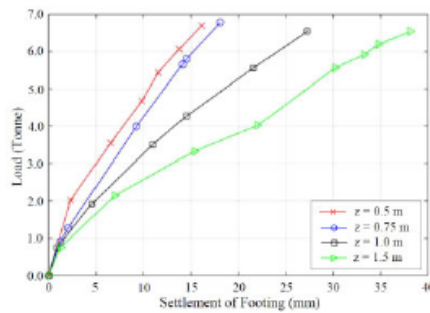


Figure 4. Variation in footing settlement with pipe burial depth.

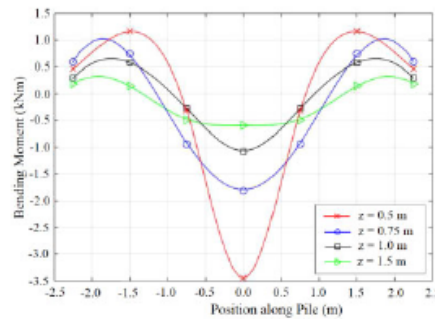


Figure 5. Variation in bending moment with pipe burial depth at applied load of 6 tonnes.

seen that a shallower pipe provides a stiffer footing settlement response signifying that the pipe is providing additional resistance to the increase in stress within the soil. Additionally, the initial small-strain stiffness appears to be very similar for each burial case suggesting that for low loads (up to 1 tonne) the soil close to the surface initially resists the additional stress and each test demonstrates the same behaviour in this part. Once the propagation of stress reaches the deeper soil, additional stiffening from the pipe comes into effect. During unloading, settlements are not fully recovered, most likely due to compaction and redistribution of sand grains.

Figure 5 presents the variation of bending moment with burial depth for these same surface loading of 6 tonnes. The moment is greatest for shallower burial depths. It can be seen that for the shallowest burial depth ($z = 0.5$ m), the bending moment peaks to a significant, sharp point directly below the load application. This is in contrast to the deeply buried pipe ($z = 1.5$ m), where the applied stress in the soil has radiated with depth and therefore when it reaches the deeper pipe, the area of influence is much greater, and

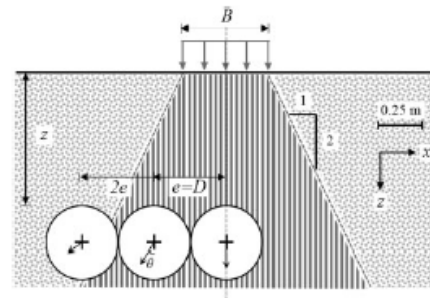


Figure 6. Schematic illustration of pipe behaviour under eccentric loading.

the stress is much less. It can be seen that the bending response is much smoother, and there is a portion of almost equal bending across the middle 2 m section as the stress is more uniformly distributed in this region. The length of this section coincides very well with theoretical approximations of a 2V:1H stress distribution with depth.

A key pipe design parameter is to minimise the very large changes in bending over short distances as well as abrupt points of inflexion as these have large shear stresses associated with them. As shown, the selection of a greater burial depth facilitates this reduction in pipe stress and could aid with the longevity of pipe lifespan.

4.2 Effect of eccentricity

In addition to varying the burial depth of the pipe, the eccentricity of the applied footing load was increased to replicate variations in surface load conditions. Eccentricities of one and two pipe diameters were investigated, with loads again applied at the mid-span of the pipe. It is expected that due to the eccentric load, the pipe is subjected to additional lateral soil pressure and therefore experiences horizontal bending and displacement as well as vertical.

Figure 6 illustrates the test dimensions of the eccentrically loaded pipes. Overlaid on this figure is the dissipation of stress within the soil depth taken to be the classical 2V:1H zone of influence. As can be seen, the pipe at $e = 1D$ is well within the bounds of this zone. The pipe at $e = 2D$ skirts the edge of this zone. Table 4 presents the observations from these tests in terms of pipe major and minor axis and resultant bending moments as well as the corresponding resultant vector direction.

It can be seen that there is a clear distinction in pipe behaviour depending on whether the pipe is within or beyond the bounds of the zone of stress influence. For example, for the two pipes fully within this zone, the magnitude of the resultant bending moment is comparable, the difference being that for the

Table 4. Pipe bending magnitude and direction due to eccentric load.

Test (#)	Max Major Mom. (Nm)	Max Minor Mom. (Nm)	Resultant Mom. (Nm)	θ (°)
2	1080	3	1080	0.1
5	754	717	1040	43.5
6	256	317	407	51.0

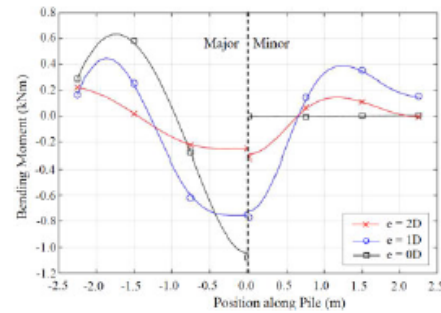


Figure 7. Variation in bending moment with load eccentricity at a burial depth of $z = 1.0$ m and applied load of 6 tonnes (N.B. D = external diameter of pipe).

pipe eccentrically loaded at $e = 1D$, the major bending moment has reduced and the minor moment has increased. This would suggest the same increase in resultant stress acting on the pipe here, but with different magnitudes of the lateral and vertical components. When the pipe is located right on the outer bound of the zone of stress influence there is a significant reduction in resultant bending moment, with both the major and minor moments reducing in parallel. The values do not reduce to zero, and the lateral stress is greater than the vertical at this location. Similar observations of bending moment reductions for eccentric loads have been made by Hosseini & Tafreshi (2010). The bending moment diagrams for each are presented in Figure 7.

Although loadings in the current study are statically applied, the observations of maximum and minimum bending moment occurring in the major and minor planes reflect the transitional stress states imposed on the buried pipe in serviceable conditions under transient loading associated with moving vehicles. Additional testing in this regard would prove highly valuable to understanding pipe longevity and deterioration owing to changes in burial confinement and relaxation that would occur with multiple transient loadings.

4.3 Effect of cyclic load

After the initial application of monotonic load, a series of 20 load cycles were applied to the footing to simulate the effect of repetitive traffic loading. The applied

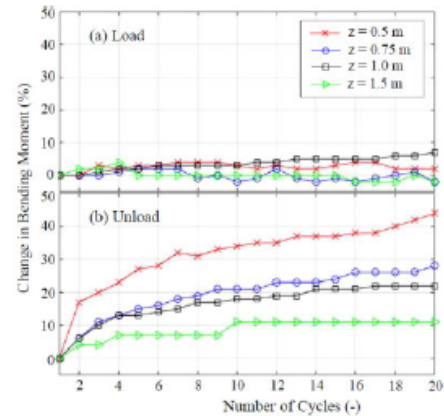


Figure 8. Evolution of (a) maximum (on load) and; (b) residual (on unload) bending moments in comparison to first cycle magnitude with number of cycles at 6 tonne load per cycle.

cyclic load simulated that of one single wheel of the articulated load and had a magnitude of 6 tonnes at prototype scale. It is admitted by the authors that 20 cycles is not a complete replication of the full cyclic loading over a lifetime pipe operation; however, it provided a preliminary insight into the cyclic behaviour with future testing in mind.

The change in bending moment (positive representing an increase in magnitude) on both the load and unload phase is shown in Figure 8. Upon each cyclic application of load, it can be seen (Figure 8a) that the maximum moment experienced within the pipe does not vary greatly with cycles. In contrast, when the load was removed the bending moment did not return to zero and residual 'locked-in' bending moment was observed (Figure 8b); increasing with cycle number. The phenomenon is clearly more pronounced for the shallower buried pipes. For the pipe buried at $z = 0.5$ m, the increase in residual bending moment is over 40% after 20 cycles which is a significant design consideration. This can be attributed to localised changes in sand grain distribution and density, and therefore new soil-structure interaction regimes on each cycle.

Upon spindown of the centrifuge, when the elevated stress field in the soil reduces, the 'locked-in' moments dissipated, confirming that this was indeed an increased confining stress within the soil restraining the pipe on unload. Over the lifetime of the pipe infrastructure, there is potential for significant 'locked-in' stresses to develop as several million cycles of load are applied to the pipe-soil configuration. This may have implications on pipe long-term performance. Strategically selected cyclic experiments investigating different loading conditions are ongoing at CEIGR in Sheffield to explore these effects.

5 CONCLUSION

A series of centrifuge modelling experiments has been carried out evaluating the behaviour of buried flexible pipes subjected to surface traffic loads, simulated by a metal footing, in dense sand. Comparison of pipes buried at different depths shows that shallower pipes are subjected to significantly greater bending moments. Footing settlement was also the lowest for the shallowest pipe suggesting increased stiffness of the system due to the pipe structure.

The buried pipes were also subjected to eccentric loads. When the pipe remained within the zone of stress influence from the eccentric load, the magnitude of the resultant bending moment remained comparable to that of the pipe loaded on the centreline. Once beyond this zone, the magnitude of resultant bending moment reduces significantly.

A series of 20 load cycles were also carried out. Upon each cyclic application of load, the maximum moment experienced within the pile remained reasonably constant. On unload on the other hand, a substantial amount of 'locked-in' bending moment was also observed, increasing with cycle number, owing to potential new soil-structure interaction regimes established. For the buried pipes at deeper depths, this phenomenon is much less pronounced suggesting less interaction.

ACKNOWLEDGMENTS

Funding support provided by the Engineering Physical Sciences Research Council (EPSRC) to establish the 4 m diameter beam centrifuge and Centre for Energy and Infrastructure Ground Research at the University of Sheffield (Grant No. EP/K040316/1) is gratefully acknowledged.

Thanks also to the support and expertise of the Department of Civil & Structural Engineering

technical staff for in-house fabrication of the pipe and loading systems.

REFERENCES

- AASHTO. 2007. AASHTO LRFD Bridge design specifications. 4th ed. *American Association of State and Highway Transportation Officials*, Washington, D.C.
- Boussinesq, J. 1883. Application des potentiels à l'étude de l'équilibre et du mouvement des solides élastiques. Gauthier-Villars, Paris.
- Bolton, M.D., Gui, M.W., Garnier, J., Corte, J.F., Bagge, G., Laue, J. & Renzi, R. 1999. Centrifuge cone penetration tests in sand. *Géotechnique* 49(4): 543–552.
- BSI. 1998. BS EN 1295-1: Structural design of buried pipelines under various conditions of loading. Part 1. General requirements. *British Standards Institution (BSI)*, London.
- Burns, J.Q., & Richard, R.M. 1964. Attenuation of stresses for buried cylinders. In *Proceedings of the Symposium on Soil-Structure Interaction*, University of Arizona Engineering Research Laboratory, Tucson, Ariz., 8-11 June 1964. American Society for Testing and Materials, West Conshohocken, Pa.: 379–392.
- Discover Water. 2017. [Date viewed: 04 October 2017]. <http://discoverwater.co.uk/leaking-pipes>
- Hosseini, S.M.M. & Tafreshi, S.M., 2000. Soil-structure interaction of buried pipes under cyclic loading conditions. *WIT Transactions on the built environment*, 48
- Marston, A. & Anderson, A.O. 1913. The theory of loads on pipes in ditches and tests of cement and clay drain tile and sewer pipes. *Bulletin 31. Iowa Engineering Experiment Station*, Ames, Iowa.
- Pocock, R.G., Lawrence, G.J.L. & Taylor, M.F. 1980. Behaviour of a shallow buried pipeline under static and rolling wheel loads. *TRRL Laboratory Report 954*, Department of Transport.
- Taylor, M.E. & Lawrence, G.J.L. 1985. Measuring the effects of traffic induced stresses on small diameter pipeline. *Pipe and Pipeline International*, 30(2): 15–19.
- Young, O.C. & O'Reilly, M.P. 1983. A guide to design loadings for buried rigid pipes. *TRRL Laboratory Report*, Department of Transport.

Part II

Development and calibration of a sand pluviation device for preparation of model sand bed for centrifuge tests

M. Hakhamaneshi, J.A. Black, A. Cargill, C.M. Cox & T. Elmrom
University of Sheffield, Centre for Energy & Infrastructure Ground Research, Sheffield, UK

ABSTRACT: A bespoke 0.068m³ (18.5 gallon) sand hopper is employed at the newly established 50gTon centrifuge facility at the University of Sheffield. The sand hopper employs a series of mesh inserts of different diameters which control the flow rate and thus the relative density of the model. A series of calibration tests on equivalent Fraction E and Fraction C sands were performed to calibrate the mesh diameter and drop height for a desired relative density. Result showed that the sand hopper is capable of delivering repeatable relative densities in the range of 30% to above 90%, for both kinds of sand grades. This wide range relative density is considered sufficient to satisfy the needs of researchers preparing dry sand models for testing in the center.

1 INTRODUCTION

Many centrifuge models aim to achieve repeatable, uniform sand bed profiles of different relative densities. It is very common for researchers to develop a series of experimental parametric studies where sand beds must be uniform across the whole test series (Hakhamaneshi et al. 2015). A non-uniform relative density with a model test bed, or variations across various models, directly affects the performance of many physical model tests in the centrifuge; examples include bearing capacity footing and pile capacity tests, liquefaction and seismic site response. Many researchers also aim to compare their experimental findings with numerical predictions (e.g. Arulanandan and Scott 1993) or the experimental results to be used as a benchmark for calibration of numerical models (e.g. Hakhamaneshi et al. 2015). It is therefore essential for every centrifuge facility to employ a pourer device capable of producing repeatable uniform relative densities of a wide range that reflect loose and dense states.

Geotechnical centrifuge facilities typically employ one or more of the following sand hopper systems based on the pour area or the number of axis to be controlled (Stringer et al. 2014): point pluviators, curtain pluviators and carpet pluviators. Point pluviators pour sand typically from a small orifice where the 3-axes of pour are all controllable manually by the user. This is the most common type of placement system currently adopted in model preparation. Compared to a point pour, curtain pluviators pour a complete line of sand but need to be moved laterally to cover the entire surface area of the container in

one sweeping motion. The most sophisticated pluviators cover full surface area of the model leaving the user to adjust the vertical axis during the pour (Chapman 1974)). Automatic sand pourers are also somewhat commonly used within the geotechnical centrifuge facilities. Fully robotic pourers are less common but some examples include those currently employed at the University of Cambridge, University of British Columbia, Technical University of Delft, Laboratoire Central des Ponts et Chaussées (LCPC), National Central University in Taiwan, and Hokkaido University in Japan (Chian et al. 2010). Previous studies on robotic pourers (Zhao et al. 2006) demonstrated the capability of such sand hoppers to produce uniform sand models of relative densities ranging from 50% to above 90%. Sweeney and Clough (1990) described the development of a large chamber for calibration of cone penetrometers in-situ; the chamber enabled soil pluviation for placement of sand, vacuum unit for removing the excess sand and an automatic data acquisition system.

Rad and Tumay (1987) reported the significance of pluviation intensity (mass flux) and falling height on the resulting relative density. In point pourers the mass flux is typically controlled via one or more steel mesh plates placed at the bottom end of the pourer. Rad and Tumay (1987) showed that number of identical steel mesh plates has small effects on the resulting relative density, except the case of adding a single mesh plate to a no-mesh system. In a point pourer falling sand is passed through a mesh (or a system of meshes) leading to a wider spread of area of falling sand and greater spatial uniformity

(Stringer et al. 2014, Sweeney and Clough 1990, Chapman 1974).

This paper aims to introduce the point pouter developed at the Centre for Energy and Infrastructure Ground Research (CEIGR) at the University of Sheffield. Relative density calibration charts (diameter of mesh insert and falling height) are provided for the equivalent of Fraction C and Fraction E sands.

2 SAND PROPERTIES

Two different types of silica sands named CH30 and CNHST95 were employed at the CEIGR. These sands are very similar to the commonly used Fraction C and Fraction E Leighton Buzzard silica sands (Chian et al. 2010). Table 1 summarizes the properties of the types of sands used for the pouter calibration. Figure 1 plots the Grain Size Distribution of these two types of sands.

Table 1. Properties of equivalent Fraction E and Fraction C sands used for pouter calibration.

Properties*	CH30	CNHST95
D_{10}	0.355 mm	0.100 mm
D_{50}	0.450 mm	0.139 mm
D_{60}	0.470 mm	0.150 mm
e_{min}	0.508	0.514
e_{max}	0.756	0.827
G_s	2.67	2.65

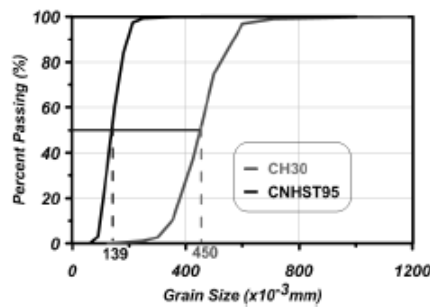


Figure 1. Grain size distribution of the equivalent Fraction C (CH30) and Fraction E (CNHST95) sands employed at CEIGR.

3 SAND PLUVIATION

3.1 Sand pouter development

The newly established 50gTon centrifuge facility at the University of Sheffield did not benefit from a pluviation system. A test container currently employed at CEIGR is a circular tub of 490mm diameter and 500mm height. A point sand pouter is developed which suits the current size of the container and enables a wide range of relative densities to be

achieved. The system is relatively easy to operate without the need of any special training, with the exception of observing Health and Safety requirements surrounding air-borne particles. The calibration charts proposed in this paper are aimed to provide a benchmark and look up table which users can refer to determine the pluviation settings that should be observed to achieve a desired relative density.

The designed and manufactured point pouter is shown in Figures 2 and 3. The sand hopper's main body was fabricated from 2mm aluminium sheet; the four sides were cut; 380mm x 425mm and each piece was tapered and folder at a 35° angle at a distance 200mm from the top of the pouter. This angle serves to ensure that sand stored in the hopper is funnelled towards to the nozzle during pluviation to maintain a constant flow of sand.

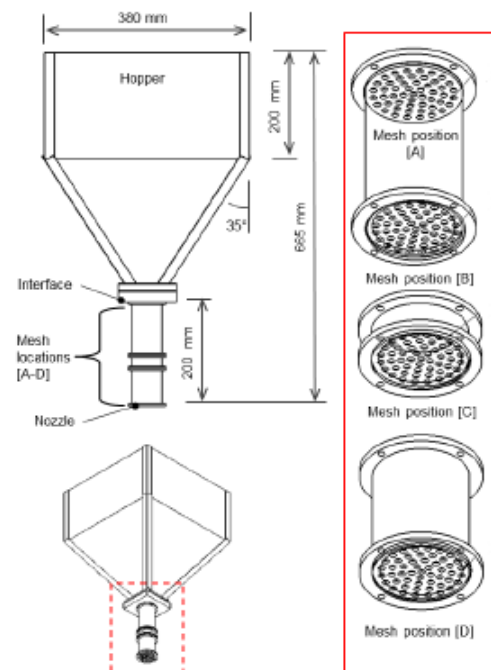


Figure 2. Schematic of the point sand pouter developed at the CEIGR along with the four allocated mesh inserts.

The hopper sides are fasted together using aluminium angle section and pop riveted to create the main pyramid shape. A base plate was fabricated at the tapered end of the hopper to interface with the end nozzle attachment. This was machined to convert the square base into a 50mm diameter outlet. The base plate was drilled and tapped to facilitate the outlet supply pipe. A length of 40mm extruded aluminium was fastened through the top of the hopper to create a lifting point so the hopper could be sus-

pended from a height adjustable pulley. This also served to strengthen the hopper overall construction. The overall capacity of the hopper is approximately 0.068m^3 .

The outlet pipe was manufactured from solid 80mm aluminium bar and consisted of 3 segmented sections and an end cap. A 50mm hole was machined through each section to correspond with the outlet from the main body. Each segment was recessed to allow a mesh filter to be inserted. Individual mesh filters were manufactured from 1 mm thick aluminium disks measuring 50mm diameter that were perforated with holes ranging from 1.5mm to 6mm. Note, the mesh reference number refers to the size of the perforations, i.e. mesh 4 has holes 4mm in diameter. It should also be noted that the mesh density decreased as the mesh diameter increased; the 1.5mm disk had a mesh density of 0.15 hole/mm^2 while the 6mm disk had a mesh density of 0.02 hole/mm^2 .

The segmented system allowed the use of up to 4 mesh filters simultaneously which offers great scope to achieve various sand densities during pluviation. For reference the mesh positions are referred to as 'A to D', with 'A' being the uppermost mesh closest to the hopper body and 'D' being the mesh at the exit position. Note, a combination of meshes are denoted in sequence; i.e. Mesh 6/-/-/2 indicates mesh sizes 6 and 2 are located in position A and D respectively, with position B and C having not mesh present.

As it will be shown later, this combination of mesh possibilities enabled a wide range of mass flux and relative densities to be achieved since they could be mounted in any combination. In this paper a number of mesh combinations are evaluated to demonstrate the variations in density that could be achieved.

3.2 Flow rate calibration

A series of experiments are performed to study the effect of mesh diameter and D_{50} on the resulting flow rate. In the tests presented herein position A contained Mesh 6 and mesh in position B was varied between Mesh 2, 3, 4, 5 and 6; for example, 6/2/-/- through 6/6/-/-. Using these mesh configurations, the two sands, CH30 and CNHST95 are evaluated and the results are summarized in Figure 4.

Zhao et al. (2006) and Chian et al. (2010) showed that larger nozzle diameters resulted in a steep increase in the flow rate. However, an aspect not considered in their investigation was the effect of fullness of the sand pourer on the outcome. It seems reasonable to think that a fuller container might lead to a smaller flow rate due to increased arching stresses in the sand particles across perforations of the outlet mesh. The current test series investigates the effect of fullness of the sand pourer when it is

completely full compared to when it is only a third full.



Figure 3. Sand pluviation configuration.

As shown in Figure 4, as diameter of the exit mesh increases, the flow rate increases accordingly for both types of sand. This is reasonable since at mesh perforation diameters larger than the grading of the sand, sand particles would flow more freely through the mesh resulting in flows that would be very similar thus making the effect of mesh diameter insignificant. This behaviour is visible in Figure 4 for mesh configurations greater than 6/4/-/-.

The finer sand (CNHST95) consistently has larger flow rate than the coarser sand (CH30). Finer sand particles can exit a certain mesh diameter faster than a coarser particle leading to a larger flow rate. However, the difference is less pronounced at larger mesh diameters (larger than 4mm in current study). Chian et al. (2010) also observed a similar pattern.

Also shown in Figure 4 is that the fine CNHST95 sand yields a smaller flow rate at the smallest mesh diameters (i.e. 6/2/-/- and 6/1.5/-/-) when the container is full compared to when it is a third full (due to arching). As mesh diameter increases, the difference between the two scenarios diminishes and the flow rate is dominated by the mesh diameter and not the fullness of the sand pourer. The coarser CH30 sand however does not show a significant difference between the two scenarios for any mesh diameter and the flow rate response is completely dominated by the mesh diameter and not the fullness of the container.

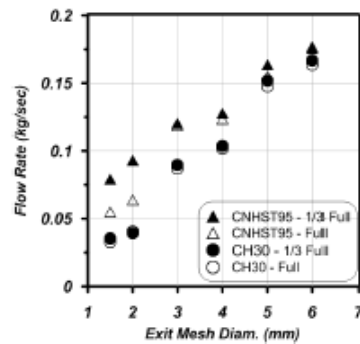


Figure 4. Effect of mesh diameter, D_{50} and fullness of sand pourer on the flow rate of the sand particles.

3.3 Sand pourer calibration test

A small cylindrical metal chamber of internal geometry 265mm diameter by 400mm high was used as a fixed volume standardized tub for the purpose of calibrating the sand pluviation system. This was achieved by measuring the mass of sand collected in the tub for different falling height and mesh diameter configurations.

Table 2 summarizes the implemented test matrix for calibration of the sand pourer. Test ID outlines the type of sand and diameter of the meshes used in the location of the hopper. The exit mesh in position B was varied between 1.5mm and 5mm while the mesh in position A was maintained as 6mm in diameter. The drop height was varied between 500mm and 900mm in most cases. A drop height of 1500mm was implemented for the CNHST95 sand to ensure a high relative density was achieved, as discussed in the next section. At the time of testing, the falling height was determined from the exit mesh position (i.e. mesh location B) to level of the soil surface. The height was manually kept constant during the pluviation to ensure a uniform relative density throughout the sample was achieved. An end cap was placed at the bottom of Mesh D to enable start/stop of the sand flow; to start the pluviation, the end cap was removed and a separate container was used to collect the sand being suddenly dropped from the exit mesh. Upon achieving a steady flow of sand particles, the extra container was removed to start the sand placement. During pluviation the nozzle was rotated slowly to cover the entire area of the calibration chamber. Classical sand pourers (Rad and Tumay 1987, Chapman 1974, Sweeney and Clough 1990) employ a vertical translation pluviation system only; in such systems the diameter of the nozzle is generally close in size to the size of the specimen. Due to the relatively small diameter of the nozzle of the proposed system compared to the diameter of the larger container (500mm), the sand pourer system will also benefit from a lateral translation system, using roll-

ers on the top of the A-frame supporting the sand pourer. The translation was not necessary for the calibration tests.

A sand height of 300mm was poured in three equal height lifts for all tests detailed in Table 2. In each lift, the sand was poured above the desired lift height (100mm) and the excess sand was then vacuumed using a dual-axis height controlled vacuum system to ensure a uniform surface is achieved in each lift. The relative density for each lift was further calculated and average values are reported in this paper. If the offset relative density of any of the three layers exceeded a value of 5% from the average relative density (e.g. D_r of layer 1 being 82% while average D_r being 88%), the test was repeated to ensure a homogenous relative density across the profile of the sample was achieved.

Table 2. Sand power calibration test matrix.

Test ID	Drop Height	Mesh 1	Mesh 2
	mm	mm	mm
CH30_6/2/-/-	500-900	6	2
CH30_6/3/-/-	500-900	6	2
CH30_6/4/-/-	500-900	6	2
CH30_6/5/-/-	500-900	6	2
CNHST_6/1.5/-/-	500-1500	6	1.5
CNHST_6/2/-/-	500-900	6	2
CNHST_6/3/-/-	500-900	6	3
CNHST_6/4/-/-	500-900	6	4
CNHST_6/5/-/-	500-900	6	5

3.4 Calibration test results

The results of the tests outlined in Table 2 (except the CNHST_6/1.5/-/- test) are summarized in Figure 5 where the achieved relative densities are plotted against the corresponding drop height. The label on each plot (e.g. 6/2/-/-) outlines the mesh combination presented. For the case of the coarser CH30 sand, a wide range of relative densities (35% to 95%) was achieved for different mesh combinations. As mesh diameter increased, the achieved relative density for a constant drop height reduced. Also, as drop height increased for each mesh configuration, increases in relative density were observed. This demonstrates the significance of the secondary effect of drop height on relative density. This is consistent to results reported by Chian et al. (2010) and Zhao et al. (2006) for sands of similar D_{50} as CH30 (0.45mm).

Evident in Figure 5 is that the effect of mesh diameter (>2mm) had less pronounced effect (about 20% change) on relative density observed for the finer CNHST95 sand compared to the CH30 sand. The achievable relative density is therefore highly influenced by the very small D_{50} (Fraction E) of the CNHST95 sand and exit mesh sizes of 2mm and greater (6/2/-/- to 6/5/-/-) do not impact the achieved relative density significantly. The ratio of mesh di-

ameter to the D_{50} is therefore too large to impact the achieved relative density. As the drop height increased in the range of 500-900mm some increases in relative density of CNHST95 sand were recorded, although not at the same rate as CH30. Generally speaking while some smaller increases were observed for CH30 over the range of variables tested, the maximum achievable relative density was never greater than 50%. In order to consolidate the data into a quick look up reference chart, the results from CH30 are compiled into a solitary plot (Figure 6). The graph serves as a useful reference lookup chart whereby user can easily cross reference a desired sample density with suitable sand hopper mesh configurations and drop height.

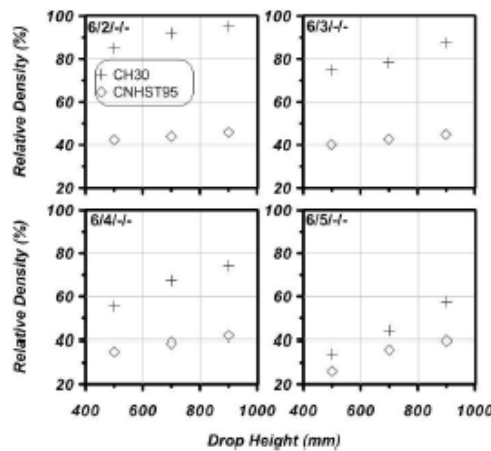


Figure 5. Effect of drop height and mesh diameter on the resulting relative density.

Evident in Figure 6 is that some overlap existing for the input variables and the output relative density. For example, if a researcher was seeking a target density of 85%, this could be achieved by mesh combination 6/3/- at a drop height of 50mm or by using mesh combination 6/4/- at a higher drop height of 900mm. A series of similar design curves have been generated for the full range of mesh combinations.

The results from the 6/1.5/- mesh combination used for the finer CNHST95 sand are plotted in Figure 7. As shown, a larger range of relative densities is achieved (between 65% and 92%) but the drop height had to be increased to 1500mm to achieve a relative density above 90%. The impact of drop height on the relative density is more pronounced than the cases shown in Figure 5. Chian et al. (2010) also reported similar impact where the drop height for the fine Fraction E sand had a larger impact on the achieved density than the coarser sand. They also reported the variation of the drop height impact on the relative density with the nozzle diameter; smaller

nozzle diameters led to a larger change in relative density with variation of drop height.

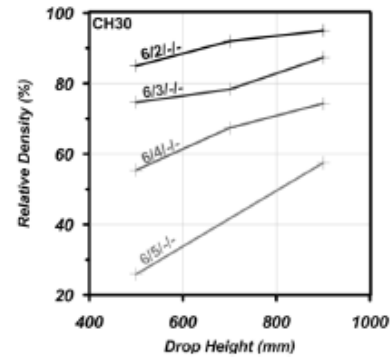


Figure 6. Relative density lookup chart for hopper input variables for CH30 sand.

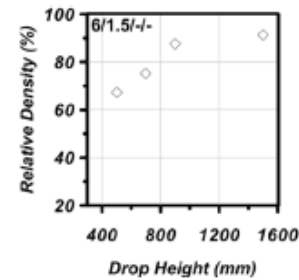


Figure 7. Effect of drop height on the relative density for the 6-1.5mm mesh for the fine CNHST95 sand.

3.5 Theoretical fall velocity

Chapra (2005) and Chian et al. (2010) proposed equations for theoretical fall velocity of a sand particle (Equations 1 & 2) with respect to the drop height (H). A lower drop height leads to a small fall velocity which further leads to a loosely packed particle arrangement. Equation 1 shows the theoretical fall velocity (v) of a sand particle of mass (m) with projected area of (A) falling from height of (H) in air during the elapsed fall time of (t); ρ is therefore density of air and C_d is the drag coefficient in air taken as 0.47.

$$v = \sqrt{\frac{m \cdot g}{\rho \cdot A \cdot C_d}} \cdot \tanh \left(\frac{t}{\sqrt{\frac{m}{\rho \cdot g \cdot A \cdot C_d}}} \right) \quad (1)$$

The elapsed fall time can further be calculated from Equation 2 below for a specific drop height (H). It should be noted that \tanh and $\operatorname{arccosh}$ are the

hyperbolic tangent and inverse hyperbolic cosine accordingly.

$$t = \sqrt{\frac{m}{\rho \cdot g \cdot A \cdot C_d}} \cdot \operatorname{arccosh} \left(e^{\frac{H \cdot \rho \cdot g \cdot C_d}{m}} \right) \quad (2)$$

Terminal velocity (maximum attainable velocity) will be achieved when the sum of all upward forces (drag and buoyancy forces) equilibrate the downward force of gravity; the sand grain will therefore have zero acceleration at the terminal velocity. Equation 3 can therefore be derived for the terminal velocity of a sand grain.

$$v_{term} = \sqrt{\frac{2m \cdot g}{\rho \cdot A \cdot C_d}} \quad (3)$$

Figure 8 plots the theoretical fall velocity for the CH30 and CNHST95 sands with respect to the drop heights. Since the drop heights were relatively small, the terminal velocity was not achieved in either of the sands. As expected from Equations 1-3, the fall velocity and terminal velocity of the finer CNHST95 (smaller grain size) are smaller than those of the coarser CH30 sand. This pattern was also reported by Chian et al. (2010) where the fall velocity of the Fraction E sand was smaller than the velocity of the coarser sand. Chian et al. (2010) also noted that the terminal velocity was not achieved due to the low drop height.

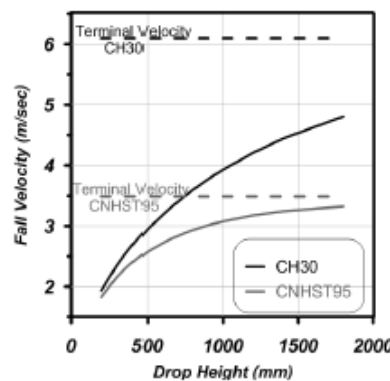


Figure 8. Variation of theoretical fall velocity with drop height.

4 CONCLUSIONS

A point sand pourer is designed and calibrated at the Centre for Energy and Infrastructure Ground Research at the University of Sheffield. The pourer was designed such that 4 mesh inserts could be used simultaneously. Effect of pour height and mesh diameter is studied to calibrate the sand hopper for different desired relative densities. Fullness of the sand hopper is also realized to impact the flow rate, a fac-

tor not previously examined in sand hopper development or sand pluviation calibration.

5 ACKNOWLEDGEMENTS

The authors would like to acknowledge the contribution by the Department of Civil & Structural Engineering technical staff for in-house technical support. Funding support provided by the Engineering Physical Sciences Research Council (EPSRC) to establish the 4 m diameter beam centrifuge and Centre for Energy and Infrastructure Ground Research at the University of Sheffield is gratefully acknowledged (EP/K040316/1).

6 REFERENCES

Arulanandan, K. & Scott, R.F. 1993. Verification of numerical procedures for the analysis of soil liquefaction problems: *Technical Papers and Discussions*, Volume 1-2. Rotterdam: A.A. Balkema.

Chapman G. A. 1974 A calibration chamber for field test equipment. *Proceedings of the 2nd European Symposium on Penetration Testing*, Stockholm, 59-65.

Chian, SC and Stringer, ME and Madabhushi, SPG, 2010. Use of automatic sand pourers for loose sand models. *Physical Modelling in Geotechnics - Proceedings of the 7th International Conference on Physical Modelling in Geotechnics*, ICPMG 2010, 1, 117-121.

Hakhamaneshi, M., Kutter, B.L., Moore, M. & Champion, C., 2015. Validation of ASCE 41-13 modeling parameters and acceptance criteria for rocking shallow foundations. *Earthquake Spectra*. (in-press)

Garnier, J., Gaudin, C., Springman, S.M., Culligan, P.J., Goodings, D., König, D., Kutter, B.L., Philips, R., Randolph, M.F., & Thorel, L., 2007. Catalogue of scaling laws and similitude questions in geotechnical centrifuge modelling. *International Journal of Physical Modelling in Geotechnics*.

Rad, N. & Tunay, M. 1987. Factors affecting sand specimen preparation by raining. *Geotechnical Testing Journal* 10(1), 31-37.

Stringer, M.E., Pedersen, L., Nuss, B.D. & Wilson, D.W. 2014 Design and use of a rotating spiral pluviator for creating large sand models. *Physical Modelling in Geotechnics - Proceedings of the 8th International Conference on Physical Modelling in Geotechnics 2014*, Perth, Australia.

Sweeney B. P. and Clough G. W. 1990 Design of a large calibration chamber. *Geotechnical Testing Journal*, 13, No. 1, 36-44.

Zhao, Y., K. Gafar, M.Z.E.B. Elshafie, A.D. Deeks, J.A. Knappe, & S.P.G. Madabhushi. 2006. Calibration and use of a new automatic sand pourer. In: C.W.W. Ng, L.M. Zhang, and Y.H. Wang (Eds.), *Physical Modelling in Geotechnics - 6th ICPMG '06*, Volume I, Hong Kong, pp. 265-270. Taylor & Francis Ltd.

Part III

Development of a 25ton consolidation press at the Centre for Energy and Infrastructure Ground Research

M. Hakhamaneshi, J.A. Black, C.M. Cox & T. Elmrom

University of Sheffield, Centre for Energy & Infrastructure Ground Research, Sheffield, UK

ABSTRACT: A 1d consolidation frame has been designed and manufactured at the Centre for Energy and Infrastructure Ground Research (CEIGR), University of Sheffield. The consolidation frame allows static consolidation of soil beds. This system comprises of a 25 ton rated press that can accommodate a range of centrifuge payload strong box configurations. The consolidation force is delivered via a hydraulic piston rated to deliver 80 kN force at 10bar supply pressure with a stroke of 500mm. A series of vertical draw-wire transducers are implemented which monitor consolidation settlement. Combined with pore pressure transducers, the user can measure the pore water pressure at the top and at the bottom of the clay sample. A bespoke LabVIEW VI visual display is implemented which offers visual/graphical feedback to the user on the range of sensor information and a live update of consolidation progress; it also incorporates data entry to capture test specific information.

1 INTRODUCTION

An essential part of centrifuge modelling is the ability to produce clay bed profiles of different over-consolidation ratio. In order to understand the consolidation characteristics of the test bed it is necessary to capture and record consolidation information during this process. This will enable knowledge of the consolidation characteristics of each test bed and also provide a means of creating reproducible homogeneous clay beds.

It is very common for researchers to develop a series of experimental parametric studies where clay bed models must be uniform across the whole test series (Hakhamaneshi et al. 2012). A non-uniform clay bed model directly affects the performance of many physical model tests in the centrifuge; examples include pile capacity tests, seismic site response, offshore platform response on soft clay. Many researchers also aim to compare their experimental findings with numerical predictions (e.g. Arulanandan and Scott 1993) or the experimental results to be used as a benchmark for calibration of numerical models (e.g. Liu et al. 2013). It is therefore essential for centrifuge facilities to employ a consolidation press capable of producing uniform clay bed models at a wide range of pre-consolidation pressures and over-consolidation ratios accordingly.

2 CENTRIFUGE FACILITY

A 25 ton consolidation press is developed at the Centre for Energy and Infrastructure Ground Research (CEIGR) centrifuge facility at the University of Sheffield. The centrifuge is a newly established University of Sheffield 50gT geotechnical beam centrifuge located in the CEIGR. The centrifuge was designed and manufactured by Thomas Broadbent and Sons Limited, United Kingdom, and commissioned in 2014. The centrifuge beam has a radius of 2 m to the base of the swing platform, of plan area 0.8 m², and can accelerate a 500 kg payload to 100 gravities (Black et al. 2014).

The 25 ton consolidation press is aimed to produce a wide range of over-consolidation ratios (OCR). A typical container employed within CEIGR is a circular tub of 490mm diameter and 500mm height, thus the maximum vertical stress that can be achieved in this configuration is 1300 kPa. It can be assumed that the thickness of a consolidated clay bed will not exceed 350mm. Therefore, the 25 ton consolidation press at full capacity is capable of producing a consolidated clay bed (assuming 350mm height and a unit weight of 18kN/m³) of OCR=2 at the bottom of the clay bed when the sample is spinning at 100 times earth's gravity (100g). On the other end of the spectrum, much higher OCRs can be produced by reducing the centrifugal acceleration.

3 DESIGN OF THE CONSOLIDATION PRESS

As shown in Figure 1, consolidation press frame consists of 4 steel flat bars as the main support of the frame, 8 C-channels as top and bottom supports of the frame, 2 L-sections bolted to the concrete floor, two steel plates as the top and bottom platforms, 2 side steel plates and 8 U-channels (4 on top and 4 on the bottom). The steel flat bars are 25mm thick, 1600mm long and 100mm wide made out of high strength carbon steel. The 4 smaller C-channels on the bottom are bolted to the concrete floor to provide additional axial support. The side L-sections are bolted to the floor and provide twisting resistance. The top and bottom larger C-channels provide additional axial and shear resistance to the steel platforms. The top steel platform and 4 U-channels support the loading piston and the reaction forces generated during loading. The bottom steel platform and U-channels support the soil container along with the consolidation loads generated from the piston. A loading plate of diameter 488.5mm transfers to consolidation load to the soil; load is being registered through a 100kN Load Cell rigidly mounted to the loading plate.

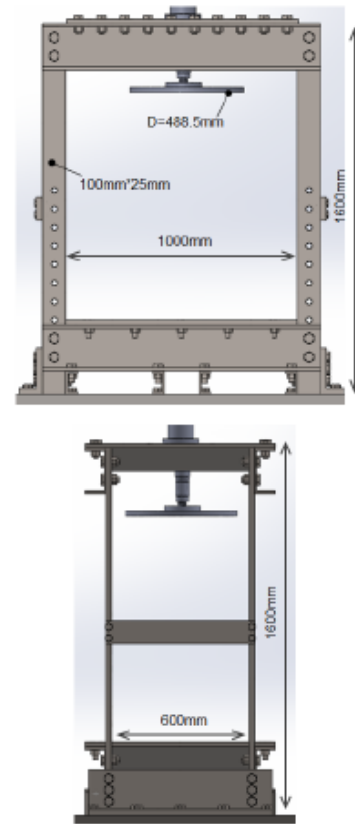
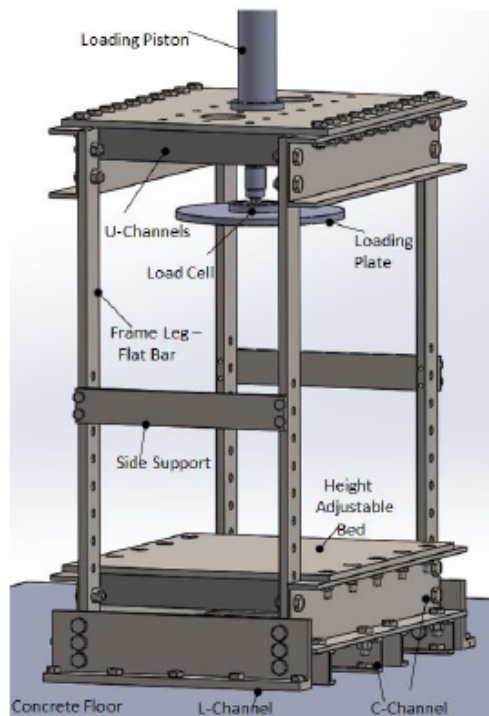


Figure 1. SolidWorks drawings of the consolidation press frame and 3D view.

A series of SolidWorks simulation under static load are conducted to evaluate the performance of the critical parts of the press frame under 25 ton of static loading. Figure 2 plots the simulation results for the steel flat bar legs and the top platform. It can be seen that the flat bars undergo a displacement of 0.02mm while the platforms deforms by 0.38mm (strain of less than 0.1% for both parts). The frame assembly is then trustfully capable of carrying 25 ton of axial loads.

4 CONSOLIDATION OF KAOLIN CLAY

4.1 Mix preparation & instrumentation

The circular tub of dimensions previously specified is used to perform a 1g consolidation test on Kaolin Clay using the consolidation press. A 30mm layer of dense sand is poured on the bottom of the container to create a uniform free draining surface. Kaolin Clay is mixed at a water content of 100% (approximately 1.3 times the liquid limit) and poured to an

initial height of 450mm (measured from bottom of the container). The slurry was covered with a vinyl sheet and allowed to self-consolidation for 24 hours.

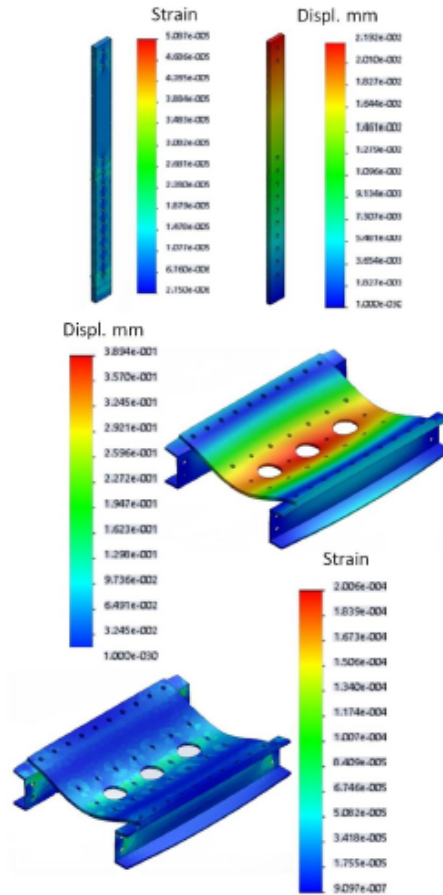


Figure 2. SolidWorks simulation results for 25 ton of static loading.

The Data Acquisition System (DAQ) consisted of a National Instruments 6001 USB device capable of measuring 8 analogue input channels. The DAQ device is packaged inside an enclosure along with sensor and signal conditioning power supplies. The sensor outputs are amplified, using amplifier Printed Circuit Boards built into the cable plugs, such that the amplified signal magnitudes (at full scale output) is a significant proportion of the input signal range, hence increasing the signal to noise ratio. The sensors used in the consolidation process are: a 100kN capacity load-cell for measuring plate load (and deriving consolidation pressure); two 500mm displacement draw-wire sensors for measuring plate movement and a pressure transducer sensor for measuring the pump pressure. The other 4 channels

are spare for connection of test specific sensors (e.g. Pore Pressure Transducers). A front Virtual Instrument (VI) was developed in the LabVIEW programming environment in order to acquire data, convert voltages to engineering units, plot and record the sensor data.

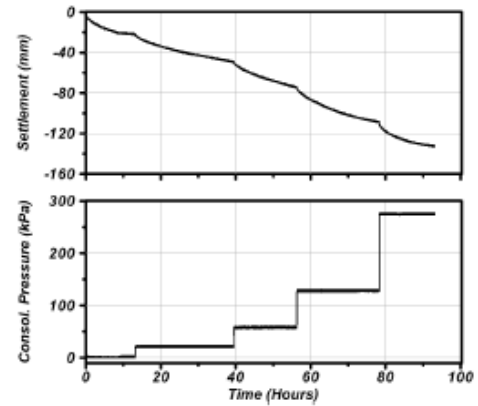


Figure 3. Settlement and consolidation pressure time history.

4.2 Consolidation test results

Figure 3 plots the settlement and consolidation pressure time history of the slurry mix. This plot does not include the settlements incurred during the self-weight consolidation of the specimen being under its own weight for 24 hours. After self-weight consolidation, initial seating pressure was set to about 13kPa and consolidation pressure was doubled during each stage increment. The achieved seating pressure without loss of material during loading is larger than seating pressure applied in typical oedometer testing (6kPa). A maximum pre-consolidation pressure of 280kPa was registered by the load cell. The weight of the steel plate is neglected in the calculation of the consolidation pressure as it is negligibly small compared to the applied axial stresses. Settlement time history plot in Figure 3 demonstrates that the sample settled 133mm (volumetric strain of about 32%). Bauer and El-Hakim (1985) reported an axial strain of 16% and 24% for Kaolin Clay slurry of 48% and 62% water content, correspondingly.

Figure 4 plots the incremental clay sample height with respect to the square root of time; the final sample height is measured to be about 287mm. Taylor (1948) method using the square root time method is used to evaluate the time required for 90% of consolidation at each stage (t_{90}). End of primary void ratio for each stage is further calculated and the resulting Normally Consolidated Line (NLC) line is shown in Figure 5. A separate oedometer testing of normally consolidated Kaolin Clay (of the same slurry mix) is performed and results are also plotted in

Figure 5. The seating pressure in the oedometer testing was set to be 6kPa and doubled for each following stage until a maximum consolidation pressure of 200kPa was achieved.

As it can be seen in Figure 5, the NCL lines from the oedometer and consolidation press are somewhat different. The difference at lower consolidation pressures is small (3% difference) and the difference gets larger with increasing consolidation pressures (up to 8%). The increased in the difference can be contributed to the variation in side friction and geometry aspect ratio between the centrifuge tub and oedometer test ring; while a thin layer of silicon grease was applied to the sides of the oedometer ring, the centrifuge tub was not treated similarly Sarsby and Vickers (1985) also discussed the effects of the side friction to the on the consolidation results and showed that the side friction can be up to 50% of the applied pressure, even when the sides were smeared with grease.

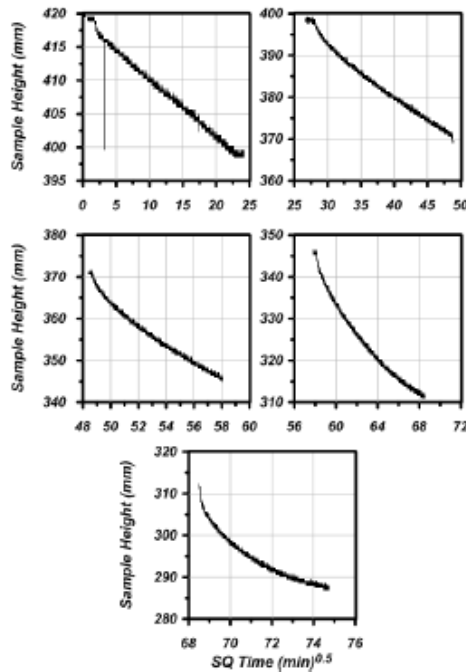


Figure 4. Caption of a typical figure. Photographs will be scanned by the printer. Always supply original photographs.

A series of water content, hand shear vane, oedometer and triaxial tests were performed on the consolidated sample produced using the consolidation press to evaluate the uniformity of consolidation within the consolidated sample. A Shelby tube sampler was used to extract a continuous sample of the entire clay profile. Water content was measured every 20mm throughout the sample. Figure 6 plots the

water content of the entire profile of the consolidated clay bed. After consolidation water content varied between 45% and 49% with the minimum water content recorded towards the middle of the clay.

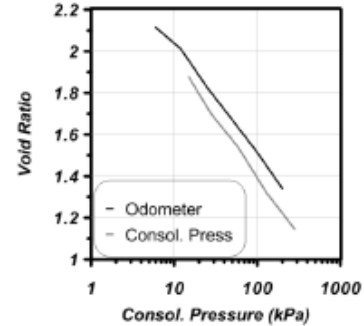


Figure 5. Void ratio versus log of consolidation pressure of Kaolin clay obtained from oedometer and consolidation press.

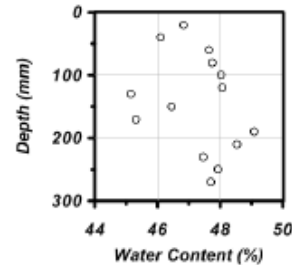


Figure 6. Water content measurements of the entire consolidated clay profile.

Figure 7 plots the results of the shear vane and triaxial tests performed at different surficial locations of different depths (triaxial samples were only taken from the middle of the clay sample). Hand vane shear tests were performed towards the middle and corners of the clay bed at a depth of 50mm followed by penetrating the vane and testing at a depth of 190mm. The undrained shear strength at a depth of 50mm varied from 23 to 28kPa while at 190mm recorded values were in the range of 24kPa and 36kPa. The measured undrained shear strength towards the middle of the container was greater than the shear strengths away from the center, with the smallest values recorded at the periphery of the chamber. The undrained shear strength of the clay bed increased with depth for samples near the center of the container. At the edges, no significant change was captured with the increase in depth. Load distribution and side friction are therefore affecting the shear strength results closer to the boundaries.

Four different triaxial test specimens (38mm in diameter) were taken from the middle of the container and at the top and bottom of the clay bed.

Tests were carried out at confining pressures of 50kPa and 200kPa. Results shown in Figure 7 reveal undrained shear strength of 26kPa for the samples taken from the surface and 37kPa for the deeper sample. These values are consistent with the undrained shear strengths recorded using the hand vane apparatus and towards the middle of the container. Effect of side friction on the samples taken from the middle of the container is minimal and therefore effect of sample surcharge on the shear strength is more pronounced in the samples taken towards the middle of the container.

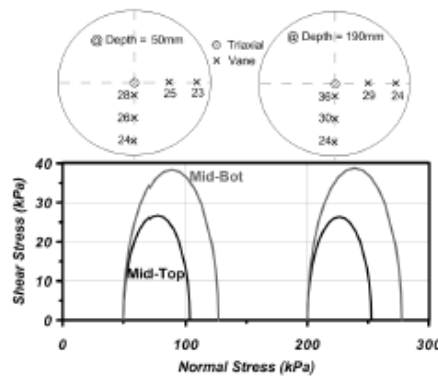


Figure 7. Hand shear vane and triaxial test results of the consolidated clay bed.

A series of 4 oedometer tests were also performed on samples at different depths and surficial locations. Two samples were taken towards the middle of the container at the surface and the bottom of the clay bed; the other samples were taken accordingly but towards the corner of the container. A maximum consolidation pressure of 800kPa (beyond their pre-consolidation pressure of 280kPa) was applied and settlement response of the samples were recorded. Taylor (1948) method was used to calculate the t_{90} and H_{90} values at each consolidation pressure stage. Figure 8 plots the void ratio of the samples versus the log of the applied consolidation pressure. The Casagrande (1936) method for determination of pre-consolidation pressure is used to evaluate the variation of this parameter at different locations of the container.

As it can be seen from Figure 8, the pre-consolidation pressure of the samples taken towards the middle of the container (both surface and deep samples) is estimated to be about 250kPa; this estimate is close to the applied 280kPa of consolidation pressure registered by the load cell. The pre-consolidation pressure of the samples taken from the edges measure equal to or less than 200kPa. The lowest value of pre-consolidation pressure is obtained from the sample taken from the edge and bottom of the clay bed. This can be correlated to com-

bined effects of load distribution and skin friction on the actual pressure at this location. Black 2007 also reported the effects of side friction in a large oedometer test on the reduced pressures with depth.

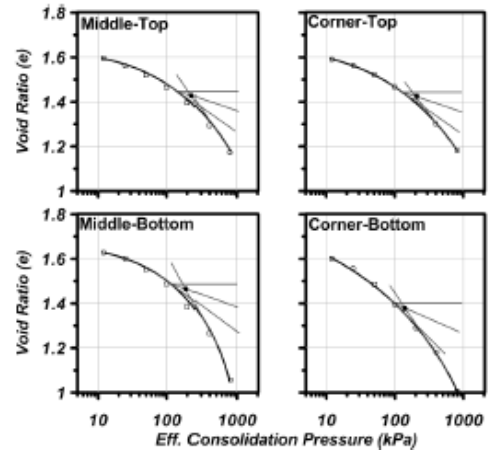


Figure 8. Oedometer testing of four samples taken towards the middle and corner of the container and at two different depths.

5 CONCLUSIONS

This paper outlines the design of a 25ton consolidation press frame. The press can be used for centrifuge testing of over-consolidated clay beds. Kaolin clay was mixed at a water content of 100% and consolidated and settlement time history of the specimen was recorded for different amplitudes of consolidation pressure. A maximum consolidation pressure of 280kPa was applied to the sample and a total axial strain of about 32% was measured at this pressure. The resulting NCL line obtained from the consolidated sample in the press was compared against an oedometer testing of a sample taken from similar initial slurry. Reasonable agreement was obtained between the two NCL lines with smaller differences in the smaller values of consolidation pressure. Effect of side friction is believed to affect the results at larger consolidation pressures. A series of shear vane, triaxial and oedometer testing was performed on the consolidated clay bed and at different surficial locations and varying depths. The undrained shear strength of the sample towards the middle of the container was measured to be greater than those measured towards the corners. There was good agreement between the hand vane and triaxial testing results throughout the clay bed. A series of 4 oedometer testing was performed from samples taken from middle and corners of the container and at different depths. The Casagrande method for determination of pre-consolidation pressure was used to estimate and compare this parameter amongst the

samples taken. It was concluded that the samples taken from the middle of the container have larger pre-consolidation pressures than those taken from the corners. This was attributed to the side friction along the container wall and the load distribution leading to smaller pressures distributed to the corners.

6 ACKNOWLEDGEMENTS

Funding support provided by the Engineering Physical Sciences Research Council (EPSRC) to establish CEIGR is gratefully acknowledged. Continued technical support by Thomas Broadbent and Son Ltd. is also appreciated. The authors would like to acknowledge the contribution by the Department of Civil & Structural Engineering technical staff for in-house technical support.

7 REFERENCES

- Arulanandan, K. & Scott, R.F. 1993. Verification of numerical procedures for the analysis of soil liquefaction problems: *Technical Papers and Discussions*, Volume 1-2. Rotterdam: A.A. Balkema.
- Bauer, G.E. & El-Hakim, Z. 1985. Consolidation testing – a comparative study. *Consolidation of Soils: Testing and Evaluation*, Issue 892, 694-710.
- Black, J.A. 2007. The settlement performance of a footing supported on soft clay reinforced with vibrated stone columns. *PhD Thesis*. Queens University Belfast, UK.
- Casagrande, A. 1936. The determination of the pre-consolidation load and its practical significance, Discussion D-34, *Proceedings of the first international conference on soil mechanics and foundation engineering*, Cambridge, Vol. III, 60-64.
- Black, J.A., Baker, N., and A. Ainsworth, 2015. Establishing a 50 g-Ton geotechnical centrifuge at the University of Sheffield. *Physical Modelling in Geotechnics ICPMG 2014*, Perth, Australia. 181-186.
- Liu, W., Hutchinson, T. C., Kutter, B. L., Hakhmaneshi, M., Aschheim, M. and Kunnath, S. 2013. Demonstration of Compatible Yielding between Soil-Foundation and Superstructure Components. *ASCE, Journal of Structural Engineering*, 139(8): 1408-1420.
- Hakhmaneshi, M., Kutter, B.L., Deng, L., Hutchinson, T.C. and Liu, W. 2012. New findings: from centrifuge modeling of rocking shallow foundations in clayey ground. *Proceedings of ASCE 2012 Geo-congress*, Oakland, March 25-29.
- Sarsby, R.W. & Brian Civkers 1985. Side friction in consolidation tests on fibrous peat. Consolidation testing – a comparative study. *Consolidation of Soils: Testing and Evaluation*, Issue 892, 485-489
- Taylor, D.W. 1948. *Fundamentals of soil mechanics*, John Wiley & Sons, Inc., New York, 700.